Robustness of WT Steel Connections during Quasi-Dynamic Loading

by

Megan E. Hayes

Report Submitted to the Faculty of the
Milwaukee School of Engineering
in Partial Fulfillment of the
Requirement for the Degree of
Master of Science in Structural Engineering

Milwaukee, Wisconsin
May 2016

Abstract

One of the most commonly used connection types in steel frame buildings is a shear connection. These connections are typically designed only for vertical shear, though previous studies have proven that shear connections have some capability to resist an interaction of shear, axial, and moment. With recent events such as the Murrah Federal Building and the World Trade Center disasters, there is a continuing need to study the robustness of connections subject to unanticipated loading scenarios.

The purpose of this research is to qualitatively and quantitatively measure the effects of the interaction of forces during a quasi-dynamic loading of a flexible WT connection. Results from this research show how a WT connection will perform during a sudden collapse of an interior support column in a steel framed building. Through the study, the robustness of the connection through both rotation and accrual of load was observed and recorded. Results of the test demonstrated the flexural resistance of the WT connection and the presence of catenary action.

To properly study and analyze the connection, physical testing of three-, four-, and five-bolt configurations of WT connections was performed. For each of the configurations, one test was loaded under a quasi-static loading rate, and three tests were loaded under quasi-dynamic loading rate. Data collected from the testing were used to calculate forces at the connection, including shear, axial, and moment.

Testing showed that as the number of bolts increased, the flexural capacity of the connection increased but the amount rotation before failure decreased. To better compare results of the two different loading types, a comparison of energy absorbed by the connection was performed. Testing showed that as the loading rate increased the net amount of rotation the connection can withstand decreases.

Acknowledgments

The completion of thesis would not have been possible without help of many people and organizations. I would like to thank Germantown Iron and Steel for their gracious donation of testing materials and specimens. I would also like to extend my thanks to Applied Bolting Technology for providing hundreds of direct tension indicating (a.k.a. “squirter”) washers.

I would like to extend a special thank you to my advisor, Dr. Christopher Raebel, for all of his help, insight, and guidance through this project. Thank you to Dr. H. Peter Huttelmaier and Dr. Richard DeVries at Milwaukee School of Engineering, and Dr. Christopher Foley at Marquette University for their expertise, guidance and continued support.

I would like to thank Dave Newman and his team (Adam Walker and Joe Tschida) in the Engineering Materials and Structural Testing Laboratory (EMSTL) at Marquette University for their help during all the experimental testing. I would like to thank Dr. Raymond Fournelle for his work performing a metallurgical analysis on the bolts used during testing.

It is also important to thank Jackie Lesser for her time and effort as she worked concurrently on her respective thesis project in conjunction with my own.

Finally, I would like to thank my family and friends for their continued support during this process.

Table of Contents

List of Figures

List of Tables

Nomenclature

Symbols

A – area

B – resultant force acting on one bolt

C – coefficient for eccentrically loaded bolt group

E – modulus of elasticity

F_u – ultimate stress of material, ksi

F_y – yield stress of material, ksi

H – normalized shear force

I – moment of interia

L_{beam} – length of beam

L_{eh} – horizontal edge distance

M – bending moment, kip-in or kip-feet

P – axial load, kips

R – nominal shear strength of one bolt at deformation

V – applied shear force, kips

e – eccentricity

t_s – thickness of the WT stem

y – distance from the neutral axis

ε – strain

Δ - deflection, inch

θ – angle of rotation, radians

ϕ – factor of safety

σ - stress

μ – micro

Abbreviations

AISC – American Institute of Steel Construction

ACI – American Concrete Institute

Avg – average

DTI – Direct Tension Indicator

DWT – Draw Wired Transducers

EMSTL - Engineering Materials and Structural Testing Laboratory

ft – Feet

IBC – International Building Code

ICOR – instantaneous center of rotation

in. – inch

ksi – kips per square inch

lbs or lb – pounds

psi – pounds per square inch

SG – strain gage

WT – wide flange tee section

Glossary

Butterworth Filter – a type of signal processing filter designed to have as flat a frequency response as possible in the passband.

catenary- curve described by a rope hung from two points on the same horizontal plane.

catenary action – tensile force acting along the geometry of a catenary.

kips – 1000 pounds.

Median Filter – nonlinear digital filtering technique used to remove high noise floor.

progressive collapse – failure in adjoining structural elements that resulted from failure in primary structural element.

quasi-dynamic – to pull down on the system at a rate of approximately 10 inches in 4 seconds.

quasi-static – to pull down on the system at a rate of 10 inches in 10 minutes.

Chapter 1: Introduction

One of the most commonly used connection types in a steel framed building is a shear connection. These connections are typically designed only for vertical shear, though previous research has proven that shear connections have some capability to resist an interaction of shear, axial force, and moment. There are several different types of shear connections such as shear tabs, single angles, double angles, end plates, seated, and tee connections.

The robustness of these connections during static loading has been a continued focus in research in the last several years. "Robustness may be thought as the building's inherent structural ability to resist loads other than those anticipated during design." [1] Events where robustness becomes a crucial part of design are accidental damage to column or beam due to impact; damage due to the concussion of a blast; strength reduction due to extreme heat during a fire; and localized accidental overload of a beam or column. These types of events have happened throughout history, with the first one that really brought robustness considerations to the forefront being the Ronan Point apartment collapse in 1968. The study of structural robustness has continued throughout the years. The events of September 11, 2001, reinvigorated the need for robustness research.

The American Institute of Steel Construction Specification [2] is unclear about the inherent robustness in steel framed buildings. ACI 318-11 [3] allows for load reductions due to inherent robustness in concrete. In recent years the International Building Code (IBC) [4] has integrated a minimum structural integrity requirement.

With all the codes adding a structural integrity component, it is becoming increasingly important to understand the robustness of the shear connection.

The purpose of this research is to evaluate the robustness of WT connection through quasi-dynamic loading. A WT is simply a wide flange section cut in half. This experimental testing will focus on the WT being bolted to both the column stub and the beam. This can be seen in Figure 1-1. To test a range of commonly used WT connections, WTs with three-, four-, and five-bolt configurations are used. During the experimental testing, the axial force, shear force, and moment in the connection are calculated through strain measurements or direct force measurements.

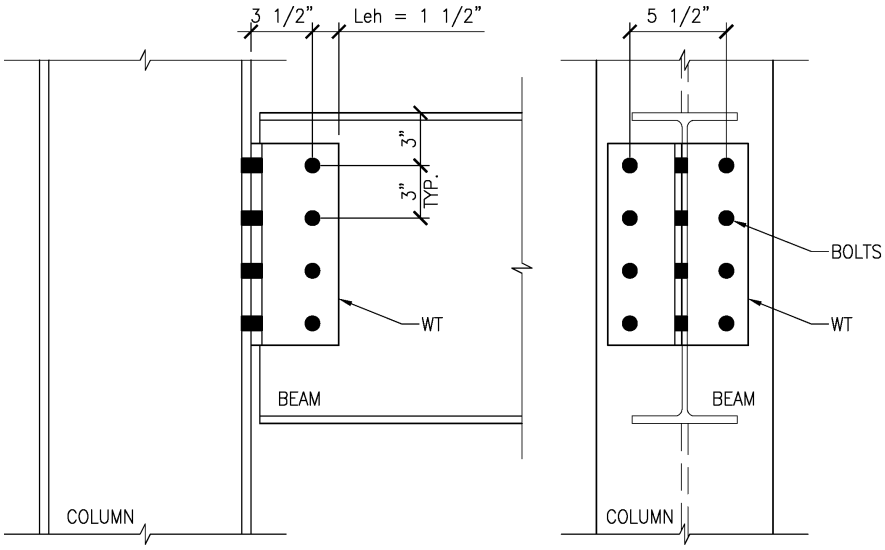

Figure 1-1: Bolted WT Connection.

Each configuration has one specimen that was loaded quasi-statically, herein called “static”, as to give a baseline and to compare to previous research. The remaining three test specimens for each configuration were loaded quasi-dynamically, herein called “dynamic.” Comparisons are made between the two loading types.

Chapter 2: Literature Review/Present Practices

Currently there is a great deal of research being conducted in regards to progressive collapse of steel framed structures that utilize simple connections. This research is in an effort to improve design guidelines and increase safety and redundancy in design. However, most of the research did not specifically consider WT bolted connections. Instead, much of the research focused on shear tabs, which have similar limit states as the WT's stem, and thus it can be used as a fair comparison. Having said this, there is a vast amount of research available regarding the design of the simple WT type connection. A summary of the research of current and past practices are included herein.

2.1 Design of Tee Framing Shear Connections by Astaneh and Nader

Shear connections should satisfy the criteria of shear strength and rotational ductility per the AISC manual. The connection should be flexible enough to rotate and release moment along with adequate shear strength to transfer the reaction of the beam. Astaneh and Nader [5] conducted experimental tests where WT connections first underwent applied moments to measure rotational flexibility and ductility. The connection was then subjected to realistic combinations of shear and rotation to measure its shear strength. The test specimens were bolted to the beam and welded to the column stub.

Moment-rotation tests were conducted by rotating the test beam up to 0.07 radians to measure the flexibility and ductility of the connection. For all but one of the test specimens, the WT connections were able to reach the 0.07 radians of rotation with only minor yielding occurring.

The WT connections then were subjected to an increasing shear force until failure. The limit states included stem shear yielding, shear rupture of net area, bolt shear failure and weld rupture. Astaneh and Nader provided a list of design guidelines based on the limit states.

2.1.1 Shear Yielding of Gross Area of Stem

The following [5] consider the full shear and neglected the effects of bending moment. These equations are based on allowable stress design procedures with a yield stress of 36 ksi, because ASTM A36 material was common at the time. Thus,

$$f_{vy} \leq F_{vy} \tag{2.1-1}$$

where

$$f_{vy} = \frac{R}{A_{vg}}, \tag{2.1-2}$$

$$F_{vy} = 0.4 \times F_y, \tag{2.1-3}$$

$$A_{vg} = L_t \times t_s \ , \tag{2.1-4}$$

L_t = Length of WT (in.),

t_s = Thickness of WT stem (in.).

2.1.2 Yielding of Tee Flange

When using a WT split from a wide flange shape, this limit state will not govern. Thus, this limit state has been omitted from this review.

2.1.3 Bearing Failure of Tee Stem or Beam Web

To avoid it being a limit state, the authors stated that using edge spacing of at least one and one-half times the bolt diameter and using a bolt spacing of three inches would be sufficient.

2.1.4 Shear Fracture of Net Area of Tee Stem

This limit state is when the critical net section of the tee stem fractures due to the shear. The research conducted showed that the critical net section was located along the edge of the bolt holes. The following equation defines the limit state:

$$f_{vu} \leq F_{vu} \tag{2.1-5}$$

where

$$f_{vy} = \frac{R_0}{A_{nse}}, \tag{2.1-6}$$

$$F_{vy} = 0.3 \times F_u, \tag{2.1-7}$$

$$A_{vg} = [L_t - n\left(\frac{1}{2}\right) \times \left(d_b + \frac{1}{16}\right) \times t_s. \tag{2.1-8}$$

Equation (2.1-8) does not use the 1/2 factor in the AISC Manual (8th Edition) [6] giving a more conservative design, which typically makes shear fracture of net area of tee stem control. All the testing and code values were based on available materials and current specification in late 1980s, which includes the fact that yield stress was 36 ksi.

2.1.5 Shear Failure of Bolts

The bolts were designed to withstand direct shear and neglected the moment caused by eccentricity during Astaneh and Nader's research [5]. The testing relies on

data from rigid or flexible connections and available bolt strengths are outdated. This limit state will need to be verified using Section J3.6 of AISC Specification [2].

2.2 A Rational Approach to Design of Tee Shear Connection by Thornton

Thornton [6] conducted an analytical study to confirm the results found by Astaneh and Nader. Thornton attempted to estimate the maximum possible force that could be applied to the bolts at the tee flange. To find this force, his assumptions state that as the connection rotates about its lower edge it will induce a force into the welds or bolts at the tee flange. Thornton neglected the effects of the shear force on the plastic moment capacity and the vertical shear on the plastic moment. The induced forces will result in a worst case scenario. The geometry of the connection is illustrated in Figure 2.2-1.

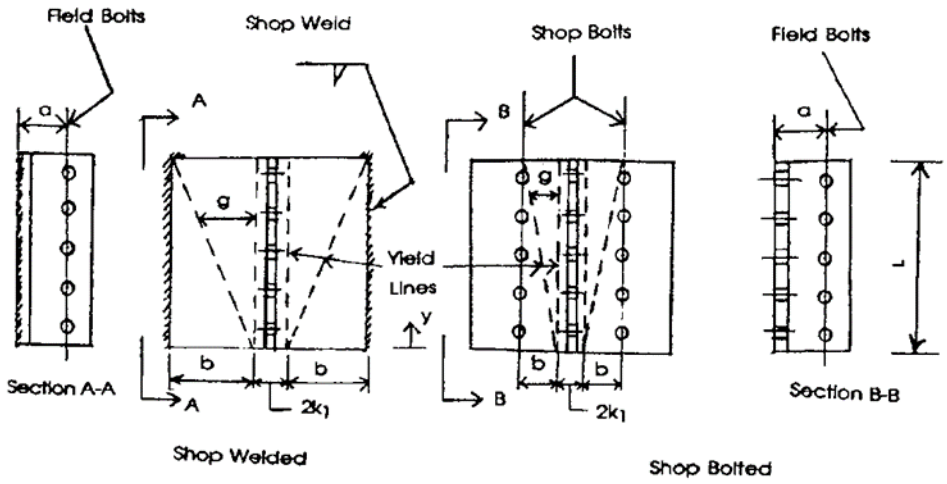

Figure 2.2-1: Tee Shear Connections [6].

From Figure 2.2-1, Thornton derived the following:

$$\emptyset = \theta\sqrt{1+\left(\frac{b}{L}\right)^2}\,, \tag{2.2-1}$$

$$\delta = \theta \times g, \tag{2.2-2}$$

$$g = \frac{b}{L} \times y\,, \tag{2.2-3}$$

where

$\emptyset$ = the rotation at the inclined yield lines,

θ = the rotation at the vertical yield lines,

δ = deflection at the center of the flange of the WT.

The virtual work equation is written as:

$$m_p \times \emptyset \times \sqrt{L^2+b^2} + m_p \times \theta \times L =$$

$$\int_0^L (V dy) \times g \times \theta = \frac{1}{2} \times V \times b \times L \times \theta\,, \tag{2.2-4}$$

where

$$m_p = \frac{1}{4} \times F_y \times t^2, \tag{2.2-5}$$

$$\eta = \frac{b}{L}\,, \tag{2.2-6}$$

V is the force per unit length of weld,

$$V = \frac{1}{2} \times F_y \times \frac{t^2}{b} \times (\eta^2 + 2). \tag{2.2-7}$$

Thornton then summed moments about the bottom of the connection to produce a connection couple:

$$M = VL^2. \tag{2.2-8}$$

From this equation, Thornton was able to compare to the experimental tests done by Astaneh and Nader [5]. The theoretical value for moment surpassed that of the physical tests when the connection rotated 0.07 radians but provided a reasonable comparison when the connection rotated 0.03 radians.

Thornton also performed the same procedure for bolted configurations even though there were no experimental data available for comparison. Thornton used the equation previously stated to design for the minimum bolt diameter and created a design procedure for the shop bolted configuration.

The maximum shear force produces a maximum couple. From equation 2.2-8:

$$M=VL^2. \tag{2.2-8}$$

Also, the stem of the tee can produce a maximum couple:

$$M = \frac{1}{4} \times F_y \times t_s \times L^2. \tag{2.2-9}$$

From Equation (2.2-8) and (2.2-9),

$$V = \frac{1}{4} \times F_y \times t_s \times L^2. \tag{2.2-10}$$

Assuming A325 bolts with an ultimate tensile strength of 90 ksi and using a bolt spacing of three inches, the maximum couple the bolts could resist that could be developed by the tee flange:

$$90 \times \frac{\pi}{4} \times d^2 \geq 3V. \tag{2.2-11}$$

Including a margin of 25 percent to account for actual yield strength exceeding specified yield strength:

$$d^2 \geq 3V \times 1.25 \times \frac{4}{\pi} \times \frac{1}{90} = 0.053V. \quad (2.2\text{-}12)$$

Thus:

$$d \geq 0.23\sqrt{V}. \quad (2.2\text{-}13)$$

The bolts must be strong enough to resist the couple that could be produced by the stem:

$$90 \times \frac{\pi}{4} \times d^2 \geq 3V = \frac{3}{4} \times F_y \times t_s. \quad (2.2\text{-}14)$$

Again adding a margin of 25 percent produces:

$$d^2 \geq \frac{3}{4} \times F_y \times t_s \times 1.25 \times \frac{4}{\pi} \times \frac{1}{4} = 0.478 \times t_s \qquad (F_y = 36\ ksi) \quad (2.2\text{-}15)$$

and

$$d^2 \geq \frac{3}{4} \times F_y \times t_s \times 1.25 \times \frac{4}{\pi} \times \frac{1}{4} = 0.663 \times t_s \qquad (F_y = 50\ ksi). \quad (2.2\text{-}16)$$

The minimum bolt diameter is determined as:

$$d \geq 0.69\sqrt{t_s} \qquad \text{(Fy=36 ksi)}, \quad (2.2\text{-}17)$$

$$d \geq 0.814\sqrt{t_s} \qquad \text{(Fy=50 ksi)}. \quad (2.2\text{-}18)$$

In Chapter 9 of the AISC Specification [2], when involving the rotational ductility Equation (2.2-17) is used. However, it would seem that the use of this limit is incorrect for the current material specification for WT shapes. Equation (2.2-18) seems to be more appropriate due to the fact that current typical yield stress is 50 ksi. The use of Equation (2.2-15) will allow for a smaller bolt diameter based on the use of material with a yield stress of 36 ksi. This discrepancy requires more research and is beyond the scope of the current project.

Using the minimum of Equation (2.2-17) or Equation (2.2-18) will give the minimum bolt diameter to ensure ductility.

Thornton includes a prescriptive design method for WT connections as follows:

1. Select a WT and determine the minimum bolt size.
2. Check that $d/t_s \geq 2$.
3. For rigid support - design shop bolts for applied shear R and moment (R)(a) at support; design field bolts for R at beam connection. The distance "a" is from the back of the tee flange to the line of bolts in the tee stem. This can be seen in Figure 2.2.1.
4. Flexible Support - Design shop bolts for applied shear R at support; design field bolts for shear R and couple (R)(a) at beam connection.
5. Perform all of the usual design checks (gross shear, net shear, etc.).

This design method can be used along with the guidance provided in the AISC Steel Construction Manual for the design of simple WT type shear connections.

2.3 Strength and Ductility Requirements for Simple Shear Connections with Shear and Axial Load by Thornton

Axial forces must be considered in combination with shear forces when designing a simple shear connection. The axial forces may be required by the applicable building code and/or due to actual forces within the connection. The addition of the axial forces reduces the rotational flexibility of the connection.

Thornton [7] focused on three types of simple connections: double angle, shear end plate, and WT connections. Thornton evaluated the effects on the ductility and strength of the connections. The limit states include those discussed by Astaneh and

Nader [5] and must also include angle leg bending and prying at the tee flange and outstanding angle leg when there is axial force present. Thornton's research investigated other limit states, but they are outside the scope of the current research. To resist these limit states, the thickness of the flange, t, must be increased or distance from tee stem to bolt line, $\tilde{b}$, decreased as seen in Figure 2.3-1. The thickness of the flange and distance from tee stem to bolt line reduce the flexibility of the connection, which in turns causes tensile stress on the upper bolts leading to possible fracture.

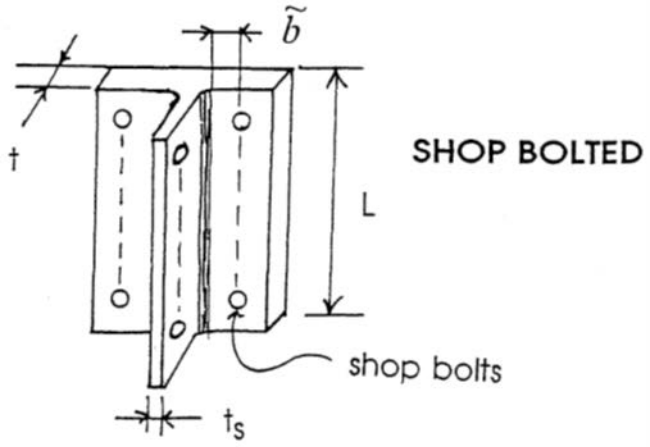

Figure 2.3-1: WT Parameters [7].

2.3.1 Ductility

Thornton [7] observes that "As the beam end rotates under gravity loads a moment will be induced by the stiffness of the tee flange. Based on yield line theory, the formula for the maximum possible moment that can be induced by the connection is as follows:"

$$M = \frac{1}{2} F_y \frac{L^2 t^2}{\tilde{b}} \left(\frac{\tilde{b}^2}{L^2} + 2 \right). \quad (2.3\text{-}1)$$

Equation (2.3-1) was deemed reasonable for predicting maximum moment based on comparisons seen by Thornton [6]. Based on that assertion, Thornton derives a number of requirements, as described below, to resist progressive failure by fracture.

For bolts subjected to tension due to connection rigidity:

$$d_{min} \geq \sqrt{\frac{5p}{2\pi}\frac{F_y}{F_{ut}}}\, t \sqrt{\frac{\eta^2+2}{\tilde{b}}}, \tag{2.3-2}$$

where

d_{min} = minimum bolt diameter (in.),

F_y = material yield strength (ksi),

F_{ut} = bolt tensile strength adjusted to gross area (ksi),

$$\eta = \frac{\tilde{b}}{L}, \tag{2.3-3}$$

p = bolt pitch (in.),

L = length of connection (in.) (from Figure 2.3-1),

$\tilde{b}$ = bending length (in.) (from Figure 2.3-1),

t = thickness of tee flange (in.).

2.3.2 Implications of the Ductility Equations for Tees

For ASTM A36 material, A325 bolts, and a pitch of three inches:

$$d_{min} \geq 0.978t \sqrt{\frac{\eta^2+2}{\tilde{b}}}. \tag{2.3-4}$$

Again, Thornton asserts that d_{min} need not exceed $0.69\sqrt{t_s}$. Similar to Thornton's previous report [7], the minimum of bolt diameter from Equation (2.3-4) and the previous limit should be used.

2.3.3 Axial Strength Design Routines

Thornton provides the following design procedure for axial capacity based on a given thickness. Thornton determines the value α', which is the ratio of the moment at the bolt line to the stem line. This provides the boundary limits to determine the axial capacity. Thus:

$$\alpha' = \frac{1}{\delta(1+\rho)}\left[\left(\frac{t_c}{t}\right)^2 - 1\right]. \tag{2.3-5}$$

$$If\ \alpha' > 1;\ T_{allow} = B\left(\frac{t}{t_c}\right)^2 (1+\delta);$$

$$If\ 0 \le \alpha' \le 1;\ T_{allow} = B\left(\frac{t}{t_c}\right)^2 (1+\delta\alpha');$$

$$If\ \alpha' < 0;\ T_{allow} = B,$$

where

$$t_c = \sqrt{\frac{8Bb'}{pF_y}}\ \text{(in.)}, \tag{2.3-6}$$

b = allowable bolt tension adjusted as required for shear interaction (kips)

$$b' = b - \frac{d}{2}, \tag{2.3-7}$$

$$b = \frac{gage - t_s}{2}, \tag{2.3-8}$$

p = bolt pitch (in.),

$$\delta = 1 - \frac{d\prime}{p}, \tag{2.3-9}$$

d’ = hole diameter (in.),

T_{allow} = allowable connection tension, per bolt (kips).

Using previous research regarding connection performance, Thornton explains that it is acceptable to use F_u in place of F_y for the design of simple connections under shear and axial forces. This allows connections to achieve their maximum rotational capacity when axial forces are present.

2.4 Simple Beam Connections in Combined Shear and Tension by Guravich and Dawe

Header angle, knife angle, single angle, and shear tab configurations were subjected to combined shear and tension as part of the Guravich and Dawe [8] investigation. The purpose of the experimental testing was to determine if a range of simple connections could develop both shear and tension, maintain structural integrity, and satisfy strength requirements for vertical and lateral load.

The specimens were rotated to 0.03 radians and had an initial shear force applied. The connections were then subjected to an increasing tensile force until failure. The test setup was designed to ensure that no additional moment was introduced after the initial rotation by applying shear as close to the connection as practical. The tensile force was applied in such a way to maintain the 0.03 radians of rotation throughout the testing. The test frame was designed to allow multiple uses of the frame, i.e., there was no damage to the support beam and column.

The knife angle connection results seem to be a valid comparison to a WT connection. As the knife angle entered into the tension zone, the heel began to separate from the column. The outstanding leg was bending about the weld along the toe of the angle, which can be seen in the yielding prevalent in the whitewash applied to the outstanding leg. The framing leg (beam leg) had less yielding due to bearing and shear. Failure occurred when cracking started in the parent metal near the end of the weld returns. The cracking continued around the tension zone corner and along the sides through the weld metal.

The limit state for all the tests using two- and three- bolt connections was weld rupture of the weld return. When the combined loads were applied, the welds had to resist bending and twisting due to in- and out-of-plate eccentricities, shear forces parallel to the weld axis, and shear force perpendicular to the weld axis. Also, the magnitude of shear load was inversely related to tension capacity for three-bolted knife angle specimens. Guravich and Dawe concluded angle thickness was a factor in tension resistance for three-bolt connection but not for the two-bolt configuration.

The results of the experimental testing resulted in significant differences in serviceability, ductility, interaction, and ultimate tension strength. It was concluded that ductility was provided through yielding due to bolt bearing, bending of angle legs, and shear yielding of the gross section. They concluded that most simple connections have the ability to carry significant amounts of tension while providing full shear capacity.

In the design recommendation the authors state, “Sufficient rotational flexibility was demonstrated by all types of connections, with the loading beam rotated 0.03 rad before shear and tension loading were initiated and this inclination maintained for the

duration of the test." [8] Guravich and Dawe stated that use of knife angle connections is unsuitable for combined shear and tension loads because prevalence of weld failure.

2.5 Behavior of Bolted Beam-Column Connection Under Catenary Action by Girhammar

Girhammar [9] researched connections' ability to withstand a sudden and unexpected load to local damage. Bolted heel connections and bolted end-plate connections were tested to study catenary action.

The test setup, seen Figure 2.5-1, uses two test frame columns, two simply supported beams, with a stub column in the center. The stub column was where the force was applied. Girhammar made a note that this center applied load is not a true representation of how the system works, but that it is irrelevant. The controlling factor is the effect of the normal force at the connection. Though, if this were a real system, the connection would have some initial rotation due to the dead load of the system and any uniform load. This initial rotation may or may not have effect on end results and needs further research.

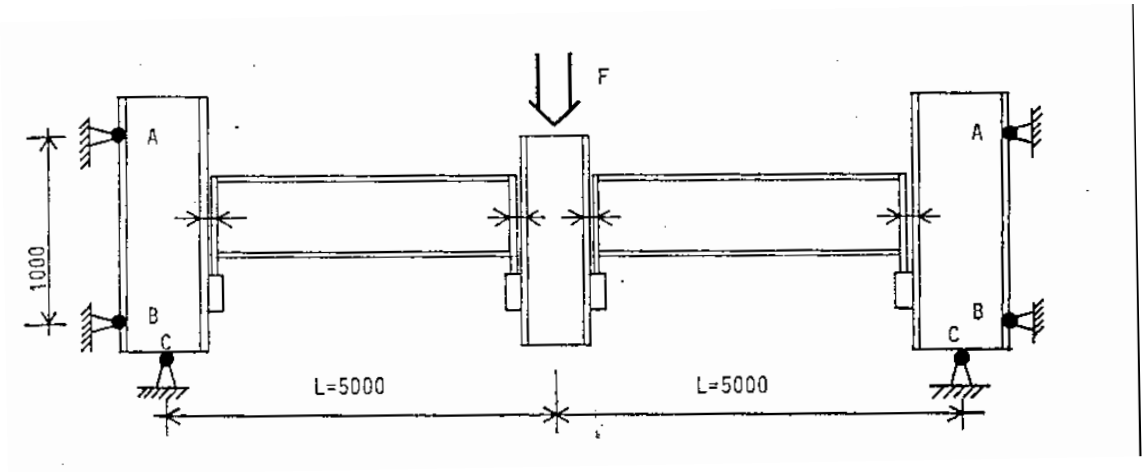

Figure 2.5-1: Girhammar Test Setup [9].

Girhammar describes that the weakest point of the structural system is the connection from the beam to column. This becomes the point of focus when local damages occurs within the beam run. He goes on to state that catenary action is the "most effective alternate load bearing system in a damaged structure in order to prevent progressive collapse." [9]

The bolted heel connection, which is considered to be "flexible", was tested first. Bolted heel connections, seen in Figure 2.5-2, are to transfer shear only through the end plate while the bolts do not transfer any load. Once local failure in the end plate occurs, then the bolts transfer the load.

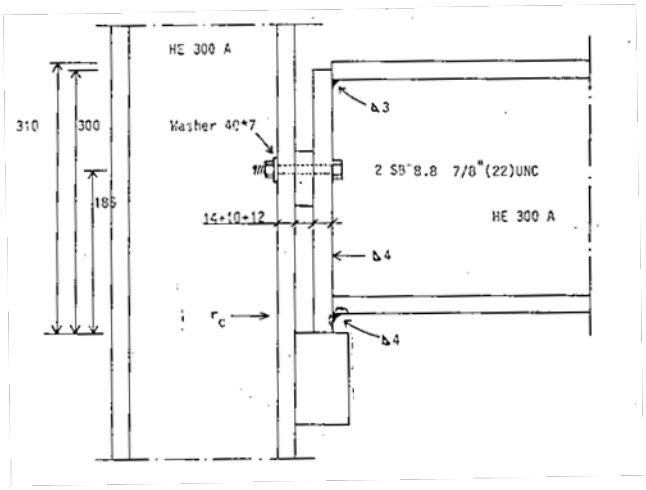

Figure 2.5-2: Flexible Bolted Heel Connection [9].

Testing the flexible bolted heel connection, a large amount of deformation occurred in the plate during the loading. Deformation continued to increase until a bolt fractured at the column stub. Girhammar noted that the bolts began to punch through the end plate. The initial amount of deflection accounts for the free movement of the beams at the connection before the bolts became engaged. The second range of deflection is

accounted for by the elastic deformation of the connection element. The final stage of deflection is due to yielding in the end plates and column flanges before failure occurred.

Girhammar set out to find the ultimate capacity of the end plate, but instead it was discovered that bolts would fail before the capacity of the plate was reached. There is one exception in Girhammar's testing, as the final bolted heel connection had bolts punch through the end plate. All other tests hold true to the graph seen in Figure 2.5-3.

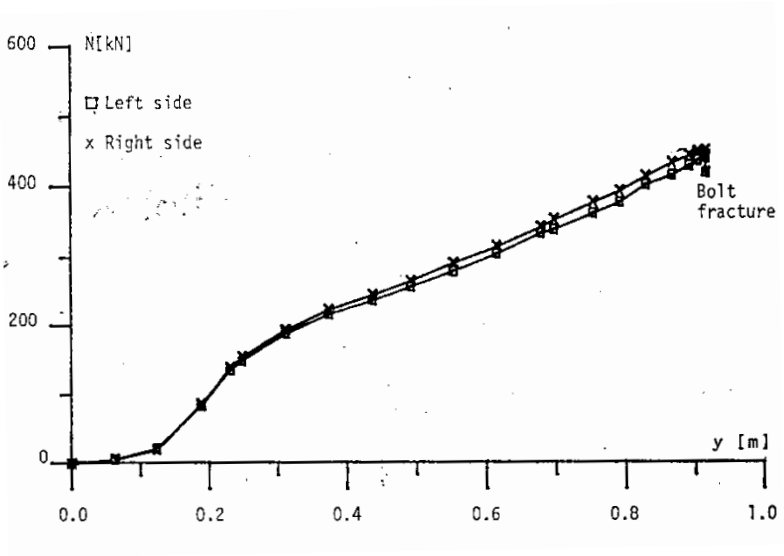

Figure 2.5-3: Bolted Heel Connection Normal Force versus Deflection [9].

From the results of experimental testing, Girhammar concluded that the ultimate load is determined by the tensile capacity of bolts and bolt punching capacity of the end plate. This is a logical conclusion because the bolted heel connection is considered "flexible," so it allows for large amounts of rotation and deformation. The bolts then become the stiffest element after local failure occurs.

The next type of connection Girhammar tested was the "semi-rigid" bolted end plate connection. This connection provides a more rigid type of connection compared to the WT connection and therefore provides an upper limit to WT experimental results.

The bolted end plate connection was designed with some moment capacity where column web buckling was the limiting factor. With this type of connection, there was not immediate collapse when a bolt fractured. There were several bolt failures before complete failure of the system. The bolted end plate connection from Girhammar's testing can be seen in Figure 2.5-4.

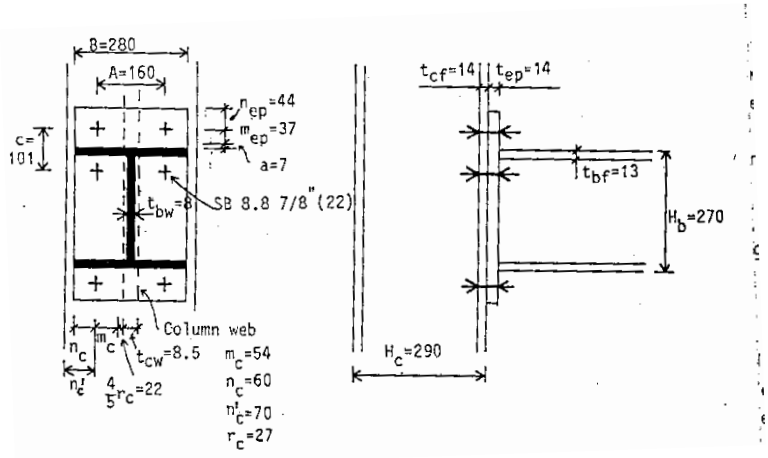

Figure 2.5-4: Bolted End Plate Connection [9].

Girhammar explains why there was not complete failure after the first bolt break. He states that as the applied force causes more deflection, the "compression bolts" become tensioned, and tensile and compressive zones of the beam switch throughout its length.

In Figure 2.5-5, it can be seen that the ultimate capacity was at three different points before collapse occurred. This proves that the rigidity of the connection allows the redistribution of the forces.

Girhammar believed that end plates were too rigid, even though they are used in standard designs. Using a thinner plate resulted in weld fracture, end plate fracture, and bolt punching. Since the end plates were thinner, they provided the connection with more flexibility, allowing for higher capacity. With an initial weld fracture, the connection dramatically decreased its capacity down to 10% of the original capacity of the thicker

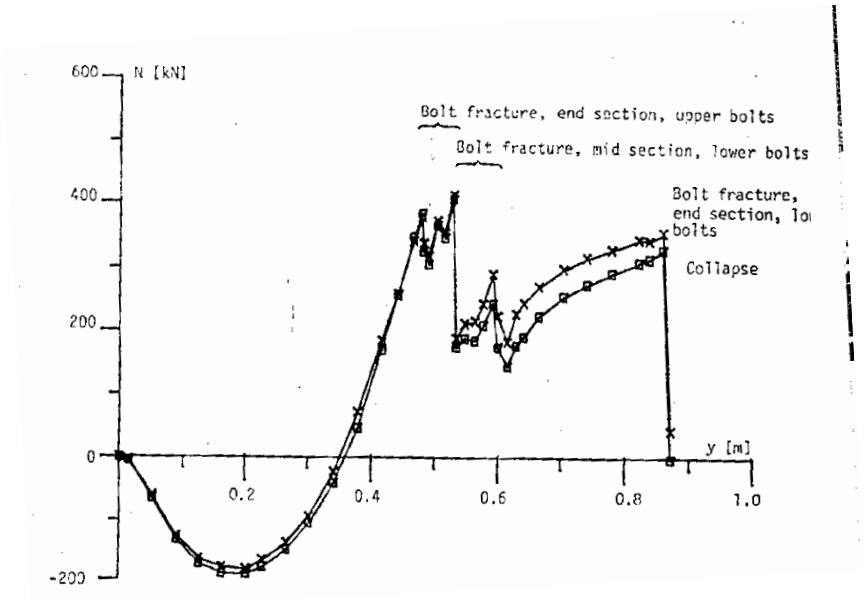

Figure 2.5-5: Thick Bolted End Plates Normal Force versus Deflection [9].

plates. After the spike downward, the system recovered and eventually reached a higher capacity than the thick end plates, seen in Figure 2.5-6.

Girhammar concluded that the ultimate load was determined by the capacity of the welds or bolt punching. He also stated that catenary action would not take place until

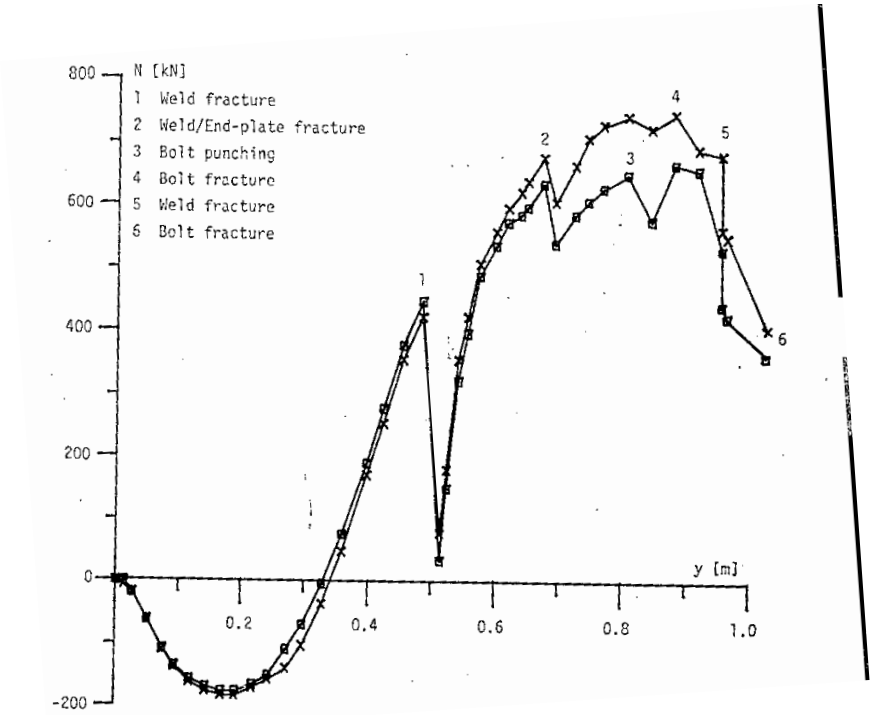

Figure 2.5-6: Thinner Bolted End Plates Normal Force versus Deflection [9].

after some failure occurred. The bolted end plate would undergo catenary action after the flexural capacity was diminished in the connection. The bolted heel connection, on the other hand, was under catenary action from the beginning.

The bolted heel connection and the bolted end plated connection created a lower and upper bound, respectively, for the WT connection. The WT will fall within the range of "flexible" and "semi-rigid" connection.

2.6 Robustness of Composite Floor Systems with Shear Connections: Modeling, Simulation, and Evaluation by Sadek, El-Tawil, and Lew

Sadek, El-Tawil, and Lew [10] investigated the behavior and failure modes of shear connections, along with the behavior and failure modes of composite floor structures during center column removal. The investigation utilized computational structural simulation with two different models. The first model is a beam-column assembly without the contribution of the floor deck, with the main focus on behavior and failure of shear connection. In the second model, the whole floor system including steel beams and their connection, columns, floor slab, and metal deck was analyzed. The first model has the most relevant information and will be the focus in this literature review.

In the model, the steel beams are connected to columns using single plate simple shear (shear tab connection), seen in Figure 2.6-1. A shear tab connection is a similar representation to that of a WT shear connection, and is a reference for comparison. The modeled system was applied to multiple computer models and analyzed because of the lack of experimental data at the time. The beam-column system had the load at the center column at a slow rate to ensure a static response. This removal of column subjected the connection to large rotation, and axial forces due to large deflection.

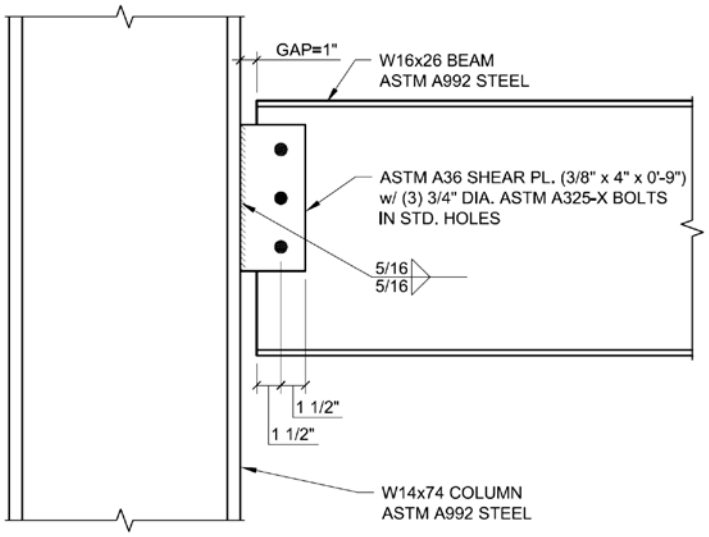

Figure 2.6-1: Shear Tab Connection (Converted to US Units) [10].

The model initially responded to the load through flexure at the connection. The flexural response occurred by transferring the moment into the top and bottom bolts of the shear tab connection. During Sadek, El-Tawil, and Lew's experimental testing, a point was reached where the flexural response changed into a cable-like behavior (catenary action), where the deflected shape of the beam is almost a straight line. This point was recorded at approximately 10 inches (254mm) of deflection at a rotation of 0.04 radians. Catenary action continued to resist the applied loading until a failure occurred. The controlling failure in this experimental testing was tear-out at the beam.

The authors stated that the shear tab and the bolts experienced substantial plastic strains, but no rupture occurred. Testing indicated that the system began to lose strength at 21 inches (533mm) displacement, which is about 0.088 radians.

In an attempt to compare results, the authors created two separate models based on studies provided in Federal Emergency Management Agency (FEMA) – 355D [11]. The first model used a set of nonlinear springs to represent the bolt with rigid members at the column and beam. A "coarse shell" was used as the second model and used a similar

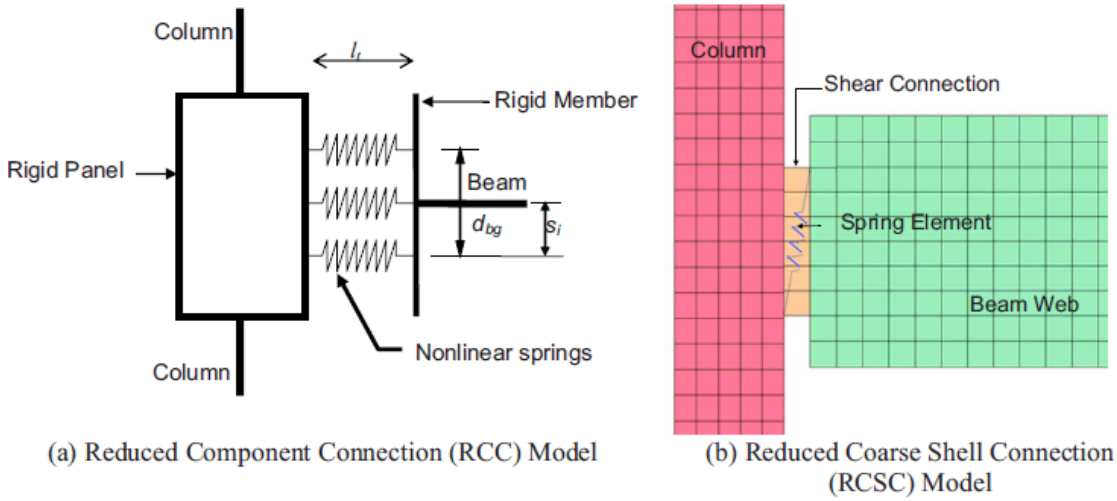

Figure 2.6-2: Shear Model Tabs [10].

spring element in place of the shear tab. These two models can be seen in Figure 2.6-2. Based on the equation and data provided from FEMA, the authors estimated that the connection would have complete failure at 0.14 radians.

When comparing the Sadek, El-Tawil, and Lew testing to the FEMA - 355D modeling results, there is a difference in rotation of 0.088 radians to 0.14 radians, respectively, at complete failure. The authors explain that the discrepancy was due to the difference in loading. FEMA had a seismic loading scenario, so the beam rotates about a center of rotation. As such, some of the bolts move towards the column and some moved

away from the column. The Sadek, El-Tawil, and Lew experimental testing had a column removal scenario and the cable forces that developed in the beam were transmitted through the bolts. This resulted in all of the bolts moving away from the column.

Sadek, El-Tawil, and Lew concluded that simple shear connections could initially resist the loading through flexural behavior and then by catenary action. Failure occurred due to increasing tensile loads from catenary action. The authors stated that even though failure was tear out of the beam web, other forms of failure are possible for alternative testing such as: fillet weld failure, bolt failure, and block shear. The maximum rotation for tear out of the beam was 0.088 radians. This rotation may vary based on the mode of failure.

2.7 Axial, Shear and Moment Interaction of WT Connections by Friedman

Friedman [12] ran experimental testing on three-, four-, and five-bolt flexible WT connections in order to investigate their inherent robustness. The WT5×22.5 were subjected to a column removal scenario. The results from this testing provided important information about how these WT can sustain large rotation while being subjected to axial tension forces.

Figure 2.7-1 is the experimental setup for testing. It can be seen that two simply supported beams were connected to a central column stub. The column stub was pulled down by a hydraulic actuator. The outputs from this experimental testing came from the strain gages located at approximately mid-span of the test beams and draw wire transducers (DWTs) connected to the top of the flanges of the central column. The test beams were connected to the test frame through a pin connection that allowed free

rotation. This setup will be replicated for the quasi-dynamic loading experimental testing in the current research initiative.

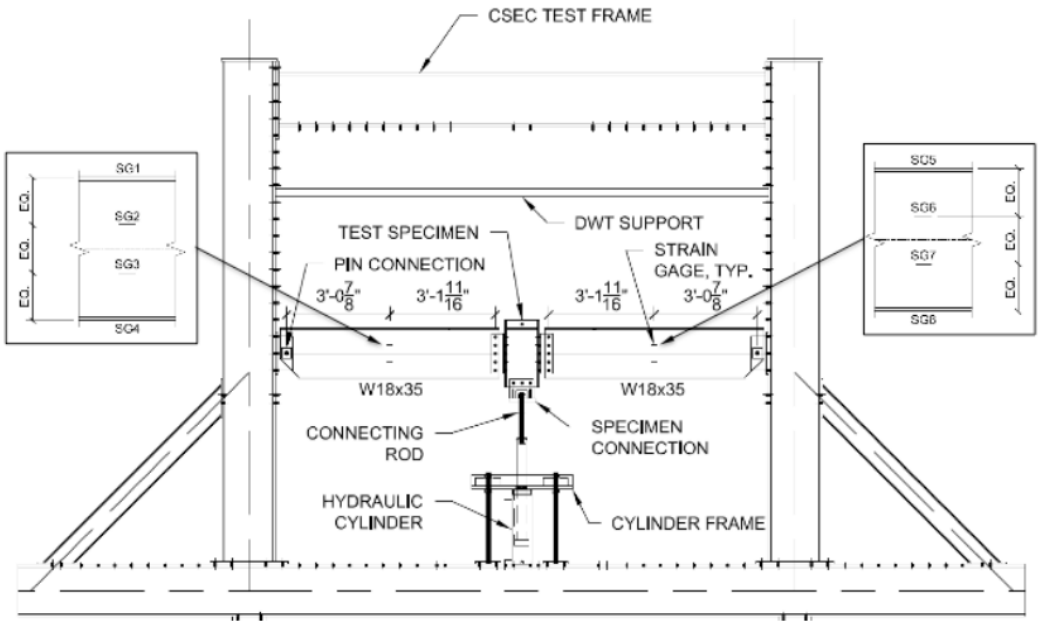

Figure 2.7-1: Fixture and Instrumental Used in Experimental Testing [12].

Friedman conducted nine experimental tests which were split evenly into the three separate bolt configurations. The strain data were used to calculate the internal axial force and moment in the W18×35 test beams. The DWTs measured the amount of displacement that occurred at the top plane of the test specimen.

Three-bolt WT specimens failed due to a bolt shear rupture at the bottom bolt of the connection. The three-bolt WT specimens also had significant bolt bearing deformation at the hole of the WT stem and minor deformation along the edge of the stem. The upper half of the connection was in compression while the lower half was in tension with rotation about the center bolt. The typical force versus rotation response can be seen in Figure 2.7-2. The flexural response of the connection was the main method of load resistance until beams rotated approximately 0.07 radians. At this rotation magnitude, the connection transitions into a catenary behavior as observed through

significant increases in axial force in the system. The axial force continues to increase until the bottom bolt fails at 0.13 radians. The maximum bending moment in 3WT ranged from 13.8-16.8 kip-ft which is 5-6% of the W18×35 beam plastic moment capacity. The rotation during the maximum moment ranged from 0.09 to 0.102 radians. The maximum axial force measured in the connections ranged from 35 to 41.4 kips. These forces were the highest at failure, at which point the rotation magnitudes of 0.125 to 0.133 radians were seen.

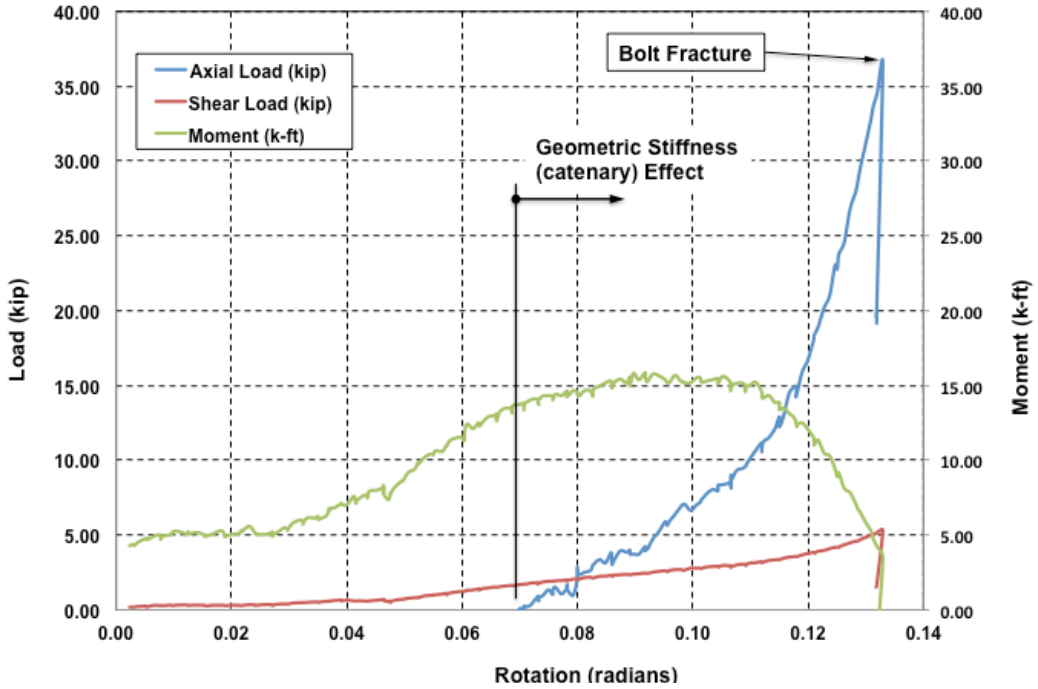

Figure 2.7-2: Typical Response of 3WT Connection (Right Beam) [12].

The four-bolt WT connection had the same bolt shear rupture limit state as the three-bolt WT connection. For two of the 4WT tests, 4WT1 and 4WT2, the specimens were loaded up to the point where one bolt fractured. The typical response for these tests can be seen in Figure 2.7-3. Test 4WT3 was loaded up to the point where two bolts fractured, which can be seen in Figure 2.7-4. The axial force at the point of the second bolt break is higher than that seen at the first bolt break. In both figures of 4WT

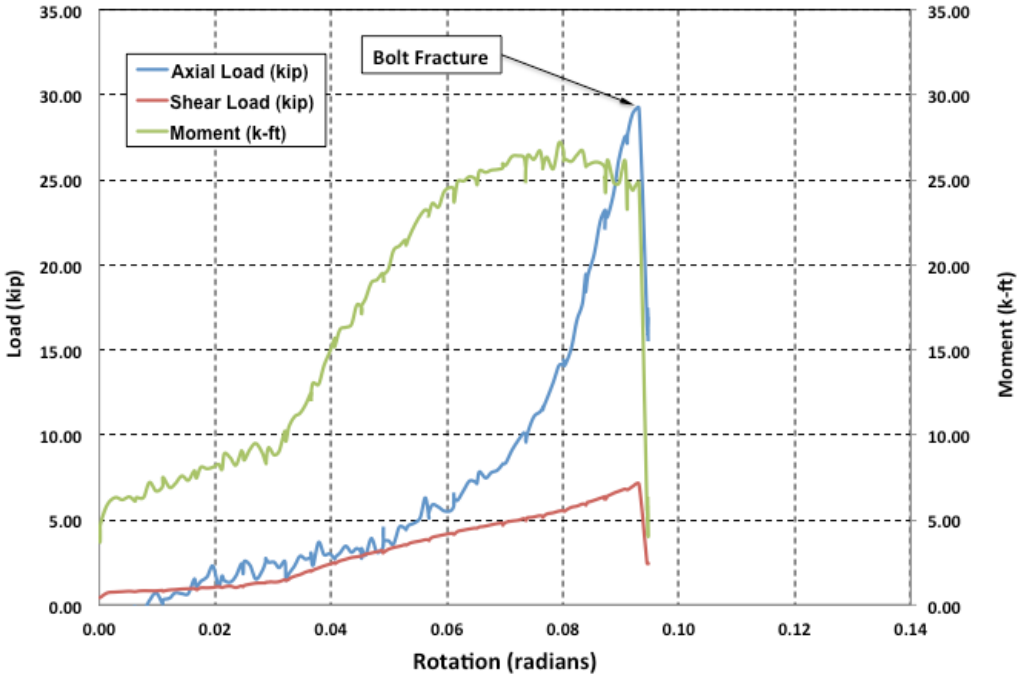

Figure 2.7-3: Typical Response for 4WT1 and 4WT2 Connection (Right Beam) [12].

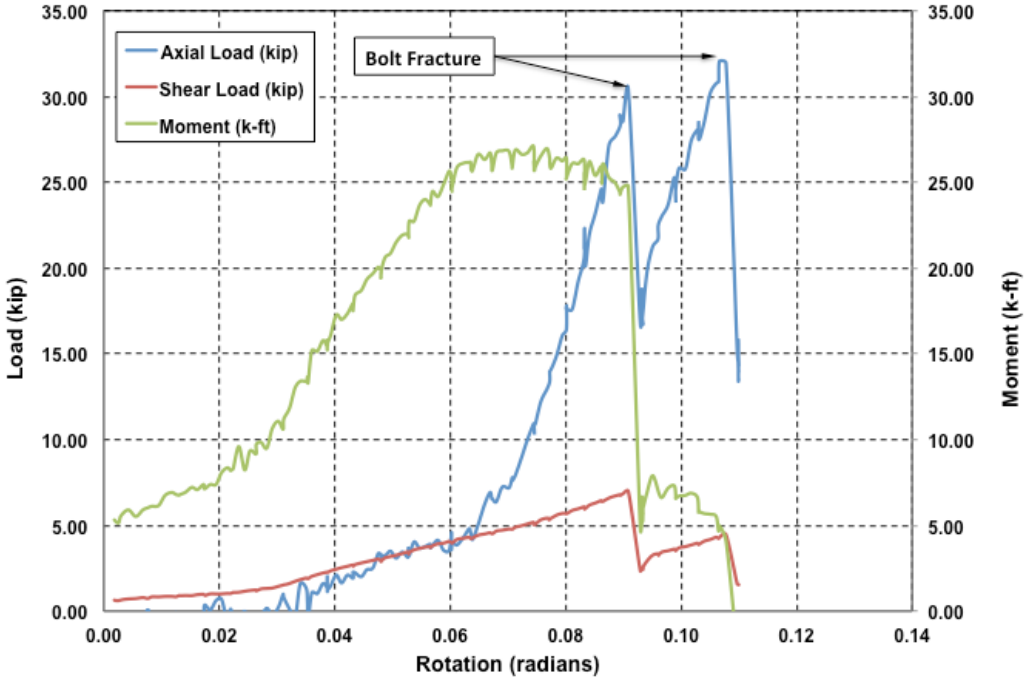

Figure 2.7-4: Response for 4WT3 Connection (Right Beam) [12].

connection, the magnitude of the bending moment is higher than what can be seen in a 3WT2 connection, which can be expected due to the additional bolt. The axial load at the point of the first bolt break is about 30 kips with about 0.09 radians in rotation. The second bolt break occurred at about 32.5 kips of axial load with about 0.11 radians of rotation.

The 5WT connection followed the same trend of having bolt shear rupture as the limiting state. The five-bolt WT connection had significantly higher moment magnitudes than three-and four- bolt WT connections, again due to the addition of a bolt in the connection. The axial loads within the connections were relatively consistent to what can be seen with the three- and four-bolt connections. Similar to the four-bolt WTs, the first and second five-bolt tests, 5WT1 and 5WT2, were terminated just after the first bolt ruptured, while the third five-bolt configuration, 5WT3, was loaded until a second bolt had failed. Figures 2.7-5 and 2.7-6 show the responses for five-bolt tests.

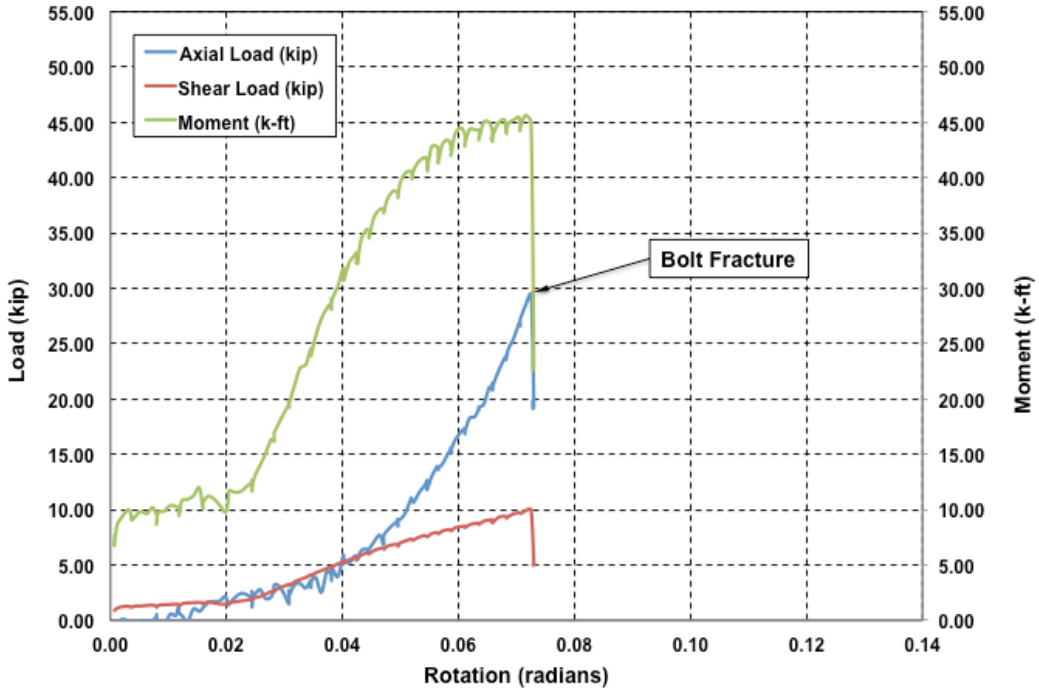

Figure 2.7-5: Typical Response for 5WT1 and 5WT2 Connection (Right Beam) [12].

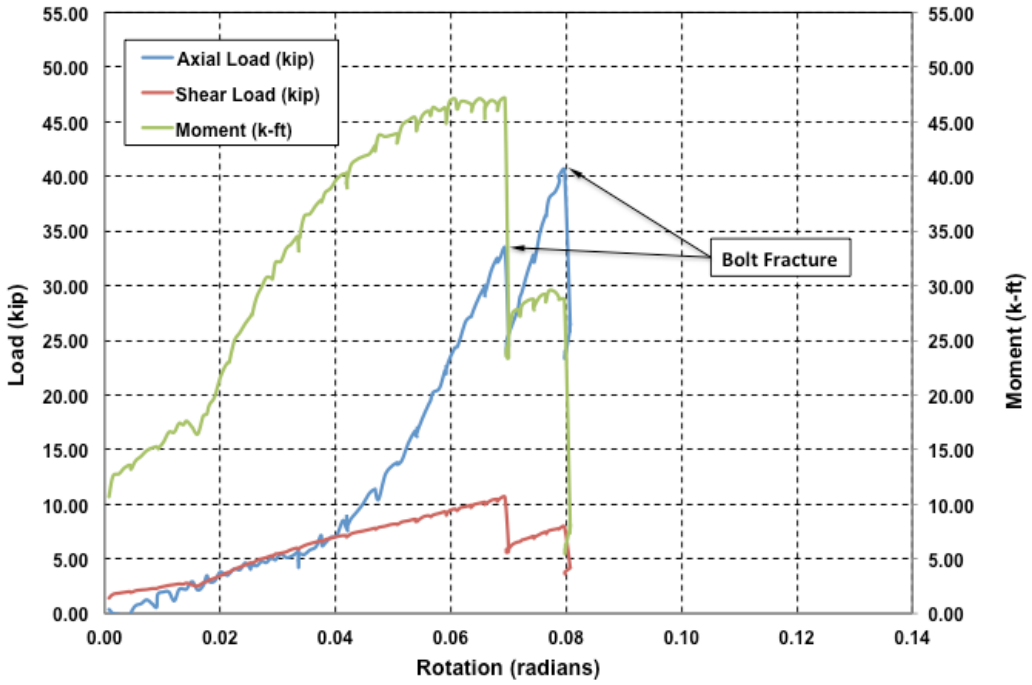

Figure 2.7-6: Response for 5WT3 Connection (Right Beam) [12].

Raebel, Foley, and Friedman [13] discussed that even though these are intended to be simple connections, they exhibited a measurable resistance to rotational and flexural demands. The catenary effects and axial forces within the beams played a role in applied load resistance in all three configurations; however, it is more pronounced in the 3WT connections because there are fewer bolts available to resist moment. In all cases, the load carrying capacity of the connection decreases after the first bolt fails. The connections had the ability to resist axial forces at the second bolt failure, but they had a significantly lower bending moment resistance.

The results of Friedman's experimental testing will be revisited often during the current research for comparison. It should be noted that Friedman's research was run in parallel with research conducted by Thompson [14]. Thompson performed similar tests using shear tab connections.

2.8 Quantifying and Enhancing the Robustness in Steel Structures by Foley, Schneeman, and Barnes

Foley, Schneeman, and Barnes [15] wrote a series of papers discussing the robustness of steel structures. The first in the series discusses the results of three-dimensional (3D) simulation of 3-,10-, and 20- story buildings exposed to compromised column scenarios and provided insights into the inherent robustness and structural integrity. The results of the 3-story building will be the focus of this literature review, because the larger buildings take multi-level force redistribution into consideration, which is not applicable to the current testing scenarios. The second paper in the series discusses methodologies for experimental testing for quantifying the catenary and membrane mechanisms.

The authors describe two procedures for evaluating progressive collapse: indirect and direct design. The indirect design approach requires that the structural system would have vertical and horizontal ties of minimum specified capacities to help engage alternative load paths. The direct design approach requires the structural engineer to explicitly create alternative load paths in the structural system and to design the members and connections for the alternative load paths.

The 3-story moment resisting frame considered by Foley, Schneeman and Barnes can be seen in Figure 2.8-1. The interior beams and girders were assumed to be connected using flexible (i.e., simple) connections, which was represented with filled-in circles at the beam ends. Beams connected with moment resisting connections are designated by a triangle at their ends. An initial critical load analysis was conducted without diaphragm stiffness which resulted in very low elastic critical load. Therefore,

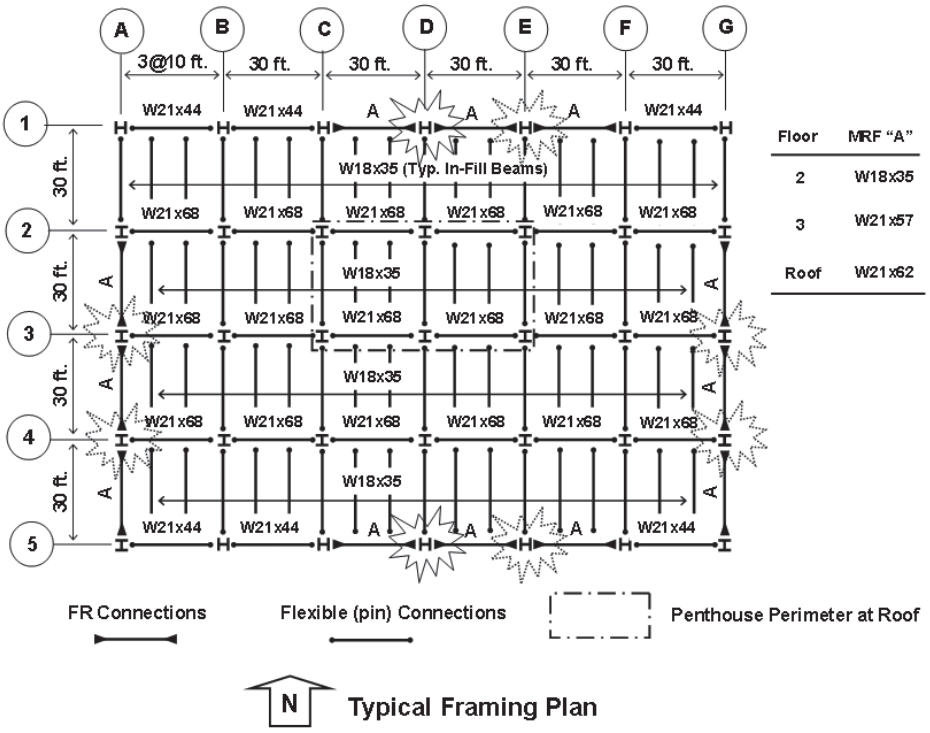

Figure 2.8-1: Typical Floor Plan for 3-Story Building [15].

massless X-bracing members were used to simulate the presence of a composite steel-concrete deck diaphragm at the floor and roof levels.

The focus of the study was to analyze the response due to removal of an external (perimeter) column at the first floor level. The first step performed was an elastic buckling analysis. The first two modes exhibited translational sway, whereas some of the other modes had high torsional buckling. An elastic dynamic analysis was performed to evaluate the effect of column loss rates and geometric nonlinearity on the response. A time history analysis was used. The gravity load and column force were applied at a 1-second interval with a 1-second pause to allow the framing system to recover from the impulse loading. When the experiment was performed, the response of the geometric nonlinearity was very similar to the linear geometric response. This was expected because the axial load compared to Euler critical load is very small. In elastic loading

analysis, the peak shear rates occurred in the columns of the framework at the top of the third story. The bending moment strain rates were comparable to the axial and shear rates.

An inelastic time-history analysis was conducted on the same model used for the elastic time-history analysis. The frame was modeled using analytical and moment hinges, which can be seen in Figure 2.8-2. The analytical hinges represented friction free pins which were modeled to conservatively simulate flexible connection behavior. Due to the previous observation that nonlinear geometric effects were negligible, a first order materially nonlinear analysis was performed. The inelastic displacement was about 50% greater than the elastic displacement. For the imposed demand of the system, a flexural hinge collapse mechanism did not form and the use of a geometrically linear analysis was

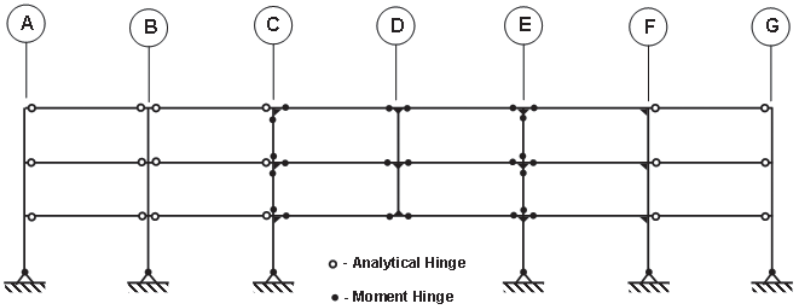

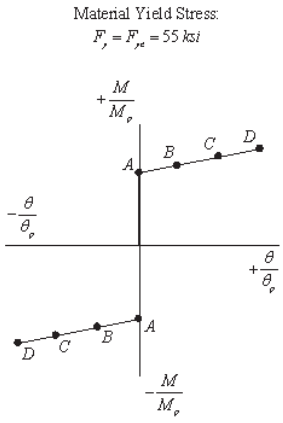

Section	Point	$\frac{M}{M_p}$	$\frac{\theta}{\theta_p}$
W18 W21	A	1.00	0
	B	1.05	8
	C	1.10	16
	D	1.15	24
W14×74	A	0.88	0
	B	0.94	8
	C	0.99	16
	D	1.04	24
W14×99	A	0.99	0
	B	1.04	8
	C	1.09	16
	D	1.14	24

Figure 2.8-2: Analytical and Moment Hinge Location and Modeling Parameters [15].

justified.

Foley, Schneeman, and Barnes reported that “During the experimental testing, the column forms the plastic hinge first and the demand in the adjacent beam is immediately capped at that moment magnitude. It is interesting that the elastic and inelastic responses dampen out to the same static bending moment capacity as required by equilibrium and yielding is temporary.” [15] In general, the peak transient bending moments seen in the members are much lower when inelastic behavior is included. The response exhibited proves that moment connections need to be designed for the full reversal of moment. The robustness in the structural steel framing system can be enhanced by designing moment-resisting connection for equal moment magnitudes in positive and negative bending.

The authors used demand-to-capacity ratio (DCR) to help quantify the extent of which the cross-section yield surface may or may not be violated. The DCR is defined as:

$$DCR = \frac{P}{P_n} + \frac{M}{M_n} + \left(\frac{V}{V_n}\right)^2. \quad (2.8\text{-}1)$$

The frame’s ability to compensate for an ineffective column and prevent disproportionate collapse is dependent on the plastic rotation demands that are placed on the connections at the ends of the beams. The plastic rotations were calculated from the displacements results taken from the inelastic time-history analysis. The girders had plastic rotation demands that were near 0.022 radians.

A major structural engineering issue that needs to be considered is the trade-off between allowing significant deflection, h, and the peak tension force, T_{max}. A free body diagram for catenary behavior can be seen in Figure 2.8-3. If the shape of the catenary is

held close to the horizontal plane (i.e., a tight rope), the catenary forces will be significantly higher. If the shape of the catenary is held close to the horizontal plane, i.e., not allowing deflection to occur, the tensile forces will become too large and make catenary action infeasible. If larger deflections were allowed, the strains will not exceed those that correspond to rupture and the tension force is reduced. More capacity is gained as the catenary is allowed to sag, but with sag comes additional strain and the rupture strain may be exceeded.

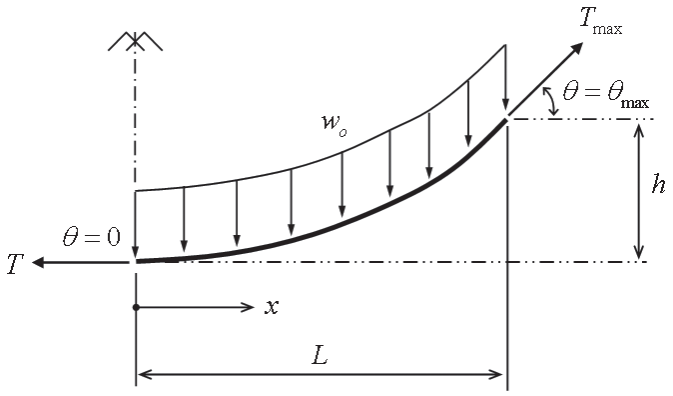

Figure 2.8-3: Free Body Diagram of Catenary Action [15].

When discussing framing connections, the authors considered a double-angle web connection. The moment, axial, and shear capacities of the connection must be found. The authors decided to use the approach of developing nonlinear tension and compression behavior for bolt elements. The bolt elements can then be assembled to form web cleats whereupon moment-rotation behavior of the connections or tension/compression response of the connection can be approximated.

A trilinear tension-deformation response for the bolt element is derived using an established procedure, though it was slightly modified. Figure 2.8-4 shows the trilinear

bolt element response, showing three characteristic points defined on the figure. Point (δ_{T1}, P_{T1}) is defined using the yield moment of the angle legs. The slope of the line from (0,0) to Point (δ_{T1}, P_{T1}), K_{T1}, is the linear elastic stiffness of the bolt elements. Point (δ_{T2}, P_{T2}) corresponds with the plastic mechanism capacity of the legs of the angle perpendicular to the beam. The stiffness K_{T2} is the post-yield mechanism. The ultimate

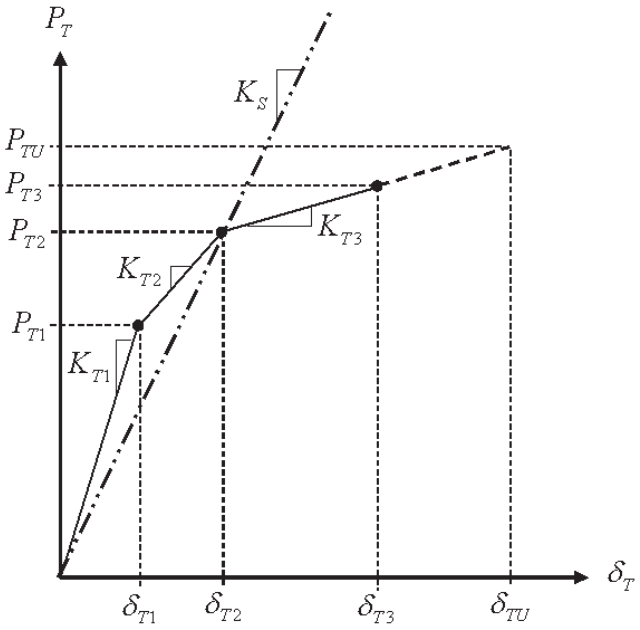

Figure 2.8-4: Double Angle Bolt Element Tension-Deformation Response [15].

loading for the bolt element was defined at Point (δ_{TU}, P_{TU}).

Point (δ_{T3}, P_{T3}) is defined through the following bolt-element limit states:

- Catenary tension fracture in the angle legs perpendicular to the beam web
- Tear-out bearing failure of the bolt in the web of the beam
- Tear-out bearing failure of the bolt in the angle
- Tension fracture of the bolts including prying action
- Tension fracture of the bolts excluding prying action
- Shear rupture of the bolts

The stiffness, K_{T3}, is defined by the deformation capacity of the bolt element.

The bolt's compression-deformation response is assumed to be bi-linear as can be seen in Figure 2.8-5. The yield Point (δ_{C1}, P_{C1}) is defined by considering three strength limit states:

- Yield in angle legs parallel to the beam web
- Yielding in the beam web
- Shear rupture of the bolts

The ultimate loading capacity of the bolt element in compression is defined through the following limit states:

- Crushing in the angle legs denoted by the ultimate stress being reached in

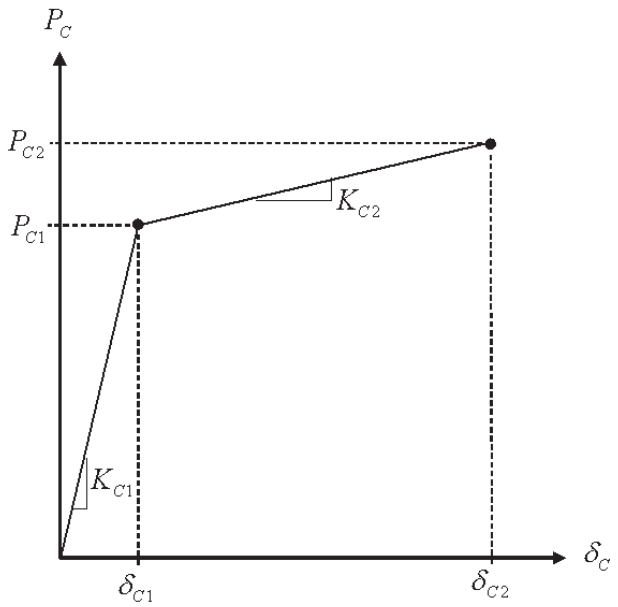

Figure 2.8-5 Bolt Element Compression-Deformation Response [15].

  the angle legs parallel to beam web
- Crushing in the beam web denoted by the ultimate stress in the beam web
- 20% increase above the ultimate bolt shear stress magnitude

The tensile capacity of the double-angle connection is determined through consideration of the following limit states:

- shear rupture of the bolts
- tension fracture of the bolts, including prying action
- block shear rupture in the angle legs parallel to the beam web
- block shear rupture in the beam web
- bearing tear out failure in the angle legs parallel to the beam web
- bearing tear out failure in the beam web
- catenary tension-rupture in the angle legs perpendicular to the beam web

The bolt's element tension- and compression-deformation response parameters were used to determine the pure moment capacity of the double-angle web connection. The controlling state deformation, δ_4, in the extreme tension angle or extreme compression angle, δ_1, was assumed. The connection rotation angle, θ, was then varied until the summation of all forces determined using the bolt element response curves is zero. Figure 2.8-6 demonstrates the procedure that was previously described.

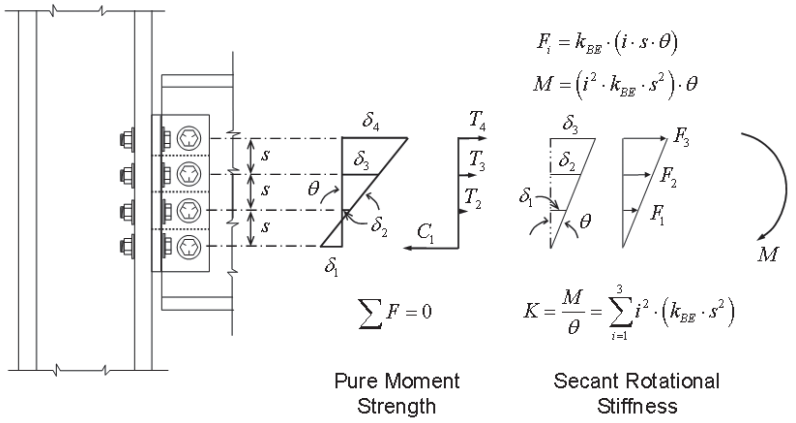

Figure 2.8-6: Schematic Illustration for Calculating Pure Moment [15].

2.9 Application of Seismic Steel Connection Experiments to Column Removal Scenario by Daneshvar and Driver

Daneshvar and Driver [16] make comparisons to seismic-type loading and progressive collapse. They first start by using the ASCE 7-05 definition of progressive collapse, which is "the spread of an initial local failure from element to element, eventually resulting in the collapse of an entire structure or a disproportionately large part of it." There are two conditions that are required for progressive collapse; one being an external cause such as abnormal loading to initiate damage and the other being inadequate structural continuity, redundancy, and ductility.

The authors discuss the previous research of identifying two causes of progressive collapse of a steel frames: material failure and inability to sustain large deformation. Connection failure is another type of failure that could lead to progressive collapse. Since there are no published standards or protocols on how to experimentally test connections under the column removal scenarios, it is obvious that more work needs to be done. Table 2.9-1 summarizes the experimental tests performed up to the time that the

Table 2.9-1: Column Removal Scenarios Test on Steel Connections [16].

No	Test Description Summary	Organisation	Reference
1	Behaviour of bolted beam-to-column connections under catenary action in damaged steel structures	Swedish Council for Building Research	(Girhammar 1980)
2	Performance of seismic moment resisting connections under column removal scenario	National Institute of Standards and Technology	(Sadek 2008)
3	Recommended performance levels for alternate path analysis of blast-damaged steel connections	Protection Engineering Consultants	(Marchand 2008)
4	Axial, shear and moment interaction of WT connections	Milwaukee School of Engineering	(Friedman 2009)
5	Axial, shear and moment interaction of single plate shear tab connections	Milwaukee School of Engineering	(Thompson 2009)

paper was published.

Beam-to-column joint deformation is complicated due to local distortion giving rise to material and geometric nonlinearities. Figure 2.9-1 shows typical moment-rotation curves of different types of connections. A large effort has been made to determine the behavior of the actual flexibility of the connection. When analytically modeling a connection for a progressive collapse scenario, rotational and axial springs

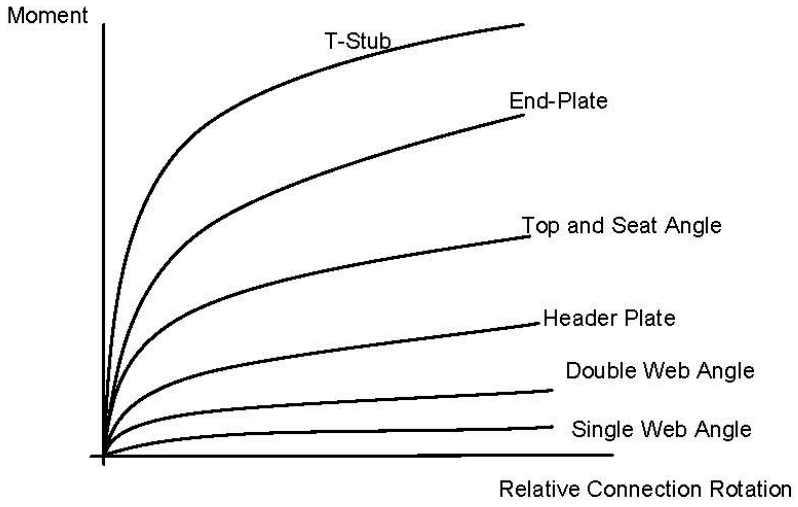

Figure 2.9-1: Typical Moment-Rotation Curves for Steel Connections [16].

should be used. The rotational spring will account for flexural capacity, while axial springs will help determine the effects of catenary action. The mechanics by which a moment-resisting frame shifts from a flexural-dominant system to a catenary-dominant system is unclear. It is clear that catenary action is a key difference between seismic connection performance and the performance of the connection in a progressive collapse scenario. A summary of key differences can be seen in Table 2.9-2.

Table 2.9-2: Key Difference Between Seismic Scenario and Progressive Collapse [16].

	Seismic Scenario	Progressive collapse Scenario
Catenary Action	Not important	Important
Type of Loading	Cyclic	Monotonic
Tension and Moment Interaction	Not important	Important
Effect of Slab	Can be Important	Need more research
Effect of Panel Zone	Can be Important	Need more research
Evaluation Parameter	Drift Angle	Chord rotation

2.10 Progressive Collapse Resistance of Steel-Concrete Composite Floor by Alashker, El-Tawil, and Sadek

Alashker, El-Tawil, and Sadek [17] performed computational simulation models of steel-concrete composite floors in which steel beams are attached to columns through shear tabs. The key parameters during this study were the deck thickness, steel reinforcement, and number of bolts in the shear tabs connections. Also discussed was the dynamic impact factor, which is widely used to account for dynamic effects within a statically modeled framework.

When modeling the shear tabs, a single row of shell elements with a thickness equal to the beam web was used. The stress-strain characteristics of these shell elements are derived from the bolt strength and deformation capacity. The first method used to load the system pushed down on the center column stub in a displacement control mode at a controlled rate. This method was called concentrated load displacement control (CL-DC). The second method applied a uniform distributed load to the entire slab and incrementally varied the load in force control mode over a period of 2.5 seconds. This method was called uniform load-force control (UL-FC).

During all the CL-DC simulations a failure in shear tab was observed. A number of simulations were then performed to see how the effects of adding extra bolts would affect the capacity of the system. The results can be seen in Figure 2.10-1. The five-bolt configuration had approximately 40% more applied load resistance than the three-bolt configuration.

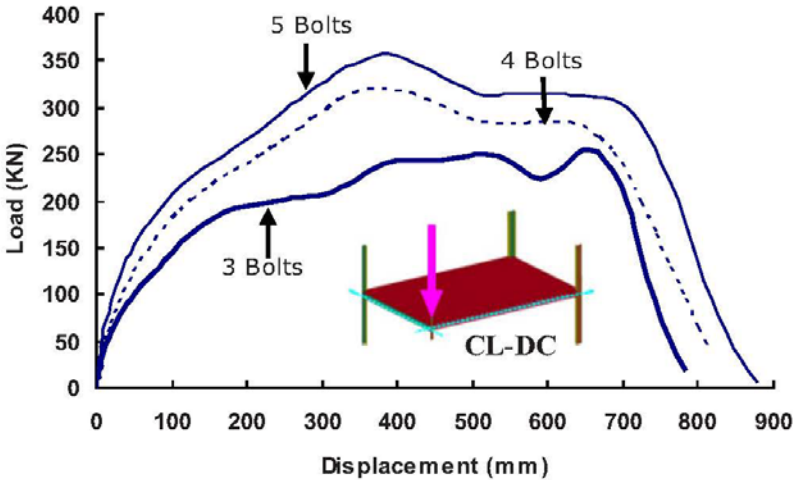

Figure 2.10-1: Concentrated Load Displacement Control Results [17].

Unlike CL-DC, the UL-FC did not show that increasing the number of bolts affected the load capacity as much. The results of increasing the number of bolts during UL-FC can be seen in Figure 2.10-2.

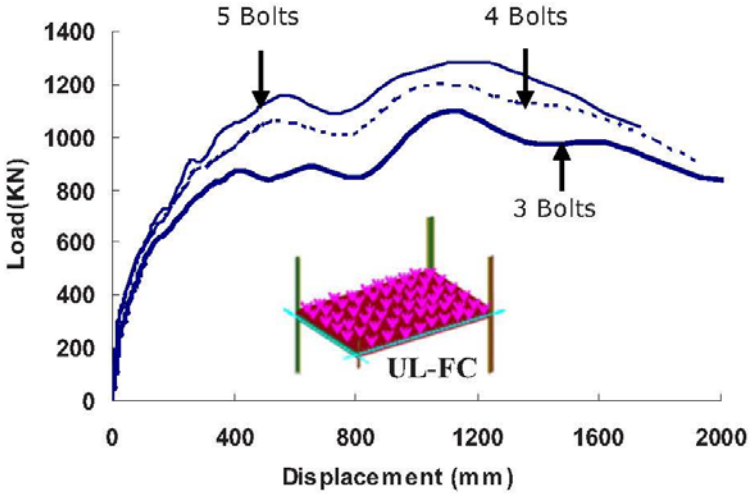

Figure 2.10-2: Uniform Load Force Control Results [17].

Another key focus during this simulation was the effect of using dynamic impact factor (DIF). Typically, a DIF of 2.0 (assuming linear structural behavior) is used to account for the dynamic effects associated with sudden placement or removal of loads in the U.S. General Service Administration guidelines. It is clear how conservative this value can be because this value does not account for the system's inelastic behavior. The dynamic impact factor was found to be 1.29 in this study for the floor system considered, a value substantially lower than the GSA's recommendation of 2.0. This result contributed to the authors' discussion of how to determine the appropriate DIF. "The appropriate value of the DIF depends on the ductility and amount of inelastic action the structure would experience during column removal scenario." [17].

2.11 An Approach to Testing the Performance of Steel Connections Subjected to Extreme Loading Scenarios by Oosterhof and Driver

Oosterhof and Driver [18] describe the design of experimental testing programs to focus on shear connection performance under extreme loading, including how to simplify the testing programs in order to more carefully examine the strength and ductility demands under column removal scenarios.

The authors first looked at Timoshenko free-body diagrams seen in Figure 2.11-1 through Figure 2.11-3. The shear force and tensile force were taken as vertical and horizontal, respectively, rather than perpendicular and parallel to the axis of beam rotation. Timoshenko's three-hinged beam can be modified to consider the rotational and axial stiffness of connections. The contribution of the moment resistance of certain types of shear connections through large rotation is expected to be significant. From this, the following equilibrium equations were developed:

$$V_4 = \frac{P}{2} = T \tan\theta_c + \frac{2M}{L}, \tag{2.11-1}$$

and for uniform loading,

$$V_5 = \omega L = 2\left[T \tan\theta_c + \frac{2M}{L}\right]. \tag{2.11-2}$$

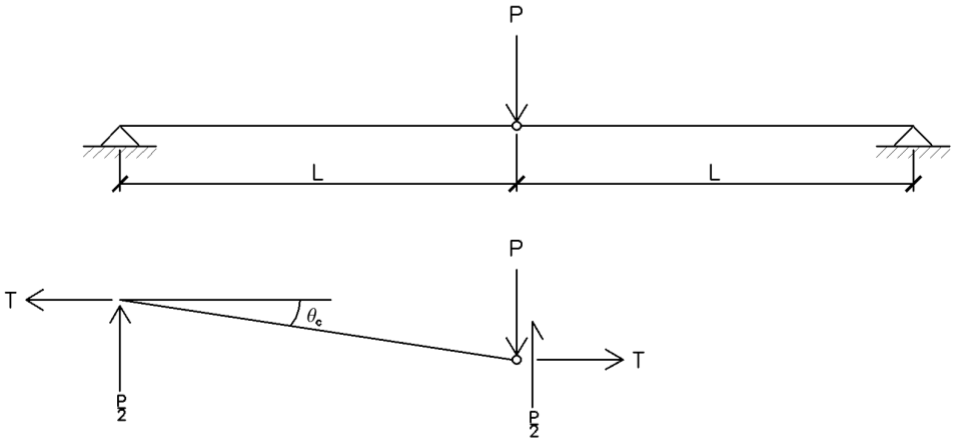

Figure 2.11-1: Three-Hinged Beam (after Timoshenko) [18].

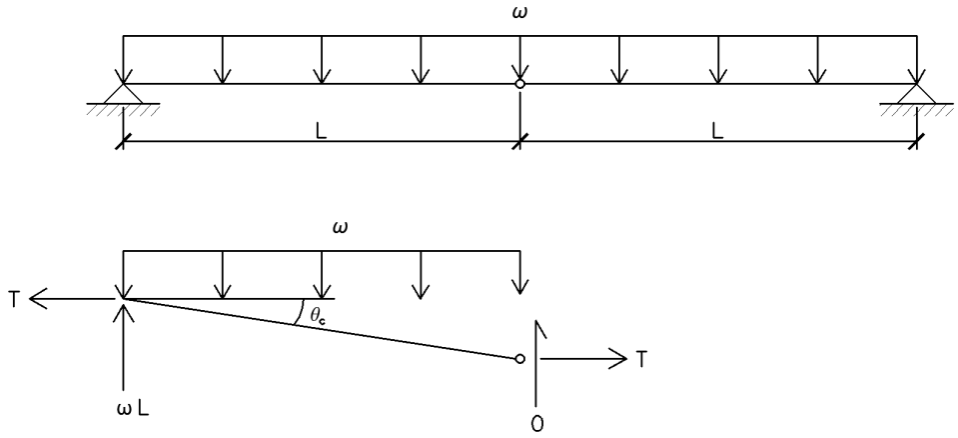

Figure 2.11-2: Three-Hinged Beam Under Uniformly Distributed Load [18].

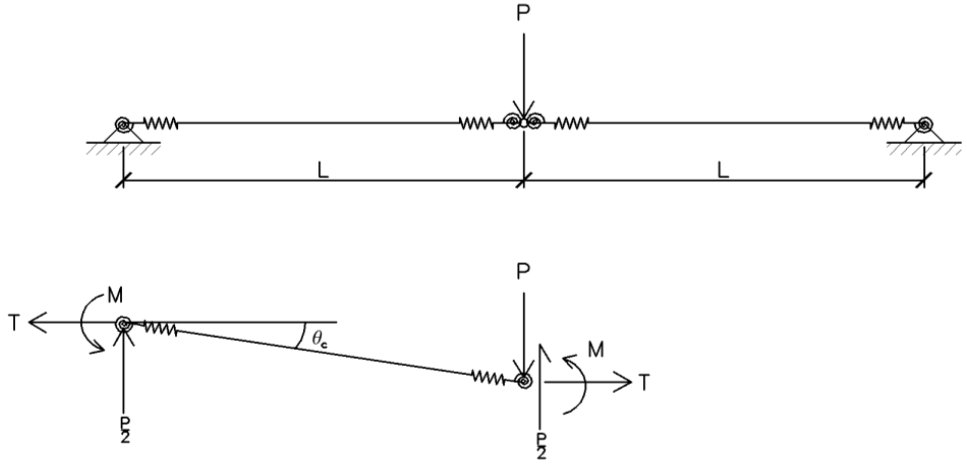

Figure 2.11-3: Modified Three-Hinged Beam with Connections Represented by Springs [18].

This was achieved by adding rotational and axial springs at each connection. Oosterhof and Driver expect that the stiffness of axial springs is quite complex due to material plasticity, deformation behavior, and the interaction among forces.

The authors then discuss the correct load history. The three histories represent the cases of a central point load, a uniformly distributed load for the connection at the removed column, and a uniformly distributed load for the connection at the remaining column. These load histories test the realistic combination of strength with ductility demands.

A load application procedure was prescribed using incremental load steps to each of the actuators shown in Figure 2.11-4. "First, Actuator 2 must be displacement-controlled, applying an incremental rotation to the system at each finite load step. Actuator 3 must also be displacement-controlled and the axial displacement to be applied is calculated using the measured rotation at the current load step. Finally, having applied controlled displacement using Actuators 2 and 3, the forces in these actuators can be measured and the equilibrium state being considered can be achieved by using Actuator 1 with force control." [18]

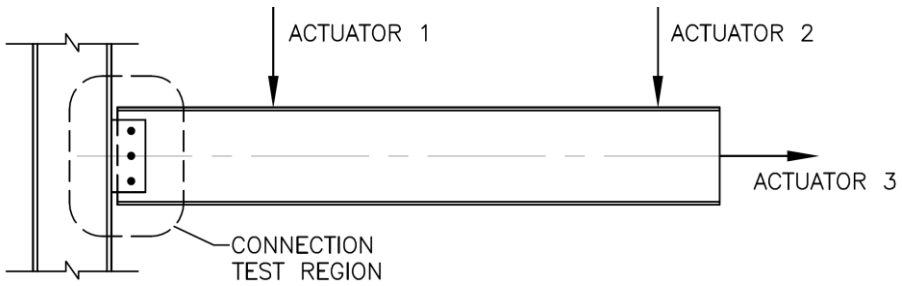

Figure 2.11-4: Schematic of Test Setup [18].

The authors created predicted plots for axial, shear, and moment versus rotation. These predicted plots were compared to Thompson's [14] experimental data as seen in Figure 2.11-5. Where the predicted plots strongly differ is that Oosterhof and Driver predicted a quick accrual of moment whereas Thompson's experimental data lag in moment development.

The authors suggest that more research needs to be performed based on the procedures discussed in their paper.

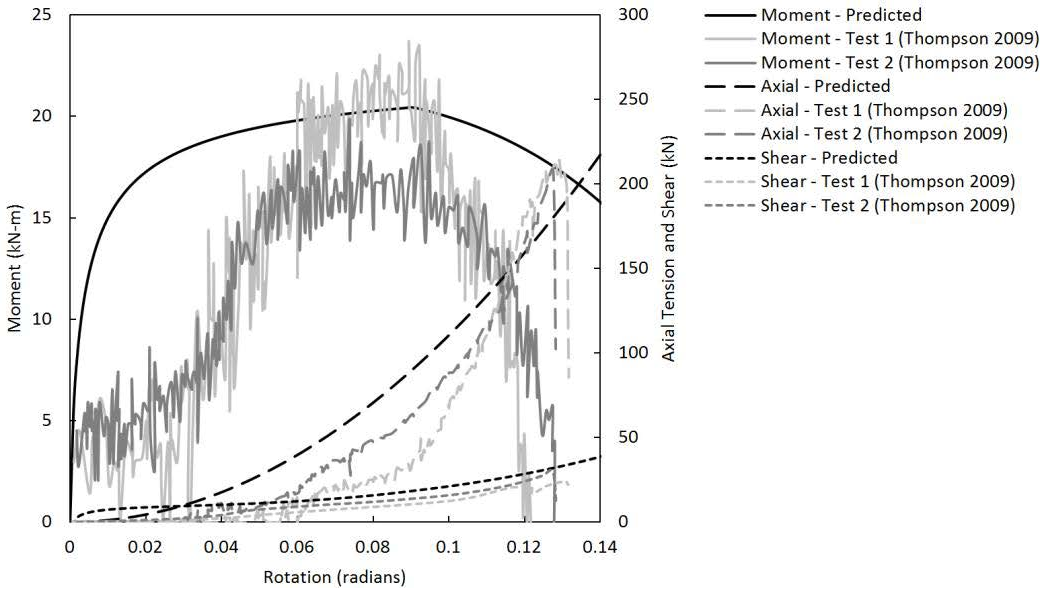

Figure 2.11-5: Predicted Load History And Physical Test Results For Shear Tab Connection [18].

2.12 Integrity of Steel Single Plate Shear Connections Subjected to Simulated Column Removal by Weigand and Berman

Weigand and Berman [19] experimentally tested the resistance of steel gravity connection subassemblages subjected to loading consistent with the removal of an interior column. An approach to determine the deformation of fibers was used to discretize the connection. This discretization was used to determine the fiber displacements at connection failure.

The experimental testing had two focuses. The first was the connection subassemblage testing conducted at University of Washington which is described in this paper. The second was the large-scale floor system testing at the University of Illinois at Urbana-Champaign and composite concrete slab on metal deck component testing at Purdue University. This paper focuses on the experimental evaluation of the response of gravity connections subjected to combined tension, shear, and flexural loading consistent with an interior column losing its vertical load carrying capacity.

The typical single shear plate subassemblage consisted of a 5-ft. – 0-in. W12×72 column stub connected to two W21×50 beams through shear plate connections. Two subassemblages used a different beam and column stub configuration, using a W14×90 column stub that was connected to two W18×35 beams. The varied connection parameters included the number of bolts, bolt diameter, ASTM bolt grade, plate thickness, horizontal plate edge distance, hole type, eccentricity with respect to the beam and simulated system span. The connection subassemblage and test setup can be seen in

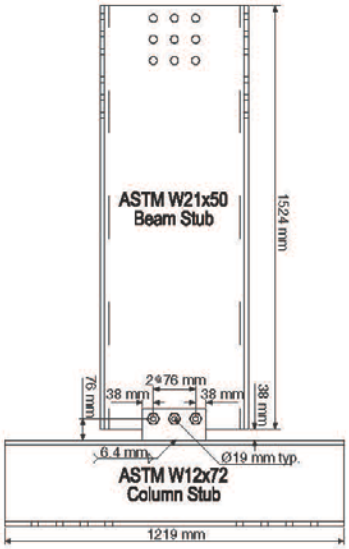

Figure 2.12-1: Typical Shear Tab [19].

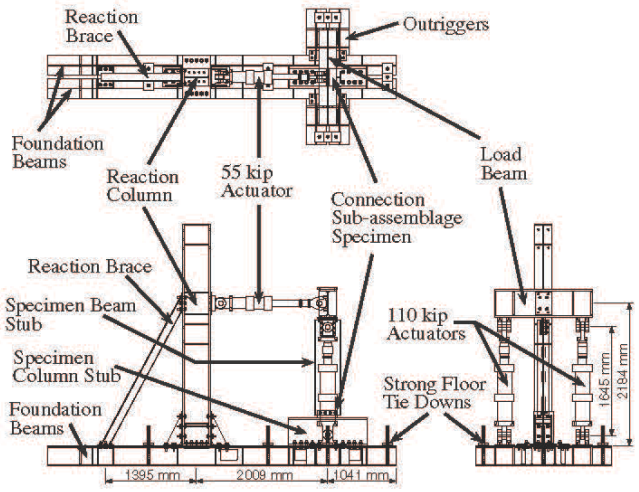

Figure 2.12-2: Connection Subassemblage Test Setup [19].

Figure 2.12-1 and 2.12-2, respectively. These subassemblages were quasi-dynamically loaded by three independent actuators.

Fiber models are often used to capture the complex behaviors of fasteners and connected element deformations in steel connections. “A connection fiber model is a simplified analytical construct that lumps connection constitutive behaviors into a discrete arrangement of axial nonlinear springs (fibers), which have fully prescribed strength and stiffness characteristics” [19]. Figure 2.12-3 shows a free body diagram of the connection. Each fiber isolates a characteristic of the connection, such as the bolt, weld, plate, or beam web. Interaction between these components is simulated by analytically placing a component spring either parallel or in series as appropriate.

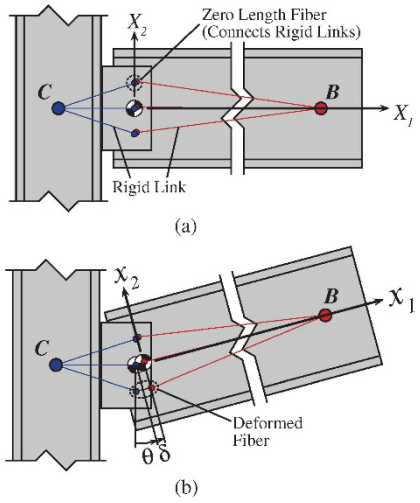

Figure 2:12-3: (a) Undeformed Configuration of Fibers; (b) Deformed Configuration of Fibers [19].

The authors observed that shear plate connections underwent four distinct phases of behavior. During Phase I, the connection resists rotation due to frictional forces developed from the pretension in the bolts. Phase II occurs after the bolts have slipped and the connection rotates without much additional accumulation in vertical force. Phase III is where the outer-most bolts begin to bear on the through-thickness faces of the shear plate and beam web. Most of the elongation of the bolt holes occurred during this

phase. Finally, Phase IV begins at the initial failure of the connection. Failure typically meant bolt fracture or rupture and subsequent tear-out of the shear plate. These phases

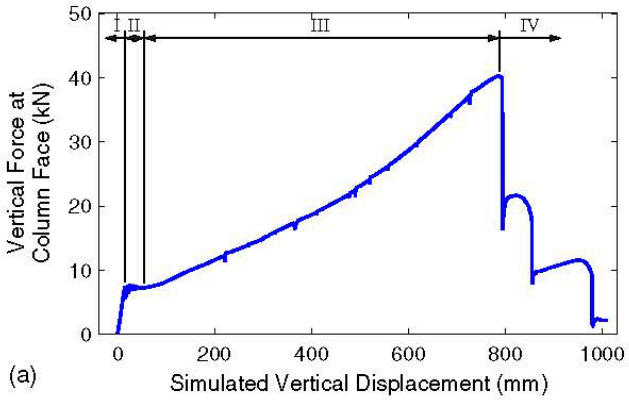

Figure 2.12-4: Phases of the Connection During Experimental Testing With STD Holes [19].

can be seen on the vertical force versus vertical displacement plot in Figure 2.12-4.

Weigand and Berman summarized their results into a couple of key points. Single shear connections failed by sequential shearing of the bolts or by tear-out of the plate. Bolt shear capacity was adversely impacted by the inclusion of bolt threads in the shear plane. The connection force-deformation and fiber displacement response was highly dependent on the system span. Single shear connections provided approximately 15% to 25% of the LRFD specified design strength under the simulated column removal scenario.

2.13 Robustness of Steel Gravity Frame Systems with Single-Plate Shear Connections by Main and Sadek

Main and Sadek [20] first discuss that the commentary of ASCE 7-10 [21] includes the two basic approaches for analyzing progressive collapse: direct design and indirect design. Foley *et al.* [15] also stated this fact and described how the methods were used. ACI [3] and IBC [4] also integrated a minimum structural integrity

requirement into their provisions. However, these minimum structural integrity requirements were based mainly on engineering judgment and the enhancements presented to resist disproportionate collapse are not well defined. Recent studies have been conducted to better understand the performance of steel framing systems during a sudden collapse. Through previous studies, much research assumed a gradual softening in post-ultimate response of the shear tab due to tear-out failure of the bolts through the beam web. However, studies by Thompson [14] and Weigand and Berman [19] exhibited sudden fracture through either bolt shear rupture or brittle rupture of the plate. Main and Sadek created two finite element models and compared the results to the experimental work done by Thompson.

Main and Sadek created a two-span assembly with a "push-down" loading on an unsupported center column. This test setup is similar to that used by Friedman [12] and Thompson [14] during their experimental programs. This configuration subjects the column to a combination of vertical shear, bending moment, and axial tension. Based on this setup, Main and Sadek created two types of finite element models, a detailed and reduced model.

The detailed modeling approach used finely meshed solid elements to represent the beam, shear tab, and bolts. Contact was defined between the bolts and the shear tab and the beam web to model the transfer of forces through the bolted connection, including friction and bolt bearing. Hand calculations prove that the weld failure was not the governing limiting state; therefore, the end nodes of shear tab were rigidly constrained to nodes of the column web. To model the material properties, a piecewise linear plasticity model was used. Material properties were based on well researched

experimental data. The properties were then run though a simulation to verify their accuracy.

The second type of finite element model used was a reduced model approach. This modeling approach used a nonlinear spring for each bolt row in the connection. The nonlinear spring represented the combined effects of bolt shear and bearing-induced deformation. "Each nonlinear spring element has distinct load-deformation curves to represent yielding and failure (1) along the beam axis and (2) in the vertical direction" [20]. The load-deformation behavior of the axial discrete beam elements captured the interaction of bending moment and axial forces of the connection, while the load-deformation behavior in the vertical direction captured the vertical shear. The axial load-deformation relationship used for the nonlinear springs was based on research by Sadek and Main [10]. Just like the detailed model, all material and component properties were based on well researched data and the accuracy of the properties were confirmed during modeling.

Main and Sadek then modeled Thompson's setup using the detailed and reduced modeling methodologies. Half of the setup was modeled using appropriate boundary conditions at the plane of symmetry. The detailed finite element model can be seen in Figure 2.13-1. The beam span between connections, where stresses remain in the elastic

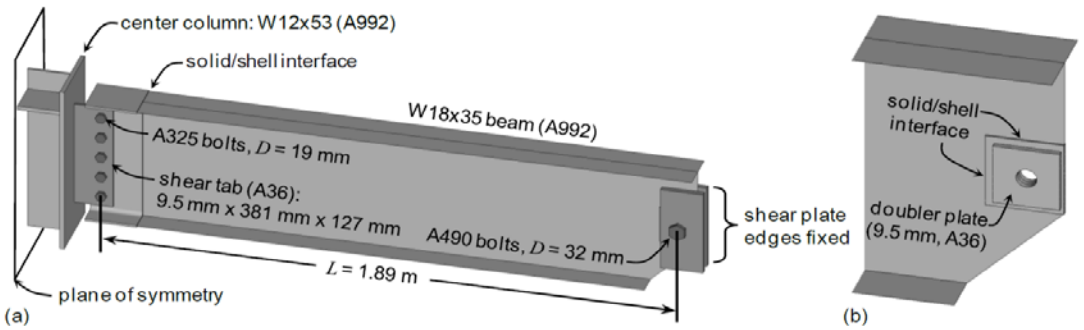

Figure 2.13-1: Detailed Model of Two-Span Assembly (a) Overview (b) Region Near Exterior Pin [20].

range, was modeled using shell elements, with nodal constraints linking the degrees of freedom of the solid and shell elements at their interface. A 1/16 in. gap was placed between the bolt and the bolt hole, as was present in the real system for a standard bolt hole. This gap was represented accurately in the solid element mesh, with the bolts initially centered in the holes, allowing some slippage before bolt bearing is engaged.

Figure 2.13-2 shows the reduced model of the assembly with five bolts per shear connection using beam elements beams and columns, nonlinear springs for each bolt row of the shear connection and rigid links to maintain proper connection geometry. The initial deformation prior to load accrual, as seen in Figure 2.13-3, represents the initial engagement of the bolts within the holes due to the gaps between the bolt shank and the standard size bolt holes. This allowed some slippage to occur before the bolt began bearing on the plate. These gaps were only included in the axial load-deformation relationship for the bolt springs. A gap element was also added to the exterior pin support.

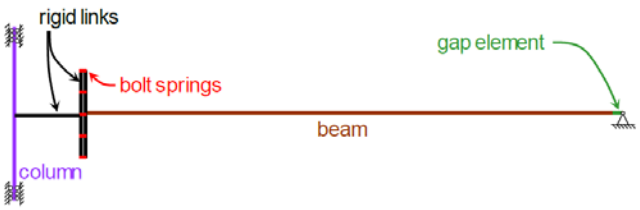

Figure 2.13-2: Reduced Model of Two-Span Assembly [20].

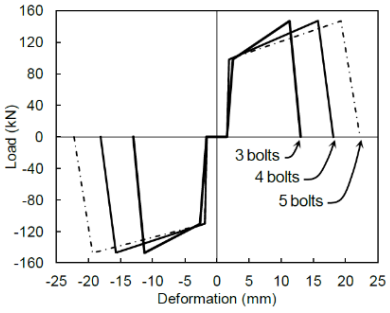

Figure 2.13-3: Load-Displacement Curve Used For Bolts [20].

Figure 2.13-4 shows the comparisons of Thompson's experimental results with Main and Sadek's detailed and reduced model computation of a) the vertical force, P, and b) the beam axial force, T, versus the vertical displacement of center column. T is the average axial force in the two beam spans. The numbered lines are from Thompson's

experimental results. These graphs show fairly good correspondence between the computational predictions and the experimental data. The detailed model predictions were within 15% of the measured mean of the vertical load. The reduced model predictions were within 21%. The axial load predictions for the detailed model underestimated P_u, while the reduced model overestimated the P_u by 10.6% in one case. The large discrepancy that can be seen in the rotation is due to points of measurement. Main and Sadek used the centerline to centerline of the bolts for their length, while Thompson used the span length from the exterior pin support to the face of the center column. The detailed and reduced models were able to capture the connection slippage in both vertical and axial forces, the flexural action, and catenary action.

The detailed model computations showed that plastic deformation were concentrated in the bolts and in bearing-induced deformation around the bolt holes. The remainder of the beam remained in the elastic range and essentially rotated as a rigid body.

The detailed and reduced models predicted that bolt shear fracture would be the failure mode in all cases; however, other limit states were seen in Thompson's experimental results. The closeness of the calculated capacities for bolt shear failure and plate bearing failure helps explain this observed variation in limit states.

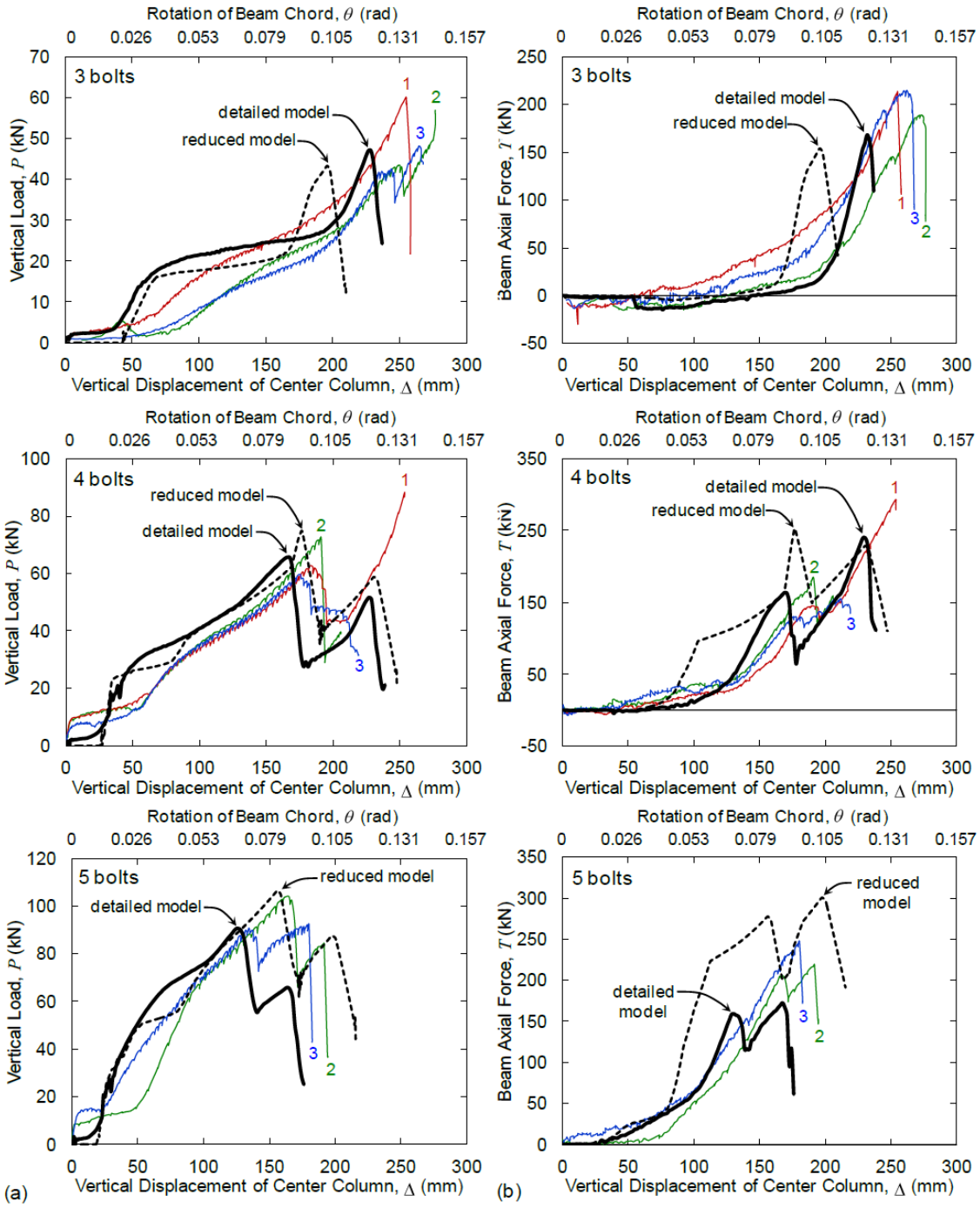

Figure 2.13-4: Comparison of Detailed and Reduced Model Results with Experimental Measurements [for Two-Span Beam Assemblies: (a) Vertical Load and (b) Axial Force Versus Vertical Column Displacement] [14, 20].

The initial failures were characterized by a fairly steep drop in resistance after the ultimate load which was captured by the detailed and reduced models. In the 4- and 5-bolt assembly tests, it was observed that the resistance increased after an initial failure until the secondary failure occurred. Tables 2.13-1 and 2.13-2 give another comparison of finite element models versus experimental data.

Table 2.13-1: Comparison of Model Predictions and Experimental Measurements of Ultimate Vertical Load [20].

	Detailed Model		Reduced Model		Experiment	
Connection Size	P_u	[Deviation*]	P_u	[Deviation*]	Mean P_u	[COV†]
3 bolts	47.1 kN	[−14.6 %]	43.4 kN	[−21.3 %]	55.1 kN	[11.3 %]
4 bolts	65.7 kN	[−10.6 %]	74.8 kN	[+1.8 %]	73.5 kN	[19.5 %]
5 bolts	90.7 kN	[−5.8 %]	106.6 kN	[+10.6 %]	96.4 kN	[7.1 %]

* Percentage deviation from mean experimental value
† Coefficient of Variation = [standard deviation]/[mean]

Table 2.13-2: Comparison of Model Predictions and Experimental Measurements of Rotation at Ultimate Load [20].

	Detailed Model		Reduced Model		Experiment	
Connection Size	θ_u	[Deviation*]	θ_u	[Deviation*]	Mean θ_u	[COV†]
3 bolts	0.120 rad	[−13.8 %]	0.103 rad	[−26.1 %]	0.139 rad	[3.4 %]
4 bolts	0.087 rad	[−21.5 %]	0.093 rad	[−16.6 %]	0.111 rad	[18.8 %]
5 bolts	0.066 rad	[−24.3 %]	0.082 rad	[−5.6 %]	0.087 rad	[9.6 %]

* Percentage deviation from mean experimental value
† Coefficient of Variation = [standard deviation]/[mean]

2.14 Behavior of Steel Connections under Column-Removal Demands by Oosterhof and Driver

Oosterhof and Driver [22] continued their work from their previous paper [18] and from the work by Daneshvar and Driver [16]. The authors did full-scale experimental testing on steel shear connections to investigate the inherent robustness. The specimens included shear tab, welded-bolted single-angle, bolted-bolted single-angle, and bolted-bolted double angle connections. Their test setup is shown in Figure 2.14-1. The test was designed to apply independent levels of moment, shear, and axial force to the beam-to-column connection. Actuator 1 and 2 were used to get the desired combination of moment and shear to the connection. Actuator 3 was oriented to apply primarily axial load along centerline of the beam.

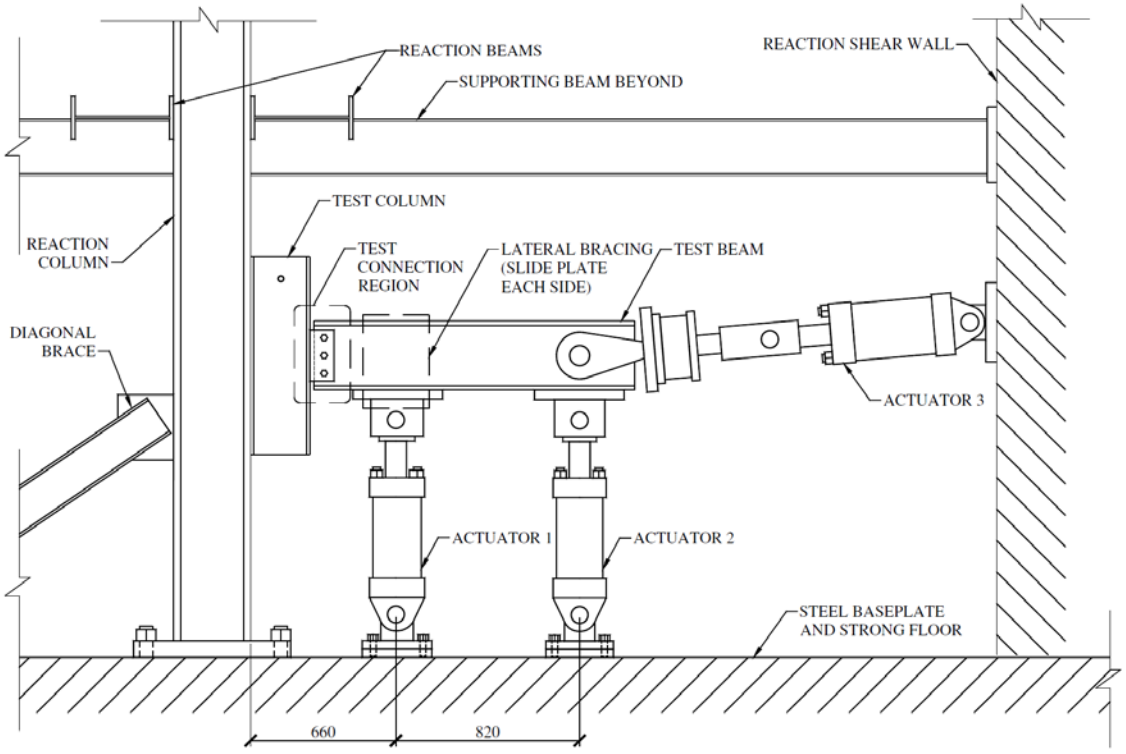

Figure 2.14-1: Test Setup [22].

When the shear tab was subjected to the loading, there was extensive local yielding of the plate. The plate's overall ductility contributed to the plate-bulging mechanism. This plate-bulging eventually led to bolt tear-out. The tear-out was the result of the catenary force being transferred to plate-by-bolt bearing, as seen in Figure 2.14-2.

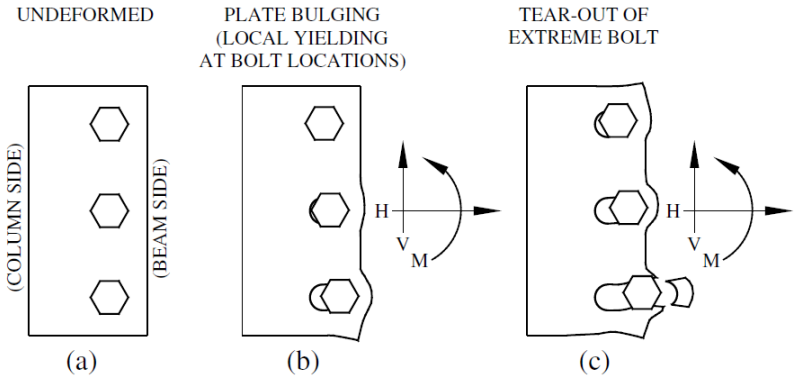

Figure 2.14-2: Deformation of Shear-Tab Connections under Combined Loading [22].

The single-angle connection that was welded to the column and bolted to the beam behaved similar to the shear tab. This is due to the fact that they are bolted cantilevered plates. The dominant deformation mechanism and failure mode in these connections was away from the weld. Therefore, the presence of the angle leg welded to the column did not affect the connection behavior.

Bolted-bolted single angle connections and double angle connections exhibit similar behavior during the loading process. Compressive arching action occurred during the early stages of bolted single angle test. Due to the fact the angle was not connected at the heel, plastic hinges in the connection were created. This can be seen in Figure 2.14-3.

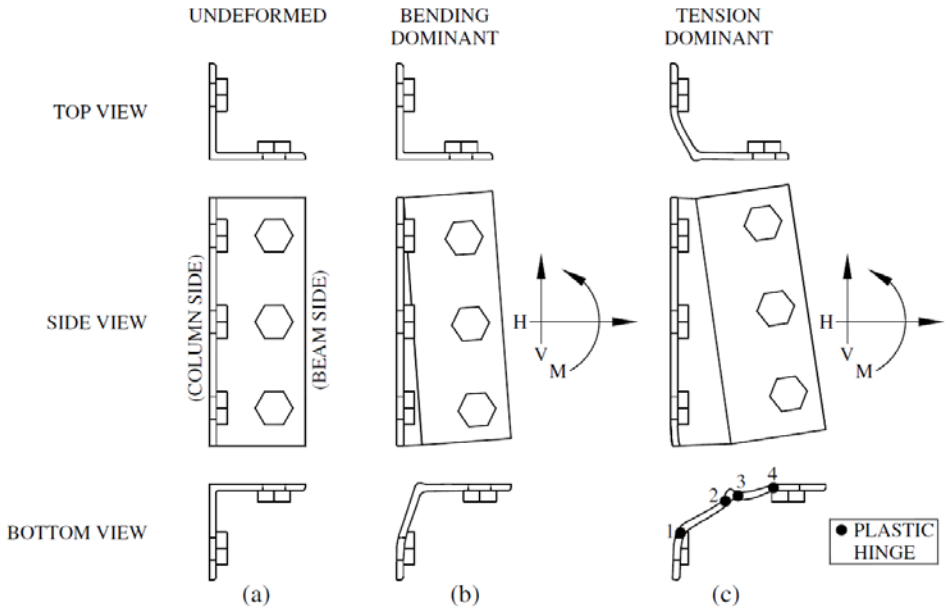

Figure 2.14-3: Deformation of Bolted Angle Connection under Combined Loading [22].

As the axial force increased, an “unfolding” mechanism gave these connections significantly lower axial and rotational stiffness. However, it did allow for higher ultimate rotation magnitudes compared to welded connections.

The compressive axial forces at low rotation resulted from a vertical eccentricity in the connection’s instantaneous center of rotation and the centerline of test beam. The compressive arching action in the bolted-bolted single angle and double angles was only found to exist in the early stages in the loading history. Therefore, it was concluded that it had a negligible effect on the performance of shear connections.

Unlike the welded connections, there was little bolt bearing deformation visible on the angle leg attached to the beam web. All of the bolted angle connections failed by the propagation of a tear that initiated at the bottom of the angle. Tears developed along one of the plastic hinges seen in Figure 2.14-3, either near the angle heel or the beam side of the line of column bolts. All connection bolts were examined for damage following

testing; no bolts failed and no significant permanent shear deformation was visible. Failure by tearing near the angle heel started to occur at low rotation, but at partial depth of the connection. As the rotation increased, the applied axial elongation led to the development of tensile axial stresses that decreased the total moment. As soon as the angle heel separated from the column flange, the moment began increase again.

Some specimens showed failure due to tearing near the column bolt line. The tear progressed upward from the bottom of the angle leg to the extreme bottom bolt. The maximum horizontal load occurred immediately before a tear initiated below the bottom column bolt hole.

Oosterhof and Driver [22] found that if the connection was welded to the column, then the failure would occur by means of tear-out in the leg attached to the beam. If the connection was a completely bolted connection, the angles would first “unfold”, then a tear would occur either in the bolts along the beam or along the bolts in the column flange.

Chapter 3: Experimental Program

3.1 Introduction

Experimental testing was conducted in the Engineering Materials and Structural Testing Laboratory (EMSTL) at Marquette University. The goal of the experimental program was to determine the robustness of various WT shear connections while under a combination of moment, axial, and shear loads. The results from this project will provide a better understanding of the interaction of the forces in shear connections during quasi-dynamic loading in comparison to static loading as determined experimentally by Friedman [12] and analytically by Sadek and Main [20] and Daneshvar and Driver [16]. The WT experimental program was done in conjunction with another experimental program involving shear tabs connections by Lesser [23].

3.2 Test Specimen Overview

A total of 12 tests were conducted using WT connections. Those 12 tests were divided evenly into three different bolting patterns: three rows, four rows, and five rows of bolts. Figure 3.2-1 demonstrates an example of the naming convention used to reference each test. Figures 3.2-2 through 3.2-4 show the general layout and geometry of each specimen.

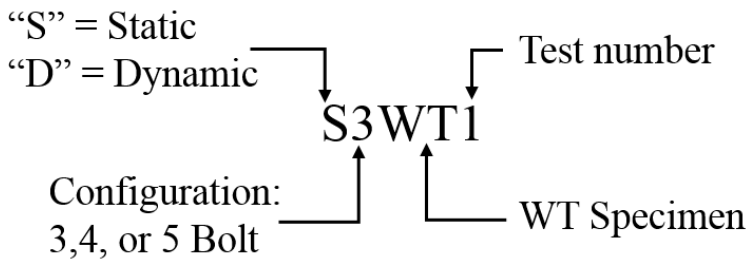

Figure 3.2-1: Naming Convention.

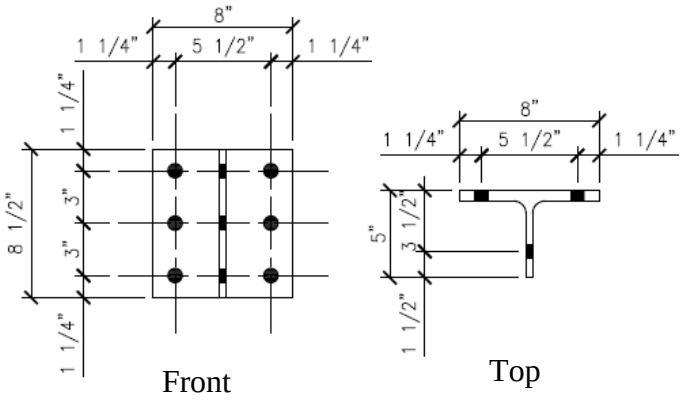

Figure 3.2-2: 3WT Specimen.

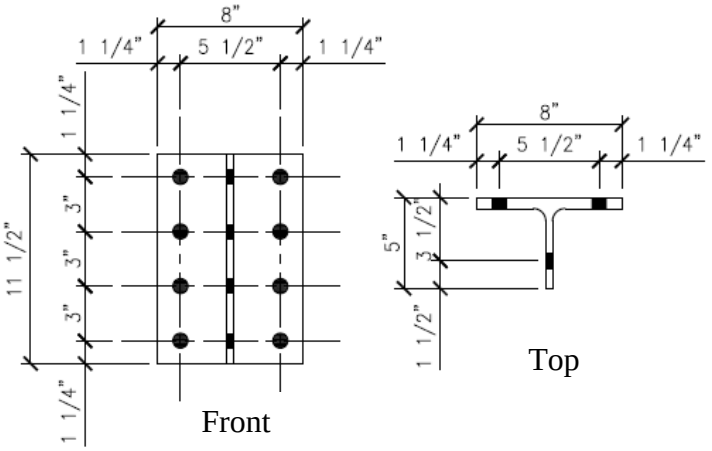

Figure 3.2-3: 4WT Specimen.

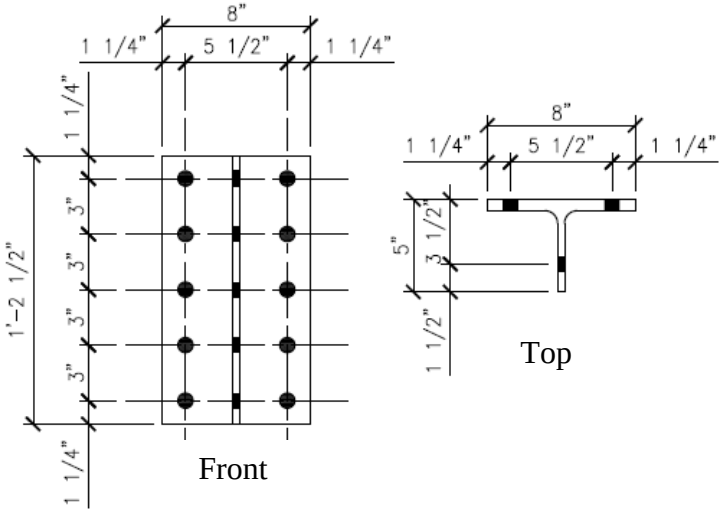

Figure 3.2-4: 5WT Specimen.

To make the tests more applicable to industry, the design of the WT connections were fabricated to match industry standards. The bolt holes were set to 13/16 in. diameter for use with 3/4 in. diameter A325 bolts. In order to compare statically loaded connections to quasi-dynamically loaded, the specimens were designed with the same geometry used by Friedman [12]. The connection design calculations and capacities can be found in Appendix A. The ultimate capacity for each failure mode is summarized in Table 3.2-1. These capacities do not include safety factors.

Table 3.2-1: WT Connection Capacity (By Limit State Without Safety Factors).

Limit States		Connection Type (kips)		
		3WT	**4WT**	**5WT**
1.	Shear Rupture of Bolts	90.0	120.0	150.0
2.	Bearing and Tear Out in WT Stem	104.9	145.9	186.8
3.	Bearing in Beam Web	105.3	140.4	175.5
4.	Block Shear Rupture of WT Stem	93.3	122.3	151.3
5.	Shear Yielding of WT Stem	76.1	107.6	139.1
6.	Shear Rupture of WT Stem	69.1	98.1	127.1
7.	Shear Rupture of Beam Web	176.4	166.1	155.9
8.	Beam Gross Shear Yield	159.3	159.3	159.3
9.	Flexural Yield of Flange	54.6	162.4	258.2
10.	Rotational Ductility	OK	OK	OK
11.	Combined Shear and Tension Interaction	107.4	143.2	179.0

The controlling limit states from Table 3.2.1 were used to determine the loading on a typical frame bay for an occupancy. With a total dead load of 70 psf and live load of 80 psf, and infill beams spaced at 10-ft.-0-in. on center, a typical girder span could be 40-ft.-0-in. for an office building bay, which that was calculated using LRFD factors. A 3WT would be able to support a 40-ft.- 0-in. girder when infill beams are 30-ft. – 0-in. long. A 4WT would be able to support a 40-ft.- 0-in. girder with 55-ft.- 0-in. long infill

beams. A 5WT would be able to support a 40-ft.- 0-in. girder with infill beams that are 80-ft.-0-in. long.

It should be noted that D3WT4, D4WT4, and D5WT4 were run at a later time than the first nine tests. This was because, after the first nine tests were completed, it was decided that one additional test of each bolt configuration would be useful for confirming results. With this difference in time, a different lot of bolts were purchased which resulted in some noticeable differences in the test results. This will be covered more in Chapter 4: Experimental Results.

3.3 Test Assembly Overview

The test assembly was designed to match the setup used by Friedman [12]. The setup was designed to utilize existing frame pieces available in the EMSTL, so a W10×88 floor beam was attached to the strong floor so that the frame could be installed at the same dimensions as the setup used by Friedman. The setup can be seen in Figures 3.3-1 and 3.3-2. The test setup was designed to emulate a typical steel framed building. As such, a column stub test specimen was centered in a two span system with end connections being a single bolt pin. The end pin connections were designed to effectively allow free rotation with minimal frictional resistance (see Figure 3.3-3).

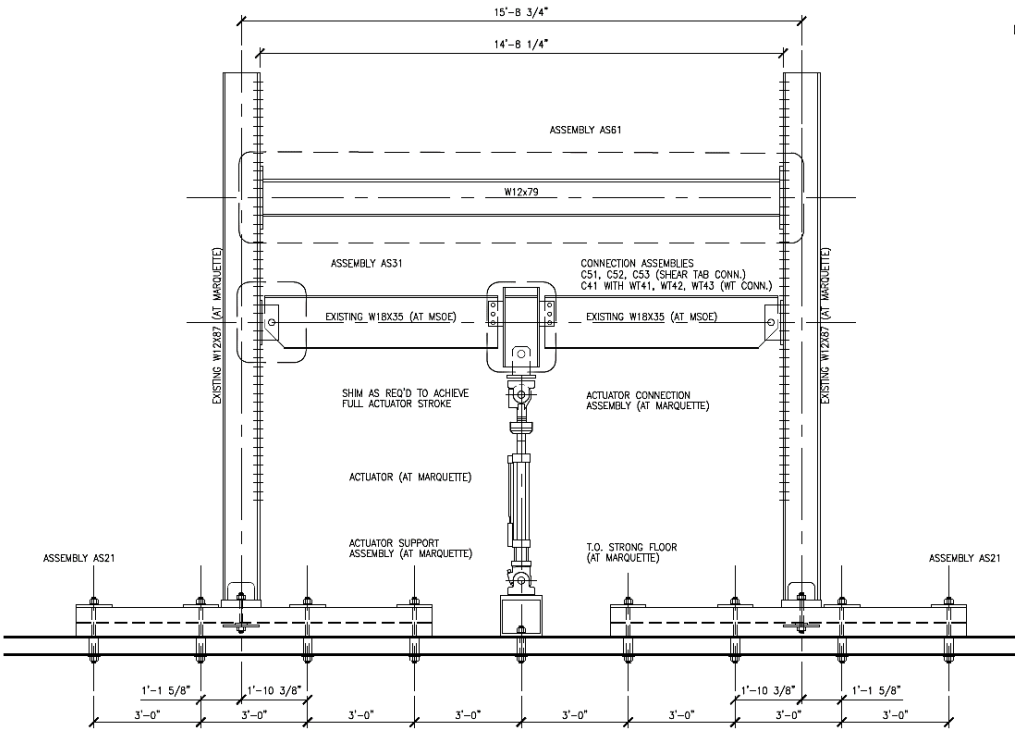

Figure 3.3-1 Overall Test Setup.

Figure 3.3-2: Test Assembly.

Figure 3.3-3 Pin Connection to Test Frame Column.

The test specimen was bolted in place using an impact driver to tighten the bolt to the proper tension. “Squirter” direct tension indicating washers (DTIs) were used to ensure that the correct bolt tension was developed when connecting the WTs to the beam and the column stub.

The loading was applied to the test assembly through an MTS 201.30T single ended actuator. The MTS actuator can pull with a force of 36.4 kips and has a full static and dynamic stroke of ten inches. The connection from the actuator to the column stub is similar to a clevis, with two plates that slide over the column stub web and are connected by means of a pin (Figures 3.3-4a, 3.3-4b and 3.3-4c). This connection allowed for a direct loading on the center of the test assembly, which was designed to replicate the effect of a column failure.

Figure 3.3-4a: Front View Connection from Actuator to Column Stub.

Figure 3.3-4b: Side View of Connection.

Figure 3.3-4c: Connection connected to Column Stub.

Multiple devices were used to collect data, including strain gages, draw wire transducers, and the force and displacement instrumentation available through the MTS 201.30T Actuator.

The strain gages were Vishay “Micro-Measurements” CEA-06-062UW-350 (350 ohm). A total of fourteen gages were used, seven per each beam. These strain gages were attached near the center of each of the beams, placing one on the center face of the top flange, one on the center of the bottom flange, one at approximately the centerline of the of web, one at approximately the top sixth point of the web, one at approximately the top third point of the web, one at approximately the bottom third point of the web and one at approximately the bottom sixth point of the web. See Figure 3.3-5 and Figure 3.3.6 for exact locations along the length and depth of the beam.

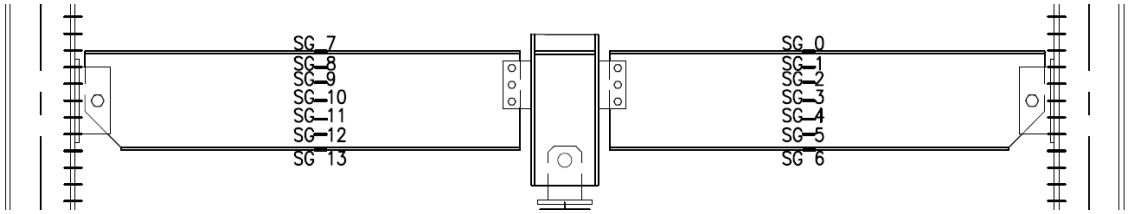

Figure 3.3-5: Strain Gage Location.

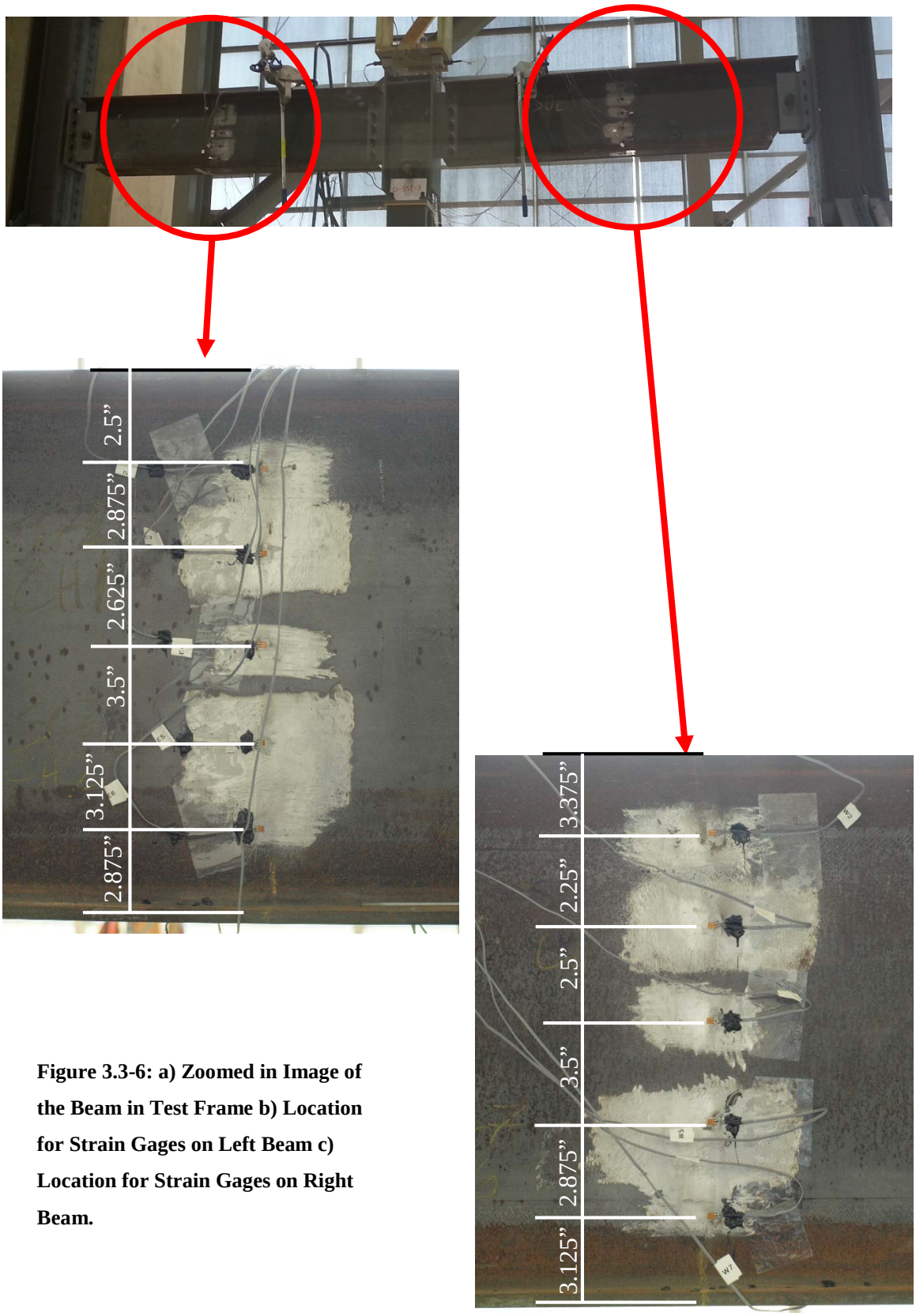

Figure 3.3-6: a) Zoomed in Image of the Beam in Test Frame b) Location for Strain Gages on Left Beam c) Location for Strain Gages on Right Beam.

Strain data were collected through the use of strain gages connected to a terminal board, then through a signal conditioner before connecting to the computer with LabView software. Though each beam had seven strain gages installed, only the strain gages on the top and bottom flange were used extensively during the data analysis. The other strain gages were installed for redundancy and for validation of the strain data collected from the top and bottom gages. The strain data were used to calculate stresses, which in turn were used to calculate axial force and moment acting at the midpoint of the beam.

Two draw wire transducers (DWT) were connected to the column stub with magnetic hooks in order to measure the overall displacement and rotation of the column stub. The DWT are Model PA-30-DS-L5M and are powered with a MPJA 14601PS DC power supply. See Figure 3.3-7 for DWT location on the test assembly.

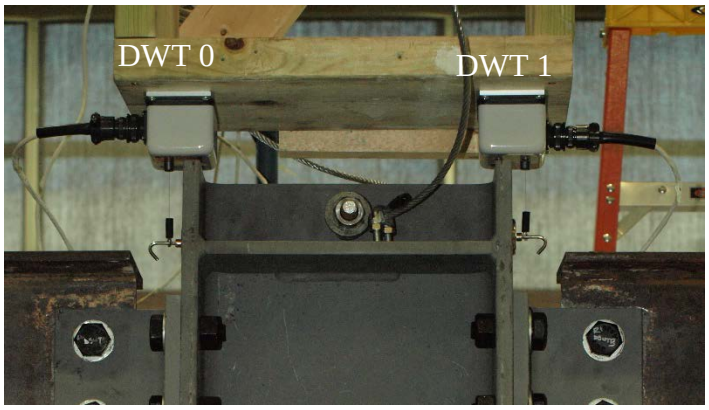

Figure 3.3-7: DWT Location.

It should be noted that the W18×35 test beams had a 1/2 in. (Fy=36 ksi) doubler plate welded to connection point of each beam. This doubler plate was installed because the test beams were intended to be used for the entire testing program (both WT and shear tab tests by Lesser [23]). The doubler plates limited deformation from occurring at the bolt holes in the beam.

Multiple safety devices were installed and utilized during the test. Hand winches were attached near the column stub on each beam, and the cables were slackened so that the vertical deformation during the test could occur but they could "catch" the test beams if there was total failure in the system. A cable was wrapped around the top cross beam of the test frame and was attached to the column stub. As with the winches, the cable was installed to catch the column stub if there was a total failure in the test system. Four winches were connected to the MTS actuator to stabilize it and keep it plumb. Lateral braces were connected to the front and back side of each of the test frame columns. Finally, safety glass (Lexan) was installed in front and behind the test specimen to protect the observers from any possible shrapnel due to bolt shear failure.

3.4 Test Procedure

3.4.1 Pre-Test Procedure

The entire setup was inspected prior to running a test. All of the bolts used to connect the test beam to the test frame were tightened down. The strain gages were checked to ensure they were working properly. The test beams were leveled by adjusting the winches. On the ground, the WT connections were bolted to the column stub, and DTI washers were used to make sure the bolts were installed at the correct tension. An impact driver and spud wrench were used to install the bolts. Once the WT was bolted to the column stub, a forklift was used to lift the column stub into place. Bolts were installed and hand-tightened. An impact driver and spud wrench were used to fully tighten the bolts, using a crisscross pattern. The winch cables were loosened to allow the column stub to displace during testing.

With the MTS actuator fully extended and the test beams and specimen at level, there was approximately an inch and a quarter (1 1/4 in.) difference in heights. This problem was remedied in two different ways, depending on the test. For the S3WT1, S5WT1, and D5WT3, a series of 1/4 in. thick shim plates were used to make up the difference (see Figure 3.4-1). On all of the other tests, the actuator was used to pull down the test beams an inch and a quarter prior to the beginning of the test. The initial pull-down was accounted for during the data analysis.

Once the actuator pin was put in place, in the frame supporting the DWTs, and the safety glass was placed (see Figure 3.4-1). The DWTs were then connected to the column stub by means of a magnetic hook. The bolts were then labeled so that they could be identified after the test. One last check of all the strain gages and DWTs was performed to ensure they were working properly. The test could now begin.

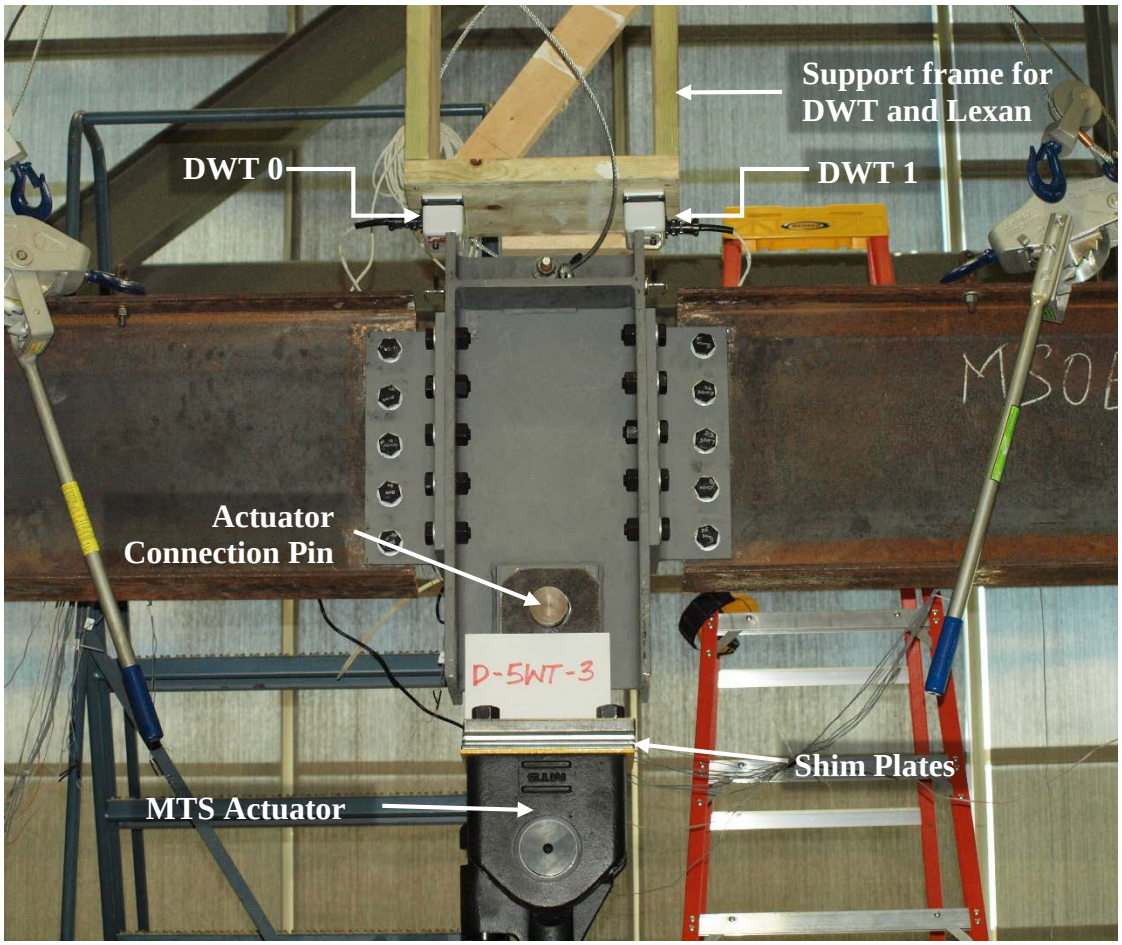

Figure 3.4-1: Pre-Test Assembly.

3.4.2 Static Test Loading

During what is referred to as a “static” experimental test, the specimen was pulled down at the rate of ten inches in ten minutes. The experiment used the full stroke of the actuator which is ten inches. Note that S3WT1 was the first test run and the actuator was not pulled to it full stroke in an effort to gage the behavior of the system for safety purposes. All other tests (both static and dynamic) exhausted the full ten inches of stroke.

3.4.3 Dynamic Test Loading

During what is referred to as a “dynamic” experimental test, the specimen was pulled down at an average rate of ten inches in approximately four seconds. The test duration was calculated for each of the nine tests and averaged, resulting in the rate of ten inches in approximately four seconds. An “average” rate is given because the actuator was programmed to retract as fast as it could. The experiments used the full stroke of the actuator.

3.4.4 Post-Test Procedure

Once the test was completed, which typically meant that the actuator had completed its full stroke, the actuator was slightly extended in order to reduce the applied load to a safe level. The test specimen remained in its deflected form. Pictures were taken at this point. A measurement of how much the column stub rotated was taken (see Figure 3.4.4-2). The test assembly was then pushed up with the actuator and the winches were tightened to prepare for disassembly.

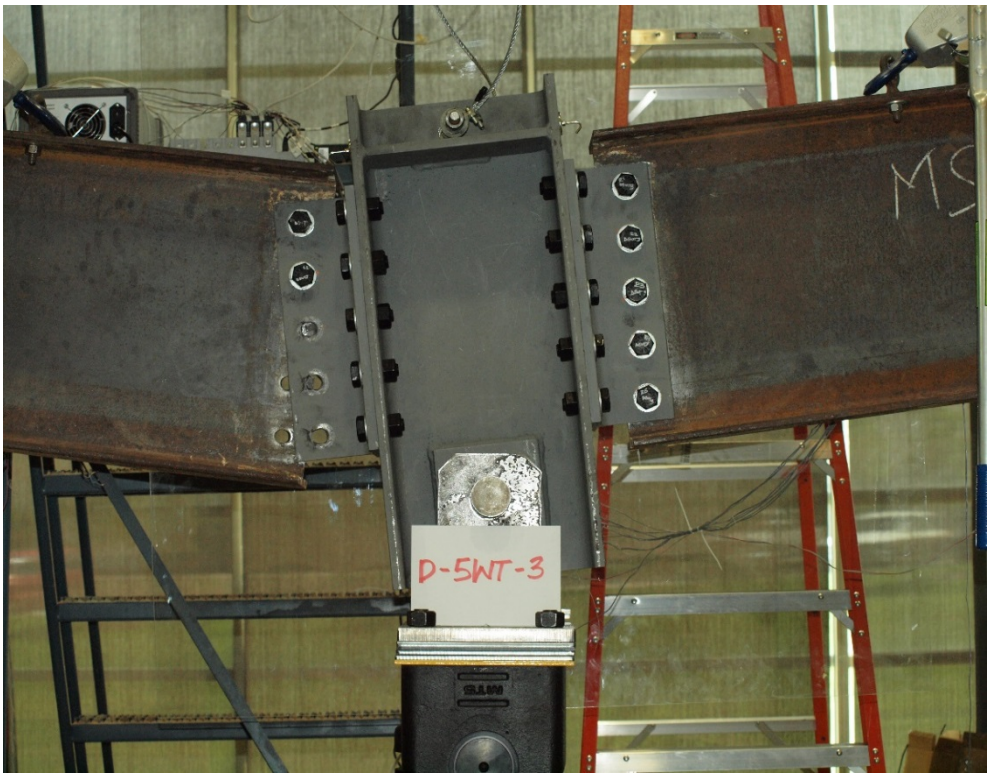

Figure 3.4.4-1: Test Specimen D5WT3 after Testing.

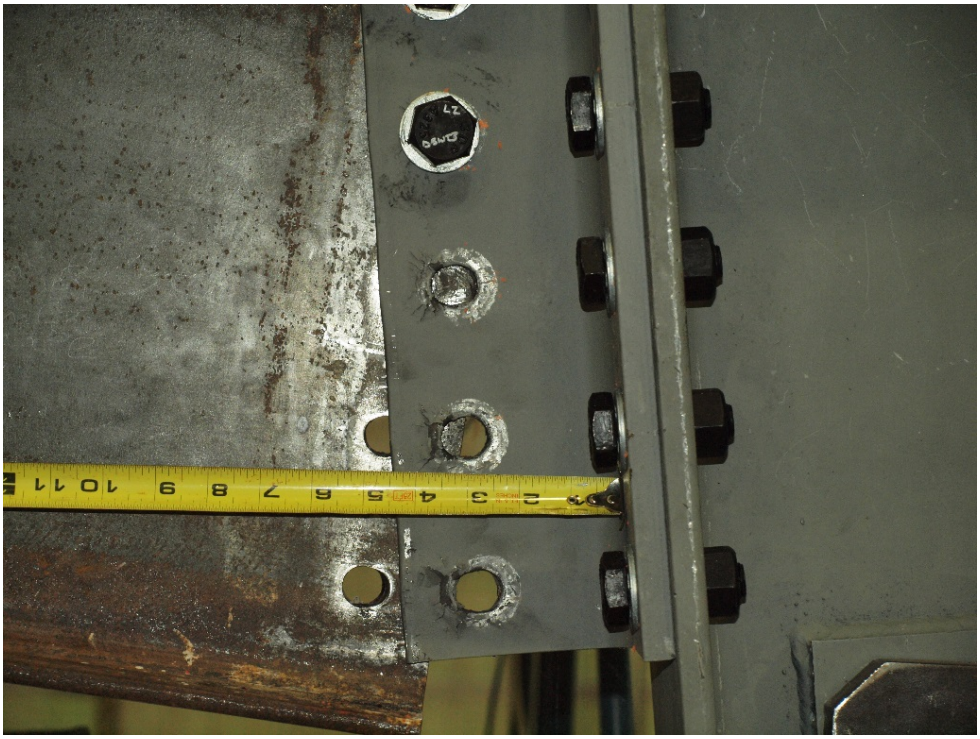

Figure 3.4.4-2: Typical Measurement of Column Stub Rotation.

Chapter 4: Experimental Results

4.1 Introduction

In the course of this experimental program, a total of twelve experiments were run. The twelve experiments were broken evenly into the three types of bolt configurations, and for each configuration one static and three dynamic tests were run. The data collected were then verified through a basic structural analysis.

4.2 Determining Forces

4.2.1 Connection Forces

The output data from the strain gages, DWTs, and the force and displacement transducers within the MTS actuator were collected through LabView. In addition, force and displacement data were collected by the MTS calibrated system. Since the LabView program was written specifically for these tests, the data collected by the MTS system provided an independent validation of the LabView output as illustrated in Figure 4.2.1-1.

Test data were plotted using the mid-stroke point of the actuator as the control point (also referred to as the "zero point" herein). As seen in Figure 4.2.1-1, the data collected were plotted using this point as the point of zero displacement, and the full extension and retraction of the actuator are at –5 in. and +5 in., respectively. The use of the control point allowed all tests to have a consistent point in space from which to base all calculations related to displacement.

The zero point was easily found in the MTS data because the system is calibrated to identify the mid-stroke point of the actuator as zero inches. The data collected through LabView were manually zeroed using the following steps:

1. The force corresponding to zero displacement in the MTS data was identified,
2. An equivalent force magnitude was identified in the LabView data, and its corresponding displacement was manually zeroed,
3. The displacements for the remainder of the LabView data were calculated using the new zero as a baseline.

As seen in Figure 4.2.1-1, the MTS load versus displacement trace is consistent with the LabView load versus displacement trace. Careful observation at the start of the data shows that the MTS trace starts with approximately 50 pounds of applied force, whereas the LabView data was programmed to zero the data prior to initiating data collection. If the MTS force measurement was also zeroed at the start of the test, it would lay right on top of LabView line. Since the MTS system is independently calibrated by an outside vendor, it is reasonable to assume that it collects accurate force and displacement measurements, thus proving that the LabView program is collecting accurate applied force and displacement measurements.

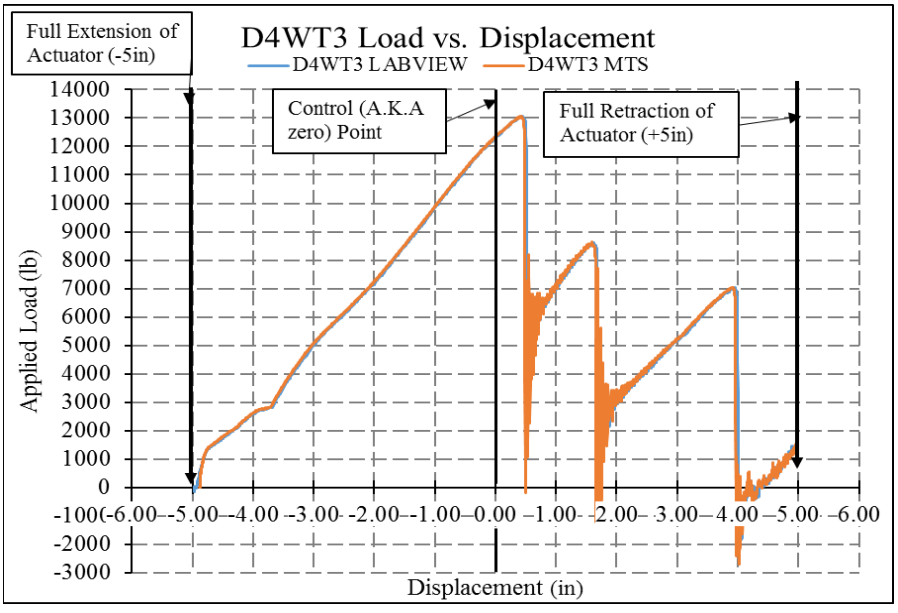

Figure 4.2.1-1: Applied Load Versus Displacement Measured by Labview and the MTS System (D4WT3 Test Shown).

The rotation as calculated from the DWT displacement measurement was then compared to the rotation as calculated from the actuator displacement measurement, as seen in Figures 4.2.1-2 and 4.2.1-3. Figure 4.2.1-2 shows the comparison between the displacements measured by DWT 0, which was connected to the left side of the column stub, to the displacement measured by the actuator. Similarly, Figure 4.2.1-3 compares the displacement measured by DWT 1, on the right side of the column stub, to the displacement measured by the actuator. In both figures, the DWT trace and the actuator trace are almost on top of one another up to the first bolt break.

Between the first bolt break and the second bolt break, the traces are less consistent. This is due to column stub rotation toward the side in which the bolt failed. The actuator continued to pull straight down at the centerline of the column stub. The DWTs were attached to the flanges of the column stub, and as such they measured the differential displacement from each side of the column stub. The rotation of the column stub can be measured using the differential displacement measurements.

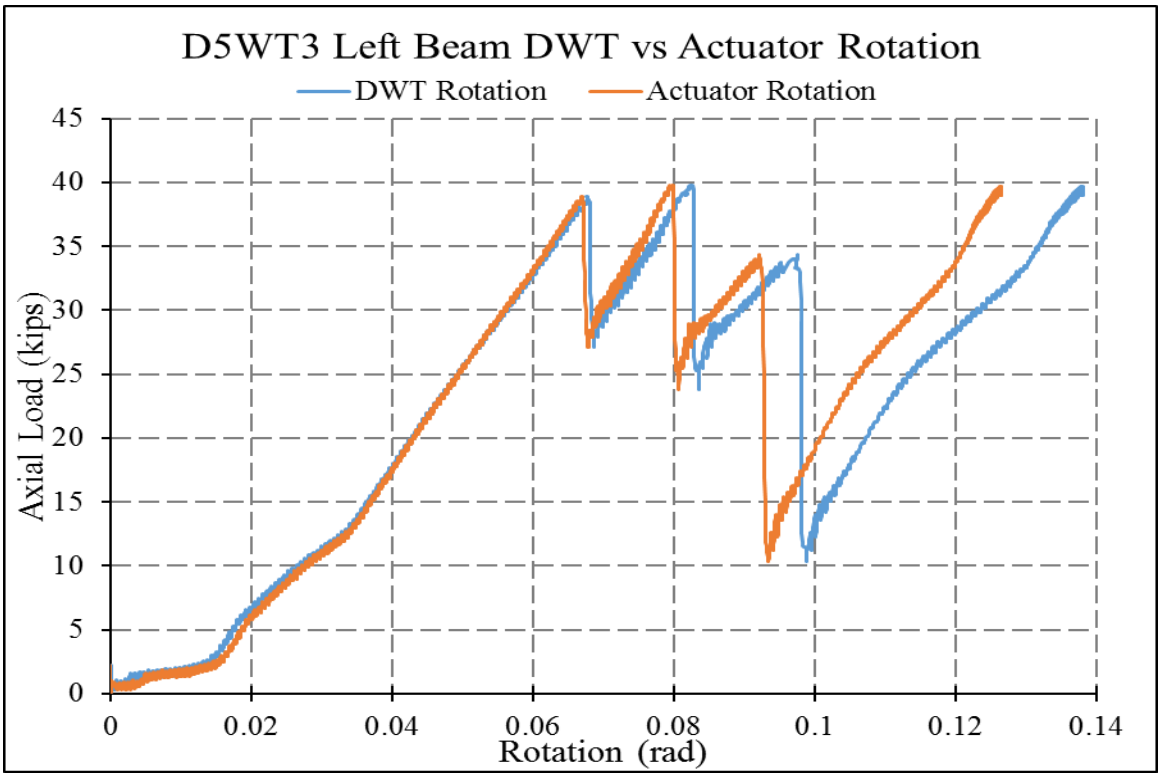

Figure 4.2.1-2: DWT 0 and Actuator Rotation versus Axial Load in Beam.

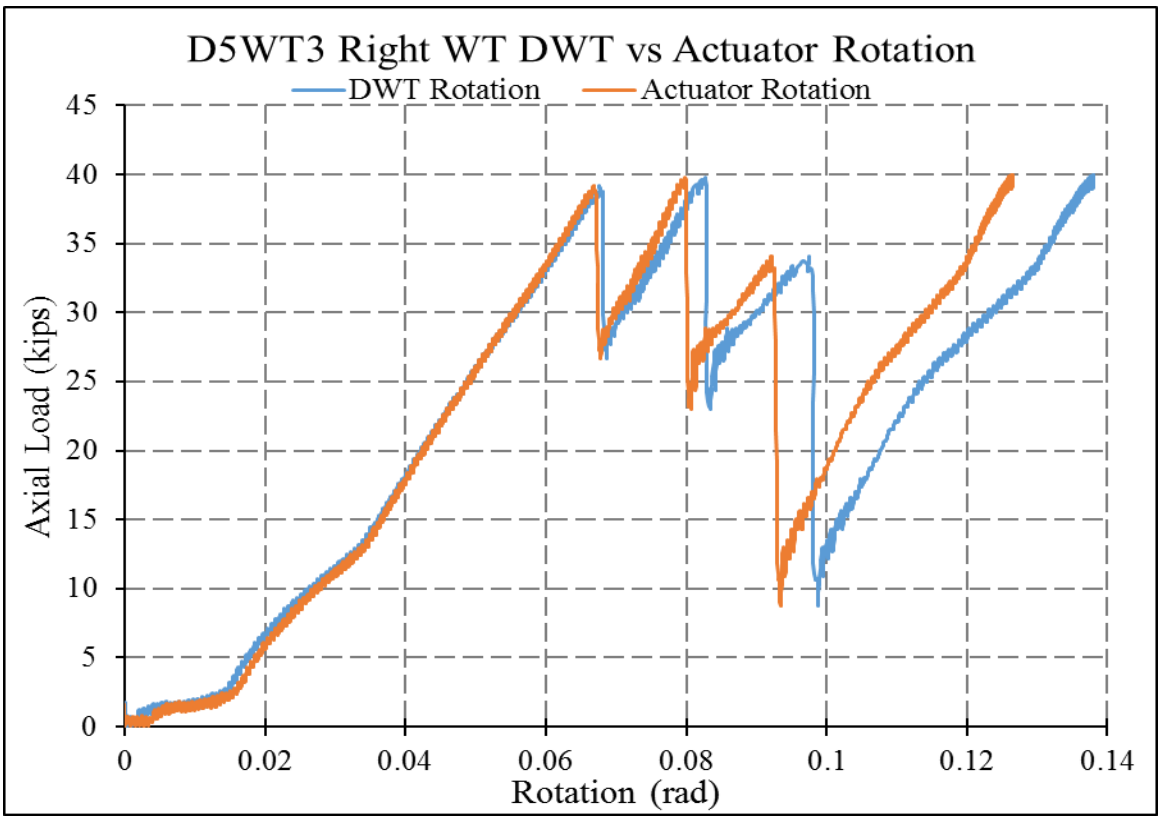

Figure 4.2.1-3: DWT 1 and Actuator Rotation versus Axial Load in Beam.

Simple geometry was used to find the rotation of the beam. Using the displacement of the column stub from one of the DWTs and geometry of the test assembly, the angle of rotation was calculated as:

$$\theta_n = \tan^{-1}\left(\frac{\Delta_n}{L_{beam}}\right) \text{ (degrees)} \quad (4.2.1\text{-}1)$$

where

Δ_n= displacement measured by DWT (in.),

n= DWT 0 or DWT 1,

L_{beam}=78.375 (in.).

Stresses were calculated by multiplying the measured strains by the modulus of elasticity of the test material. Direct tension tests conforming to ASTM E8 [24] were conducted on several WT material samples. It was found that the average modulus of elasticity was 29,200 ksi. The strain gages were applied to the beam and no material test was conducted on the beam; thus, the modulus of elasticity was assumed to be the standard 29,000 ksi. The stress at the location of the strain gage is calculated as:

$$\sigma = \mu\epsilon \times E \quad (4.2.1\text{-}2)$$

where

$\mu\epsilon$ = measured microstrain,

E = modulus of elasticity, 29,000 ksi.

The internal axial force and moment was determined using principles of mechanics of materials. The normal stress can be calculated using the interaction equation for axial and flexural stress:

$$\sigma = \frac{P}{A} \pm \frac{My}{I} \quad (4.2.1\text{-}3)$$

where

P = axial force, unknown (kips),

A = area of the beam (in^2),

M = moment in the beam (in-kips),

I = moment of inertia of beam (in^4),

y = distance to the strain gage from the neutral axis.

A matrix form of Equation (4.2.1-3) was used to solve for measured axial force and measured moment at the strain gages:

$$\begin{bmatrix} P \\ M \end{bmatrix} = \begin{bmatrix} \frac{1}{A} & \frac{-y_1}{I} \\ \frac{1}{A} & \frac{-y_2}{I} \end{bmatrix} \begin{bmatrix} \sigma_1 \\ \sigma_2 \end{bmatrix} \qquad \begin{pmatrix} kips \\ in. - kips \end{pmatrix}. \tag{4.2.1-4}$$

The internal axial force in the beam, P, and the internal moment, M, are calculated using "opposing" strain gages. For the left beam, the strain values from strain gages 7 and 13 are used, which are located at the top and bottom of the flanges, 8.85 in. above and below the beams neutral axis, respectively. For the right beam, the strains values are taken from gages 0 and 6, which are also located on the top and bottom flange. The other strain gages were used to validate the results, but were not directly used when calculating the internal forces and moments.

These internal axial forces and moments are calculated at the point where the strain gages are applied, which is some distance away from the connection to the stub column. The internal axial force is constant throughout the beam; thus, the axial force at the connection is of the same magnitude. The internal moment in the beam varies linearly from a magnitude of zero at the pinned connection to the test frame column to a maximum magnitude at the stub column connection. The moment at the point of the connection was determined by multiplying the moment at the strain gages by a constant.

This constant was based on the test assembly geometry and the assumption that the beam remains linear-elastic during testing.

The moment at the connection is

$$M_{conn} = \frac{c_s * M}{12} \qquad (ft - kips) \qquad (4.2.1\text{-}5)$$

where

M = Moment in beam at the strain gages in (in.-kips),

$$c_s = \frac{L_{horiz}}{L_{SG,n}}, \qquad (4.2.1\text{-}6)$$

$$c_L = \frac{78.38''}{36''} = 2.18 \qquad (unitless),$$

$$c_R = \frac{78.38"}{36.125"} = 2.17 \qquad (unitless),$$

s= left or right beam,

$L_{horiz.}$ = horizontal distance from the pin connection to the bolt group centroid,

78.38 in.,

$L_{SG,n}$ = horizontal distance from pin connection.

The shear at the each of the WT connections is the total applied load divided in half:

$$V_{applied} = \frac{P_{total}}{2} \qquad (kips) \qquad (4.2.1\text{-}7)$$

where

P_{total} = Load applied by the MTS actuator, kips.

From the collected data, the following values were calculated: measured rotation, measured axial force, measured moment at the connection and shear force.

4.2.2 Determination of Bolt Forces

The instantaneous center of rotation method (ICOR) was used to determine the resultant shear force in each bolt. Free-body diagrams have been included to illustrate the forces acting on the connection.

Three forces act on the bolt group. The axial force, P, acts along the line of action from the pin connection at the test frame column to the centroid of the bolt group at the WT connection. Shear force, $V_{applied}$, acts at the face of column stub and applies a load with some eccentricity on the bolt group. The moment, M, is resolved at the bolt group centroid. The forces and moment can be seen on Figure 4.2.2-1.

The forces were then broken into components so that they could be used to calculate bolt forces using the ICOR method, which can be seen on Figure 4.2.2-2. The axial force was broken into its components acting vertically and horizontally. The vertical and horizontal components were then each divided by the number of bolts in the bolt group, n.

The axial force components are calculated as

$$P_x = P * \sin\theta \qquad (kips), \tag{4.2.2-1}$$

$$P_y = P * \cos\theta \qquad (kips). \tag{4.2.2-2}$$

The moment was resolved into a normalized shear force, H, acting at an eccentricity, e. Normalizing the moment eliminated an unknown variable from the equation. The normalized shear force was given a value of 1.0 kips, and the eccentricity was used to scale the moment to the appropriate magnitude:

$$e = \frac{M\ (inch-kips)}{H\ (kips)} \qquad (in.). \tag{4.2.2-3}$$

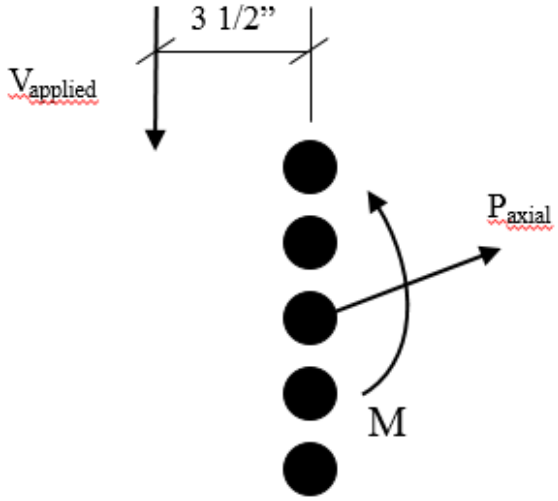

Figure 4.2.2-1: Connection Forces.

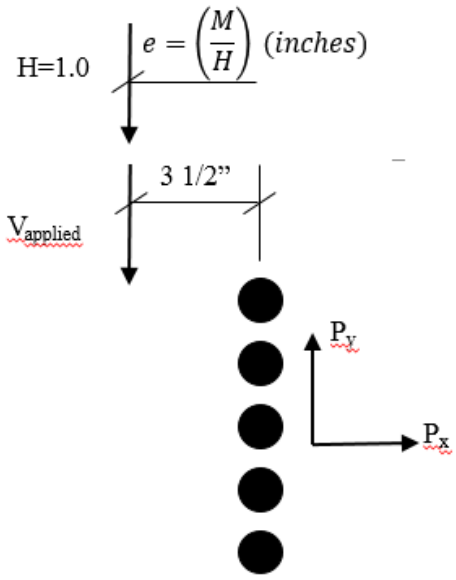

Figure 4.2.2-2: ICOR Input Forces.

The ICOR method is based on the bolt deformation. Thus, the analysis only provides accurate bolt forces up to the point of maximum bolt deformation. As explained by Kulak *et al.* [25], the maximum bolt deformation is considered to be 0.34 in. Bolt deformation is only one of the limiting factors, the other being base metal deformation. The connecting elements have a minimum yield stress of 50 ksi, so it is likely that bolt deformation occurred before the connection elements deformed. Once deformation occurs in the base material, the ICOR method no longer provides an accurate result. Thus, the bolt forces were only calculated at the maximum moment, where no plastic deformation has occurred.

From Kulak *et al.* [25], the following equation was developed for single fastener loaded in double shear:

$$R = R_{ult} * (1 - e^{-\mu\Delta})^{\lambda} \quad (4.2.2\text{-}4)$$

where

R = nominal shear strength of one bolt at deformation Δ (kips),

R_{ult} = ultimate shear strength of one bolt (kips),

Δ = total deformation, including shear, bearing and bending deformation in the bolt and bearing deformation of the connection element),

e = 2.718….., base of the natural logarithm.

An iterative process based on measured loads, rotation, and connection geometry was used to determine the bolt forces. Kulak *et al*. [25] showed that the ultimate shear stress of bolts at rupture is approximately 80 ksi; therefore, the expected maximum force at rupture based on 3/4 in. diameter bolts is approximately 35.4 kips. This number is used in the analysis to determine the point at which a bolt reaches its maximum deformation of 0.34 in. within the maximum moment measured in the testing. It should be noted that for the maximum moment, an average was taken of the top one percent of the moment magnitudes. Figure 4.2.2-3 shows all of the forces acting upon one bolt as determined using the ICOR method. The resultant bolt force on one bolt is the square root of the all the forces acting in the vertical direction squared plus all the forces acting in the horizontal direction squared, as seen in Figure 4.2.2-4.

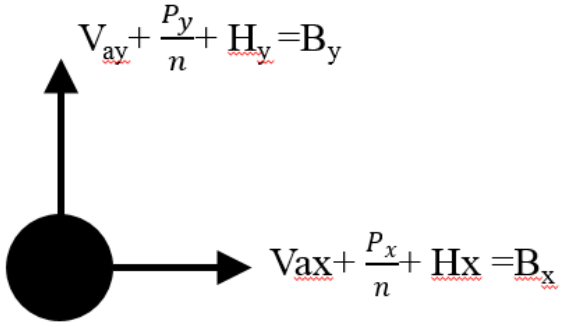

Figure 4.2.2-3: All the Forces Acting on One Bolt in Their Component Form.

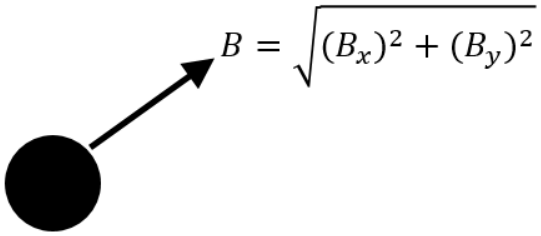

Figure 4.2.2-4: Resultant Force Acting on One Bolt.

4.3 Results of Experimental Testing

The following sections are organized by bolting configuration and include a description of the tests, pictures before and after failure, and graphs of the calculated forces and moment at the connection based on measured strains.

4.3.1 Three-Bolt WT Tests

Four three-bolt tests were conducted: one statically loaded test and three dynamically loaded tests. S3WT1, D3WT2, and D3WT3 were tested at the same time, and the bolts purchased for these tests were within the same lot. D3WT4 was tested at a later time, and as such, the bolts purchased were from a different lot. S3WT1 was the first test for all the experiments. This test did not utilize the whole stroke of the actuator in an effort to learn how the test would progress and promote a safe laboratory environment. D3WT2 and D3WT3 failed after maximum moment had peaked and the connection has extended into catenary action. D3WT4 did not break any bolts even though full stroke of the actuator had been exhausted.

It is clear that bottom bolts accrue the maximum shear force. The load path can be explained in the free-body diagram shown in Figure 4.3.1-1. The axial force pulls all the bolts in the direction of the force. The assumption was that the axial force is distributed

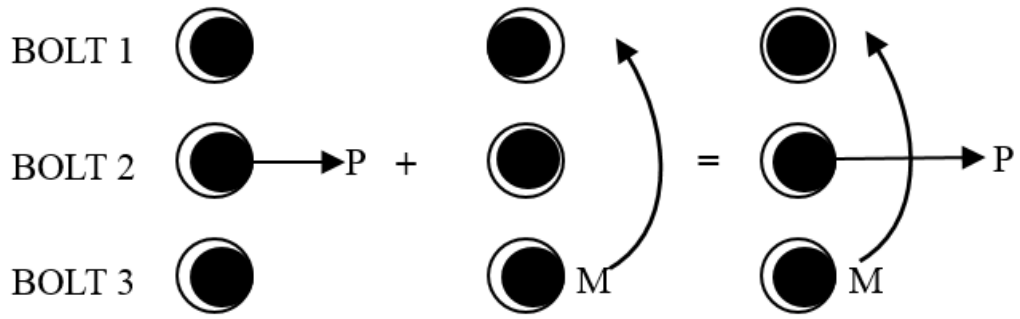

Figure 4.3.1-1: Bolt Location Due to Load.

evenly among the bolts, though it was not likely that axial load was actually evenly distributed to each bolt at the connection beyond the flexural resistance range. The moment was acting about the center bolt of the bolt group. This resulted in a force couple pushing towards and away from the column stub. These forces are creating shear on the bolts, and will be described as "compressive" and "tensile" force, respectively, herein. Since the bottom-most bolt was resisting the largest amount of combined forces, it was the failure point.

Initially, the data acquisition program was set to a very high resolution. This caused a "band" of data to be collected (see Figure 4.3.1-2) for tests D3WT2 and D3WT3. In order to manage the volume of data points, the data were sent through two different filters. The first filter was a low pass Butterworth Filter, which is a type of signal processing filter designed to reduce the frequency response in the pass band. The second filter was a median filter, which is a nonlinear digital filter used to reduce the amount of noise. With this band of data, there were too many points of data to be analyzed, so the amount of points was reduced by 90%. Figure 4.3.1-2 shows an

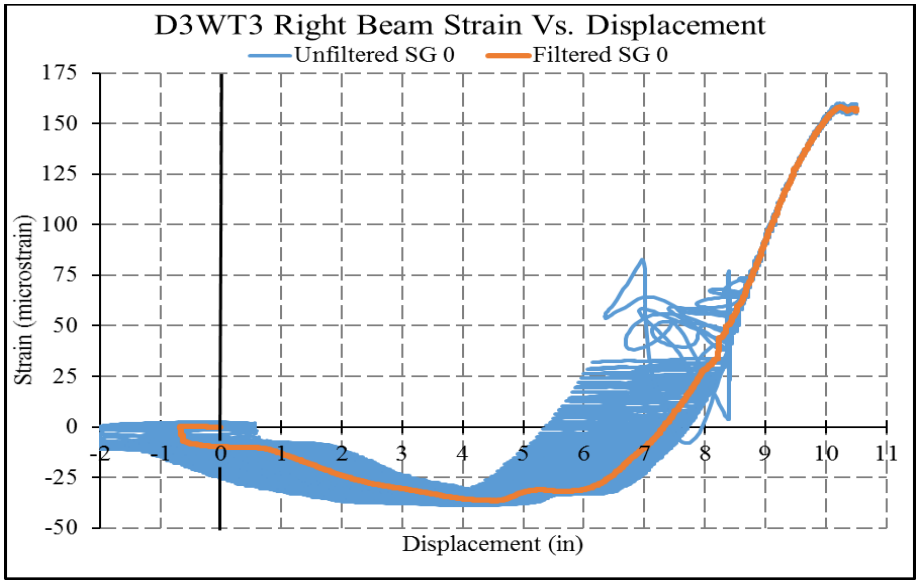

Figure 4.3.1-2: Unfiltered Data versus Filtered Data.

example of the pre-filtered data as compared to filtered and reduced data. The data acquisition program was adjusted after these two tests and fewer data points were collected, making data management easier. Filters were applied to other data sets if deemed appropriate to do so.

4.3.1.1 S3WT1 Statically Loaded Test

Figure 4.3.1.1-1 shows the pre-test setup for S3WT1. This test is the one test that did not exhaust the full stroke of the actuator because it was the first test run on this test assembly and there was a desire to ensure the test assembly was safe and working properly. Also, this is one of the few tests that had five 1/4 in. shim plates placed between the connection from the column stub to the clevis end of the MTS actuator. The test specimen was pulled down at a rate of one inch per minute. The post-test position can be seen in Figure 4.3.1.1-2. Though this test specimen did not experience bolt rupture, it can be seen in Figure 4.3.1.1-3 and Figure 4.3.1.1-4 that deformation occurred at the bottom bolt hole on each side. The bottom bolts were significantly deformed whereas other bolts showed visual signs of minor deformation, as seen in Figure 4.3.1.1-5.

Figure 4.3.1.1-1: S3WT1 Pre-Test Position.

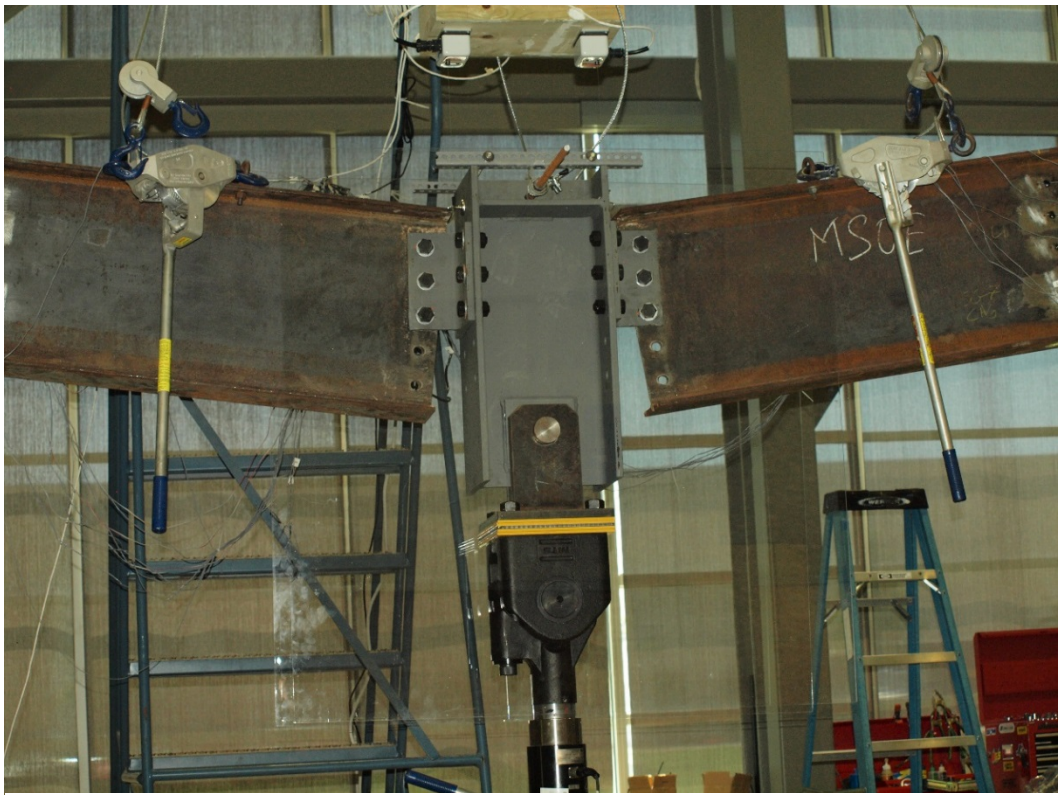

Figure 4.3.1.1-2: S3WT1 Post-Test Position.

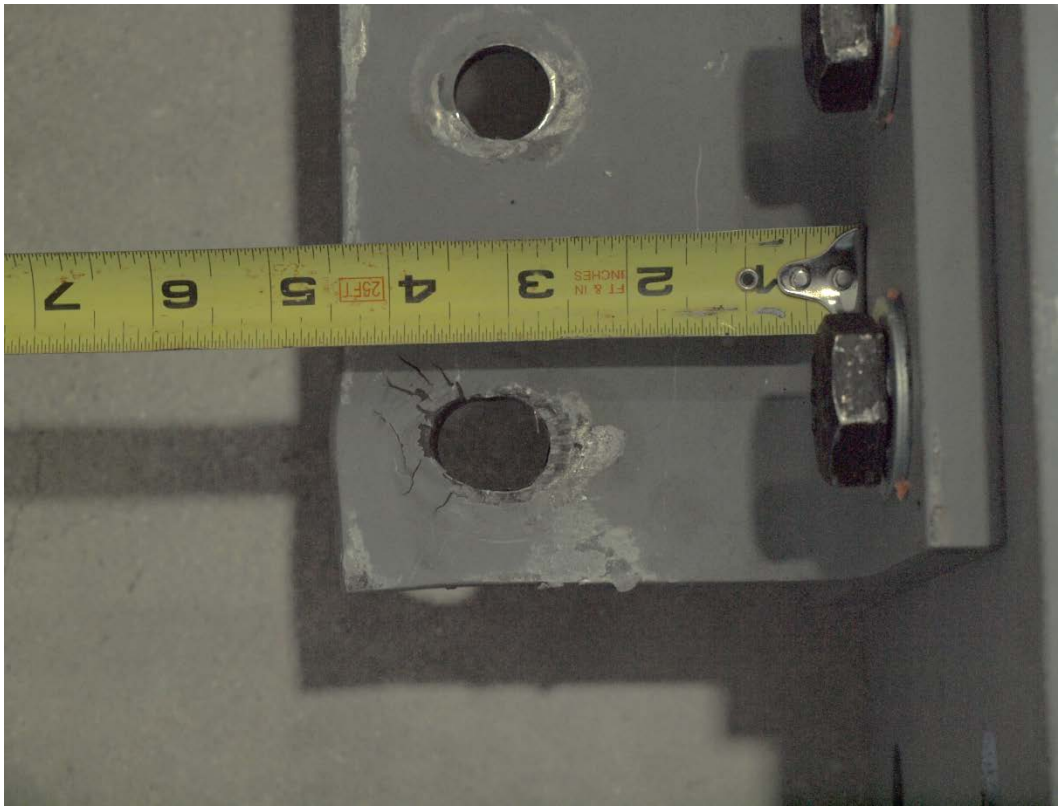

Figure 4.3.1.1-3: S3WT1 Left WT Specimen Post-Test.

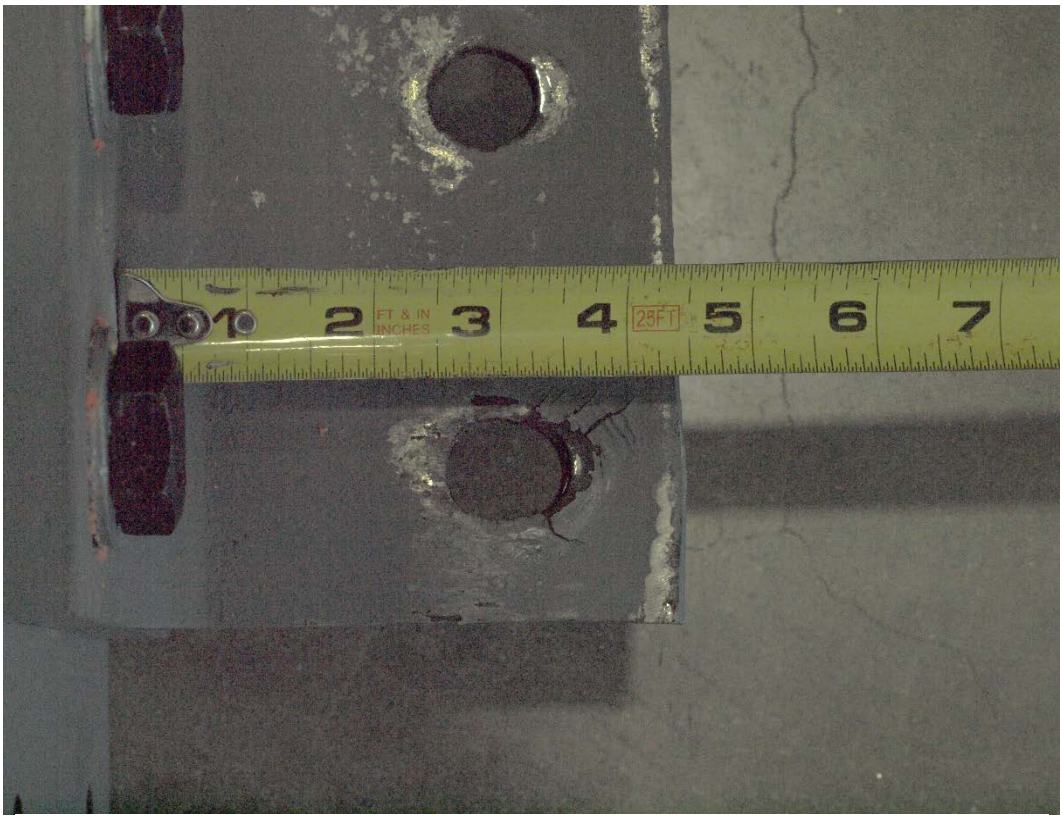

Figure 4.3.1.1-4: S3WT Right WT Specimen Post-Test.

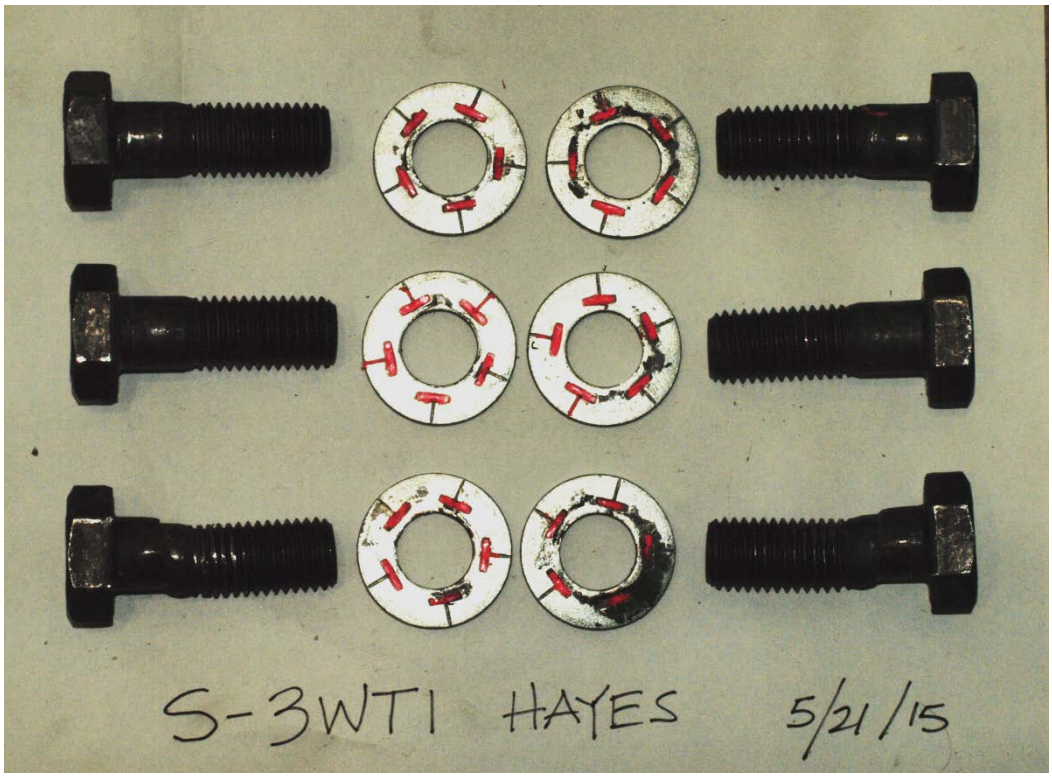

Figure 4.3.1.1-5: S3WT1 Bolts After the Test.

Figures 4.3.1.1-6 and 4.3.1.1-7 show the internal forces and moment at the point of the connection throughout the duration of the test. The connection resisted applied forces through flexural resistance up to approximately 0.07 radians. After that point, the flexural resistance decreased and catenary action took over. The catenary action caused plastic deformation in bolts and the stem of the WT. The axial load within the connection quickly accrued, but as it, did the increase in rotation diminished.

The value for maximum moment in the connections was averaged from the top 1% of maximum moment measured. Thus, the maximum moment is 11.65 kip-ft in the left WT and 12.74 kip-ft in the right WT. These moments are approximately 4.5% of the plastic moment capacity of the W18×35 beam. The maximum moment occurred between 0.06 and 0.08 radians of beam rotation. The maximum axial force in the WT was 42.04 kips in the left WT and 41.54 kips in the right WT. The maximum applied shear to each side was 5.90 kips. Note that the maximum magnitudes occurred at different rotation magnitudes.

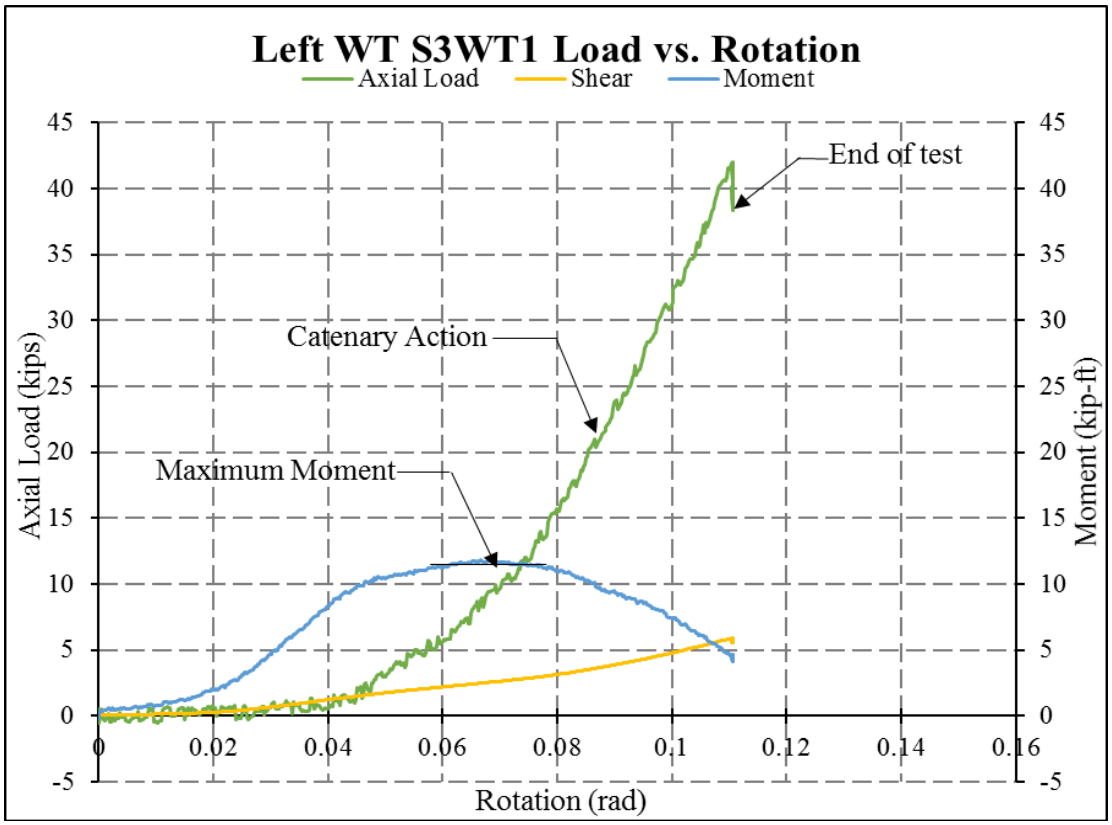

Figure 4.3.1.1-6: Left WT S3WT1 Load versus Rotation.

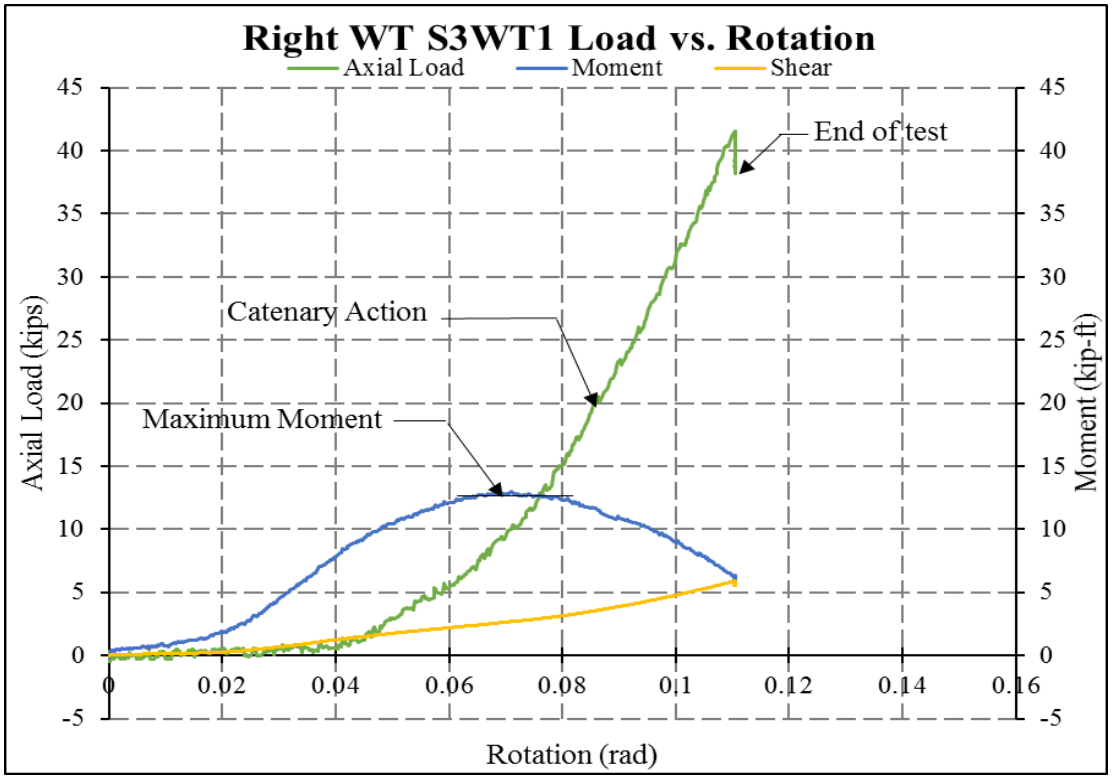

Figure 4.3.1.1-7: Right WT S3WT1 Load versus Rotation.

4.3.1.2 D3WT2 Dynamically Loaded Test

This was the first dynamic test run of the three-bolt configuration. It was also the first test that had bolts break. This test used one shim plate under the connection from the column stub to the actuator. Prior to commencing the test, the actuator was used to pull the test specimen down approximately 1.25 in., as seen in Figure 4.3.1.2-1. The full stroke of the actuator (ten inches) was reached in four seconds. During this test, the bottom bolt and the middle bolt broke on the left WT. The post-test configuration can be seen in Figure 4.3.1.2-2 and bolts after testing in Figure 4.3.1.2-3.

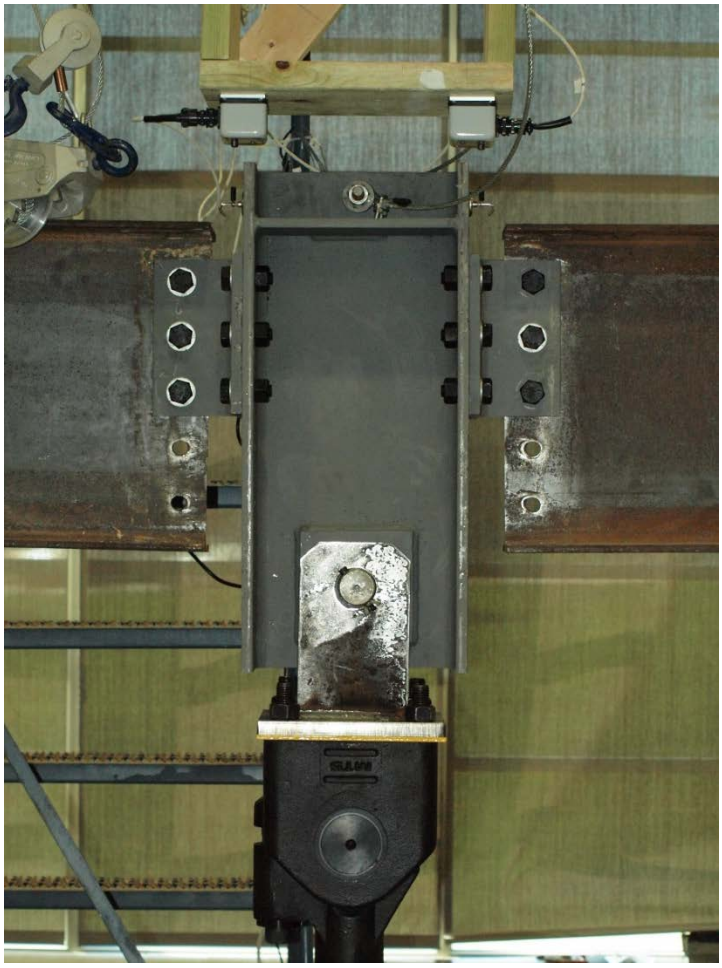

Figure 4.3.1.2-1: D3WT2 Pre-Test Position.

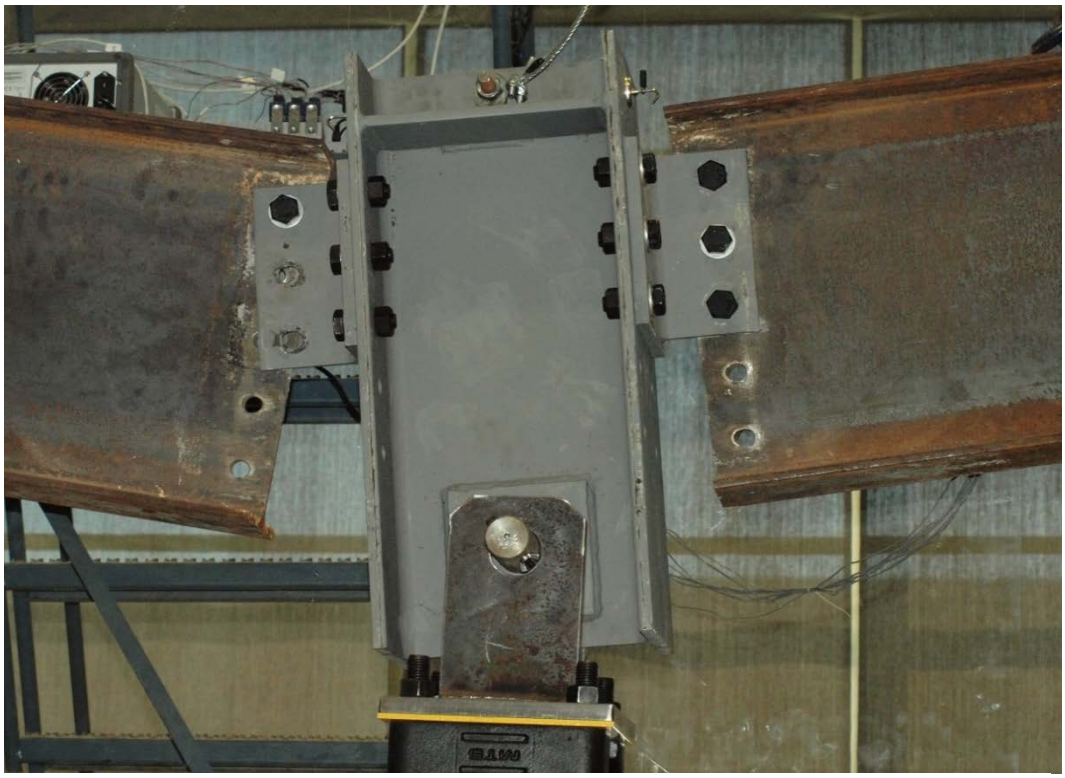

Figure 4.3.1.2-2: D3WT2 Post-Test Position.

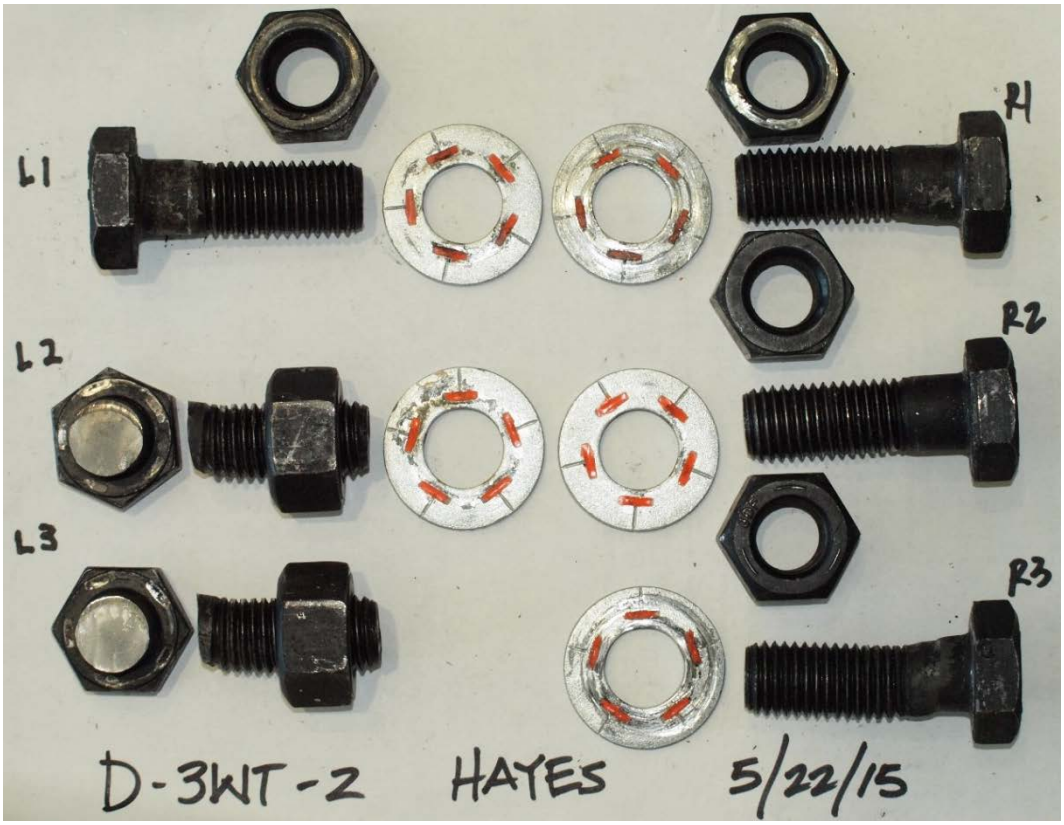

Figure 4.3.1.2-3: D3WT2 Bolts After the Test.

Figures 4.3.1.2-4 and 4.3.1.2-5 show the internal forces and moment at the point of the connection throughout the duration of the test. At approximately 0.09 radians, the flexural resistance of the connection decreased and the catenary action takes over. The catenary action causes plastic deformation in bolts and the stem of the WT. The axial load significantly increased with a small amount of additional rotation accruing until the bottom bolt on the left WT broke. At this point, the system loses approximately 10 kips in axial load and 2 kips in applied shear. The connection then reengages and accumulates applied and axial load with the system resisting these forces through catenary action. Once the first bolt breaks, the column stub begins to rotate, so the measured rotations no longer are the same between the two graphs. When the middle bolt on left WT breaks, the shear and axial load in the system significantly decreases and the column stub undergoes more pronounced rotation. Once again, the system reengages and picks up a little more load before the end of the test.

The value for maximum moment in the connections was averaged from the top 1% of maximum moment measured. The maximum moment range occurs before the first bolt break. The maximum moment is 14.64 kip-ft in the right WT and 15.31 kip-ft in the left WT. These moments represent approximately 5.5% of the plastic moment capacity of the W18×35 beam. The maximum moment occurred between 0.07 and 0.09 radians of beam rotation. The first bolt broke at an internal axial force of 27.9 kips and at approximately 0.11 radians of rotation. The second bolt broke at a maximum axial force of 42.02 kips and 41.87 at the left WT and right WT, respectively. Each WT had an applied shear of 4.35 kips.

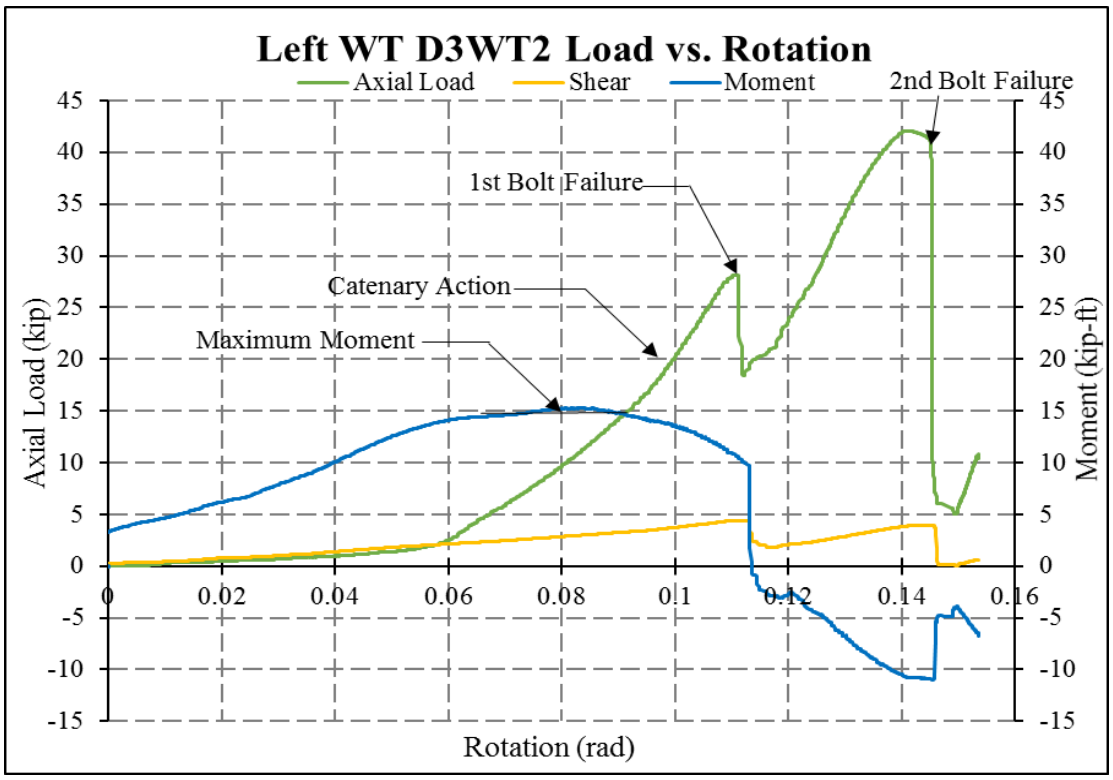

Figure 4.3.1.2-4: Left WT D3WT2 Load versus Rotation.

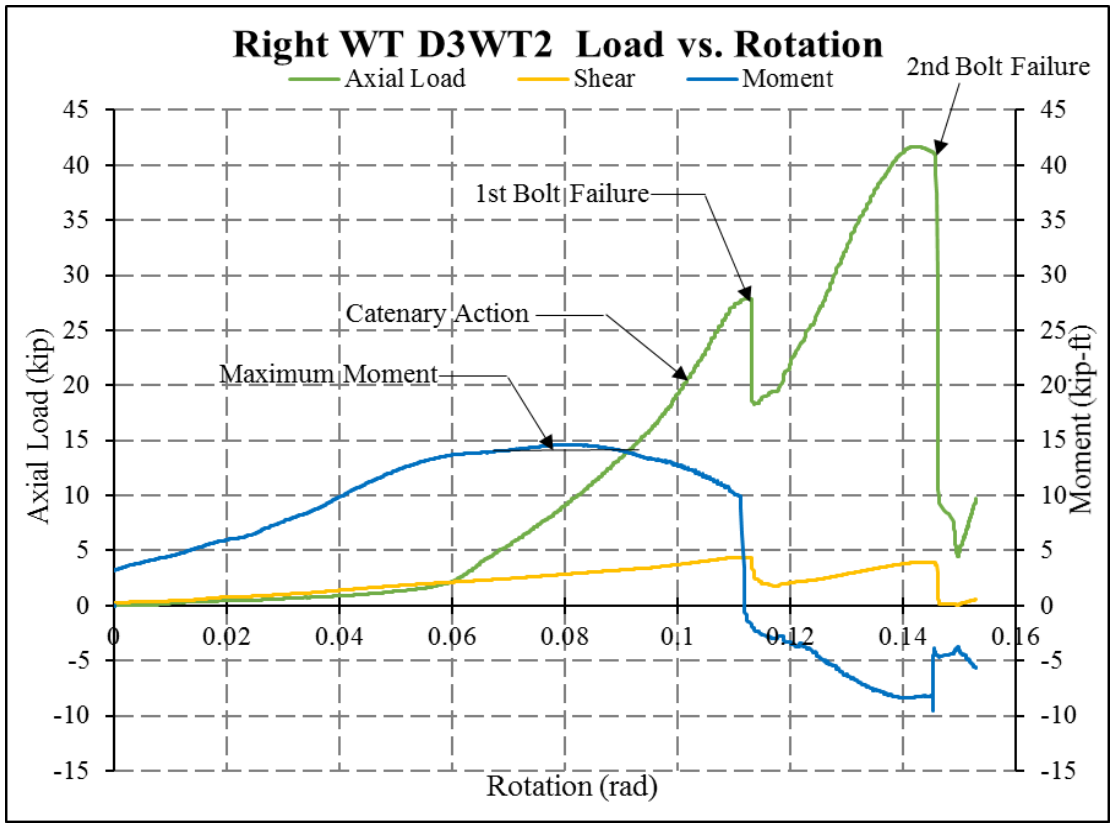

Figure 4.3.1.2-5: Right WT D3WT2 Load versus Rotation.

4.3.1.3 D3WT3 Dynamically Loaded Test

This was the second dynamic test run with the three-bolt configuration and also used one shim plate under the connection from the column stub to the actuator. Prior to commencing the test, the test assembly was pulled down approximately 1.25 in. in order to put the actuator pin through the column stub. The pre-test configuration can be seen in Figure 4.3.1.3-1. Like D3WT2, this test was pulled at the rate ten inches in four seconds. The bottom bolt in the left WT broke during the experiment. The post-test configuration and bolts can been seen in Figures 4.3.1.3-2 and 4.3.1.3-3, respectively.

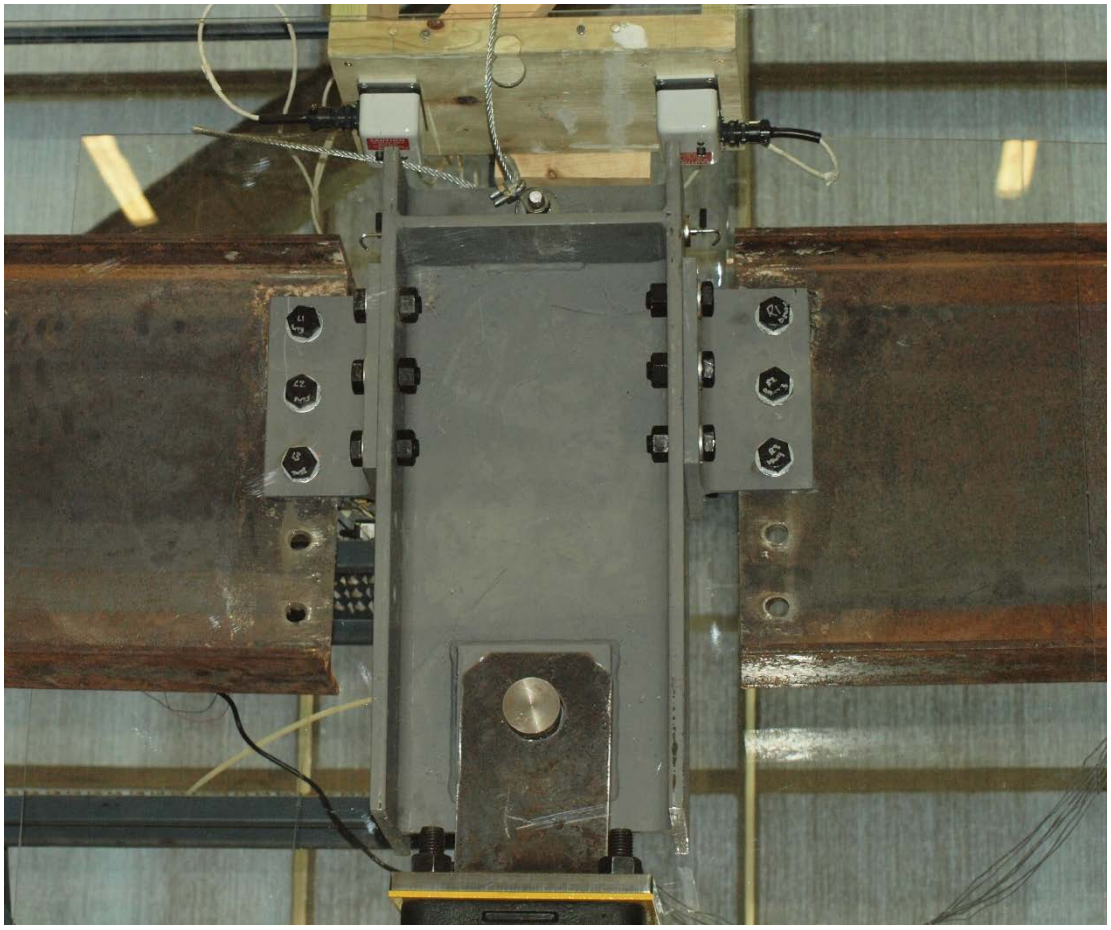

Figure 4.3.1.3-1: D3WT3 Pre-Test Position.

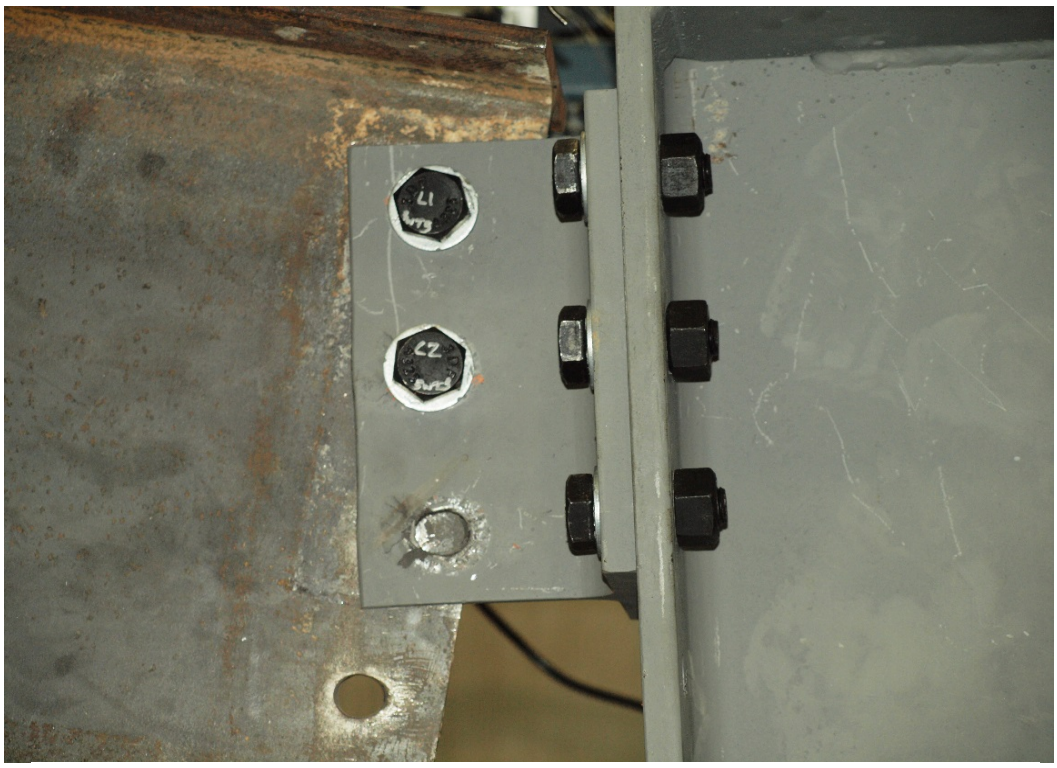

Figure 4.3.1.3-2: D3WT3 Post-Test, Enlarged View of Left WT.

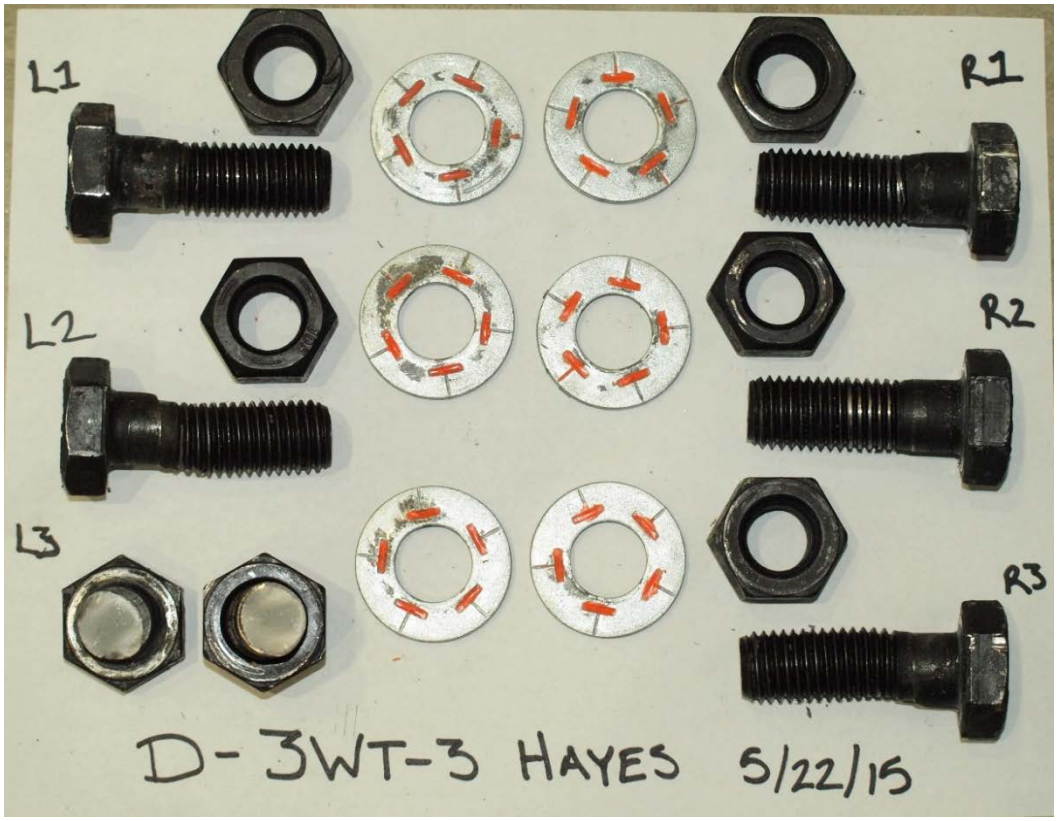

Figure 4.3.1.3-3: D3WT3 Bolts After Testing.

Figures 4.3.1.3-4 and Figure 4.3.1.3-5 show the internal forces and moment at the point of the WT connections throughout the duration of the test. The flexural resistance decreases at approximately 0.09 radians, at which point catenary action dominates. Catenary action quickly increases the axial load in the system without significant additional rotation in the test assembly. The bottom bolt fractured at the left WT at a beam rotation of approximately 0.10 radians. With that bolt break, the system lost approximately 10 kips in axial force and about 2 kips in shear. The connection then reengaged and quickly accrued axial force and shear with the connection resisting those forces through catenary action.

The magnitude of maximum moment in the connections was averaged from the top 1% of maximum moment measured. The maximum moment range occurs before the first bolt break, between approximately 0.06 to 0.75 radians. The maximum moment is 16.33 kip-ft in the left WT and 16.43 kip-ft in the right WT. These moments represent approximately 5.9% of the plastic moment capacity of the W18×35 beam. The bolt broke at an axial force of 21.2 kips. The end of the test was nearing another bolt break, and the axial forces were 41.2 kips and 41.5 kips in the left and right WT, respectively. The maximum shear force in the WT was not realized until the end of test, and was 4.2 kips to each WT.

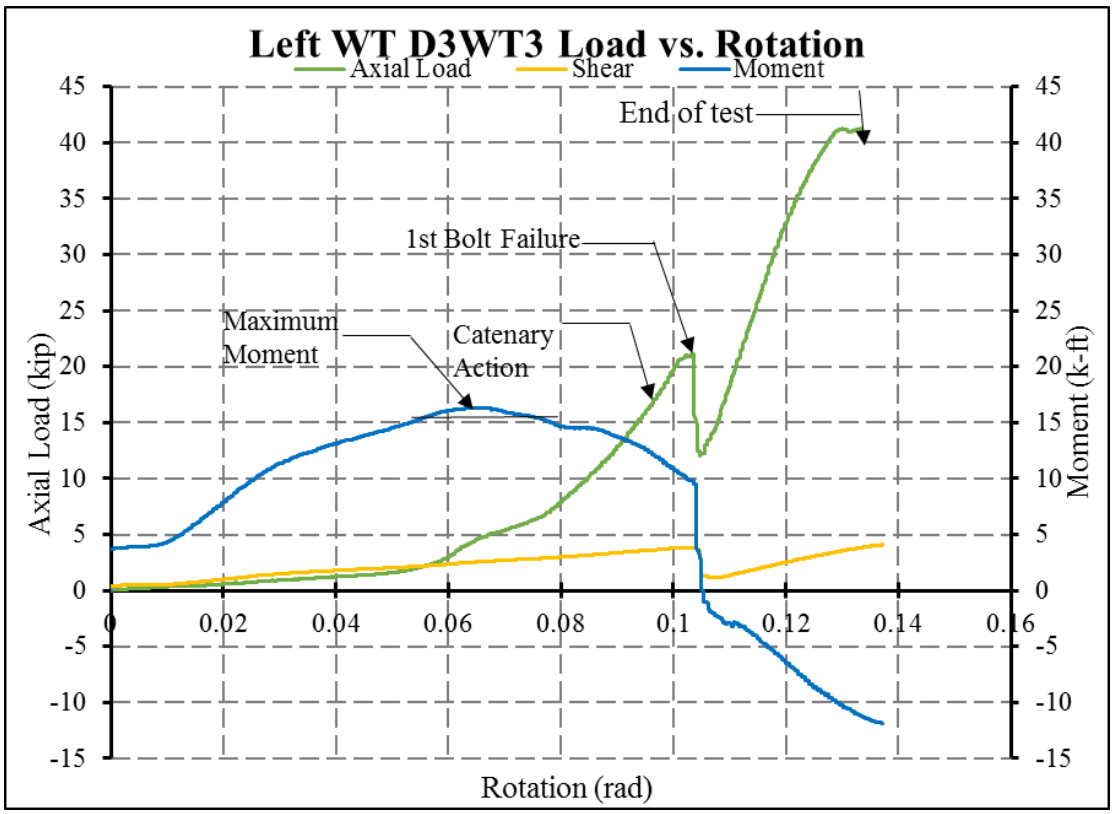

Figure 4.3.1.2-5: Left WT D3WT3 Load versus Rotation.

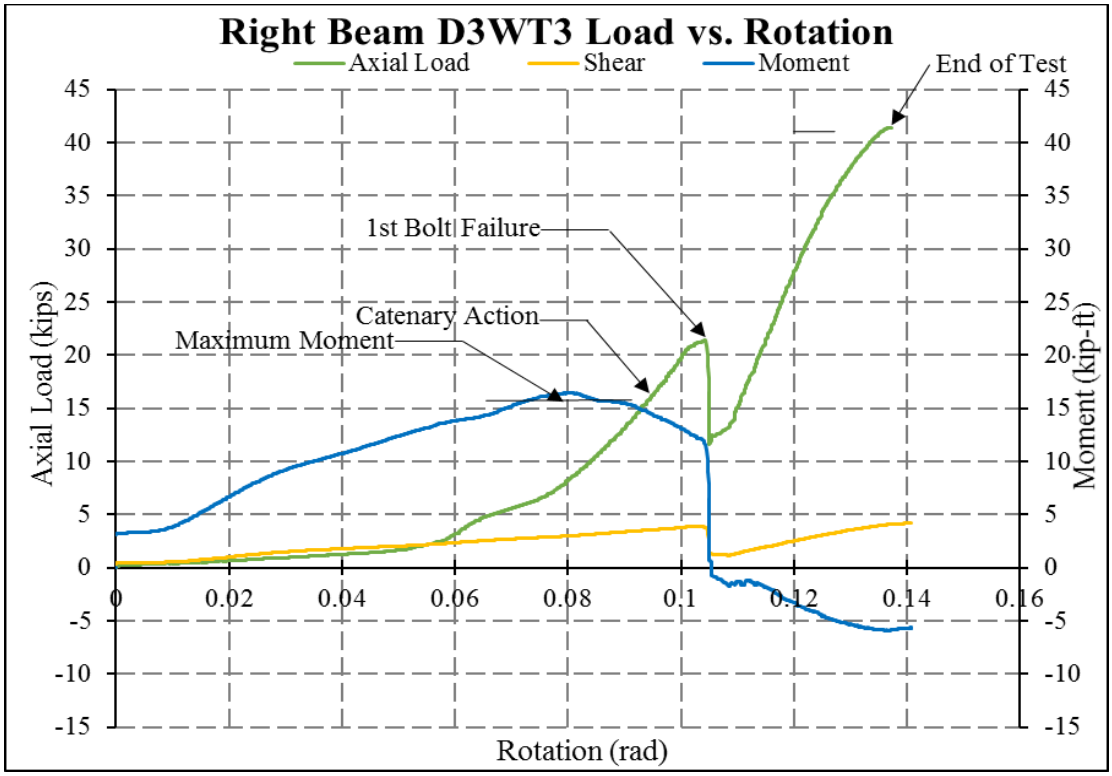

Figure 4.3.1.3-5: Right WT D3WT3 Load versus Rotation.

4.3.1.4 D3WT4 Dynamically Loaded Test

D3WT4 was the third and final dynamic test of the three-bolt configurations. This test was run at a later date than the first three tests. D3WT4 used one shim plate under the connection from the column stub to the actuator. Prior to commencing the test, the assembly was pulled down approximately 1.25 in. in order to insert the actuator pin into the column stub. The pre-test position can be seen in Figure 4.3.1.4-1. Since it was run at a later date, a different lot of bolts was used. These bolts proved stronger than those used in earlier tests, and D3WT4 showed the highest strength and the bolts did not break. The post-test position of the system is seen in Figure 4.3.1.4-2 through Figures 4.3.1.4-4, and the post-test condition of the bolts is seen in Figure 4.3.1.4-5.

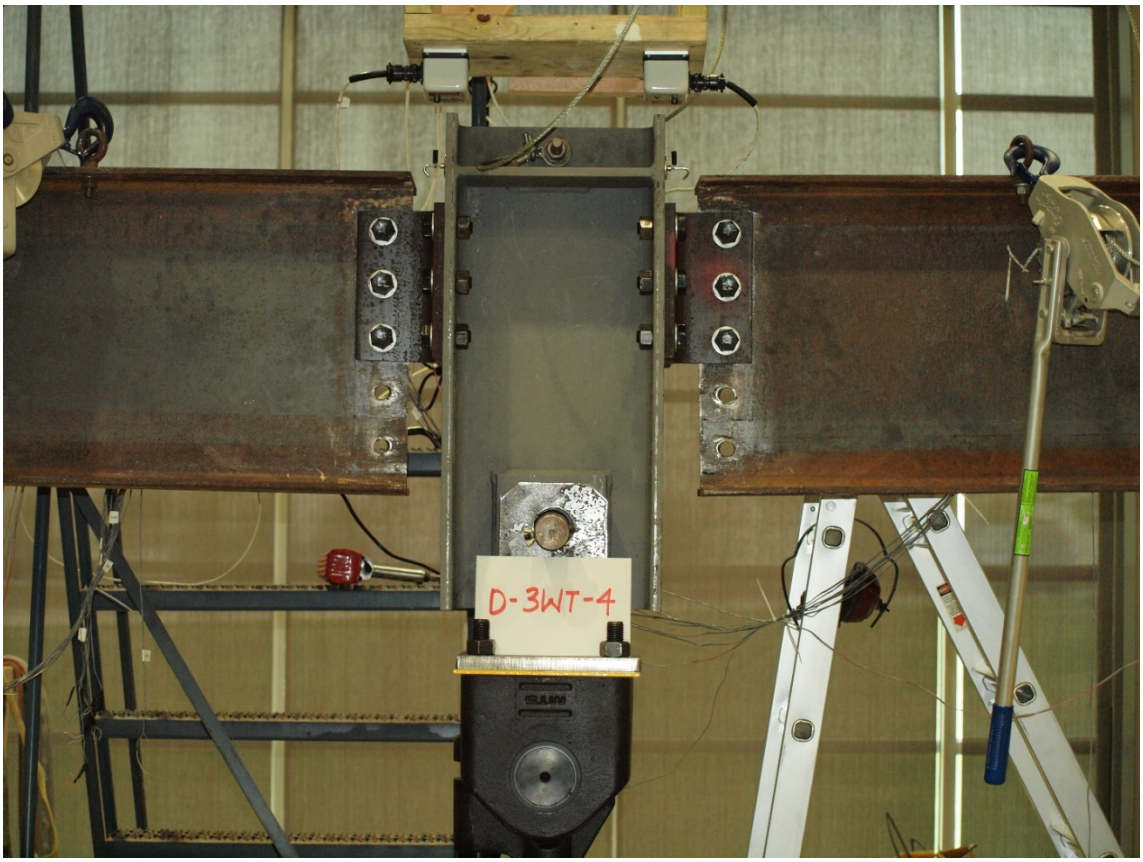

Figure 4.3.1.4-1: D3WT4 Pre-Test Position.

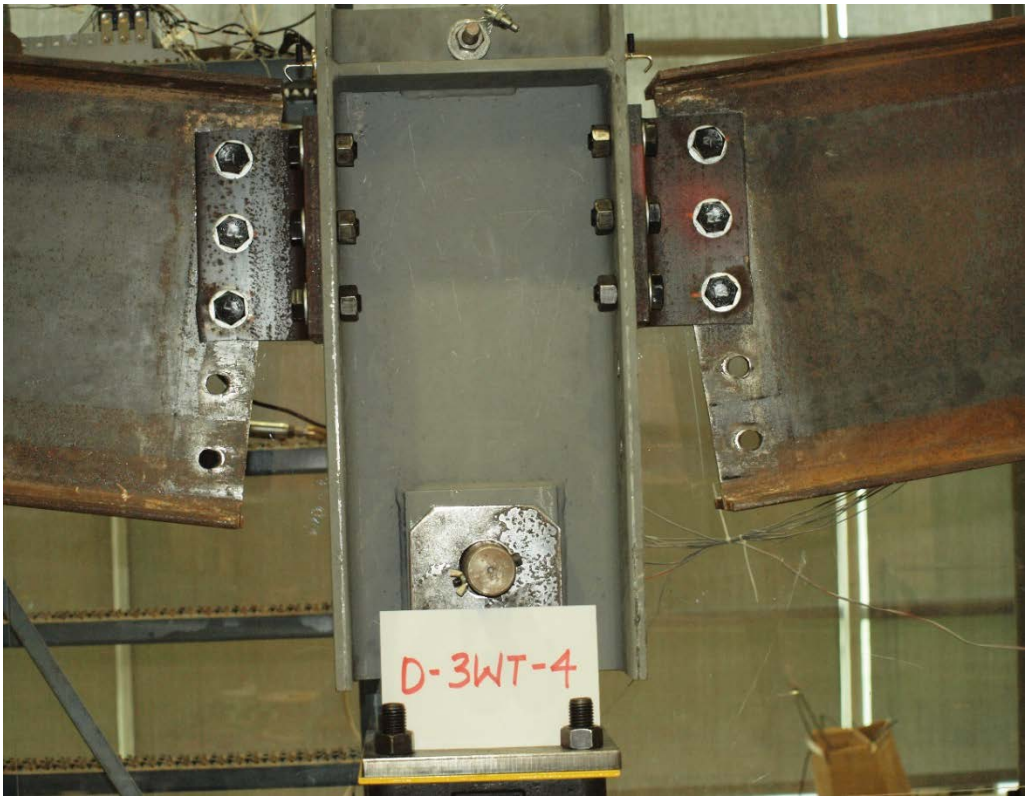

Figure 4.3.1.4-2 D3WT4 Post-Test Position.

Figure 4.3.1.4-3: D3WT4 Left WT After Testing.

Figure 4.3.1.4-4: D3WT4 Right WT After Testing.

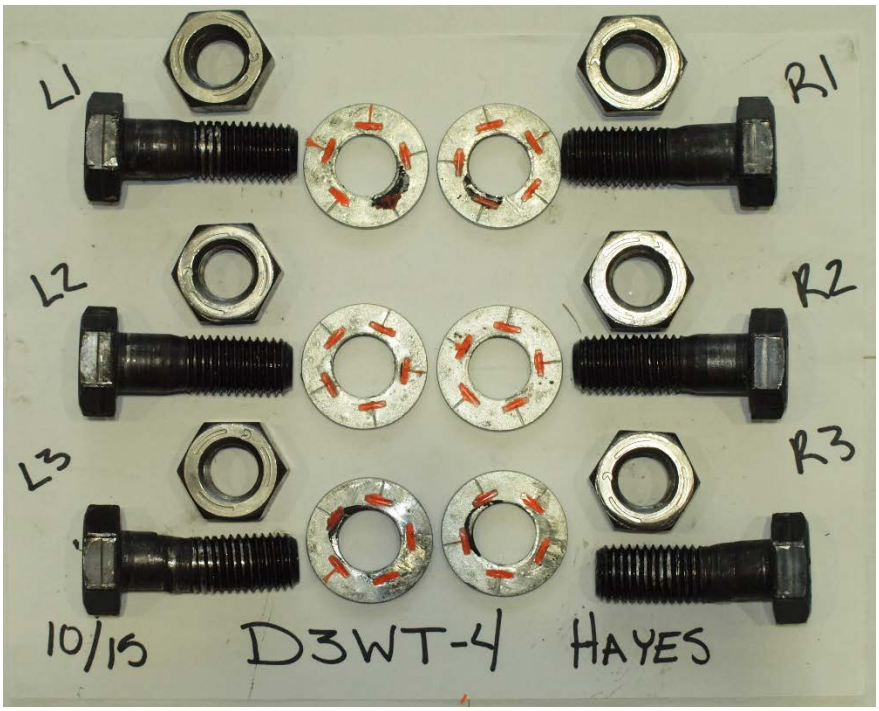

Figure 4.3.1.4-5: D3WT4 Bolts After Testing.

The force and moment versus rotation graphs for the D3WT4 connection can be seen in Figure 4.3.1.4-6 and Figure 4.3.1.4-7. The flexural resistance of the connection decreases at approximately 0.09 radians. At that point, catenary action begins to control and is maintained until the end of the test. D3WT4 did not break any bolts, which was uncommon for a dynamically loaded test. D3WT4 had the axial capacity 50% more than the rest of the three-bolt configurations. This is attributed to a different lot of bolts being purchased for this test.

The top 1% of the measured moments for test D3WT4 falls within the range 0.06 to 0.08 radians. The left WT measured a maximum moment of 16.35 kip-ft and the right WT measured a maximum moment of 16.89 kip-ft, which are approximately 6% of the plastic moment capacity of the W18×35. The maximum axial force seen in the test system was 57.67 kips and 57.13 kips in the left and right, respectively. The maximum of applied shear force in each WT was 7.65 kips.

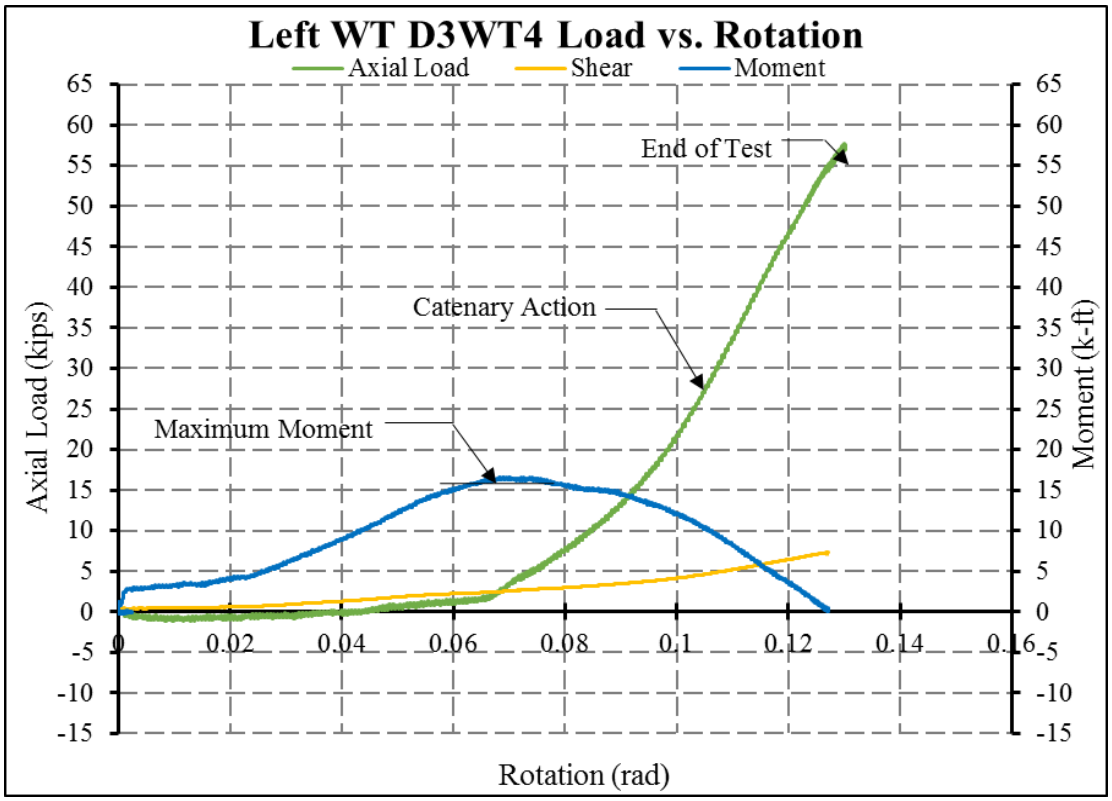

Figure 4.3.1.4-6: Left WT D3WT4 Load versus Rotation.

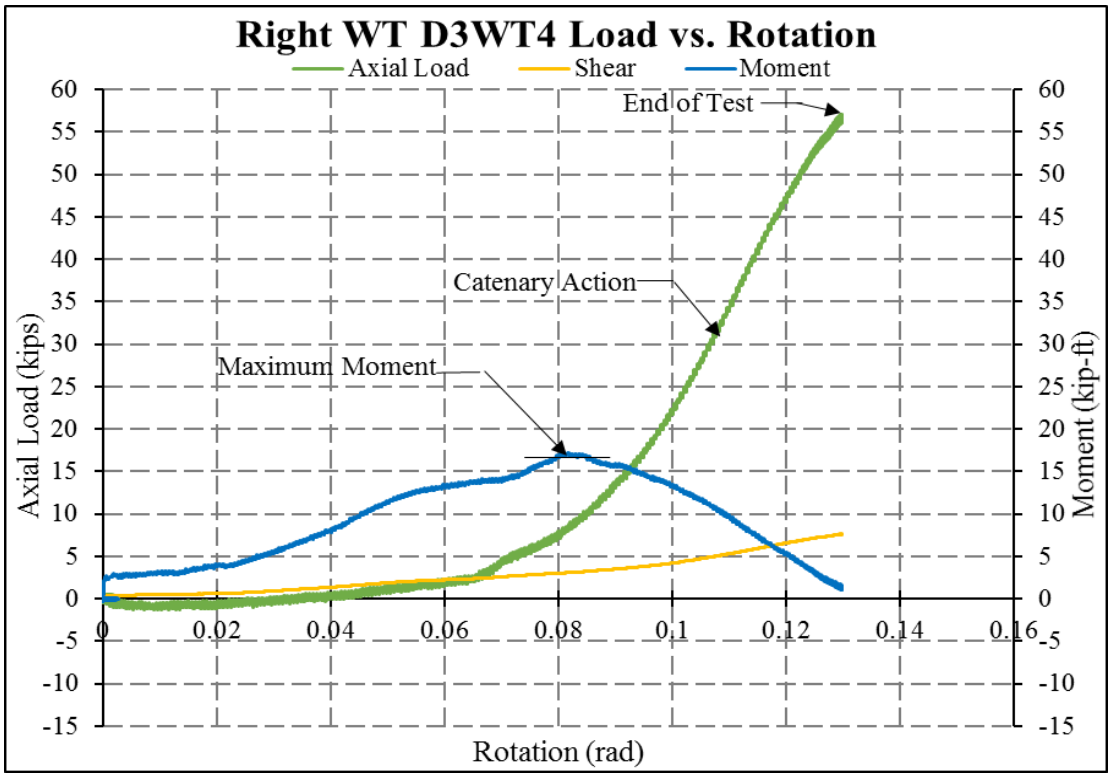

Figure 4.3.1.4-7: Right WT D3WT4 Load versus Rotation.

4.3.1.5 3WT Test Summary

A left WT comparison of a typical dynamic test to the static test is illustrated in Figure 4.3.1.5-1. This figure has been manually shifted to match the zero point described in Section 4.2.1. This graph clearly shows that the dynamically loaded test breaks with less rotation than the statically loaded test. It should be noted that even though D3WT4 had higher strength, the trend of catenary action being the main resistance of applied force is consistent with other dynamic tests.

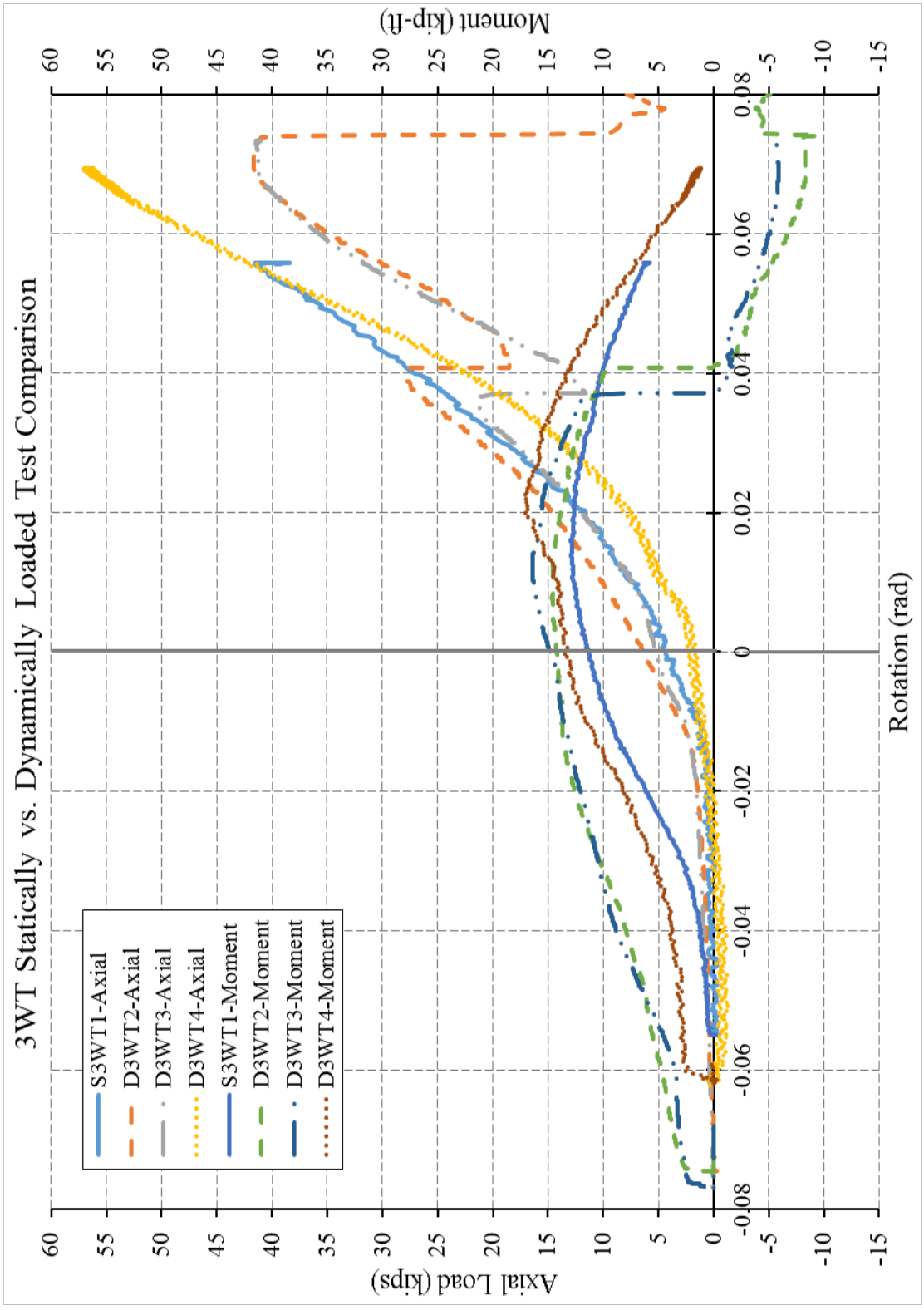

Figure 4.3.1.5-1: 3WT Statically versus Dynamically Loaded Tests.

Table 4.3.1.5-1 compares the test values at the first bolt break in all four 3WT tests. Though S3WT1 and D3WT4 did not break a bolt, they were included to keep with the consistency of the tables. These values were calculated using the procedure described in Section 4.2.1. This table shows the rotation, the applied shear, the measured axial force and moment to the left and right WT, respectively. The initial failures can be seen as the critical point after which the test specimen lost significant loading carrying capacity.

Table 4.3.1.5-1: Connection Forces of the Four 3WT Test Specimens at 1st Bolt Failure.

Test	Left WT				Right WT			
	Rotation (rad)	Applied Shear (kips)	Measured Axial (kips)	Measured Moment (kip-feet)	Rotation (rad)	Applied Shear (kips)	Measured Axial (kips)	Measured Moment (kip-feet)
S3WT1	NA							
D3WT2	0.11	4.20	27.90	9.71	0.11	4.20	22.51	4.07
D3WT3	0.10	3.73	21.46	11.64	0.10	3.73	15.51	3.53
D3WT4	NA							

Table 4.3.1.5-2 compares the second bolt failure in the test specimens. This is similar to the first bolt failure table as it is comparing rotation, applied shear, measured axial force and moment in the left and right WT, respectively. Only the first dynamic test, D3WT2, broke a second bolt.

Table 4.3.1.5-2: Connection Forces for the Four 3WT Connections at the 2nd Bolt Failure.

Test	Left WT				Right WT			
	Rotation (rad)	Applied Shear (kips)	Measured Axial (kips)	Measured Moment (kip-feet)	Rotation (rad)	Applied Shear (kips)	Measured Axial (kips)	Measured Moment (kip-feet)
S3WT1	NA							
D3WT2	0.14	3.87	41.62	-8.35	0.13	3.87	41.99	-10.78
D3WT3	NA							
D3WT4	NA							

As noted previously, the estimated maximum moment was taken from the average of top 1% of the measured moments. The range of data for axial force and shear force corresponding to the top 1% moment was used to calculate connection force. These forces can seen in Table 4.3.1.5-3.

Table 4.3.1.5-3: Connection Forces for the Four 3WT Connection at the Top 1% Measured Moment.

Test	Left WT				Right WT			
	Rotation (rad)	Applied Shear (kips)	Measured Axial (kips)	Measured Moment (kip-feet)	Rotation (rad)	Applied Shear (kips)	Measured Axial (kips)	Measured Moment (kip-feet)
S3WT1	0.07	2.53	8.93	11.66	0.07	2.53	8.55	12.74
D3WT2	0.08	2.93	9.97	14.58	0.08	2.93	10.17	15.23
D3WT3	0.07	2.77	6.23	15.51	0.07	2.77	6.17	15.64
D3WT4	0.07	2.64	8.82	16.89	0.08	2.64	3.94	16.35

These forces are not at the point of bolt shear failure, but at the point which the bolts deformed and load began to be redistributed within the connection. Table 4.3.1.5-4 can be directly compared to the expected maximum bolt force from the *Guide to Design Criteria for Bolted and Riveted Joints* [25] of 35.4 kips. The percent difference that is shown in the table is the bottom (Bolt 3) versus the *Guide* value. All the values are within 6% of the *Guide's* value except for S3WT1. This is because, as mentioned previously, S3WT1 was not run to the actuator's full stroke, and no bolts approached shear rupture.

Table 4.3.1.5-4: Bolt Forces Found from Using ICOR in the 3WT Experimental Testing.

Test	Left				Right			
	Bolt 1 (kips)	Bolt 2 (kips)	Bolt 3 (kips)	% Difference from the Guide	Bolt 1 (kips)	Bolt 2 (kips)	Bolt 3 (kips)	% Difference from the Guide
S3WT1	22.04	3.18	27.92	21%	24.01	3.07	29.63	16%
D3WT2	28.84	3.61	35.51	0%	27.59	3.55	34.13	4%
D3WT3	30.91	2.44	34.93	1%	30.62	2.47	34.69	2%
D3WT4	32.17	1.45	34.76	2%	31.63	2.97	37.46	6%

4.3.2 Four-Bolt WT Tests

Four four-bolt tests were conducted: one being statically loaded and three being dynamically loaded. Similar to the three-bolt tests, S4WT1, D4WT2, and D4WT3 were tested at the same time and the bolts purchased for these tests were within the same lot. D4WT4 was tested at later date with a different lot of bolts. All the bolts met A325 standards, but as with the three-bolt tests, it was found that the second lot of bolts were stronger than the initial lot.

Bolts broke in all four tests, and interestingly all in the right WT. The following free-body diagram, shown in Figure 4.3.2-1, demonstrates the action of the bolts under combined loading. Since there is another bolt in each WT compared to the previous three-bolted WT connection, the four-bolted WT connections had a larger flexural capacity within the system. As described in the three-bolted WT, "compressive" and "tensile" forces are the shear forces due to the couple force from the moment, M, seen in Figure 4.3.2-1. The additional bolt decreased the amount of compression force applied to the top bolt because a second bolt exists above the centroid of the bolt configuration. Similarly, the bottom two bolts are handling the tension in connection. Since the axial force is also present, the bottom-most bolt will break because of the additive forces.

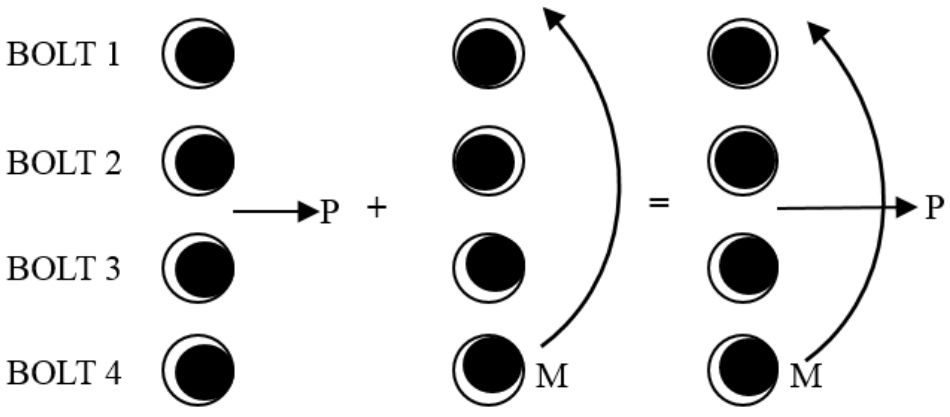

Figure 4.3.2-1: 4WT Bolt Locations Due to Loading.

4.3.2.1 S4WT1 Statically Loaded Test

S4WT1, as seen in Figure 4.3.2.1-1, was the first test run of the four-bolt WT tests. S4WT1 used one shim plate under the actuator connection and the column stub was pulled down 1.25 in. before the test began. S4WT1 was pulled down at a rate of ten inches in ten minutes. Three bolts in the right WT broke, as seen in Figure 4.3.2.1-2. The bolts after testing can be seen Figure 4.3.2.1-3.

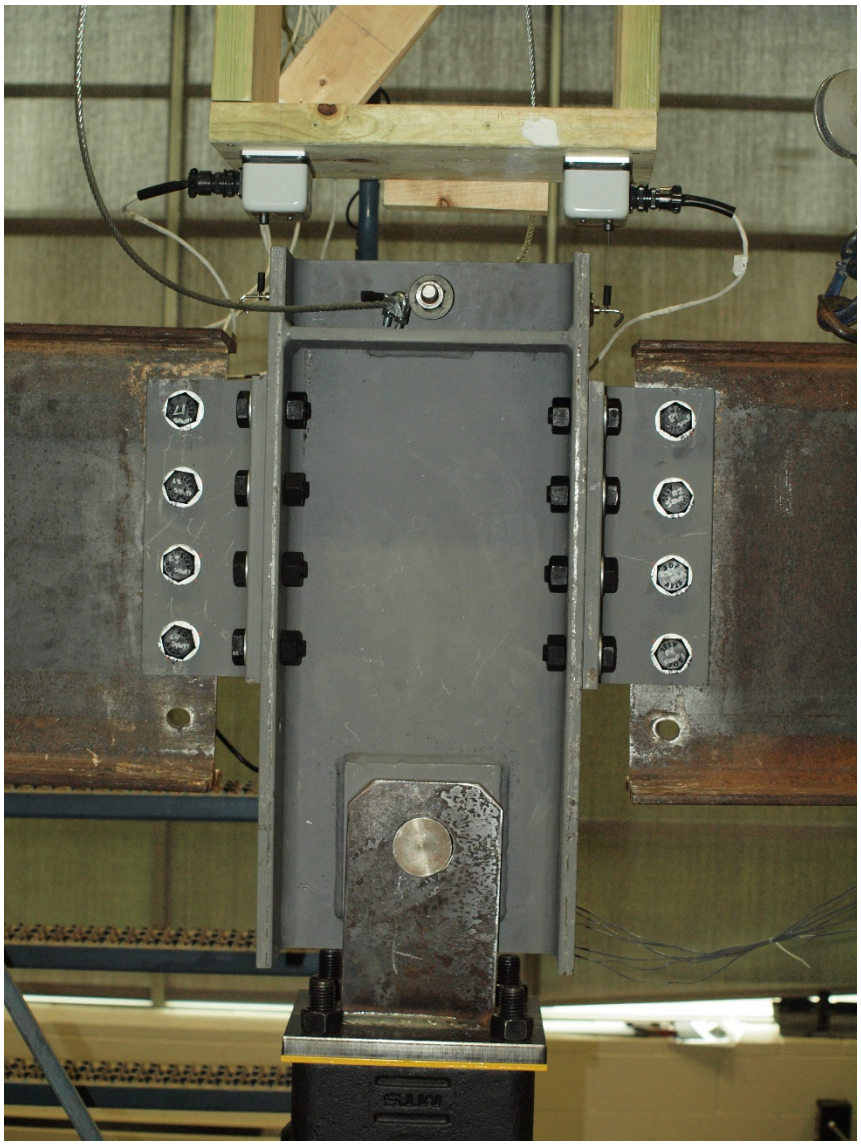

Figure 4.3.2.1-1: S4WT1 Pre-Test Position.

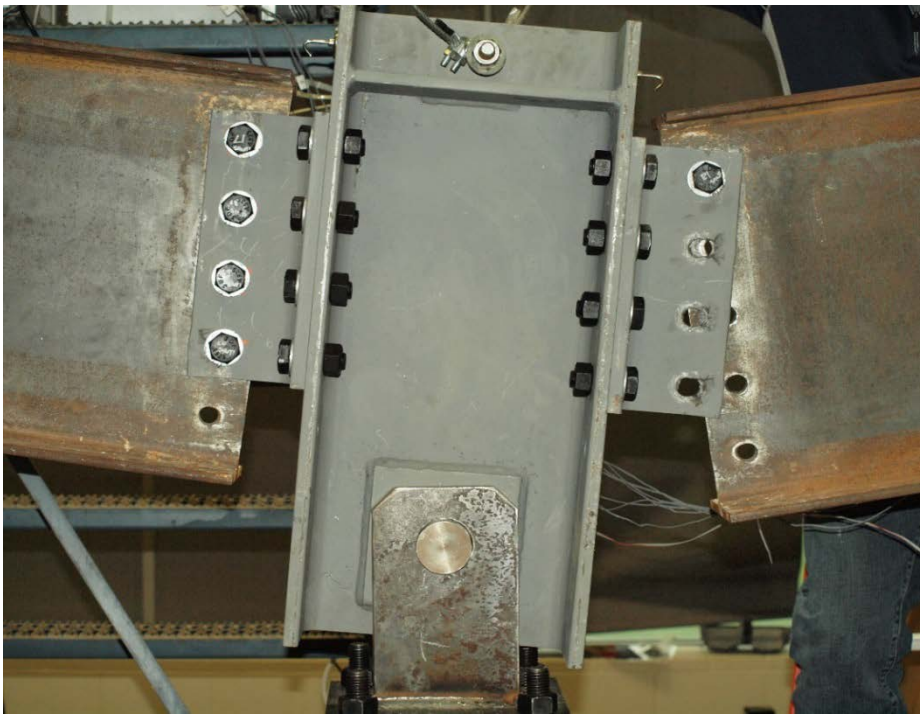

Figure 4.3.2.1-2: S4WT1 Post-Test Position.

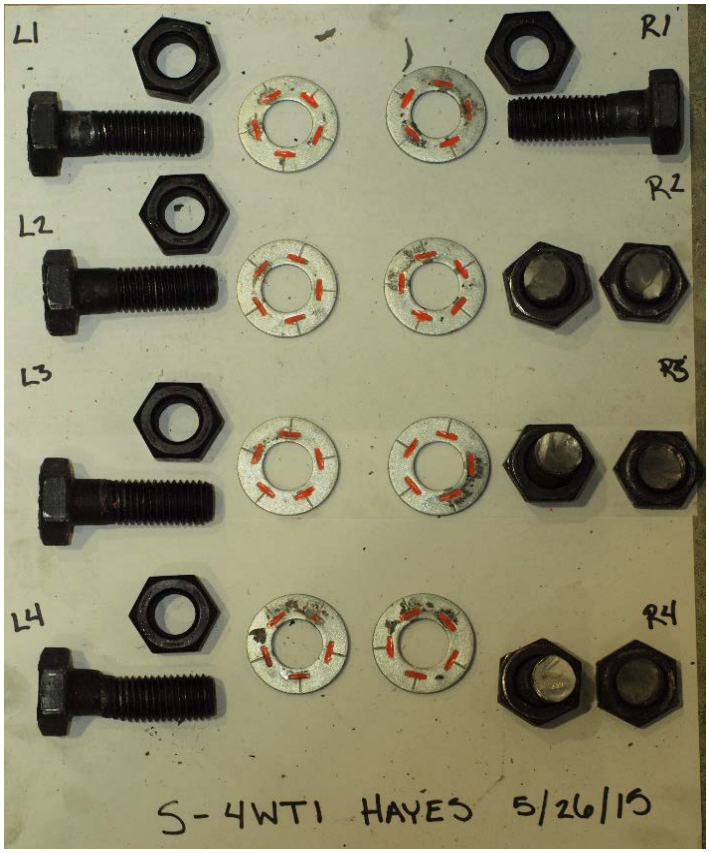

Figure 4.3.2.1-3: S4WT1 Bolts after Testing.

As stated before, the four-bolt WT connections have a larger flexural capacity than do the three-bolt WT. The following graphs, Figure 4.3.2.1-4 and Figure 4.3.2.1-5, show the forces within the connection throughout the duration of the test. As with the three-bolt tests, catenary action increased and eventually took over most of the resistance of the loading. However, unlike the three-bolt tests, the moment did not drop off significantly at the point of initial bolt fracture. After the first bolt break, the moment resistance dropped significantly and the catenary effects resisted the loading for the rest of the experiment. The first two bolts broke within 0.01 radians of each other. That is because the bottom of the beam was in tension and the bottom two bolts were responding to the combined tension forces due to axial and moment interaction. The third bolt broke 0.022 radians after the second, which doubles the amount of rotation seen between the first two bolt breaks.

The value for maximum moment was again averaged from the top 1% of measured moment. This was recorded between approximately 0.075 radians and 0.09 radians of beam rotation. The left WT had a maximum moment calculated at 28.73 kip-ft, which is 10.4% of the plastic moment capacity of W18×35. The right WT had maximum moment of 28.97 kip-ft, which is about 10% of the plastic moment capacity of the W18×35. The maximum axial force the WTs reached was 42.69 kips and 42.62 kips, left and right WT, respectively. The maximum shear force applied was 7.99 kips to each WT.

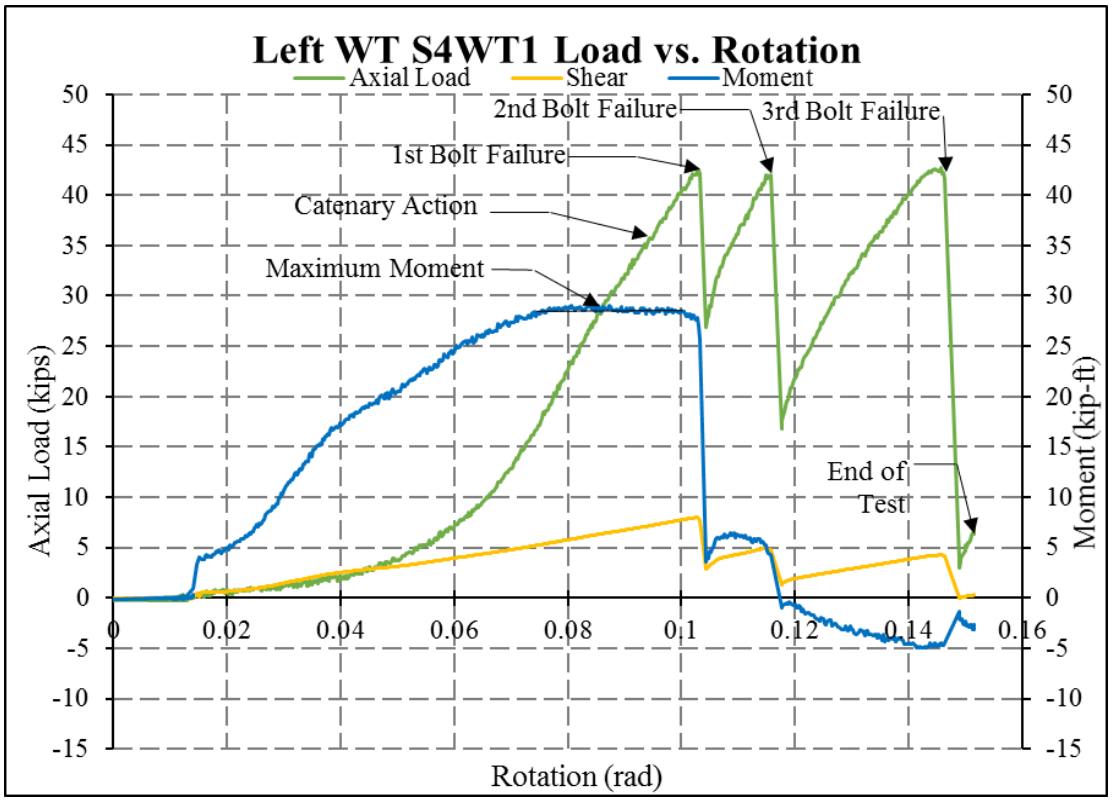

Figure 4.3.2.1-4: Left WT S4WT1 Load versus Rotation.

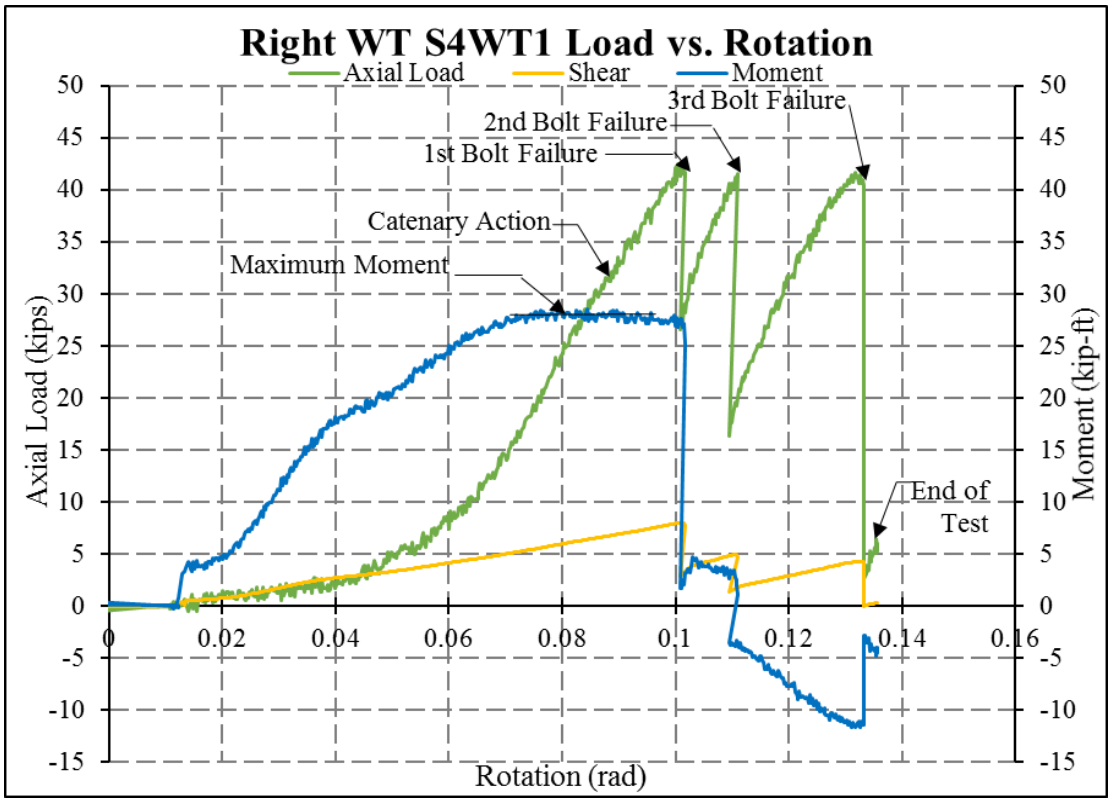

Figure 4.3.2.1-5: Right WT S4WT1 Load versus Rotation.

4.3.2.2 D4WT2 Dynamically Loaded Test

This was the first dynamically loaded test for the four-bolt WTs. It was loaded at a rate of ten inches in four seconds. This test used one shim plate and the actuator was used to pull the system down 1.25 in., as seen in Figure 4.3.2.2-1. D4WT2 had bands of data, so the original output was run through filters and the data quantity was reduced. During the test, three bolts in the right WT broke. The post-test position and bolts after testing can be seen in Figure 4.3.2.2-2 and 4.3.2.2-3.

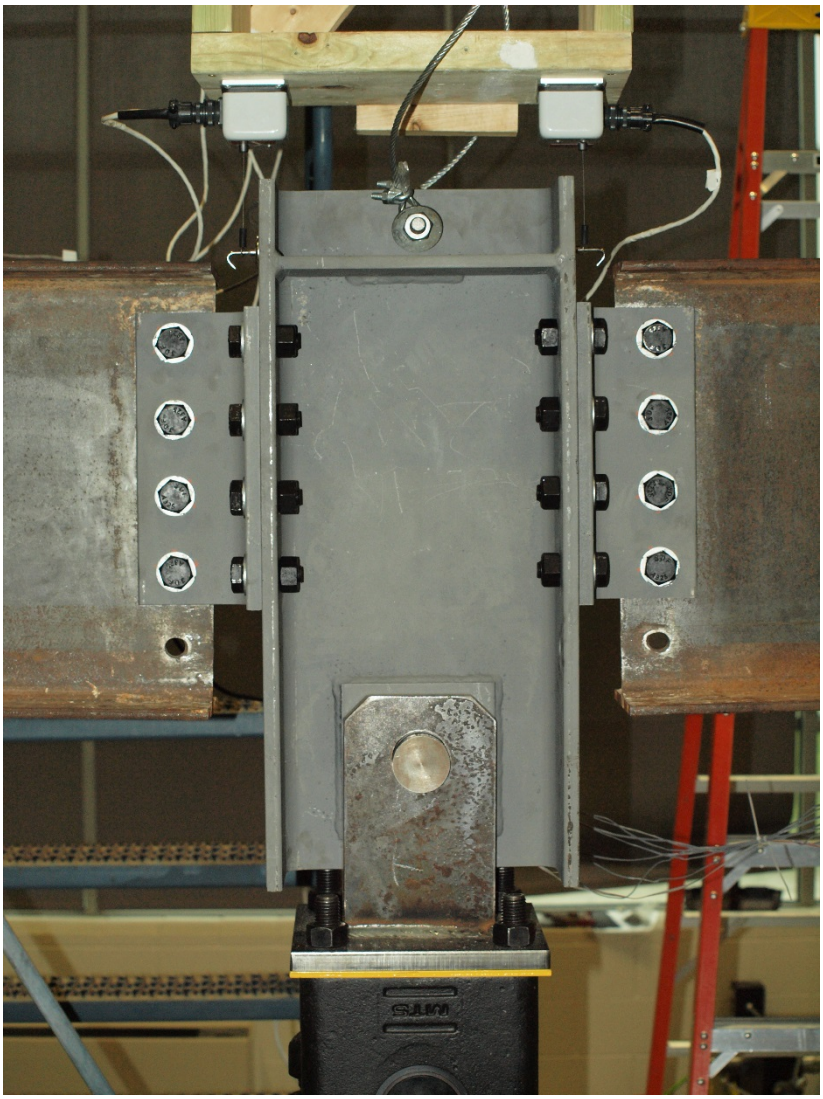

Figure 4.3.2.2-1: D4WT2 Pre-Test Position.

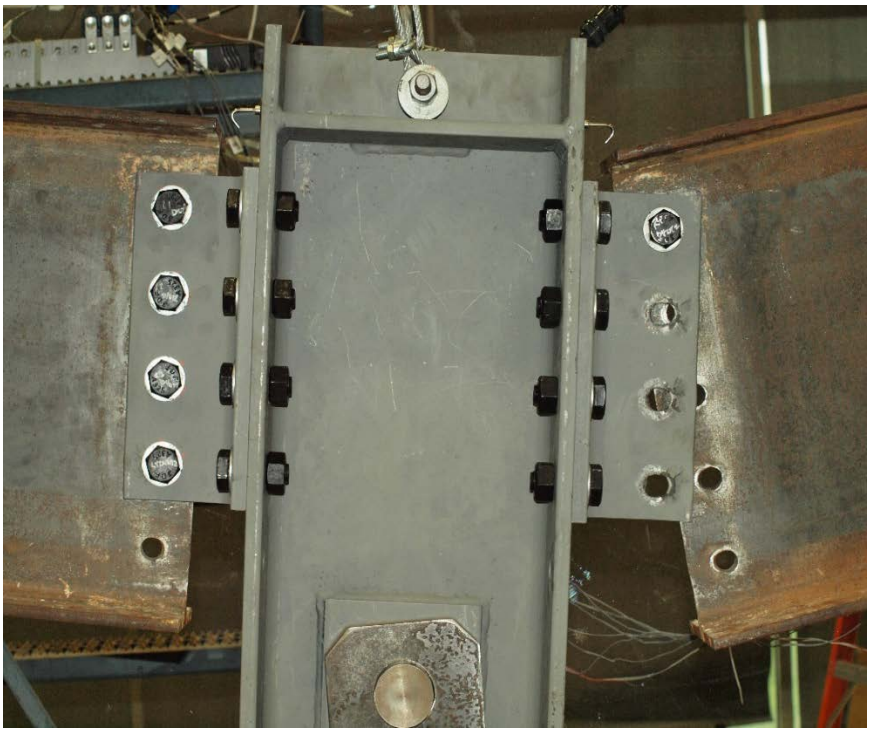

Figure 4.3.2.2-2: D4WT2 Post-Test Position.

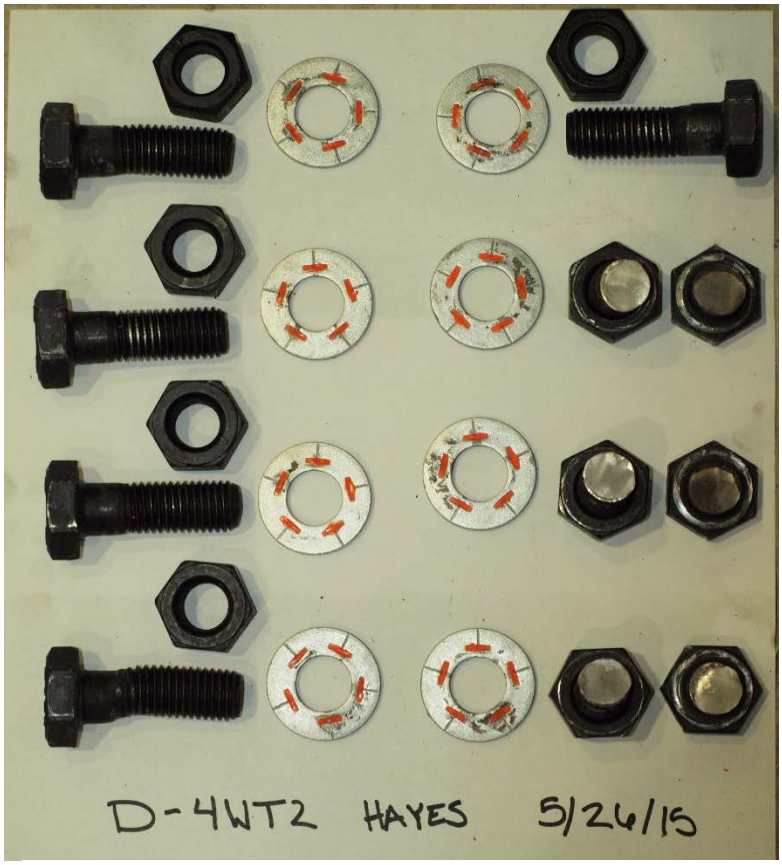

Figure 4.3.2.2-3: D4WT2 Bolts after Testing.

Figure 4.3.2.2-4 and Figure 4.3.2.2-5 shows the internal forces and moment at the point of the connection throughout the test. Similar to S4WT1, the moment did not decrease significantly prior to initial bolt fracture, even as the axial forces increased and resisted most the load. After that, the moment resistance dropped significantly. Two bolts broke within 0.02 radians of each other, while the third bolt broke at the end of the test, approximately 0.03 radians after the second. It is interesting to note that the last bolt to break had the largest axial load associated with it. Again, this had to do with the moment at the connection and the fact that the top two bolts were in compression and the bottom bolts were in combined axial tension and tension due to moment.

The value for maximum moment was averaged from the top 1% of measured moment, and was recorded between approximately 0.07 radians and 0.085 radians of beam rotation. The left WT had a maximum moment of 27.0 kip-ft, which is 9.8% of the plastic moment capacity of the W18×35, while the right WT had maximum moment of 29.32 kip-ft, which is 10.6% of the plastic moment capacity. The maximum axial force the WTs reached was 42.09 kips and 40.92 kips, left and right WT, respectively. The maximum shear force applied was 7.22 kips to each WT.

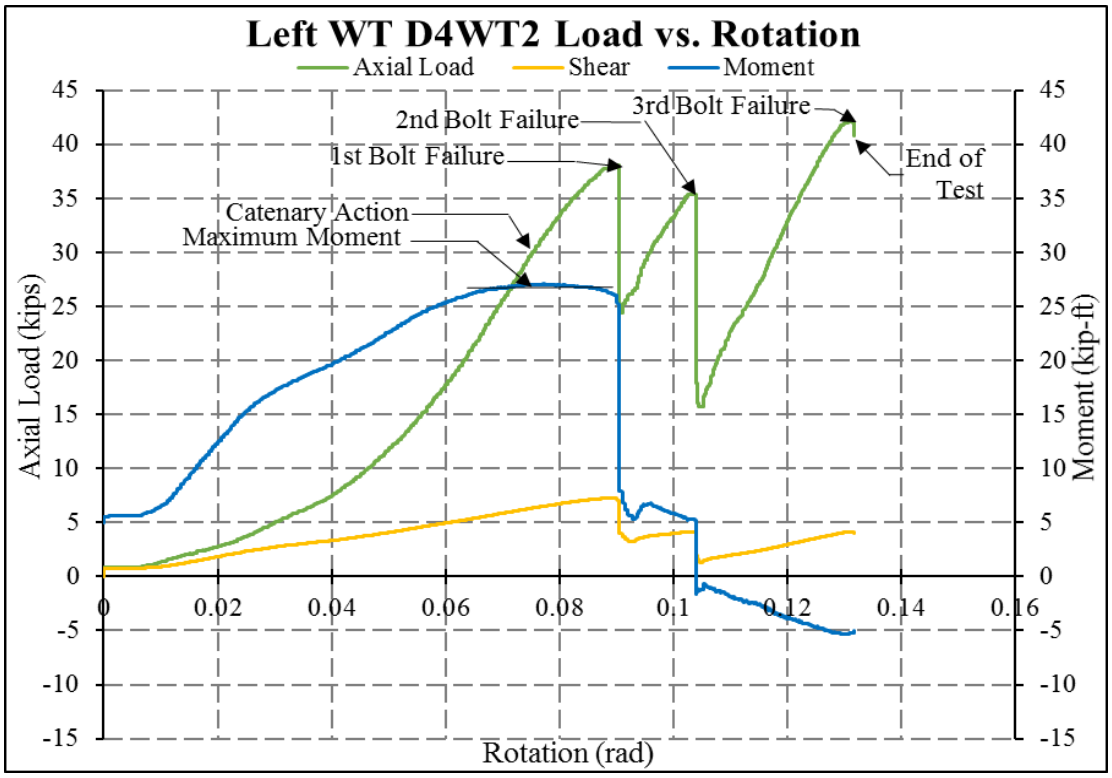

Figure 4.3.2.2-4: Left WT D4WT2 Load versus Rotation.

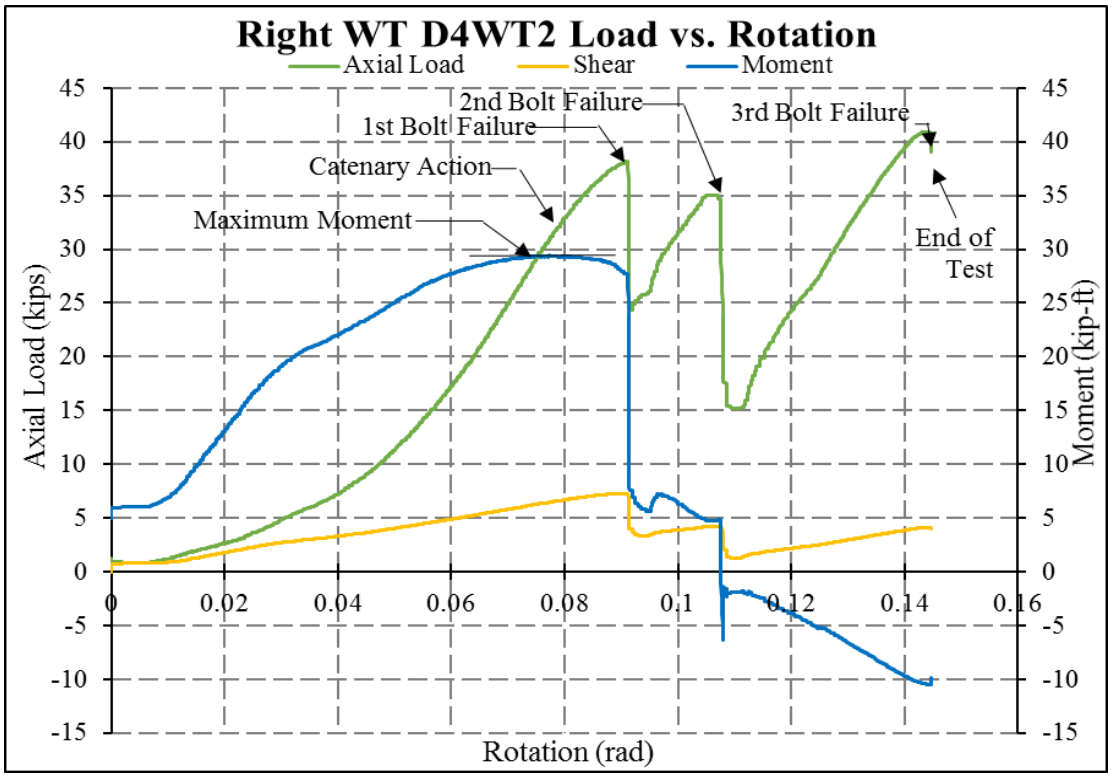

Figure 4.3.2.2-5: Right WT D4WT2 Load versus Rotation.

4.3.2.3 D4WT3 Dynamically Loaded Test

D4WT3 is the second dynamically loaded test using the four-bolt configuration. The column stub was pulled down at a rate of ten inches in four seconds. In Figure 4.3.2.3-1, it can be seen that one shim plate was used under the actuator connection; thus, the test specimen was pulled down 1.25 in. before the test was run. Three bolts broke in the right WT during this test, which can be seen in the post-test configuration in Figure 4.3.2.3-2 and post-test bolts in Figure 4.3.2.3.

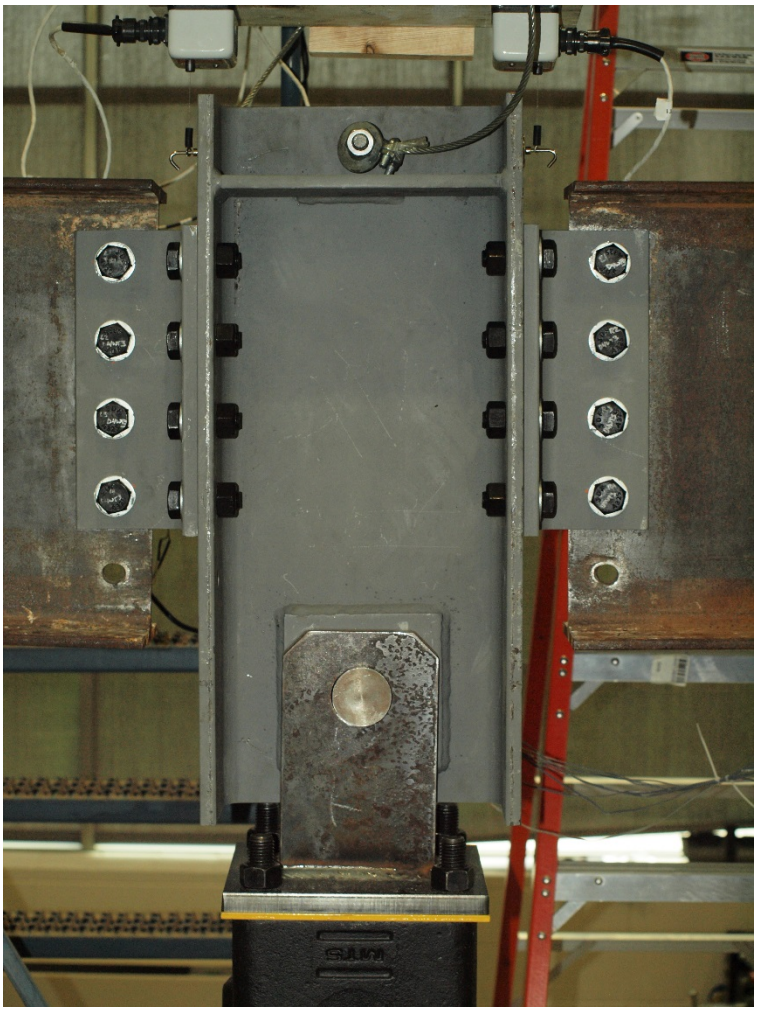

Figure 4.3.2.3-1: D4WT3 Pre-Test Position.

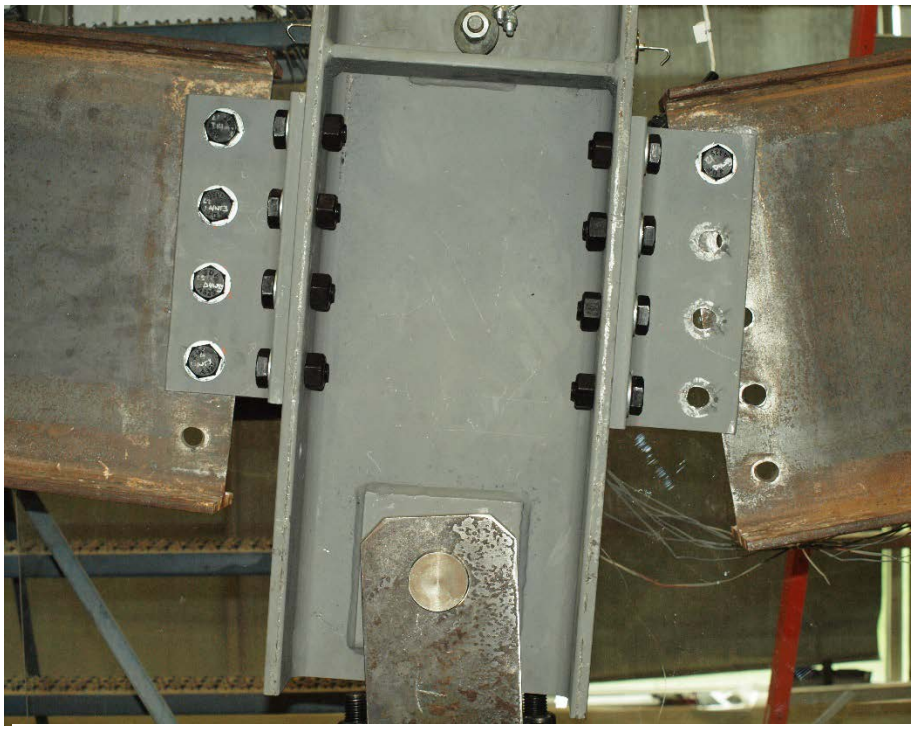

Figure 4.3.2.3-2: D4WT3 Post-Test Position.

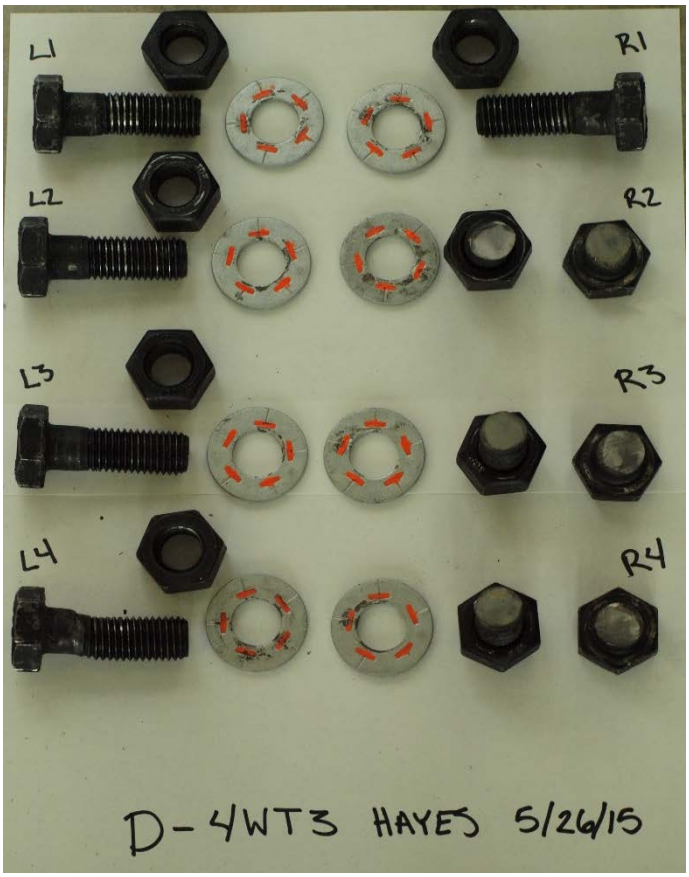

Figure 4.3.2.3-3 D4WT3 Bolts after Testing.

It was noticed after the test was performed that there was a data acquisition problem. This problem was also seen in Lesser [23]. The data acquisition problem was when the software in Labview was started, the program began running, but the processor did not begin at the same time. These caused a subset of data to be missing while the processor tried to "catch up." These missing data will be described as "gap data" herein. Once the processor and the software were running at the same speed, good data could be collected.

In Figure 4.3.2.3-4 and Figure 4.3.2.3-5, the axial and moment start at non-zero magnitude. The test had gap data at the beginning of the test. The rest of the measured results following the range of gap data gave comparable results to what was seen in other tests.

Figure 4.3.2.3-4 and Figure 4.3.2.2-5 show the internal forces and moment at the point of the connection throughout the test. Due to the data acquisition issue, the moment did not cross over axial load in the left WT connection. The axial forces and moment in both WT are similar to what can be seen in both S4WT1 and D4WT2. Catenary action took over in resisting the applied load at approximately 0.05 radians of rotation.

The value for maximum moment was averaged from the top 1% of measured moment, and was recorded between approximately 0.06 radians and 0.075 radians of beam rotation. The left WT had a maximum moment of 25.1 kip-ft, which is 9.1% of the plastic moment capacity of the W18×35, while the right WT had maximum moment of 30.8 kip-ft, which is 11.1% of the plastic moment capacity. The maximum axial force the WTs reached was 45.2 kips and 48.9 kips, left and right WT, respectively. The maximum shear force applied was 6.53 kips to each WT.

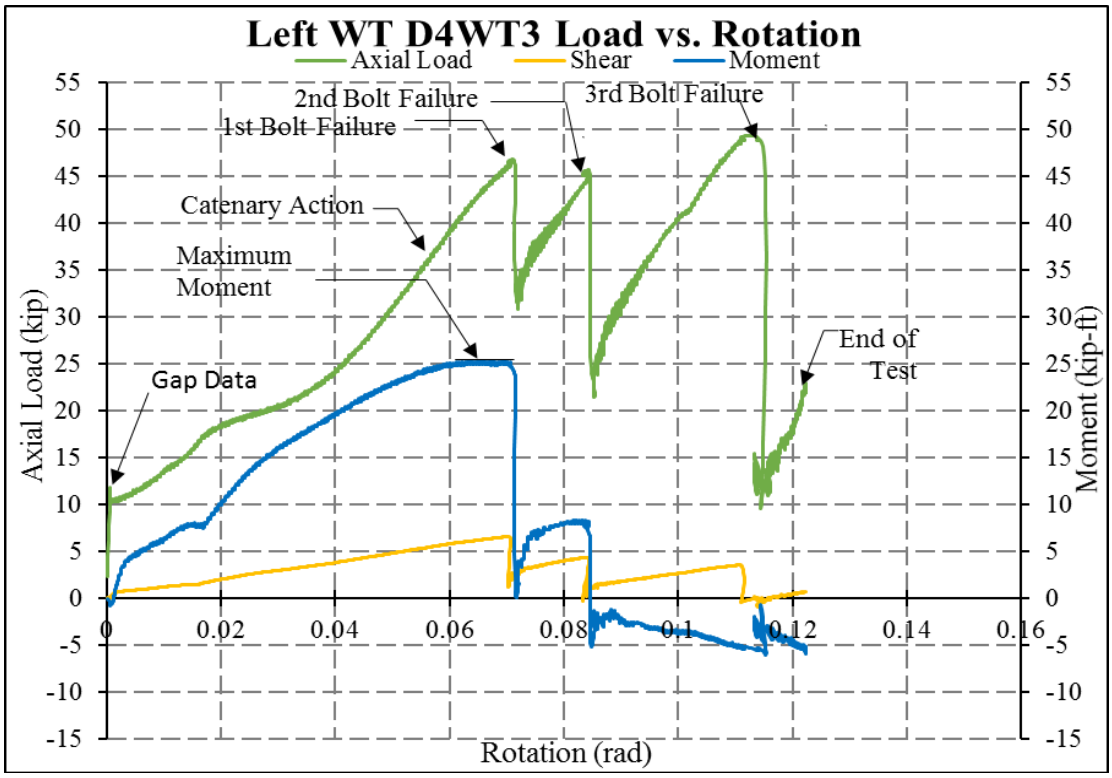

Figure 4.3.2.3-4: D4WT3 Left WT Load versus Rotation.

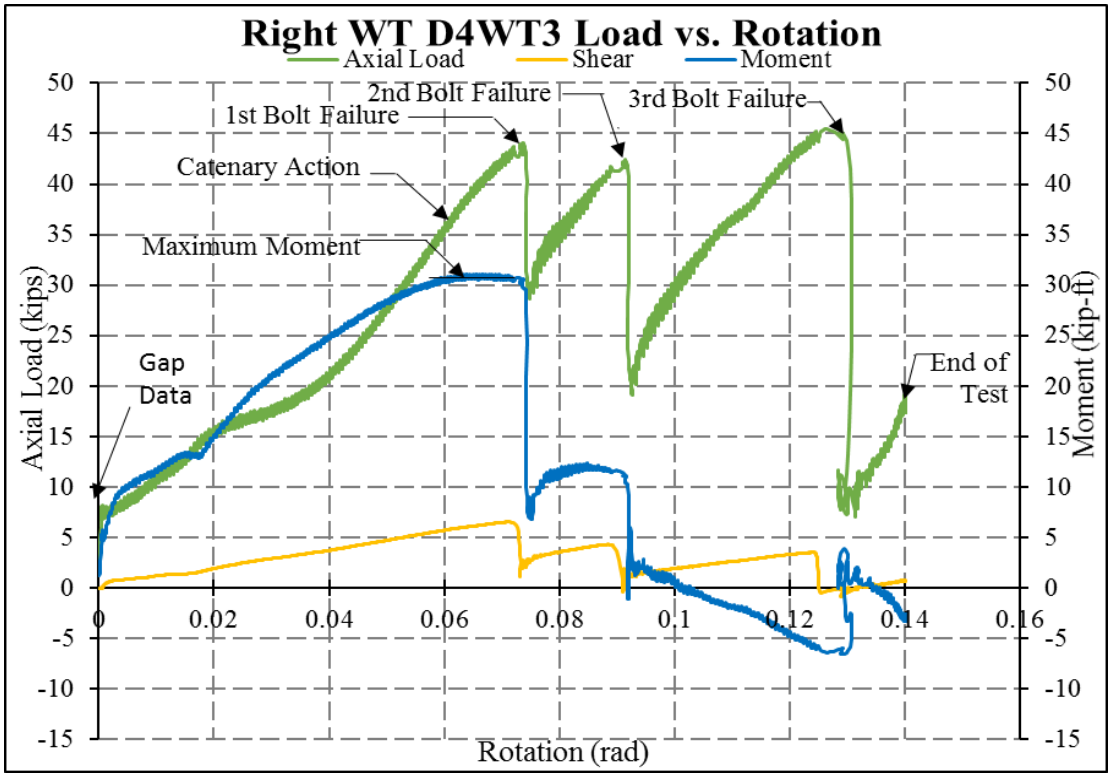

Figure 4.3.2.3-5: D4WT3 Right WT Load versus Rotation.

4.3.2.4 D4WT4 Dynamically Loaded Test

This is the third and last dynamic test of the four-bolt WT connections. This test was run at a later date and therefore used a different lot of bolts than those used in the first three four-bolt tests. The bolts turned out to be stronger; therefore, the system was able to carry a higher axial force and moment than the previous four-bolt tests. This system also used one shim plate under the actuator and the column stub was pulled down 1.25 in. to insert the actuator pin into the column stub. The pre-test setup is shown in Figure 4.3.2.4-1. The test was pulled down at a rate of ten inches in four seconds and broke two bolts on the right side. The post-test position can be seen in Figure 4.3.2.4-2, and post-test bolts in Figure 4.3.2.4-3.

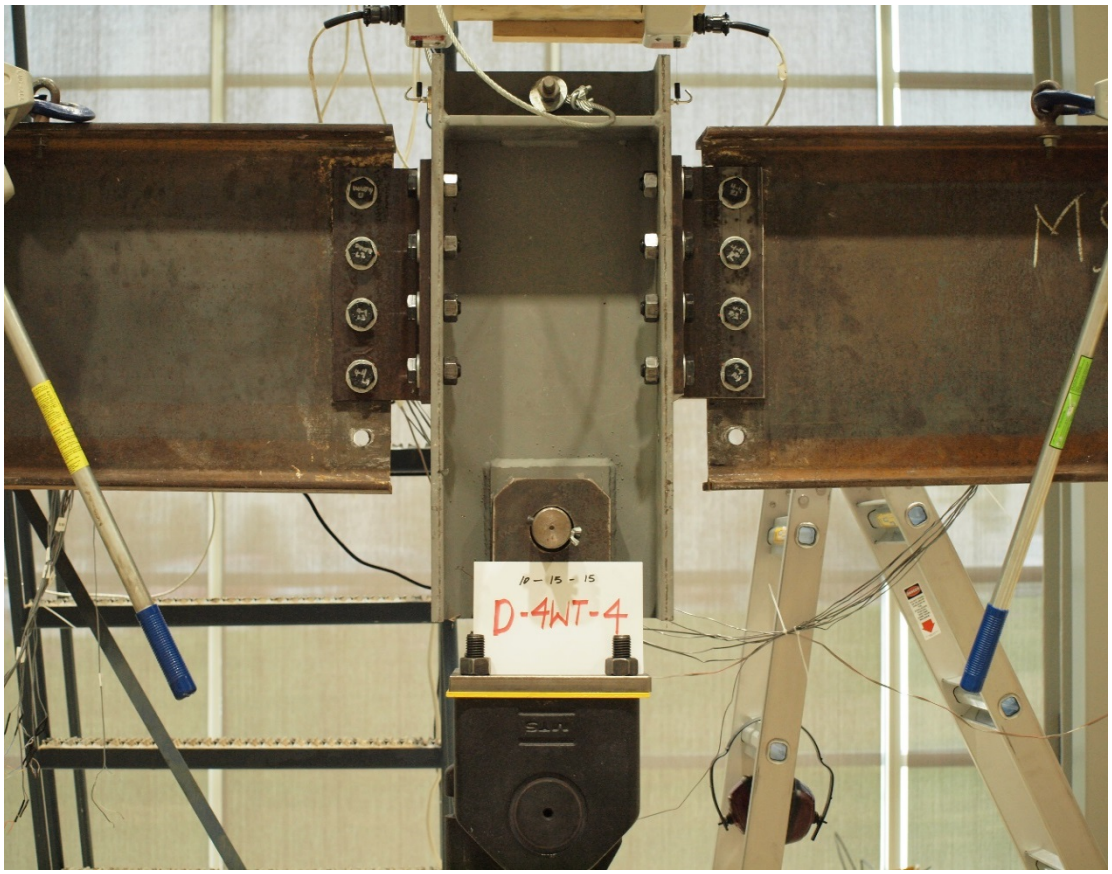

Figure 4.3.2.4-1: D4WT4 Pre-Test Position.

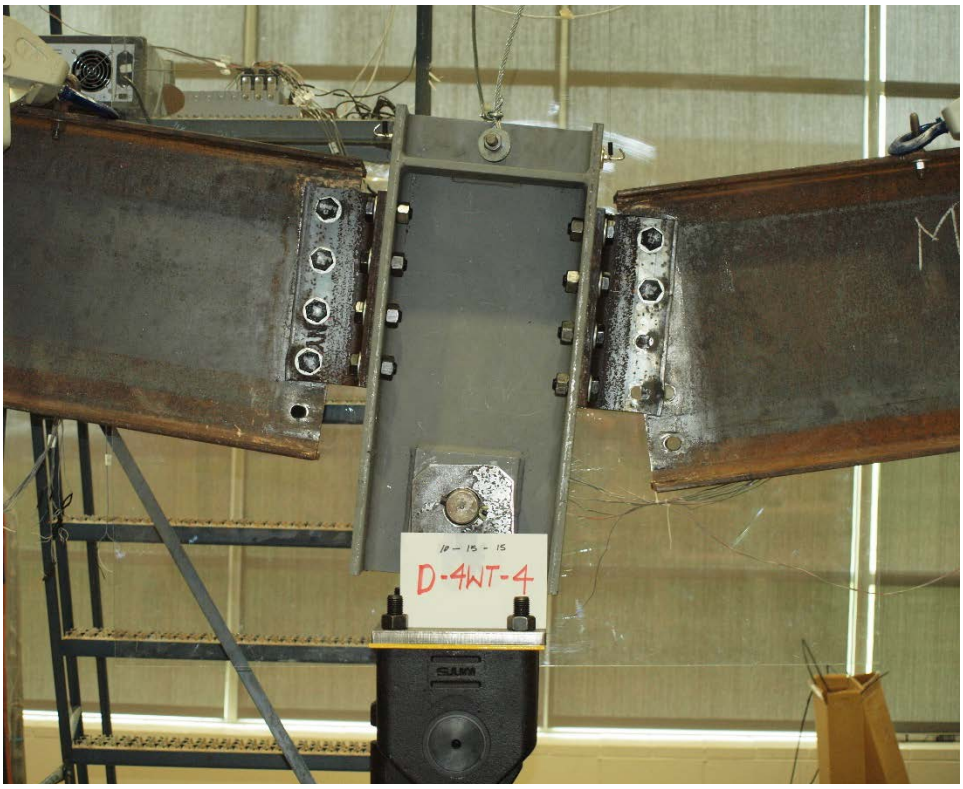

Figure 4.3.2.4-2: D4WT4 Post-Test Position.

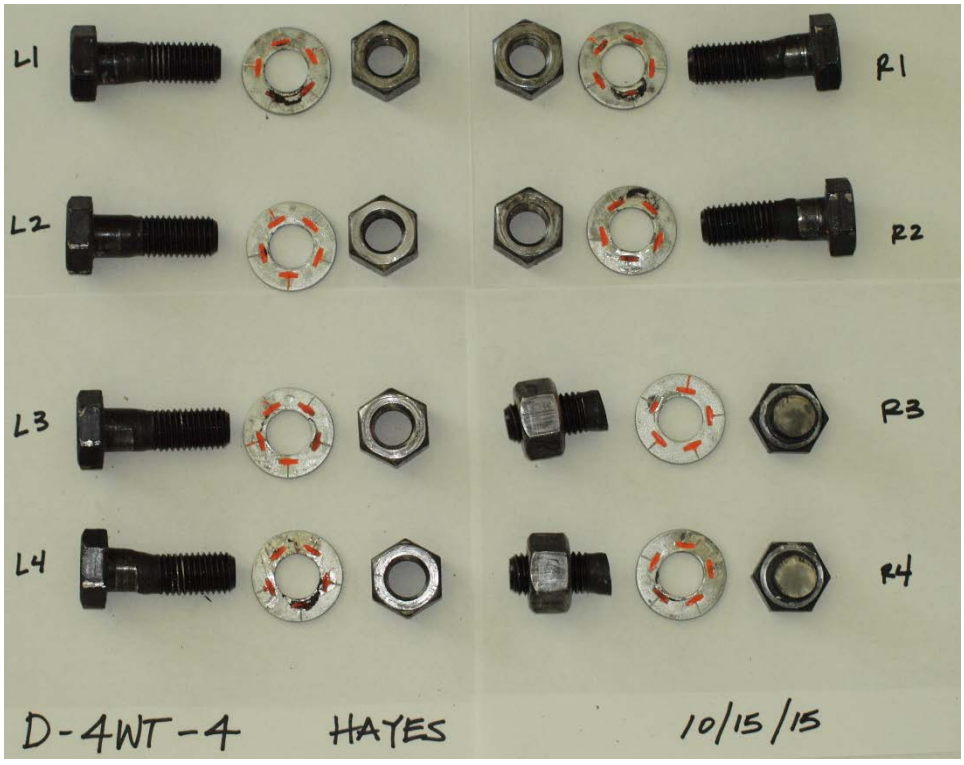

Figure 4.3.2.4-3: D4WT4 Bolts after Testing.

Axial, moment, and shear in both the left and right WT throughout the duration of the test can be seen in Figure 4.3.2.4-4 and Figure 4.3.2.4-5, respectively. Unlike the previous tests run, D4WT4 broke two bolts almost simultaneously, as seen in the figures. This action of two bolts breaking at nearly the same time and with such high axial loads caused the left WT to measure a backwards movement in rotation; that is, a rebounding effect. The difference in rotation between the two bolt breaks was 0.003 radians. After the second bolt break, the internal axial force, shear and moment magnitudes dropped significantly. Catenary action took over as the main way of resisting the loading until the end of the test.

The top 1% of the maximum moment was recorded between 0.07 and 0.086 radians of beam rotation. The maximum moments during the D4WT4 were similar to the previous tests at 30.47 kip-ft and 29.89 kip-ft, left and right WT, respectively. The left WT moment magnitude was about 11% of the plastic moment capacity of the W18×35 while the right WT was 10.8%. Though the moments were similar, the maximum axial forces were much higher than the other tests. The left WT reached 52.70 kips, where the right WT reached 52.66 kips. The shear force was also higher than previous tests at a maximum of 10.03 kips in each WT.

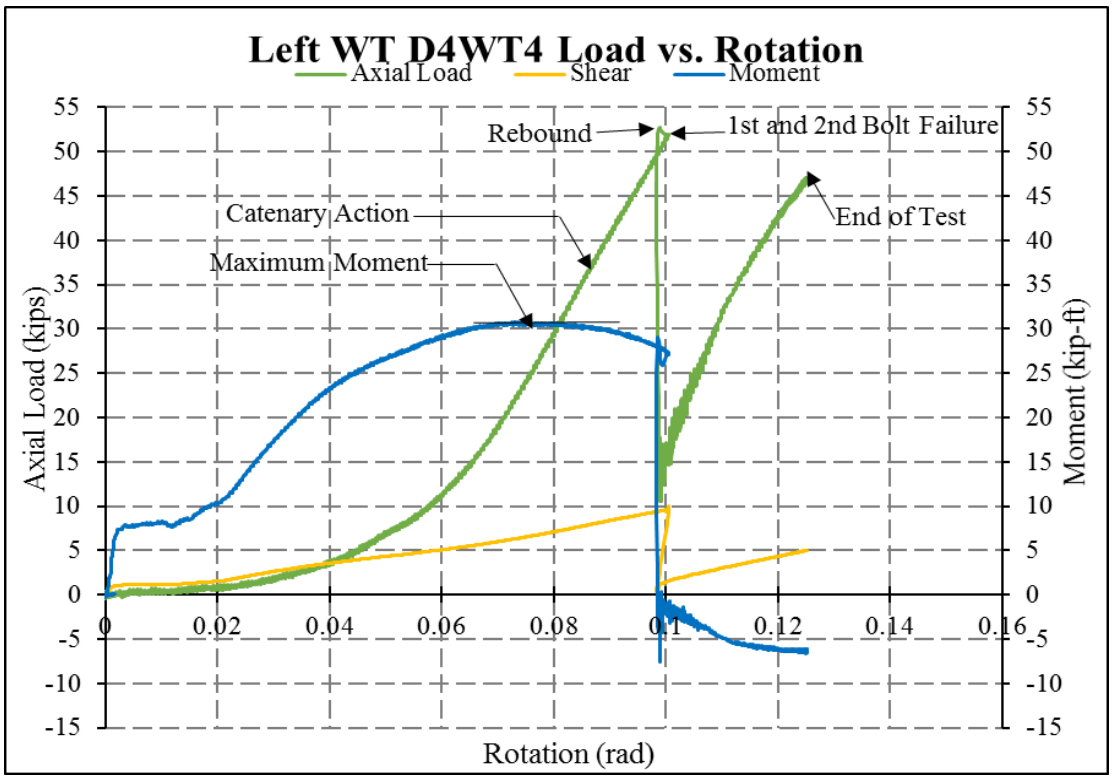

Figure 4.3.2.4-4: Left WT D4WT4 Load versus Rotation.

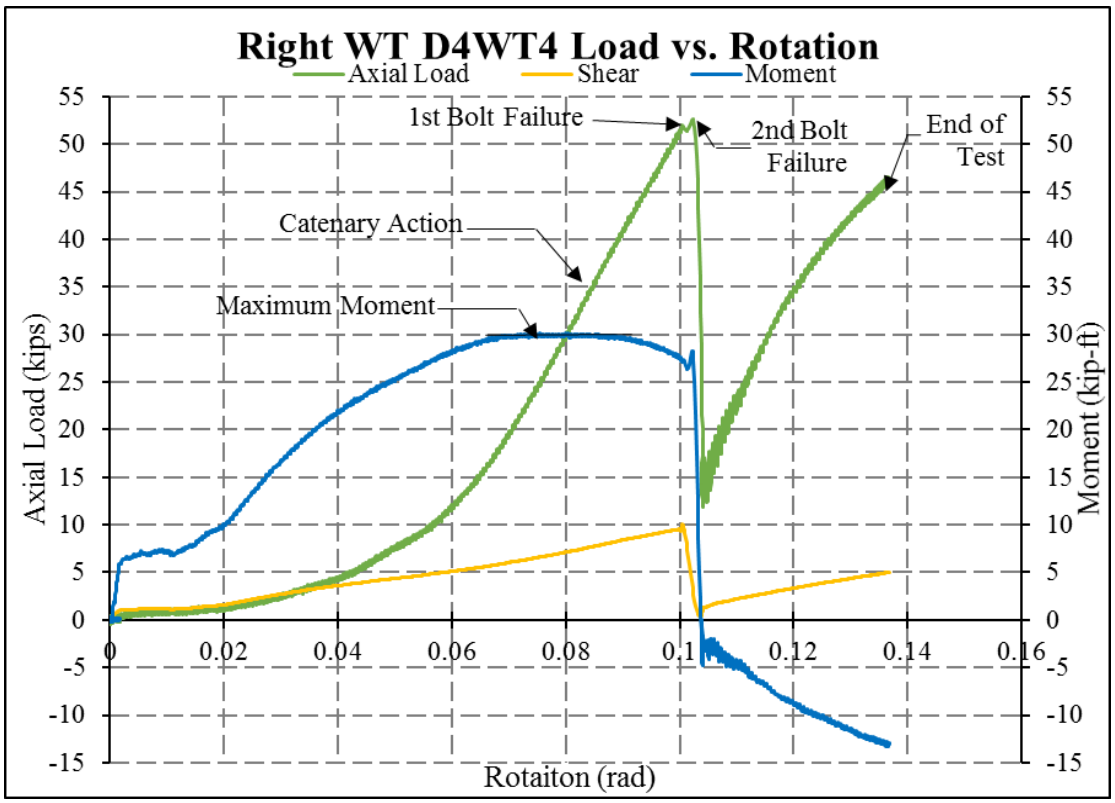

Figure 4.3.2.4-5 D4WT4 Right WT Load versus Rotation.

4.3.2.5 4WT Test Summary

A left WT comparison of a typical dynamic to a typical static test is illustrated in Figure 4.3.2.5-1. This figure has been manually shifted to match the zero point described in Section 4.2.1. This graph clearly shows that the dynamically loaded test breaks with less rotation than the statically loaded test. It should be noted that even though D4WT4 had higher strength, the trend occurs of catenary action being the main resistance of applied force.

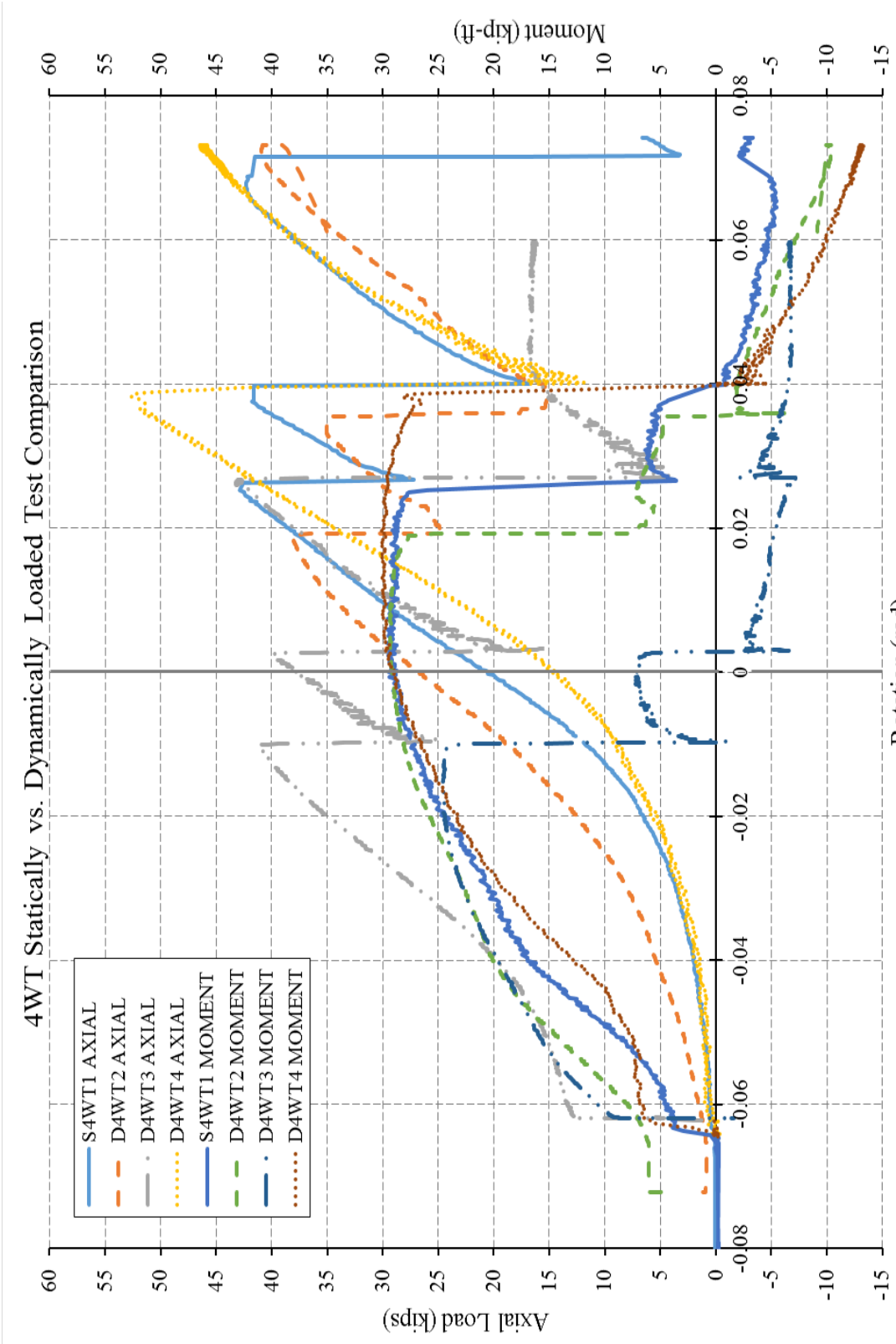

Figure 4.3.2.5-1: 4WT Statically versus Dynamically Loaded Tests.

Tables 4.3.2.5-1 through 4 summarize the measured connection forces throughout key points in the experimental testing. All the 4WT had bolts break in the right WT which is why all of the values are slightly higher than in the left WT. Table 4.3.2.5-1 summarizes the test values at the first bolt break in all four 4WT tests. These values were calculated from the procedure described in Section 4.2.1. This table shows the rotation, shear force, axial force and moment to the left and right WT, respectively. These initial failures can be seen as the maximum point before the test specimen lost significant loading carrying capacity.

Table 4.3.2.5-1: Forces Measured at the Connection at 1st Bolt Failure.

Test	Left WT				Right WT			
	Rotation (rad)	Applied Shear (kips)	Measured Axial (kips)	Measured Moment (kip-feet)	Rotation (rad)	Applied Shear (kips)	Measured Axial (kips)	Measured Moment (kip-feet)
S4WT1	0.10	7.99	42.63	26.73	0.10	7.99	42.66	27.80
D4WT2	0.09	7.22	38.17	27.56	0.09	7.22	37.88	25.79
D4WT3	0.07	2.73	44.11	29.76	0.07	2.73	46.76	24.66
D4WT4	0.10	9.48	51.06	27.63	0.10	9.48	50.96	27.56

Table 4.3.2.5-2 summarizes the second bolt failure in the test specimens. This is similar to the first bolt failure table as it is comparing rotation, shear, axial force and moment in the left and right WT, respectively. All of the 4WT broke at least two bolts. It should be noted that while the first and second bolt failures occurred at similar axial force values, the moments are quite different in magnitude. After the first bolt break, the symmetry of the connection has gone away, which decreases the moment by a significant amount.

Table 4.3.2.5-2: Forces Measured in the WTs at the 2nd Bolt Failure.

Test	Left WT				Right WT			
	Rotation (rad)	Applied Shear (kips)	Measured Axial (kips)	Measured Moment (kip-feet)	Rotation (rad)	Applied Shear (kips)	Measured Axial (kips)	Measured Moment (kip-feet)
S4WT1	0.11	4.75	41.59	1.06	0.12	4.75	42.01	4.32
D4WT2	0.10	4.15	34.69	4.83	0.11	4.15	35.37	5.21
D4WT3	0.08	0.76	42.41	10.46	0.09	0.76	45.45	7.53
D4WT4	0.10	3.29	52.66	28.25	0.10	3.29	52.59	26.73

Some of the 4WT tests had three bolts break. The forces and moments can be seen in Table 4.3.2.5-3. Once again, the axial force magnitudes are similar to that of the first and second bolt failures, but the moment resistance is effectively not existent.

Table 4.3.2.5-3: Forces Measured in the Left and Right WTs at the 3rd Bolt Failure.

Test	Left WT				Right WT			
	Rotation (rad)	Applied Shear (kips)	Measured Axial (kips)	Measured Moment (kip-feet)	Rotation (rad)	Applied Shear (kips)	Measured Axial (kips)	Measured Moment (kip-feet)
S4WT1	0.13	4.26	41.43	-11.62	0.15	4.26	42.69	-4.51
D4WT2	NA							
D4WT3	0.11	-0.67	45.17	-6.56	0.13	-0.67	48.88	-5.28
D4WT4	NA							

Table 4.3.2.5-4 shows the axial, shear and moment forces magnitudes at the point when moment is maximum. These magnitudes were found using the instantaneous center of rotation (ICOR) methodology.

Table 4.3.2.5-4: Average of the Top 1% of the Measured Maximum Moment within the 4WTs.

Test	Left WT				Right WT			
	Rotation (rad)	Applied Shear (kips)	Measured Axial (kips)	Measured Moment (kip-feet)	Rotation (rad)	Applied Shear (kips)	Measured Axial (kips)	Measured Moment (kip-feet)
S4WT1	0.08	6.23	26.84	27.97	0.08	6.23	27.15	28.73
D4WT2	0.08	6.44	30.71	29.32	0.08	6.44	30.91	26.99
D4WT3	0.07	6.25	40.41	30.77	0.07	6.25	43.47	25.06
D4WT4	0.08	6.87	27.37	29.89	0.08	6.87	27.21	30.47

The values in Table 4.3.2.5-5 can be directly compared to the expected bolt force of 35.4 kips [25]. The percent difference that is shown in the table is for the bottom bolt (Bolt 4) versus the expected value.

The values in Table 4.3.2.5-5 are higher than the values for the 3WT tests. This result can be attributed to the fact that 4WTs have higher moment capacity and can handle more applied force.

Table 4.3.2.5-5: Bolt Forces for 4WT Found by Using ICOR.

Test	Left					Right				
	Bolt 1 (kips)	Bolt 2 (kips)	Bolt 3 (kips)	Bolt 4 (kips)	% Difference from the Guide	Bolt 1 (kips)	Bolt 2 (kips)	Bolt 3 (kips)	Bolt 4 (kips)	% Difference from the Guide
S4WT1	25.44	19.30	32.54	38.83	10%	24.72	18.73	31.79	37.94	7%
D4WT2	22.75	16.92	32.03	38.02	7%	25.46	18.30	33.32	40.62	15%
D4WT3	17.52	12.09	33.49	39.09	10%	24.33	17.79	37.69	44.37	25%
D4WT4	27.47	20.92	34.16	40.89	16%	26.83	20.39	33.71	40.33	14%

4.3.3 Five-Bolt WT Tests

The five-bolt WT was the last bolt configuration, and similar to other configurations, four tests were run. The statically loaded test, S4WT1, and the first two dynamically loaded tests, D5WT2 and D5WT3, were run at the same time, and then at a later time, D5WT4, the last dynamically loaded test, was run with a different lot of bolts. All the bolts met A325 standards. Although D5WT2 was run and pictures were taken, an error occurred in the data acquisition process and only force and actuator displacement data were collected.

In all four tests, bolts broke in the left WT, ranging from three to four bolts breaking. Figure 4.3.3-1 is a free-body diagram of the bolts' movement from the internal loading during these tests. Similar to the four-bolt tests, the five-bolt configuration affects how forces are resisted within the bolt group. The extra bolt creates a larger moment arm, so the bolts are able to resist a larger moment than other configurations. This resulted in the system's ability to continue to accrue moment and axial force in the connection simultaneously.

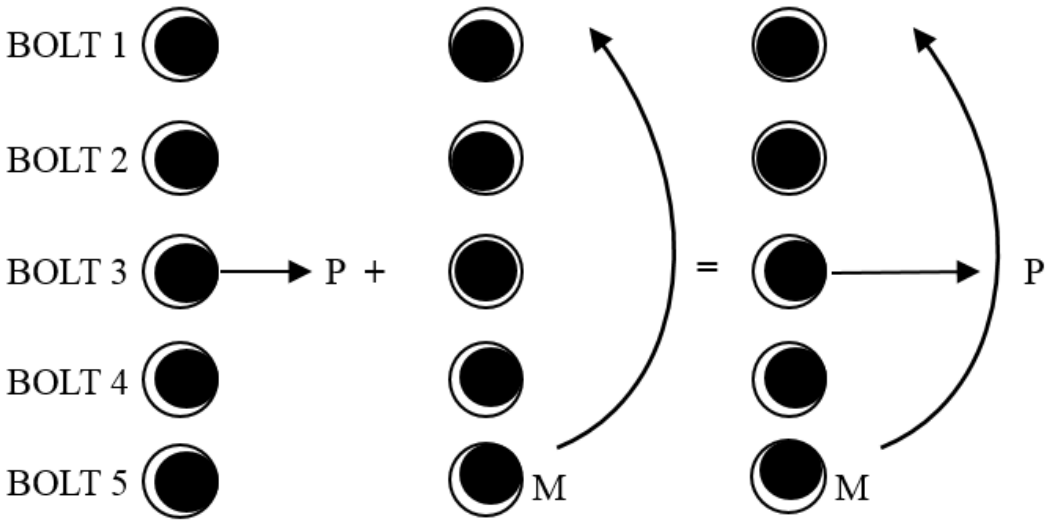

Figure 4.3.3-1: Free Body Diagram of the Five-Bolt Configuration.

As what was described with the three-bolt WT, the compressive and tensile forces described herein are actually shear forces acting on the bolts.

Similar to the three- and four-bolt tests, the top 1% of the measured moments were averaged for the maximum moment when figuring out bolt forces. This being said, it is recognized that the top 1% is at the first bolt failure point in all of the 5WT tests, and some plastic deformation in the bolts has occurred at this point.

4.3.3.1 S5WT1 Statically Loaded Test

The first of the five-bolt WT tests run was statically loaded. With the additional five 1/4 in. plates under the actuator connection (seen in Figure 4.3.3.1-1), there was no need to pull the column stub down 1.25 in. before starting the test. The column stub was pulled down by the actuator at a rate of ten inches in ten minutes. During this test, three bolts broke in the left WT, which can be seen in the post-test configuration in Figure 4.3.3.1-2 and post-test condition of the bolts in Figure 4.3.3.2-3.

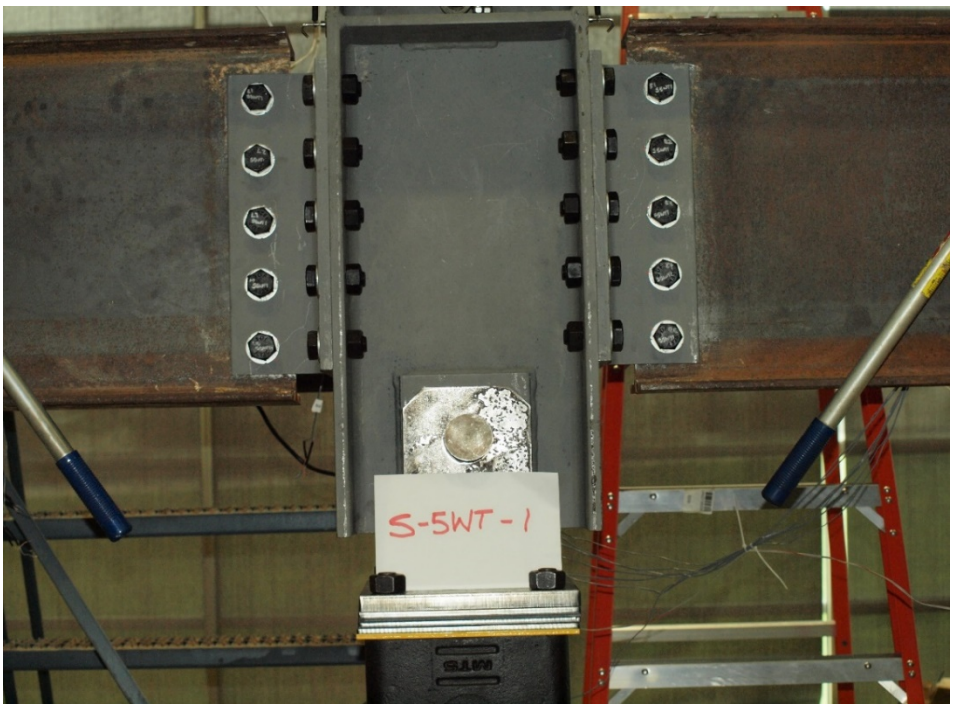

Figure 4.3.3.1-1: S5WT1 Pre-Test Position.

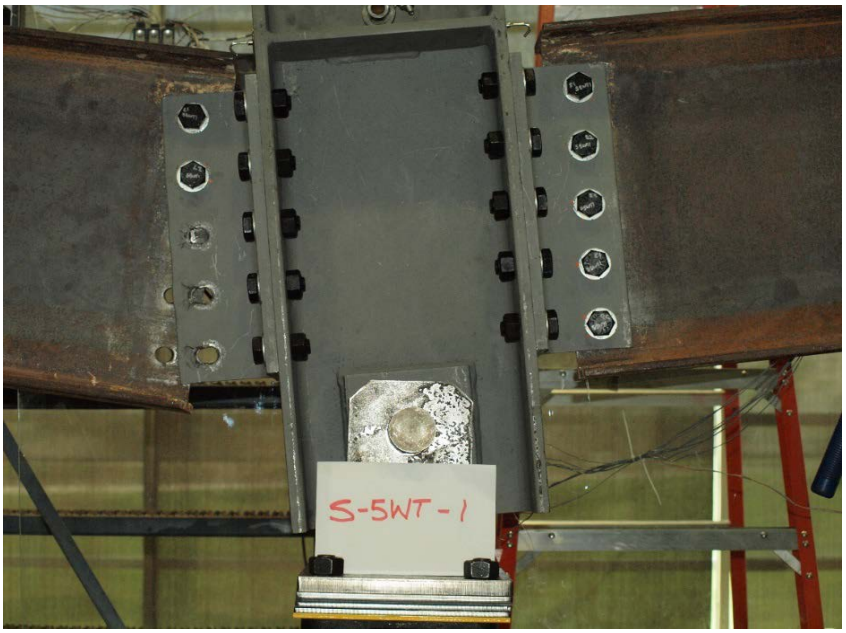

Figure 4.3.3.1-2: S5WT1 Post-Test Position.

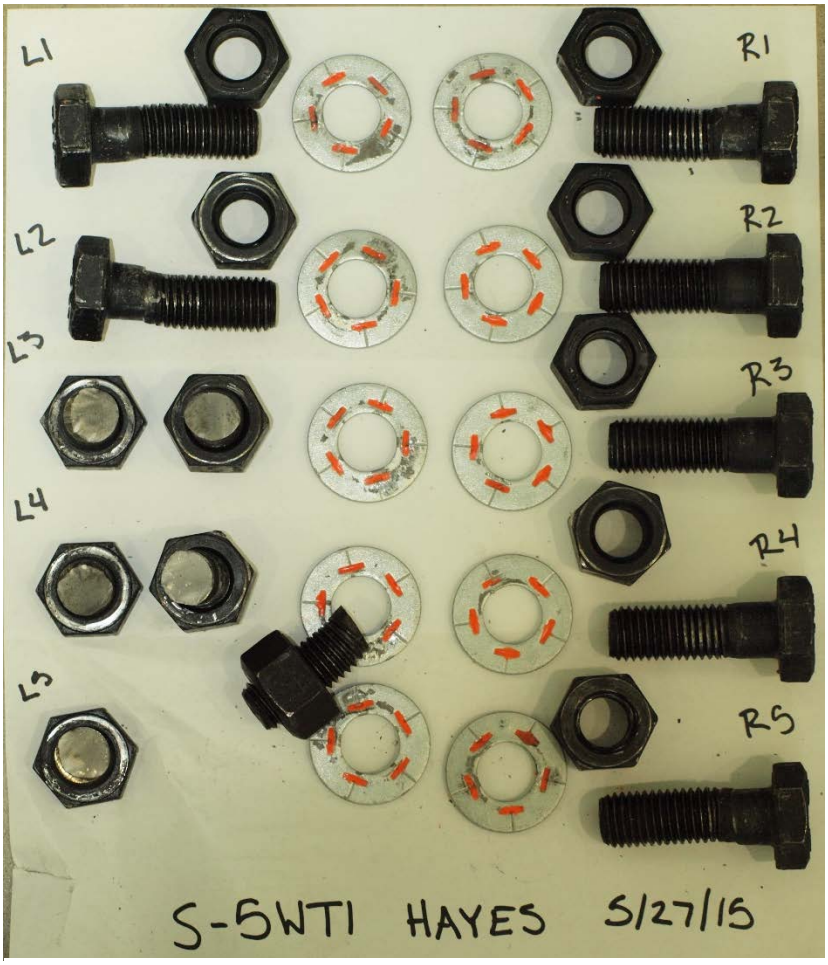

Figure 4.3.3.1-3: S5WT1 Bolts after Testing.

As mentioned, S5WT1 broke three bolts during the test. Figures 4.3.3.1-4 and 4.3.3.1-5 show the force and moment versus rotation response throughout the test. The bottom bolt broke at approximately 0.07 radians of beam rotation, which was also the point of highest maximum moment in the test of 49.89 kip-ft with a corresponding axial force of 38.7 kips. That bolt break released about 28 kip-ft of moment but only about 10 kips of axial force. The second bolt break occurred after another 0.015 radians of beam rotation at an axial load of 41.62 kips, but at a much lower moment of 31.7 kip-ft. The third bolt broke after another 0.01 radians of rotation, but the axial force and moment were lower than the previous two bolt breaks. The test completed after full actuator stroke.

The top 1% of the measured moment was averaged from a very small range between 0.067-0.07 radians. This is because the maximum moment occurred at the first bolt break. The maximum moments are 46.72 kip-ft and 49.89 kip-ft, left and right, respectively. These are approximately 17.9% and 16.9% of the plastic moment of the W18×35. The axial forces for the WT were in line with the rest of the tests with the left WT at 41.4 kips and right WT at 41.6 kips. Each WT had a maximum shear of 9.54 kips.

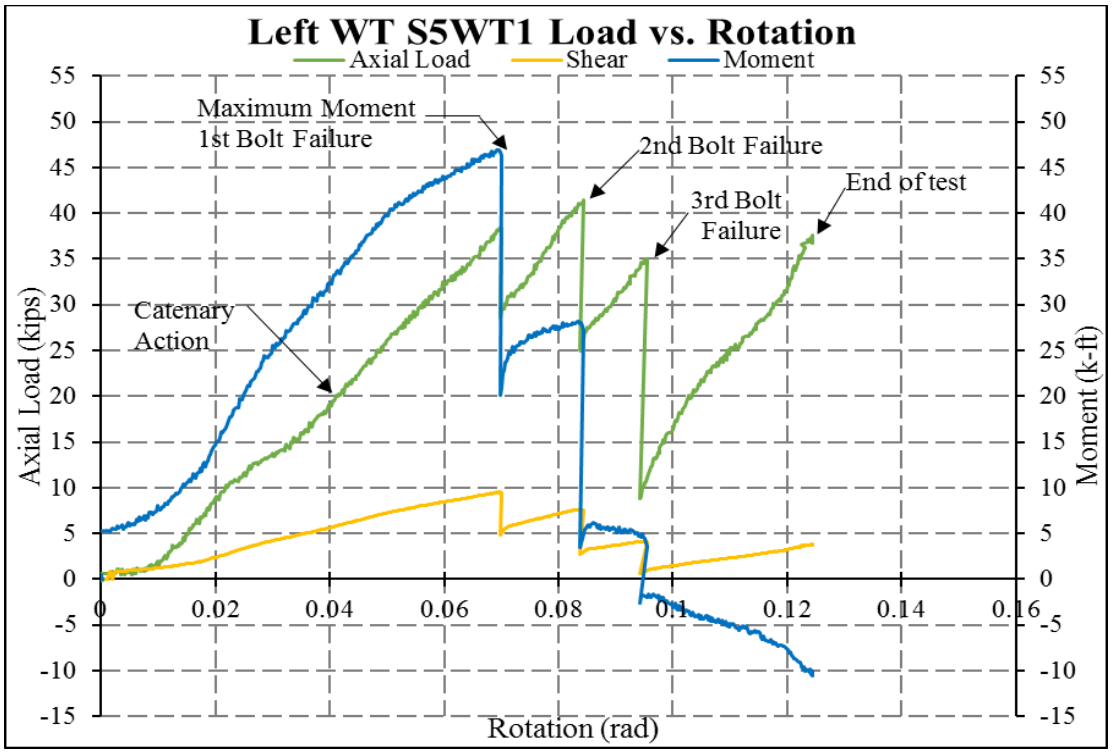

Figure 4.3.3.1-4: Left WT S5WT1 Load versus Rotation.

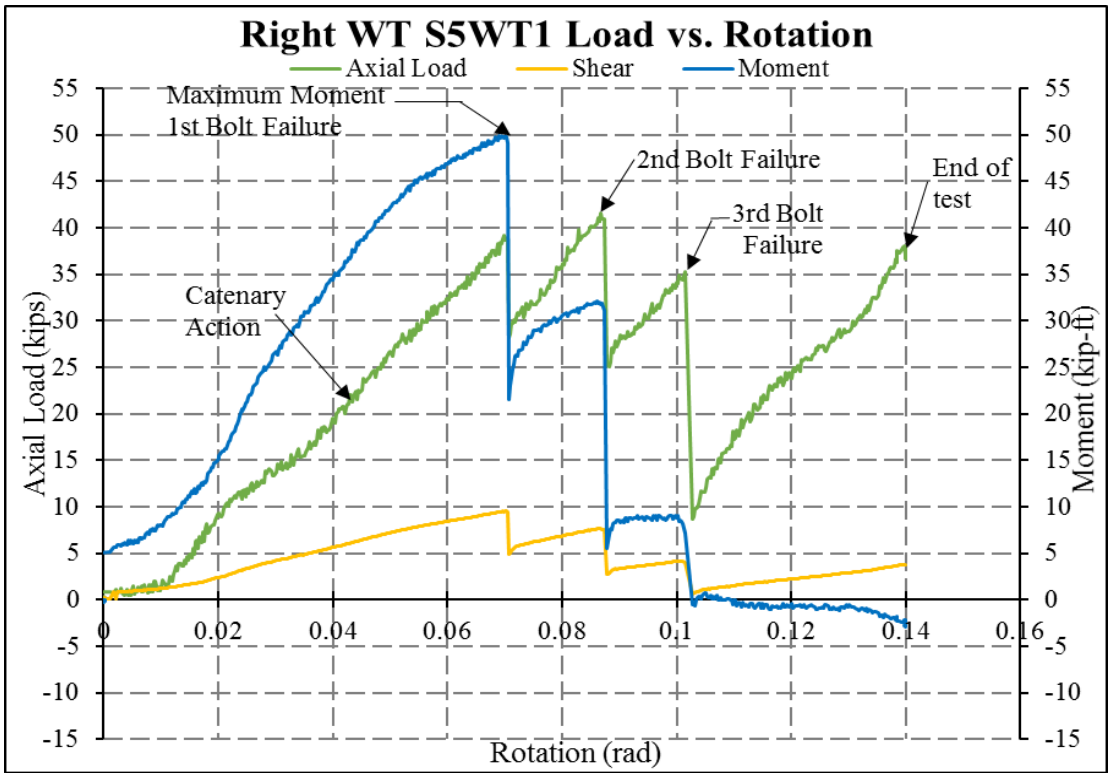

Figure 4.3.3.1-5: Right WT S5WT1 Load versus Rotation.

4.3.3.2 D5WT2 Dynamic Loading

As mentioned before, this test did not have any data collected other than force and actuator displacement from the MTS system. A graph of the load applied versus displacement in inches is seen in Figure 4.3.3.2-2.

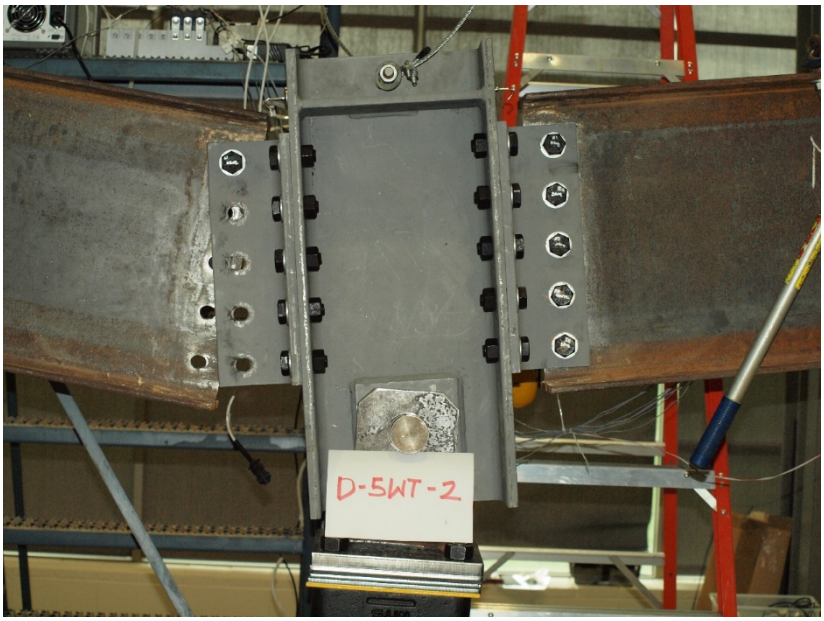

Figure 4.3.3.2-1: End Test Results from D5WT2.

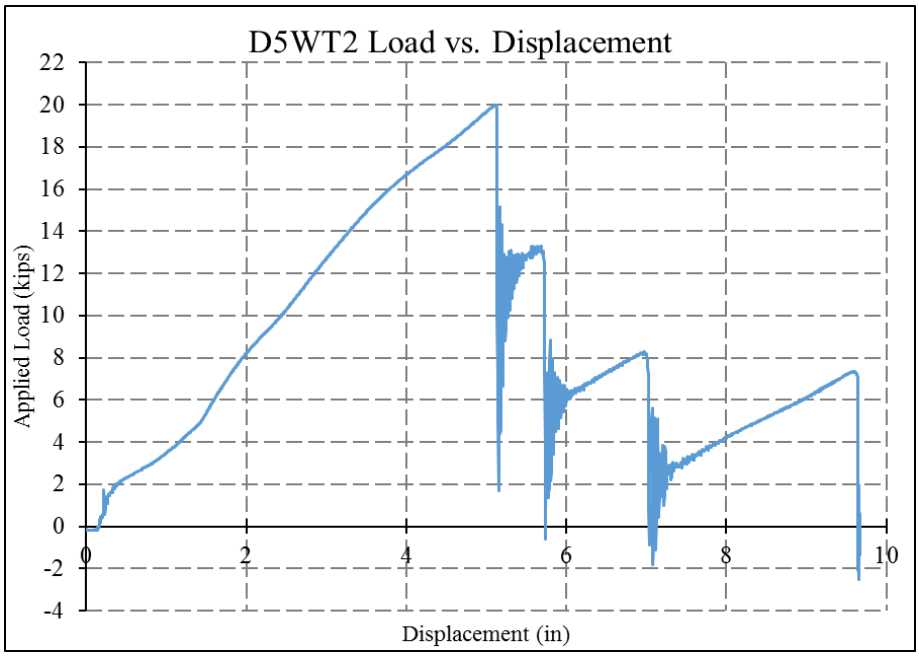

Figure 4.3.3.2-2: D5WT2 Load versus Displacement.

4.3.3.3 D5WT3 Dynamically Loaded Test

D5WT3 was the second dynamically loaded test of the five-bolt configuration. The test specimen was loaded at a rate of ten inches in four seconds. This test utilized five 1/4 in. shim plates between the connection of the actuator to the column stub. The pre-test set up can be seen in Figure 4.3.3.3-1. During this experimental test, three bolts broke in the left WT, which can be seen in the post-test configuration in Figure 4.3.3.3-2 and the post-test condition of the bolts in Figure 4.3.3.3-3.

Figure 4.3.3.3-1: D5WT3 Pre-Test Position.

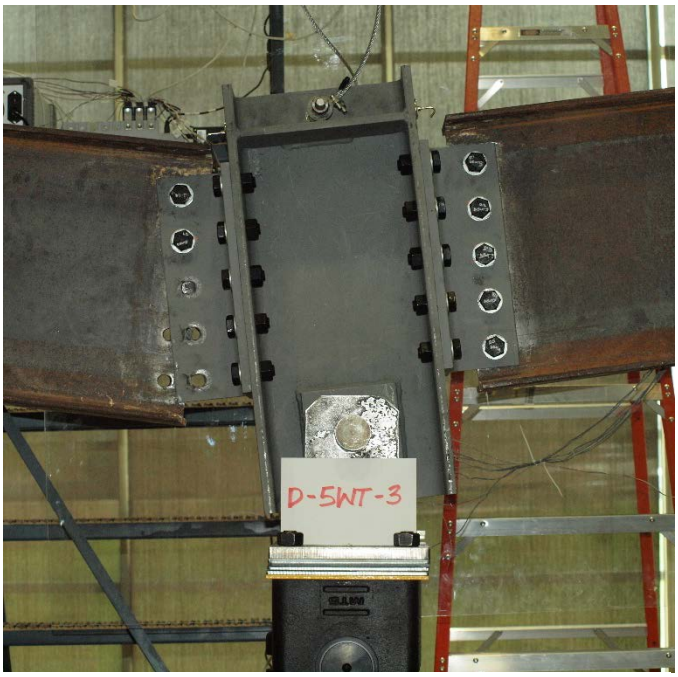

Figure 4.3.3.3-2: D5WT3 Post-Test Position.

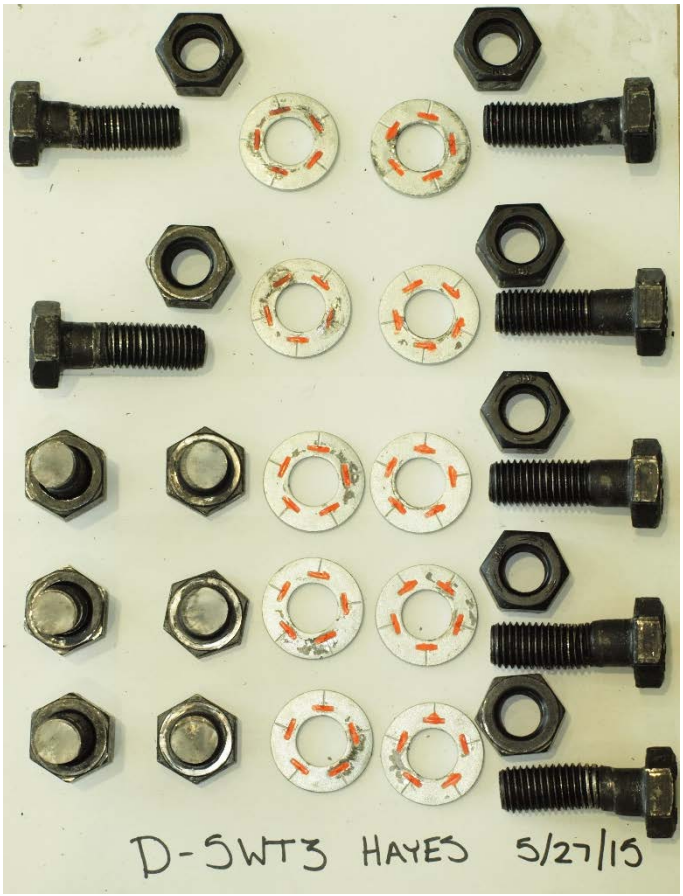

Figure 4.3.3.3-3: D5WT3 Bolts after Testing.

Figures 4.3.3.3-4 and 4.3.3.3-5 show the force and moment versus rotation responses for the D5WT3 connection. As mentioned before, this test broke three bolts in the left WT. The first bolt broke at the point of maximum moment, which occurred at 0.063 radians of beam rotation. After that, the second and third bolts broke at equal rotation increments of 0.015 radians between each bolt break. The maximum moment occurred at the first bolt break but the second bolt break had the highest axial force for the test at 39.8 kips. The flexural resistance controlled until the first bolt break, and after that, catenary action is the main method of resistance. Catenary action remained dominant for the rest of the test.

The maximum moment was averaged from the top 1% of the measured moments. The maximum moment and axial load in left WT was 51.0 kip-ft and 39.8 axial force. The right WT had maximum moment of 48.2 kip-ft and 39.8 kips axial force. Each WT had a maximum shear force of 9.67 kips.

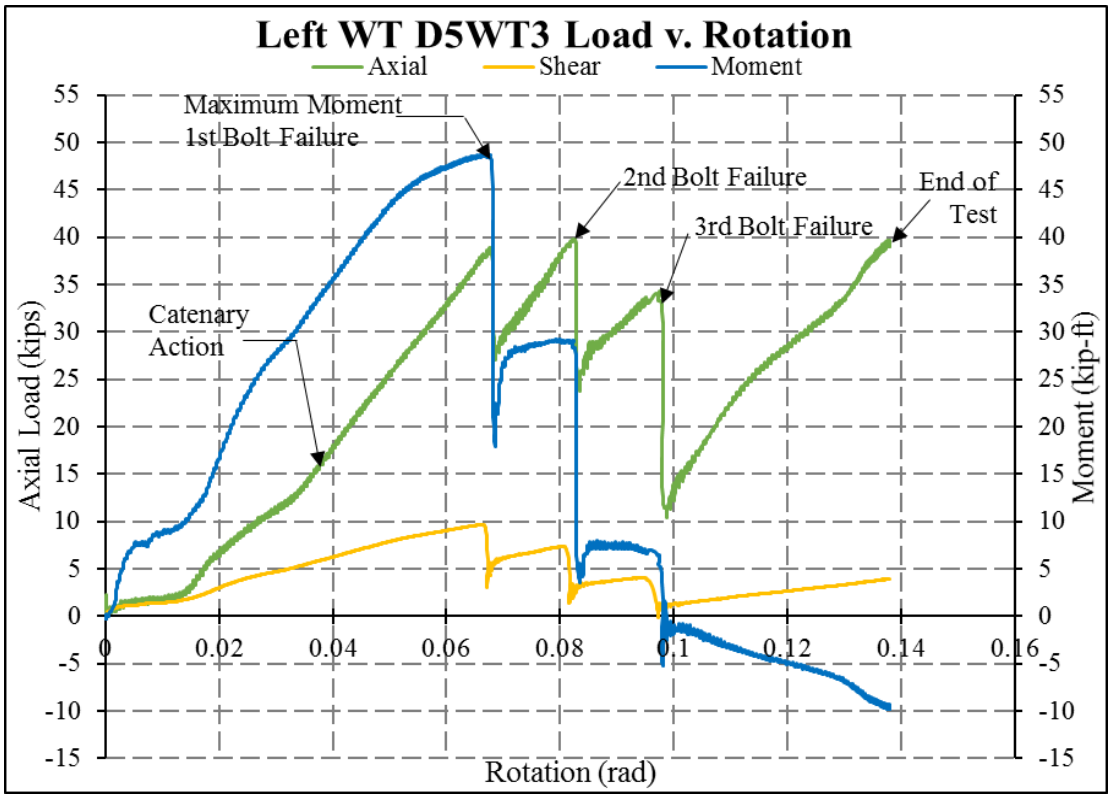

Figure 4.3.3.3-4: Left WT D5WT3 Load versus Rotation.

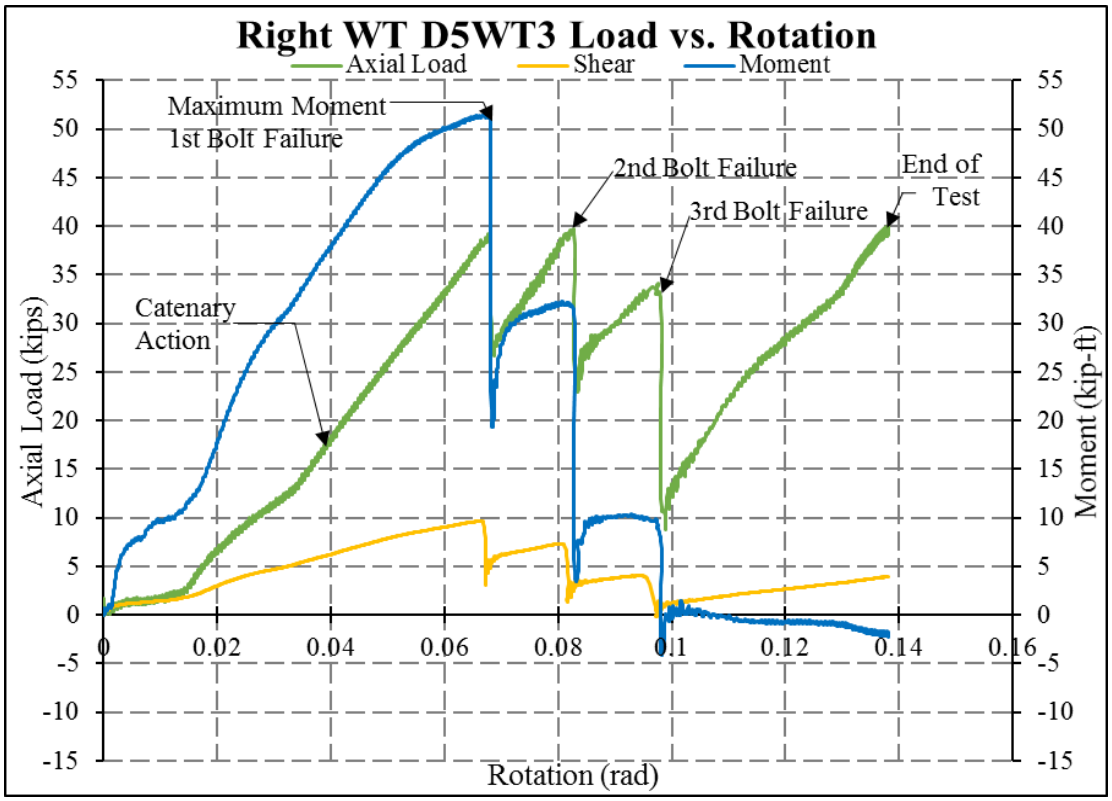

Figure 4.3.3.3-5: Right WT D5WT3 Load versus Rotation.

4.3.3.4 D5WT4 Dynamically Loaded Test

D5WT4 was the fourth test run and the third dynamically loaded test of the five-bolt WTs. This test did not utilize additional shim plates, as seen Figure 4.3.3.4-1, under the actuator connection and therefore the column stub was pulled down 1.25 in. before the test began. The loading rate was ten inches in six seconds. This test was run at a later date (compared to other 5WT tests) and it used a different lot of bolts as compared to the first three 5WT tests. The bottom three bolts on the left WT broke, and there was significant deformation in the WT before the first bolt broke. The first and second bolts broke almost simultaneously and the third broke after approximately 0.015 radians of additional beam rotation. The post-test configuration can be seen in Figure 4.3.3.4-2. Figure 4.3.3.4-3 shows the deformation at the bottom bolt hole in the left WT, and Figure 4.3.3.4-4 shows the post-test bolt configurations.

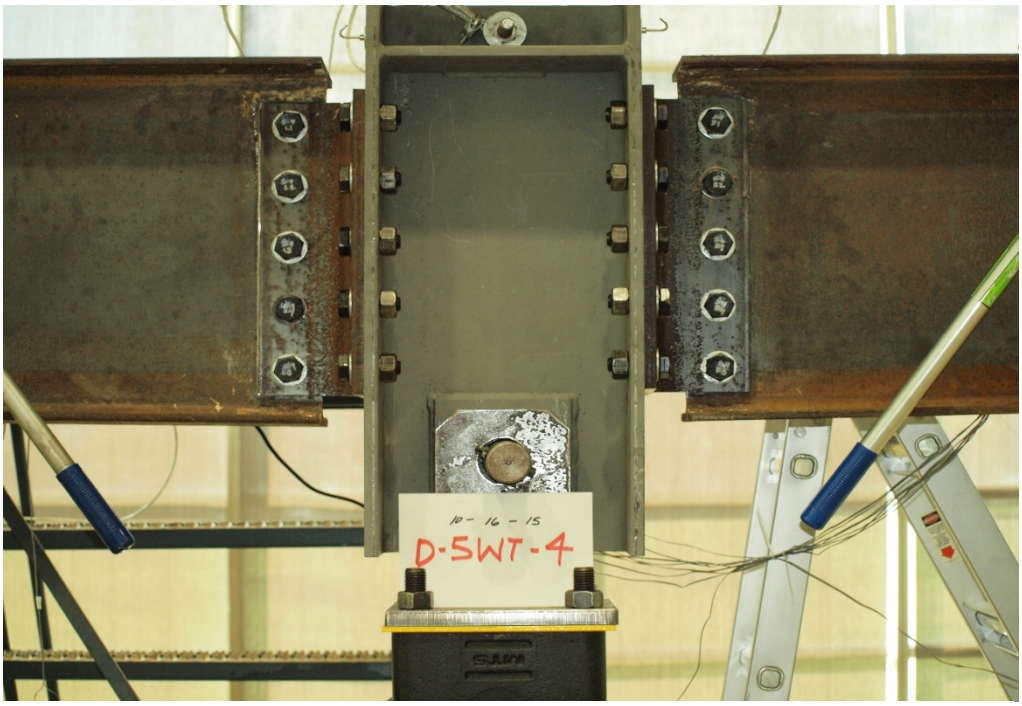

Figure 4.3.3.4-1: D5WT4 Pre-Test Position.

Figure 4.3.3.4-2: D5WT4 Post-Test Position.

Figure 4.3.3.4-3: D5WT4 Left WT Zoomed in on Bottom Bolt after Testing.

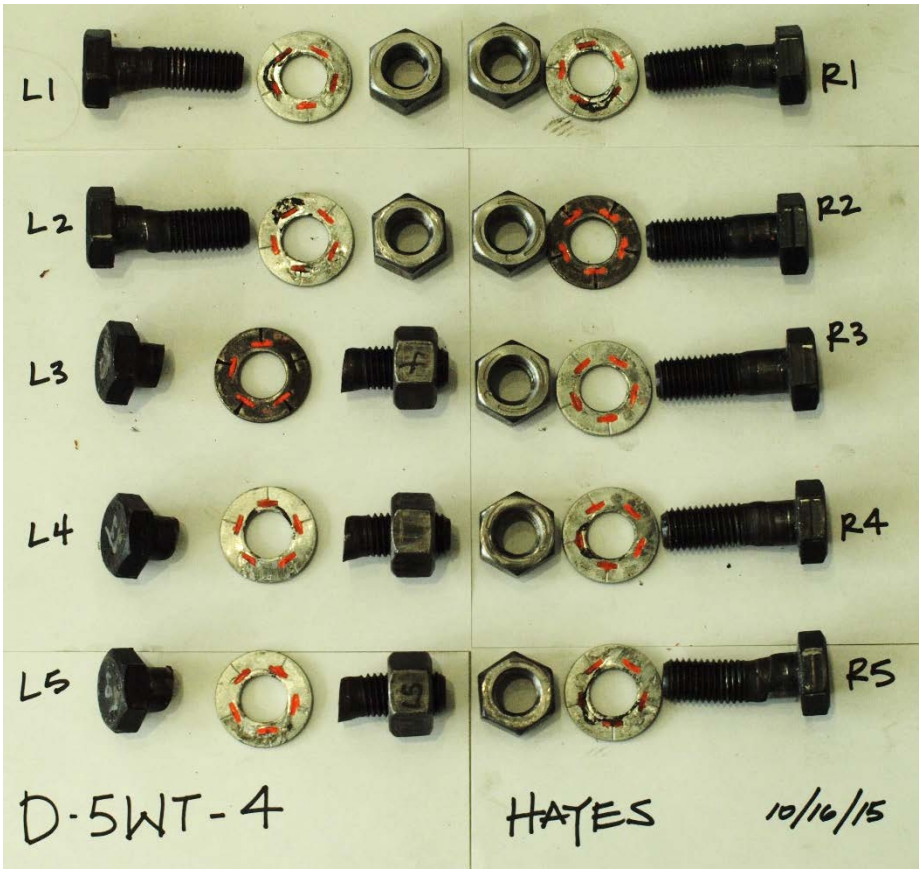

Figure 4.3.3.4-4: D5WT4 Bolts after Testing.

The measured axial force, shear and moment for each WT throughout the duration of test can be seen in Figures 4.3.3.4-4 and 4.3.3.4-5. Since this test was run with the second lot of bolts, the forces are higher than the rest of five-bolted WTs. Catenary action starts almost immediately, but the flexural resistance of the system controls until approximately 0.11 radians. The first two bolts fractured nearly simultaneously, with 0.0005 radian of rotation of the beam separating the two bolt breaks. The third bolt fractured after an additional 0.013 radians of beam rotation. After the third bolt break, catenary action continued for the remainder of the test.

D5WT4 proved to be much stronger than the previous tests of the five-bolt WT. The maximum moment was taken from the average of the top 1% of the measured moments. For the left WT, the maximum moment was 55.1 kip-ft, which is approximately 18.8% of the plastic moment capacity of the W18×35. The right WT had a maximum moment of 58.1 kip-ft, which is 21.5% of the plastic moment capacity of the beam. The maximum axial load at second bolt break and was 71.28 kips and 70.96 kips, left and right WT, respectfully. The maximum shear force in each WT was 15.45 kips.

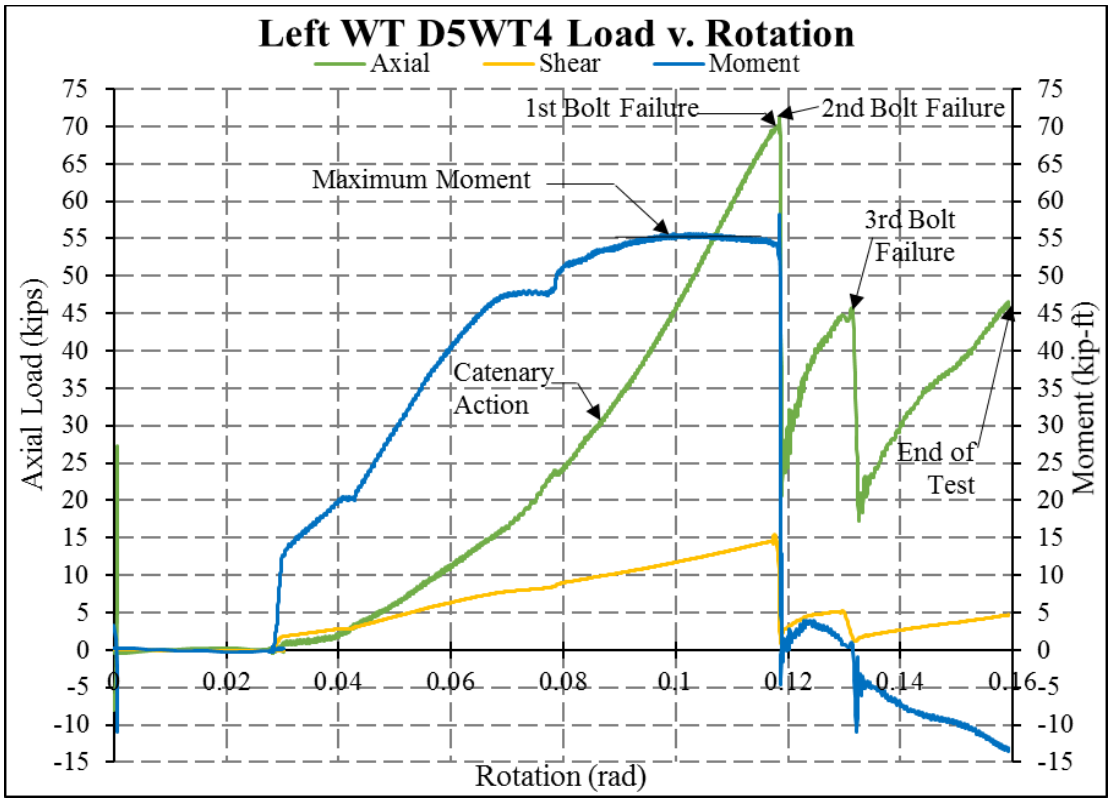

Figure 4.3.3.4-5: Left WT D5WT4 Load versus Rotation.

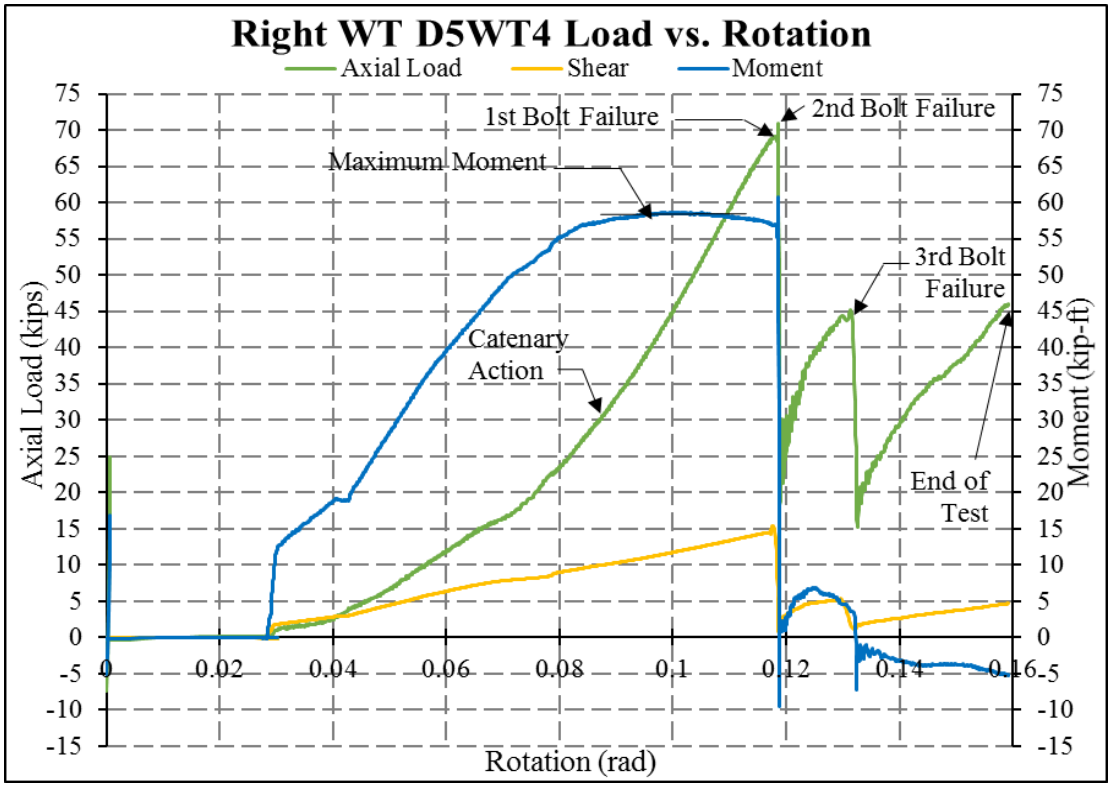

Figure 4.3.3.4-6: D5WT4 Right WT Load versus Rotation.

4.3.3.5 5WT Test Summary

Figure 4.3.3.5-1 compares a typical dynamic to static 5WT test. This figure has been manually shifted to match the zero point described in Section 4.2.1. This graph clearly shows that the dynamically loaded test breaks with less rotation than the statically loaded test. It should be noted that even though D5WT4 had higher strength, the trend of catenary action was the main resistance of applied force.

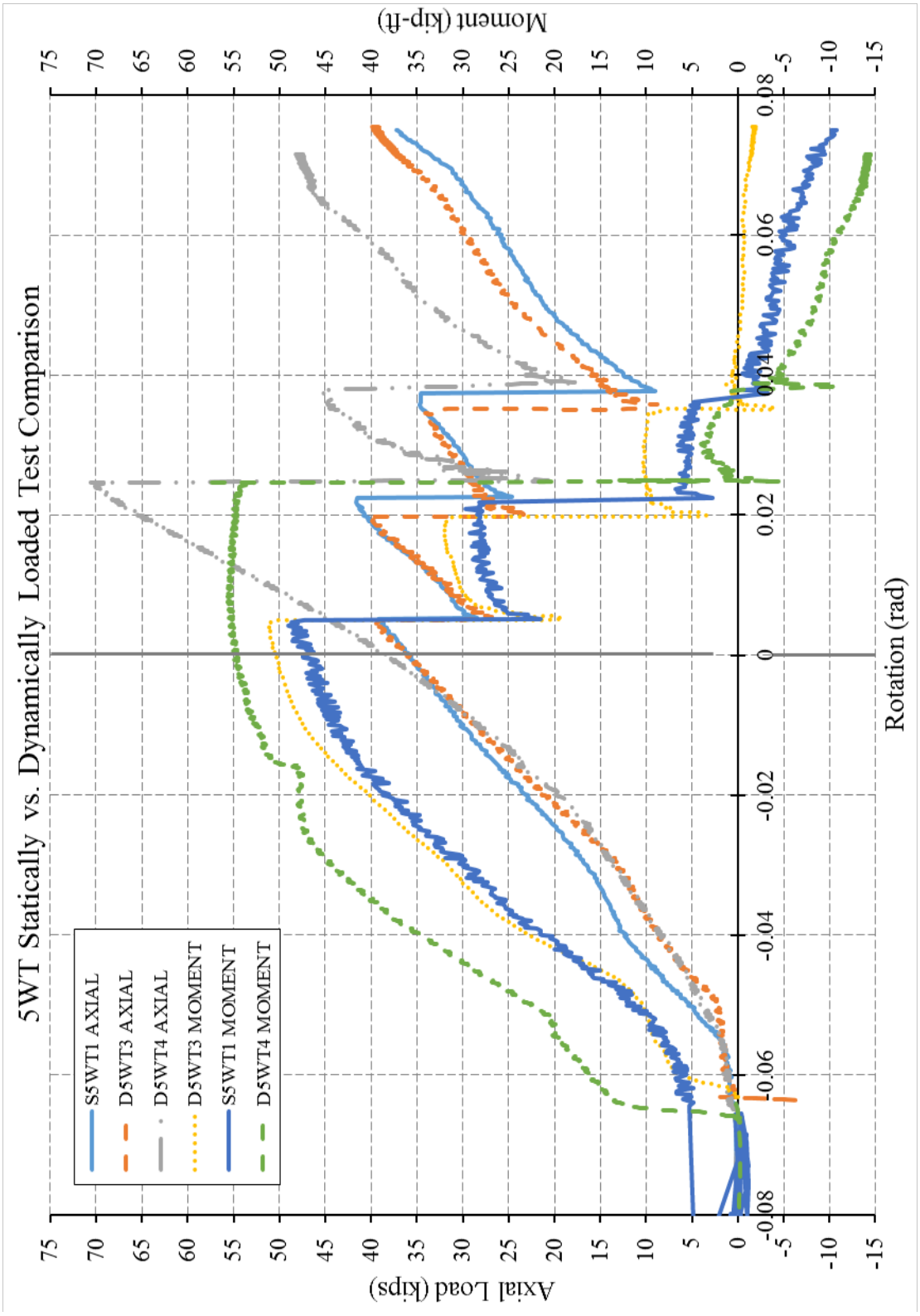

Figure 4.3.3.5-1: 5WT Statically versus Dynamically Comparison.

Tables 4.3.3.5-1 through 4 summarize the key values for the 5WT tests. All the 5WT had bolts break in the left WT, making the values slightly higher than in the right WT. D5WT2 is indicated in all the tables even though, as mentioned previously, there were no strain data collected for this test, thus forces and moments could not be calculated.

Table 4.3.3.5-1 summarizes the test values at the first bolt break in the three 5WT tests. These values were calculated from the procedure described in Section 4.2.1. This table shows the rotation, the shear force, axial load and moment to the left and right WT, respectively. These initial bolt failures can be seen as a maximum point at which the test specimen lost a significant amount of load carrying capacity.

Table 4.3.3.5-1: Forces Measured at the Connection at 1st Bolt Failure.

Test	Left WT				Right WT			
	Rotation (rad)	Applied Shear (kips)	Measured Axial (kips)	Measured Moment (kip-feet)	Rotation (rad)	Applied Shear (kips)	Measured Axial (kips)	Measured Moment (kip-feet)
S5WT1	0.07	9.47	39.15	49.67	0.07	75.47	75.22	46.94
D5WT2	NA							
D5WT3	0.06	5.01	39.23	51.13	0.06	5.01	38.87	48.73
D5WT4	0.12	13.81	69.17	56.99	0.11	13.81	70.07	54.04

Table 4.3.2.5-2 summarizes the data at the second bolt failure in the test specimens. This is similar to the first bolt failure table, as it is comparing rotation, shear, axial force, and moment in the left and right WT, respectively. It should be noted that although the first and second bolt failures have similar axial values, the moments differ. Though there is a spike downward in the moment capacity in the 5WTs after the initial bolt fractures, but the jump is not as significant as seen in the 4WTs. This is because even with one bolt failure, there is a bolt far enough away from the centroid of the connection to redistribute and resist the moment.

Table 4.3.3.5-2: Forces Measured in the WTs at the 2nd Bolt Failure.

Test	Left WT				Right WT			
	Rotation (rad)	Applied Shear (kips)	Measured Axial (kips)	Measured Moment (kip-feet)	Rotation (rad)	Applied Shear (kips)	Measured Axial (kips)	Measured Moment (kip-feet)
S5WT1	0.09	7.60	41.62	31.68	0.08	7.60	41.13	27.98
D5WT2	NA							
D5WT3	0.08	5.34	39.78	31.30	0.07	5.34	39.78	28.13
D5WT4	0.12	2.49	70.96	60.57	0.11	2.49	70.62	55.36

All of the 5WTs broke three bolts, which gives interesting results, seen in Table 4.3.3.5-3. This is the first time the axial loads are not consistently near 40 kips (as they were prior to the first two bolt fractures) and the moments are very low because of the lack of moment capacity in the connection after several bolts have fractured. This is the first time the axial capacity in the 5WTs is significantly higher than in the measured moment.

Table 4.3.3.5-3: Forces Measured in the Left and Right WTs at the 3rd Bolt Failure.

Test	Left WT				Right WT			
	Rotation (rad)	Applied Shear (kips)	Measured Axial (kips)	Measured Moment (kip-feet)	Rotation (rad)	Applied Shear (kips)	Measured Axial (kips)	Measured Moment (kip-feet)
S5WT1	0.10	4.13	34.92	8.41	0.09	4.13	34.64	4.93
D5WT2	NA							
D5WT3	0.09	5.58	34.09	9.24	0.08	5.58	34.31	6.14
D5WT4	0.13	1.72	45.29	3.62	0.12	1.72	45.67	0.70

Bolt forces were calculated using the instantaneous center of rotation methodology. The forces used were those associated with the maximum moment range, which can be seen in Table 4.3.3.5-4. It should be noted that the maximum moment recorded was near the first bolt break; thus, the bolt forces are slightly higher than were seen in other tests and some plastic deformation had occurred.

Table 4.3.3.5-4: Average of the Top 1% of the Measured Maximum Moment of 5WTs.

Test	Left WT				Right WT			
	Rotation (rad)	Applied Shear (kips)	Measured Axial (kips)	Measured Moment (kip-feet)	Rotation (rad)	Applied Shear (kips)	Measured Axial (kips)	Measured Moment (kip-feet)
S5WT1	0.07	9.44	38.52	49.56	0.07	9.44	37.96	46.72
D5WT2	NA							
D5WT3	0.06	7.15	37.63	50.98	0.06	7.15	37.30	48.21
D5WT4	0.11	6.58	56.07	59.64	0.10	6.58	55.59	52.15

Table 4.3.3.5-5 shows the bolt forces in each of the 5WT experiments. The bottom bolt force was then compared to the recommendations by Kulak *et al.* [25] of 35.4 kips. This comparison is shown as a percent difference in the table.

Table 4.3.3.5-5: Bolt Forces for 5WT Found by Using ICOR.

Test	Left						Right					
	Bolt 1 (kips)	Bolt 2 (kips)	Bolt 3 (kips)	Bolt 4 (kips)	Bolt 5 (kips)	% Difference from the Guide	Bolt 1 (kips)	Bolt 2 (kips)	Bolt 3 (kips)	Bolt 4 (kips)	Bolt 5 (kips)	% Difference from the Guide
S5WT1	26.69	23.28	7.80	38.18	41.66	18%	28.54	24.96	7.91	40.08	43.74	24%
D5WT2	NA						NA					
D5WT3	26.45	23.31	7.46	38.14	41.31	17%	28.63	24.28	7.53	39.25	43.62	23%
D5WT4	26.28	22.72	11.06	44.71	48.29	36%	31.29	27.28	11.17	49.47	53.51	51%

4.4 Data Validation

The data were validated for each test run. A statics check was done by considering a range of data. The range was determined by looking at all the tests run for a specific bolt configuration (e.g., all the 3WTs were considered together). The range was selected where the individual tests had similar slopes in the axial force trace. This means that each range of data was taken from different starting and ending rotations.

Figure 4.4-1 shows a free body diagram of the forces within the test setup. These forces included the axial force, P; moment, M; and shear, V, as the beam undergoes a rotation, θ. The rotation was calculated based on actual geometry, up to and including the shim plates in the connection assembly (if present). To determine the internal forces within the system, forces were summed in the x-direction and y-direction and moments were summed about the pin. It should be noted that the length from strain gages to the pin was determined to be 36 in. and 36 1/8 in., left and right beam, respectfully.

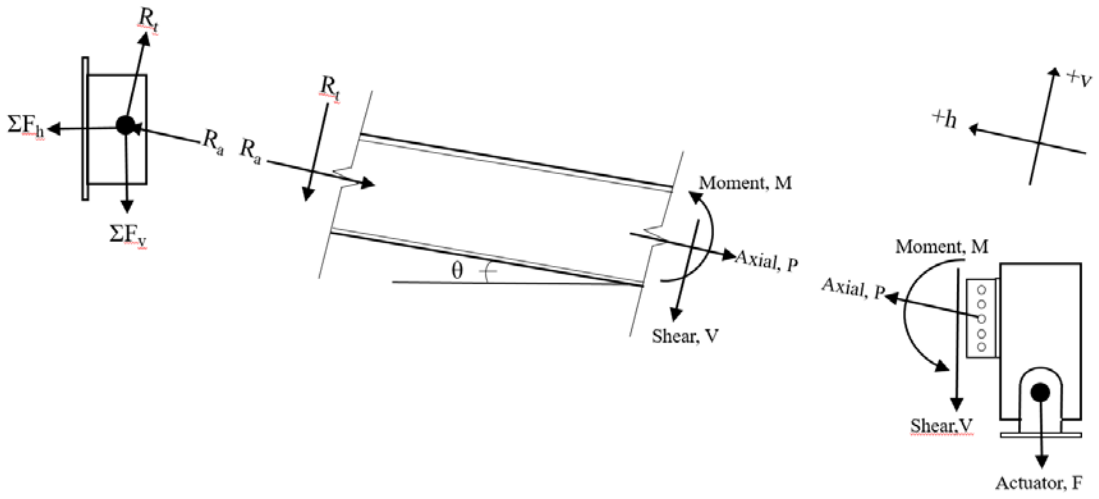

Figure 4.4-1: Free Body Diagram of Static Evaluation.

To determine the internal axial force going into the left pin, R_a, the sum of forces in the horizontal direction, F_h gives

$$\Sigma F_h = P\text{-}R_a = 0, \tag{4.4-1}$$

$$\therefore\ R_a = P \text{ (kips)}. \tag{4.4-2}$$

To determine the transverse reaction at the pin, R_t, the sum of moments at the left pin, M, gives

$$\Sigma M = M\text{-}(R_t \times 36) = 0, \tag{4.4-3}$$

$$\therefore\ R_t = \frac{M}{36} \text{ (kips)}.$$

The previous solved forces, R_a and R_t, were found for the longitudinal axis for the beam (local axis), but in order to compare the forces to actuator forces, they need to be transposed with respect to the global axes. To resolve R_a and R_t to the global axes, the forces needed to be multiplied by the geometric functions sine and cosine:

$$R_{a\ \text{vertical}} = R_a * \sin(\theta), \tag{4.4-4}$$

and

$$R_{t\ \text{vertical}} = R_t * \cos(\theta). \tag{4.4-5}$$

The same calculations were performed on the right beam using the appropriate dimensions to the pin connection. The vertical components from both the left and right beams were summed:

$$\Sigma F_v = F - R_{a,\ \text{vertical left beam}} - R_{t,\ \text{vertical left beam}} - R_{a,\ \text{vertical right beam}} - R_{t,\ \text{vertical right beam.}} \tag{4.4-6}$$

The remaining vertical loads were compared to the actuator force, F, to determine the percent difference. Table 4.4-1 shows the average percent difference, maximum percent difference, minimum percent difference, the standard deviation, and the range at which this percent difference was calculated.

Table 4.4-1: Static Check Percent Error Table for WT Connection Test.

Static Check Percent Error					
Test	Average	Maximum	Minimum	Standard Deviation	Range
S3WT1	12.39%	14.7%	7.8%	1.5%	0.07-0.09
D3WT2	6.39%	6.48%	5.54%	0.17%	0.07-0.10
D3WT3	0.86%	1.17%	0.00%	0.31%	0.07-0.11
D3WT4	5.78%	11.46%	0.01%	3.50%	0.07-0.12
S4WT1	10.03%	10.85%	8.49%	0.59%	0.065-0.085
D4WT2	7.39%	7.67%	6.96%	0.15%	0.045-0.065
D4WT3	19.75%	21.10%	18.87%	0.38%	0.045-0.065
D4WT4	2.08%	2.59%	1.65%	0.18%	0.065-0.085
S5WT1	5.60%	6.92%	3.84%	0.77%	0.03-0.05
D5WT2	NA				
D5WT3	0.76%	1.75%	0.00%	0.48%	0.03-0.05
D5WT4	5.76%	6.73%	3.75%	0.38%	0.04-0.06

Chapter 5: Data Comparisons

5.1 Introduction

The data collected during the experimental testing were compared in two different ways. The first was to focus on the graphical data of a statically loaded test versus the dynamically loaded tests for a given bolting configuration. The second was to compare the two different loadings, static and dynamic, through the amount of work done by each of the connections, thus showing how much energy the system could absorb. The work calculated for the statically loaded test from the present research was compared to the work from the Friedman statically loaded tests [12].

5.2 Visual Data Comparison

The following graphs are an example of the statically loaded test versus one of the dynamically loaded tests. Figures 4.3.1.5, 4.3.2.5, and 4.3.3.5 demonstrate the statically loaded test versus all the dynamically loaded tests, again for a given bolting configuration. These graphs allow one to focus on the trends of the dynamically loaded tests as compared to the statically loaded test. The data have been manually re-zeroed through the procedure described in Section 4.2.1. Again, this point was convenient for data comparison because of its consistent spatial location for all tests.

5.2.1 S3WT1 versus D3WT2

Figure 5.2.1-1 demonstrates the statically loaded three-bolt test, S3WT1, with one of the dynamically loaded three-bolt tests, D3WT2. The first thing to note is the first bolt in test D3WT2 broke with 0.015 radians less rotation as compared to the first bolt break in S3WT1. Even though S3WT1 was stopped early, it is clear that the test specimen was close to failure. The first bolt break in the D3WT2 happened at a lower axial force

magnitude than the static test. The axial force in the system at the point of the second bolt break in D3WT2 had a similar axial magnitude to that of the end of the static test (approximately 41 kips). The axial force graph for both static and dynamic tests has similar slopes, but the dynamic test shows the axial force accruing under slightly less rotation. D3WT2 has a higher moment capacity than the statically loaded test, but this may be due to the fact that it had an initial spike in moment. Without considering the initial spike in moment resistance, the two tests show similar magnitudes.

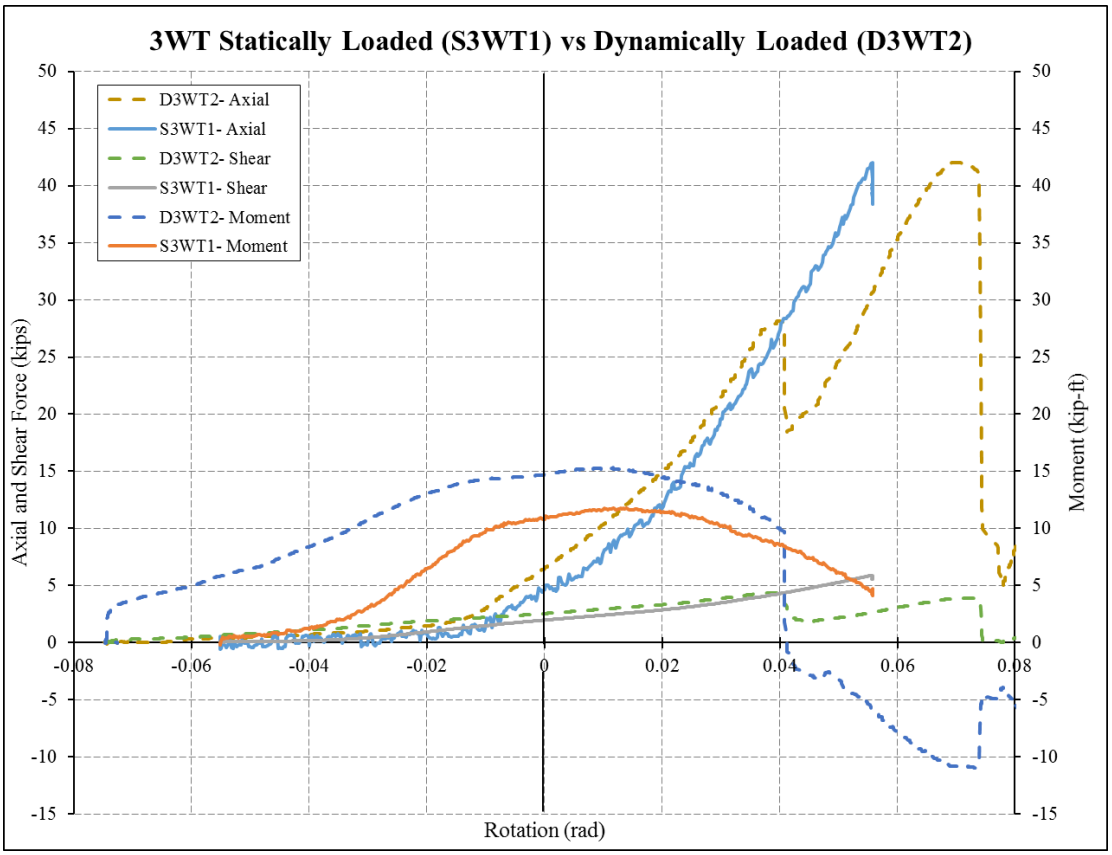

Figure 5.2.1-1: 3WT Statically Loaded versus Typical Dynamically Loaded.

5.2.2 S4WT1 versus D4WT2

Figure 5.2.2-1 illustrates a comparison between the statically loaded four-bolt test, S4WT1, with one of the dynamically loaded four-bolt tests, D4WT2. Similar to the dynamic 3WTs, the 4WTs broke with less rotation, about 0.017 radians less than what was seen in the statically loaded test. Both S4WT1 and D4WT2 had axial force magnitudes close to 40 kips at the point of every bolt break. For both the statically and dynamically loaded 4WT, the third bolt failure had the highest axial load. As with the three-bolt comparison, both the static and dynamic axial force traces have similar slopes, but the dynamic test shows the axial force accruing under slightly less rotation. Unlike the 3WTs, the moment magnitude in the 4WT tests are much closer. As the number of

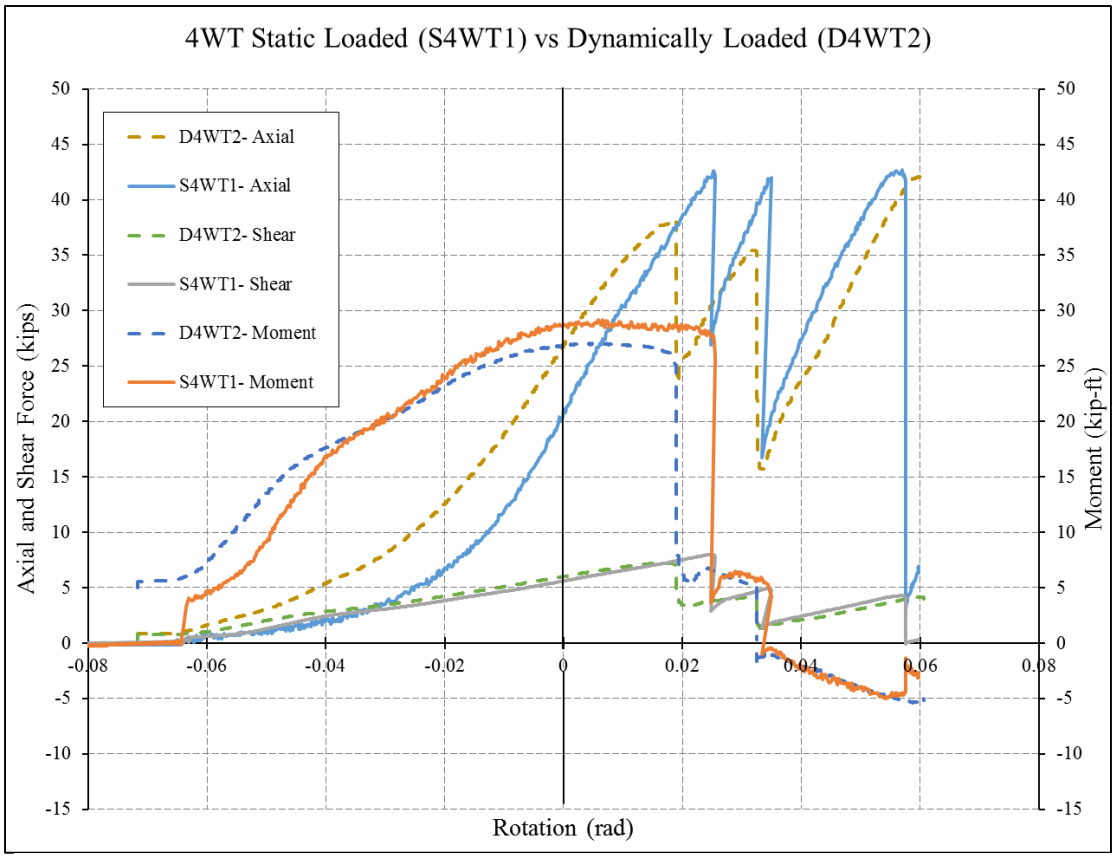

Figure 5.2.2-1: 4WT Statically Loaded versus Dynamically Loaded.

bolts increase, the amount of flexural resistance in the connection increases and becomes a primary factor in the resistance of applied load.

5.2.3 S5WT1 versus D5WT3

Figure 5.2.3-1 demonstrates the statically loaded five-bolt test, S5WT1, with one of the dynamically loaded five-bolt tests, D5WT3. Unlike the three- and four-bolt WTs, the 5WT statically and dynamically loaded tests had their first bolt breaks effectively at the same magnitude of rotation. The maximum axial forces are approximately 40 kips, which is similar in magnitude to the 3WT and 4WT configurations, for the first two bolt breaks. The axial force decreases for the third bolt break (the bolt at the centerline of the beam). D5WT3 shows a higher moment magnitude than is seen in the statically loaded test. It is interesting that D5WT3 was edging toward a plateau at its initial bolt fracture,

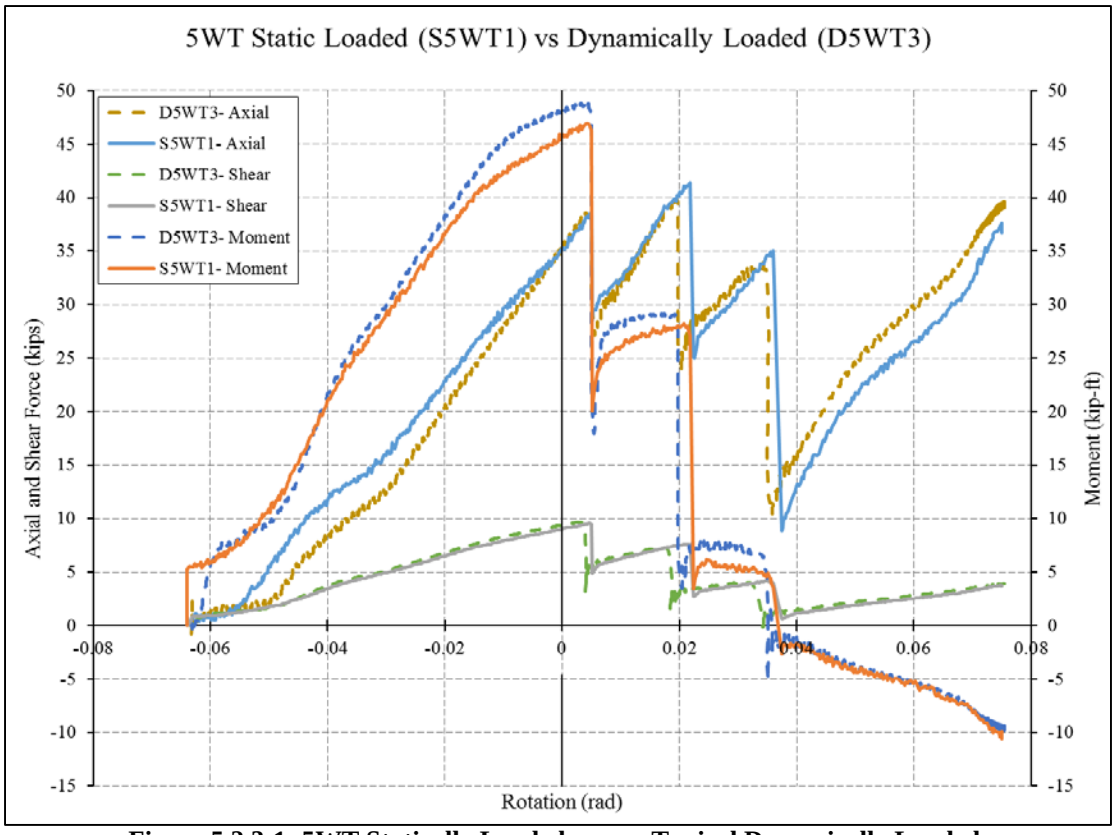

Figure 5.2.3-1: 5WT Statically Loaded versus Typical Dynamically Loaded.

whereas S5WT1 was still accruing moment force when the initial bolt fractured.

5.3 Calculation of Internal Work and Energy Dissipation

A primary objective of the current research is to compare the performance of the WT connections under different rates of applied loading (quasi-static versus quasi-dynamic). The work done by the connections can be used to compare connection performance under differing applied load rates. Work allows one to consider the forces and moment acting on the connection and how they interact with each other. No matter what type of loading the connection may be subjected to, the amount of energy that a given connection can absorb before a failure must be consistent.

Using the results of the experimental program, the work is found by taking the area under three curves: shear force versus vertical displacement, moment versus rotation, and axial force versus elongation of the connection parallel to the beam. These areas are then added to find the total work being done by the connection. These areas were calculated up to the point of initial bolt fracture, signifying that a governing limit state had occurred. A MATLAB filter was used to produce a smooth line and reduce some of the experimental noise within the data. Since some of the tests have already been filtered due to the data acquisition problem discussed in Section 4.3.1, Table 5.3-1 was created to explain which filters were applied to each test. The MATLAB scripts performed can be seen in Appendix E.

Table 5.3-1: MATLAB Filters.

MATLAB Filters			
TEST	Butterworth Low Pass Filter 1	Median Filter 1	Butterworth Low Pass Filter 2
S3WT1	--	--	X
D3WT2	X	X	--
D3WT3	X	X	--
D3WT4	--	--	X
S4WT1	--	--	X
D4WT2	X	X	--
D4WT3	--	--	X
D4WT4	--	--	X
S5WT1	--	--	X
D5WT2	--	--	X
D5WT3	--	--	X
D5WT4	--	--	X

Butterworth Low Pass Filter 1 – sampling frequency: 30, cutoff frequency 0.40
Butterworth Low Pass Filter 2 – sampling frequency: 10, cutoff frequency 0.65

The energies calculated from both the static and dynamic tests are consistent since the area under consideration extends to the initial bolt fracture. The traces are not a consistent function, so the trapezoidal rule is used to calculate the areas under each of the graphs. An example of the area found underneath the curve can be seen in Figures 5.3-1, 5.3-2, and 5.3-3. Each graph area was calculated as:

Work done by moment:

$$Area = \left(\frac{|M_i|+|M_{i+1}|}{2}\right) * \left|\theta_{n_{i+1}} - \theta_{n_i}\right| \text{ (kip-in)}, \quad (5.3\text{-}1)$$

where,

M = Moment (kip-in),

i = time step.

Work done by shear force:

$$Area = \left(\frac{|V_i|+|V_{i+1}|}{2}\right) * \left|\Delta_{n_{i+1}} - \Delta_{n_i}\right| \text{ (kip-in)}, \quad (5.3\text{-}2)$$

where,

V = Shear (kips),

i = time step.

Work done by axial force:

$$Area = \left(\frac{|A_i|+|A_{i+1}|}{2}\right) * \left|EL_{n_{i+1}} - EL_{n_i}\right| \text{ (kip-in)}, \quad (5.3\text{-}3)$$

where,

A = Axial Force (kips),

$$EL_n = \left|L_{beam} - \sqrt{{L_{beam}}^2 + {\Delta_n}^2}\right| \text{ (in)},$$

i = time step.

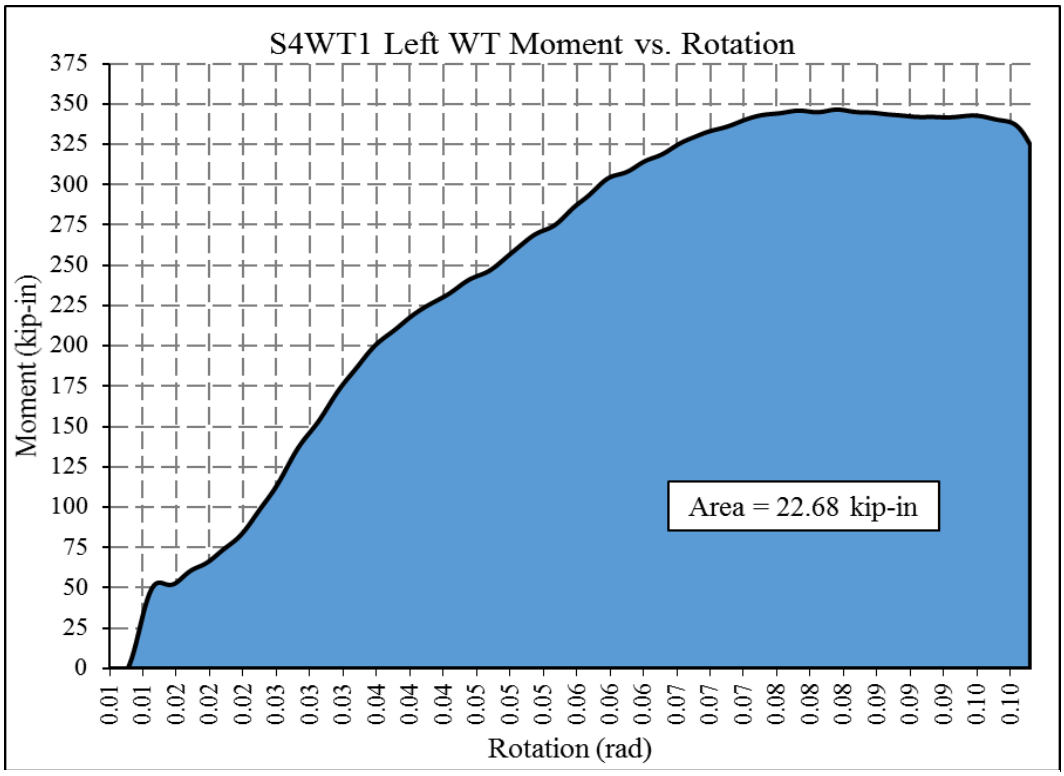

Figure 5.3-1: Sample of Work Calculated for Moment versus Rotation.

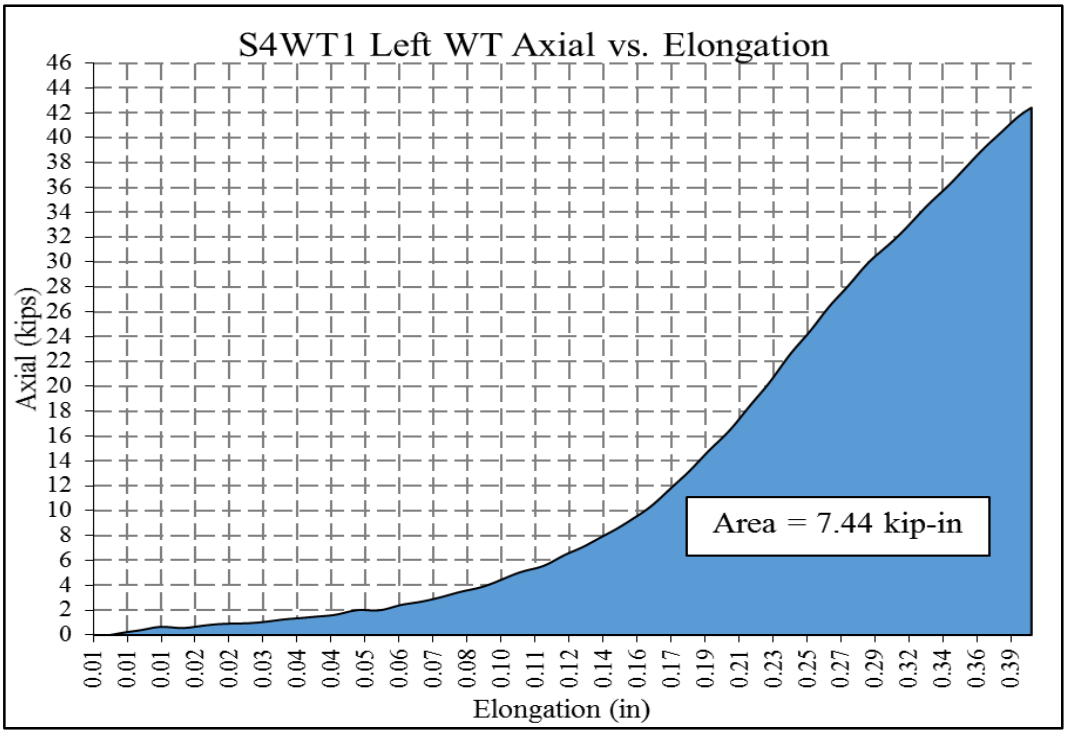

Figure 5.3-2: Sample of Work Calculated for Axial Versus Elongation of the WT Connection.

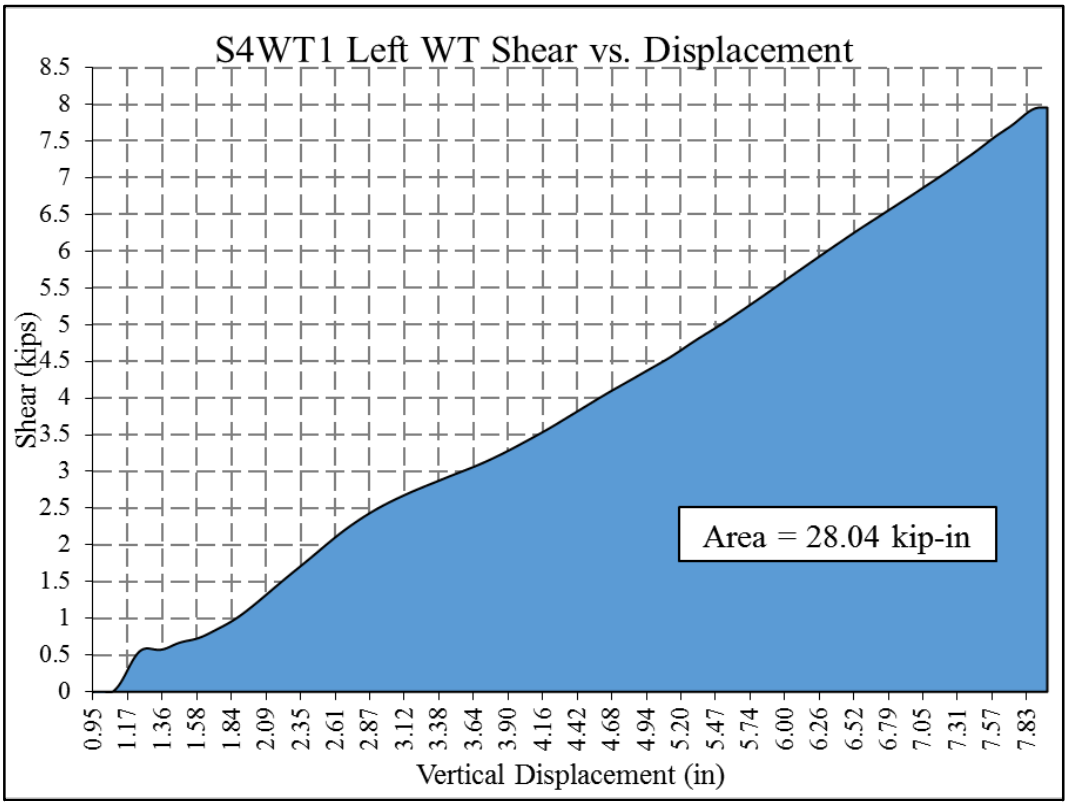

Figure 5.3-3: Sample of Work Calculated for Shear versus Vertical Displacement Measured by DWT.

5.4 Work Comparison between Friedman and Current Results for Static Tests

The statically loaded test that was performed as part of the current research initiative was for two purposes: (1) to compare to the statically loaded test conducted in 2009 by Friedman [12] and (2) to compare to the dynamically loaded tests. The data from Friedman [12] were analyzed using the same procedure seen in Section 5.3. The values were compared to the current research and a percent difference was calculated. The results of this analysis can be seen in Tables 5.4-1 through 3.

Table 5.4-1: Work Done on Three-Bolt Configuration.

Work Done on 3 Bolt Configuration				
Year Conducted	Hayes (2016)	Friedman (2009)		
Test	**S3WT1**	**3WT1**	**3WT2**	**3WT3**
	Work (k-in)	Work (k-in)	Work (k-in)	Work (k-in)
Left WT	46.94	44.50	38.37	40.77
Right WT	49.11	42.18	38.16	40.80
Average	48.03	43.34	38.27	40.79
Percent Different	NA	10%	20%	15%

Table 5.4-2: Work Done on Four-Bolt Configuration.

Work Done on 4 Bolt Configuration				
Year Conducted	Hayes (2016)	Friedman (2009)		
Test	**S4WT1**	**4WT1**	**4WT2**	**4WT3**
	Work (k-in)	Work (k-in)	Work (k-in)	Work (k-in)
Left WT	58.17	55.42	45.99	44.48
Right WT	56.70	53.93	45.58	44.54
Average	57.44	54.67	45.78	44.51
Percent Different	NA	5%	20%	23%

Table 5.4-3: Work Done on Five-Bolt Configuration.

Work Done on 5 Bolt Configuration				
Year Conducted	Hayes (2016)	Friedman (2009)		
Test	**S5WT1**	**5WT1**	**5WT2**	**5WT3**
	Work (k-in)	Work (k-in)	Work (k-in)	Work (k-in)
Left WT	57.06	55.29	55.57	65.36
Right WT	54.64	51.57	52.72	61.84
Average	55.85	53.43	54.14	63.60
Percent Different	NA	4%	3%	14%

The results in the tables show certain trends. Table 5.4-1 shows that the work done by S3WT1 compares well to 3WT1 an average of 10% difference. 3WT2 and 3WT3 do not compare as well to S3WT1 (between 20% and 15% difference), but they compare well to each other.

Similar trends hold true for the other bolt configurations. For the four-bolt configuration, S4WT1 compares favorably to 4WT1 as shown by a 5% difference in the magnitudes of work done. 4WT2 and 4WT3 compare well between themselves, but have a larger percent difference (20% to 23%) when compared to S4WT1. The work done by S5WT1 compares well to both 5WT1 and 5WT2 (4% difference or less), but 5WT3 has a larger percent difference (up to 14%) when its work is compared to S5WT1.

Percent differences up to 25% are not unexpected, considering the differences between Friedman's tests and the current research. The tests completed by Friedman were quasi-statically impulse loaded (i.e., force was slowly added manually to the system and the system was then given time to redistribute the loading before additional load was added). The load applied to the statically loaded tests performed in the current research was continuously increased as the test specimen was pulled through the actuator's full

stroke of ten inches in ten minutes. This constantly increasing load created a slightly higher magnitude of work.

Another difference between Friedman's study and the current research is in the materials used. Friedman's tests resulted in lower internal force and moment values for the three- and four-bolt configurations as compared to the results of the current research. The internal force and moment in the five-bolt configurations are closer, mainly due to their higher moment capacity.

5.5 Work Comparison between Static and Dynamic Tests

Tables 5.5-1 through 3 summarize the magnitudes of work done for the static and dynamic tests as part of the current research. A percent difference between the dynamically loaded and the statically loaded tests is included for each test.

Table 5.5-1: Static versus Dynamic Work Done on Three-Bolt Configuration.

Work Done on 3 Bolt Configuration				
Test	**S3WT1**	**D3WT2**	**D3WT3**	**D3WT4**
	Work (k-in)	Work (k-in)	Work (k-in)	Work (k-in)
Left WT	46.94	57.61	49.29	84.65
Right WT	49.11	55.60	48.07	85.03
Average	48.03	56.60	48.68	84.84
Percent Different	NA	18%	1%	77%

Table 5.5-2: Static versus Dynamic Work Done on Four-Bolt Configuration.

Work Done on 4 Bolt Configuration				
Test	**S4WT1**	**D4WT2**	**D4WT3**	**D4WT4**
	Work (k-in)	Work (k-in)	Work (k-in)	Work (k-in)
Left WT	58.17	54.98	40.21	73.56
Right WT	56.70	57.23	45.23	73.06
Average	57.44	56.10	42.72	73.31
Percent Different	NA	2%	26%	28%

Table 5.5-3: Static versus Dynamic Work Done Five-Bolt Configuration.

Work Done on 5 Bolt Configuration				
Test	**S5WT1**	**D5WT2**	**D5WT3**	**D5WT4**
	Work (k-in)	Work (k-in)	Work (k-in)	Work (k-in)
Left WT	57.06	--	55.21	119.30
Right WT	54.64	--	54.49	122.72
Average	55.85	--	54.85	121.01
Percent Different	NA	--	2%	117%

The 3WT and 5WT tests showed excellent correlation between the work being done by the static tests (S3WT1 and S5WT1) and the dynamic tests conducted during the same time frame (D3WT2 and D3WT3; D5WT3). All of these tests were conducted as part of the first round of testing, and all of these tests used bolts purchased at the same time.

One of the four-bolt dynamic tests, D4WT2, was similar in work magnitude to the static test S4WT1. D4WT3 has a significantly lower magnitude of work done than S4WT1, but that can be attributed to the data acquisition problem discussed in Section 4.3.2.3.

Tests D3WT4, D4WT4, and D5WT4 had much higher magnitudes than the rest of the tests. These tests were conducted at a later time with a different lot of bolts. The work done on the system was higher because the strength of the bolts was significantly higher. The limit state in connection remained as bolt shear rupture, even though the bolts had a higher capacity. D4WT4 had a lower axial magnitude of work being done in comparison to D3WT4 and D5WT4.

Chapter 6: Discussion and Conclusion

6.1 Introduction

This section summarizes and discusses the results from the current research. It focuses on trends and occurrences that may have happened during the experimental testing. Conclusions are drawn.

6.2 Discussion of Experimental Results

When comparing the results from the dynamic tests to static tests, the dynamic 3WT and 4WT tests consistently had an initial bolt fracture under less rotation than the corresponding static test. This is due to the fact the connection does not have as much time to redistribute the applied loads, and therefore, the system acts more brittle. In the deeper 5WT connections, the additional bolts enhance the rotational resistance so the rate at which the connection is loaded does not have a significant effect on the amount of rotation the system can withstand.

In the shallower connections, the connection could withstand more rotation but had a lower flexural capacity. The 5WT had a higher flexural capacity, but since it was connected to the whole depth of the web of the beam it also resisted rotation.

It was seen in the experiments conducted that the limit state of bolt shear rupture governs regardless of the rate of loading. The exception to this was D3WT2 and D3WT3, which broke at a lower axial force. This is discussed in further detail in Section 6.3.

Chapter 5 concluded that work done on the connection is not significantly affected by the rate of loading. The three-, four-, and five-bolt connections all have similar work done, but when looking at each individual bolt configuration, it is seen that

a similar number of rows of bolts will have similar amounts of energy absorbed before failure.

6.3 Observations in Axial Force

The three-bolt dynamic tests break with less axial force than the four- and five-bolt tests. Axial force distribution was considered as one reason for this behavior. The dynamic tests broke with less rotation than the static tests because the connection did not have time to redistribute the loads. The center of gravity for the 3WT connection is above the center of gravity for the beam (see Figure 6.3-1). Therefore, the load from the axial force has a straight line from the bottom bolt to the pin connection in the test frame. Although not directly measured as part of the current experimental research, this load path likely plays a role as to why the 3WT dynamic tests had a lower axial load at failure. Figure 6.3-1 shows a possible line of action for the axial forces in each configuration. The blue arrows illustrate the shear forces in the bolt group due to moment when taken about the center of gravity of the connection. The green arrows illustrate a likely shear force distribution due to axial force in the beam. The five-bolt connection shows the axial force being distributed uniformly to each of the five bolts because the center of gravity for both the connection and the beam are aligned.

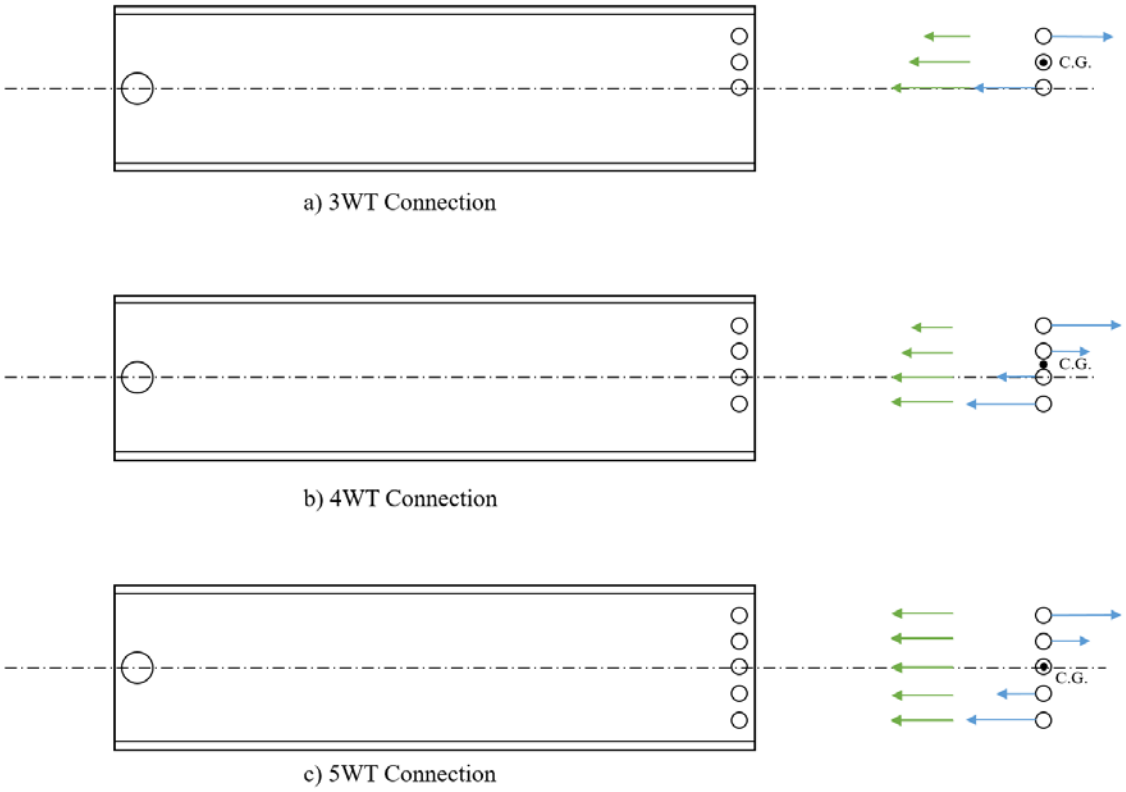

Figure 6.3-1: Free Body Diagram of Potential Forces in Connection.

6.4 Conclusion

A number of conclusions can be made about robustness of WT connections during quasi-dynamic loading. These conclusions stem from both the experimental testing conducted as part of the research initiative and also from the comprehensive literature review conducted as part of the project.

As the depth of the WT approaches the depth of the beam, the flexural capacity increases. As the flexural capacity increases, the amount of rotation the connection goes through decreases. When comparing the quasi-dynamic loading to the quasi-static loading, connections that are less than the full depth of the beam (i.e., three- and four-bolt connections used in the present study) will fail with less rotation as the loading rate

increases. Connections that are approximately the full depth of the beam, the 5WTs, behave similarly to quasi-dynamic loading as they would behave to quasi-static loading.

In the four- and five-bolt connections, a bolt failed when the axial force reached approximately 40 kips. In the three-bolt connection, the first bolt broke at a much lower axial force than 40 kips, but the second bolt failure approached an axial force magnitude of 40 kips. This is due to the moment demand being resisted by the connection.

For all the connections, the governing limit state for design was something other than shear rupture in the bolts. However, the limit state found for all experimental tests was shear rupture in the bolts. This observation can be validated through the material tests performed on the tees, as the actual steel strengths were somewhat higher than the minimum values used in the design calculations.

For WTs with similar parameters (i.e., same number of rows of bolts, same lot of bolts, and same material properties), the amount of work done (energy dissipated) by the WTs will be approximately the same. The rate at which the WT is loaded does not significantly affect the amount of energy that can be absorbed by the system.

6.5 Future Research

The testing in this project looked at a particular configuration for the WT connection with a specific rate of loading. Testing also had the initial assumption that the connection would be the weak link (the column stub and beam were designed to remain in the elastic range). Future research could consider a number of different related topics. One of these topics includes determining the true axial force distribution in each of the bolts, as was discussed in Section 6.3. Another would be finding and applying a loading rate that would match actual strain rates in a progressive collapse. Another important topic that could follow this experimental testing is finite element modeling that correlates to the experimental results. Finally, it would be useful to conduct research to compare the WT results to a similar connection type, such as a bolted double angle connection.

It was interesting to find that many of the connections exhibited bolt failures when the axial load in the connection had reached 40 kips. This would be an interesting topic that could use some further research. If this is consistent with additional tests and with other types of shear connections, it could lay groundwork for refined code provisions in progressive collapse resistance.

References

[1] Raebel, Christopher. 2011. “A Quantitative Study of Robustness Characteristic in Steel Framed Structures.” Ph. D. diss., Marquette University.

[2] AISC. 2010a. *ANSI/AISC 360-10: Specifications for the Design of Steel Buildings (and Commentary),* American Institute of Steel Construction, Chicago, IL.

[3] American Concrete Institute (ACI). 2011. *318-11: Building Code Requirements for Structural Concrete and Commentary.* Framington Hills, MI

[4] International Code Council (ICC). 2012. International Building Code 2012. Country Club Hills, IL.

[5] Astaneh, A. and M. Nader. 1989. “Design of Framing Shear Connections.” *AISC Engineering Journal.* First Quarter, 1989, pp. 9-20.

[6] Thornton, W.A. 1996. “A Rational Approach to Design of Tee Shear Connections.” *AISC Engineering Journal.* First Quarter, 1996, pp. 34-37.

[7] Thornton, W.A. “Strength and Ductility Requirements for Simple Shear Connections with Shear and Axial Loads.” In AISC Conference Proceedings. 1997.

[8] Guravich, S.J. and J.L. Dawe. 2006. “Simple Beam Connections in Combined Shear and Tension.” *Canadian Journal of Civil Engineering*. Vol. 33, pp. 357-372.

[9] Girhammar, U.A. 1980. *Behaviour of Bolted Beam-Column Connections under Catenary Action in Damaged Steel Structures.* Lolea: Swedish Council for Building Research.

[10] Sadek, F., S. El-Tawil and H.S. Lew. 2008. “Robustness of Composite Floor Systems with Shear Connection: Modeling, Simulation, and Evaluation.” *ASCE Journal of Structural Engineering*. Vol. 134 (11), pp. 1717-1725.

[11] Federal Emergency Management Agency (FEMA). 2000. *FEMA-355D State of the Art Report on Connection Performance*. Washington, DC: FEMA.

[12] Friedman, Adam D. 2009. “Axial, Shear and Moment Interaction of WT Connections.” Master’s thesis, Milwaukee School of Engineering.

[13] Raebel C., C. Foley and A. Friedman. “Experimental Evaluation of the Robustness of Flexible WT Steel Connections.” In International Structural Specialty Specialty Conference. 6-9 June 2012.

[14] Thompson, Scott. 2009. “Axial, Shear and Moment Interaction of Single Plate ‘Shear Tab’ Connections.” Master’s thesis, Milwaukee School of Engineering.

[15] Foley C., C. Schneeman and K. Barnes. “Quantifying and Enhancing the Robustness in Steel Structures.” *Engineering Journal*. Fourth Quarter, 2008, pp. 247-286.

[16] Daneshvar H. and R.G. Driver. “Application of Seismic Steel Connection Experiments to Column Removal Scenario.” In 2nd Specialty Conference on Disaster Mitigation. 9-12 June 2010.

[17] Alashker Y., S. El-Tawil and F. Sadek. “Progressive Collapse Resistance of Steel-Concrete Composite Floor.” *Journal of Structural Engineering*. October 2010. Pp.1187-1196.

[18] Oosterhof S. and R.G. Driver. “An Approach to Testing the Performance of Steel Connections Subjected to Extreme Loading Scenarios. In Interactional Engineering Mechanics and Materials Specialty Conference. 14-17 June 2011.

[19] Weigand J. and J. Berman. “Integrity of Steel Single Plate Shear Connections Subjected to Simulated Column Removal.” *Journal of Structural Engineering.* December 2013.

[20] Main J. and F. Sadek. July 2012. *Robustness of Steel Gravity Frame Systems with Single-Plate Shear Connection.* Technical Note 1749. Engineering Laboratory, National Institute of Standards of Technology.

[21] American Society of Civil Engineers. 2010. *Minimum Design Loads for Buildings and Other Structures 7-10.* Reston, VA.

[22] Oosterhof S. and R.G. Driver. “Behavior of Steel Shear Connection under Column-Removal Demands.” *Journal of Structural Engineering.* July 2014.

[23] Lesser J. 2016. “Robustness of Shear Plate under Quasi-Dynamic Loading.” Working Paper. Master’s thesis. Milwaukee School of Engineering.

[24] ASTM International. ASTM Committee E28 on Mechanical Testing. Subcommittee E28.04 on Uniaxial Testing. 1 April 2004. Standard Test Methods for Tension Testing of Metallic Materials. Designation E8 – 15. In annual Book of ASTM Standards. Volume 03.01. West Conshohocken, PA: ASTM International.

[25] Kulak, Geoffrey L., J. Fisher and J.H.A. Struik. 2001. *Guide to Design Criteria for Bolted and Riveted Joints Second Edition*. United States: Research Council on Structural Connection.

Appendix A: WT Connection Calculation

Given:

The capacity of WT5×22.5 three-bolt connection based on the geometry presented in Figure A-1. All the calculations were performed using 3/4 in. diameter ASTM A325-X bolts with standard holes. The column stub was assumed to be infinitely strong compared to the connection. The following is the calculation for the three WT. Table 3.2-1 summarized the results for the three, four, and five WT connections.

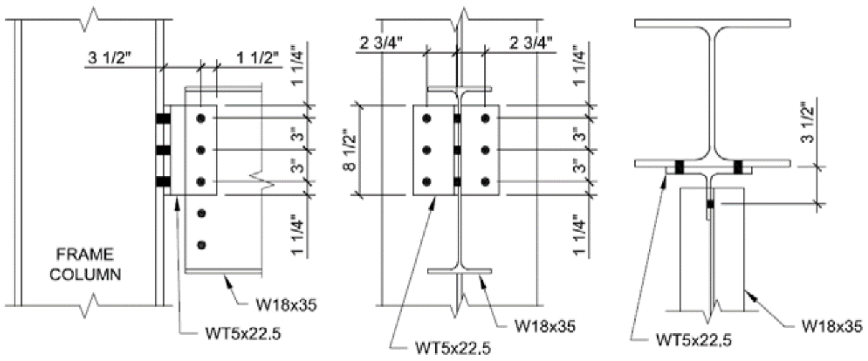

Figure A-1: Connection Layout.

Geometric and Material Properties

WT5x22.5

$t_s := 0.35$ in $d_{wt} := 5.05$ in $t_{fwt} := 0.62$ in $b_{fwt} := 8.02$ in $k := \frac{13}{16}$ in

ASTM A992 $F_y := 50$ ksi $F_u := 65$ ksi

Edge Distance lev := 1.25 leh := 1.5 Bolt Spacing s := 3 gage := 5.5 lw := 8.5

BEAM: W18x35

$t_{wb} := 0.300$ in $d_b := 17.7$in $t_{fb} := 0.425$ in

ASTM A992 $F_y := 50$ ksi $F_u := 65$ ksi

COLUMN: W12x53

$t_{wc} := 0.345$ in $d_c := 12.1$ in $t_{fc} := 0.575$ in

ASTM A992 $F_y := 50$ ksi $F_u := 65$ ksi

WT Connection Limit States

1. Shear Rupture of Bolts
2. Bearing and Tear Out in WT Stem
3. Bearing in Beam Web
4. Block Shear Rupture of WT Stem (L-Shape)
5. Shear Yielding of WT Stem
6. Shear Rupture of WT Stem
7. Shear Rupture of Beam Web
8. Beam Gross Shear Yield
9. Flexural Yield of Flange
10. Rotational Ductility
11. Combined Shear and Tension Interaction

3 Bolt Design

$n := 3$

1. SHEAR RUPTURE OF BOLTS

$rn := 30$

$R_n := rn \cdot n$ (A-1)

$R_n = 90$ kips

2. Bearing and Tear Out in WT Stem

Edge Bolt Tear Out

$lc := lev - \frac{13}{32} = 0.84$ (A-2)

$R_{eb} := 1.2 \cdot lc \cdot t_s \cdot F_u = 23.03$ (A-3)

Non-edge Bolt Tear Out

$lc := s - \frac{13}{16} = 2.19$ (A-4)

$R_{enb} := 1.2 \cdot lc\, t_s \cdot F_u = 59.72$ (A-5)

Bearing for Edge or Nonedge Bolts

$d := 0.75$

$R_{ebr} := 2.4 \cdot d \cdot t_s \cdot F_u = 40.95$ (A-6)

Bearing for Nonedge Bolt Controls Tearout for Edge Bolt

$Rn := R_{eb} + (n - 1) \cdot R_{ebr}$ (A-7)

$Rn = 104.93$ kips

3. Bearing in Beam Web

$R_{ebr} := 2.4 \cdot d \cdot t_{wb} \cdot F_u = 35.1$ (A-8)

$Rn := n \cdot R_{ebr}$ (A-9)

$Rn = 105.3$ kips

4. Block Shear Rupture in WT Stem

L Shape Block Shear

$$A_{gv} := (lw - lev)\cdot t_s = 2.54 \quad \text{(A-10)}$$

$$A_{nv} := A_{gv} - (n - 0.5)\cdot\left(\frac{7}{8}\right)\cdot\left(t_s\right) = 1.77 \quad \text{(A-11)}$$

$$A_{nt} := \left[leh - 0.5\cdot\left(\frac{7}{8}\right)\right]\left(t_s\right) = 0.37 \quad \text{(A-12)}$$

$$Ubs := 1$$

$$Rn := \begin{cases} \left(0.6\cdot F_u\cdot A_{nv} + Ubs\cdot F_u\cdot A_{nt}\right) & \text{if } \left(0.6\cdot F_u\cdot A_{nv} + Ubs\cdot F_u\cdot A_{nt}\right) \le \left(0.6\cdot F_y\cdot A_{gv} + Ubs\cdot F_u\cdot A_{nt}\right) \\ \left(0.6\cdot F_y\cdot A_{gv} + Ubs\cdot F_u\cdot A_{nt}\right) & \text{otherwise} \end{cases} \quad \text{(A-13)}$$

Rn = 93.27 kips

5. Shear Yielding of WT Stem

$$Rn := 0.6\cdot F_y\cdot A_{gv} \quad \text{(A-14)}$$

Rn = 76.12 kips

6. Shear Rupture of WT Stem

$$Rn := 0.6\cdot F_u\cdot A_{nv} \quad \text{(A-15)}$$

Rn = 69.1 kips

7. Shear Rupture of Beam Web

$$A_{nv} := \left[d_b - n\cdot\left(\frac{7}{8}\right)\right]\cdot t_{wb} = 4.52 \quad \text{(A-16)}$$

$$Rn := 0.6\cdot F_u\cdot A_{nv} \quad \text{(A-17)}$$

Rn = 176.38 kips

8. Beam Gross Shear Yield

$$A_w := \left(d_b\right)\cdot t_{wb} = 5.31 \quad \text{(A-18)}$$

$$Rn := 0.6\cdot F_y\cdot A_w \quad \text{(A-19)}$$

Rn = 159.3 kips

9. Flexural Yield of WT Flange

$$S_x := \frac{\left(t_s\cdot lw^2\right)}{6} = 4.21 \quad \text{(A-20)}$$

$$e := \left(\frac{b_{fwt}}{2}\right) - \left(\frac{t_{wb}}{2}\right) = 3.86 \quad \text{(A-21)}$$

$$Rn := \frac{\left(F_y\cdot S_x\right)}{e} \quad \text{(A-22)}$$

Rn = 54.59 kips

10. Rotational Ductility

$$b := \frac{(gage - 2\cdot k)}{2} = 1.94 \quad \text{(A-23)}$$

$$d_{min} := \begin{cases} \left[0.163\cdot t_{fwt}\cdot\sqrt{\left(\frac{F_y}{b}\right)\cdot\left[\left(\frac{b^2}{lw^2}\right)+2\right]}\right] & \text{if } 0.163\cdot t_{fwt}\cdot\sqrt{\left(\frac{F_y}{b}\right)\cdot\left[\left(\frac{b^2}{lw^2}\right)+2\right]} \le 0.69\cdot\sqrt{t_{fwt}} \\ \left(\left(0.69\cdot\sqrt{t_{fwt}}\right)\right) & \text{otherwise} \end{cases} \quad \text{(A-24)}$$

$d_{min} = 0.54$

$$d_{mincheck} := \begin{cases} \text{"NO GOOD"} & \text{if } d_{min} > 0.75 \\ \text{"OK"} & \text{otherwise} \end{cases} = \text{"OK"}$$

11. Combined Shear and Tension Interaction

Max loading if bolt shear

$r_{uv} := 17.9$

$P_u := r_{uv}\cdot(2\cdot n) = 107.4$ (A-25)

$e := 3.5$

$dm := 9$

$Ab := \pi\cdot\frac{0.75^2}{4}$ (A-26)

$r_{ut} := \frac{(P_u\cdot e)}{(4\cdot dm)} = 10.44$ (A-27)

$F_{nt} := 90$

$F_{nv} := 54$

$F_{ntprime} := 1.3\cdot F_{nt} - \left(\frac{F_{nt}}{F_{nv}}\right)\left(\frac{r_{uv}}{Ab}\right) = 49.47$ (A-28)

$R_{ntensile} := F_{ntprime}\cdot Ab = 21.86$ (A-29)

Rntensile > rut

If bolt tension maximum will never happen

$Rn := P_u = 107.4$ kips

Appendix B: Shop Drawings

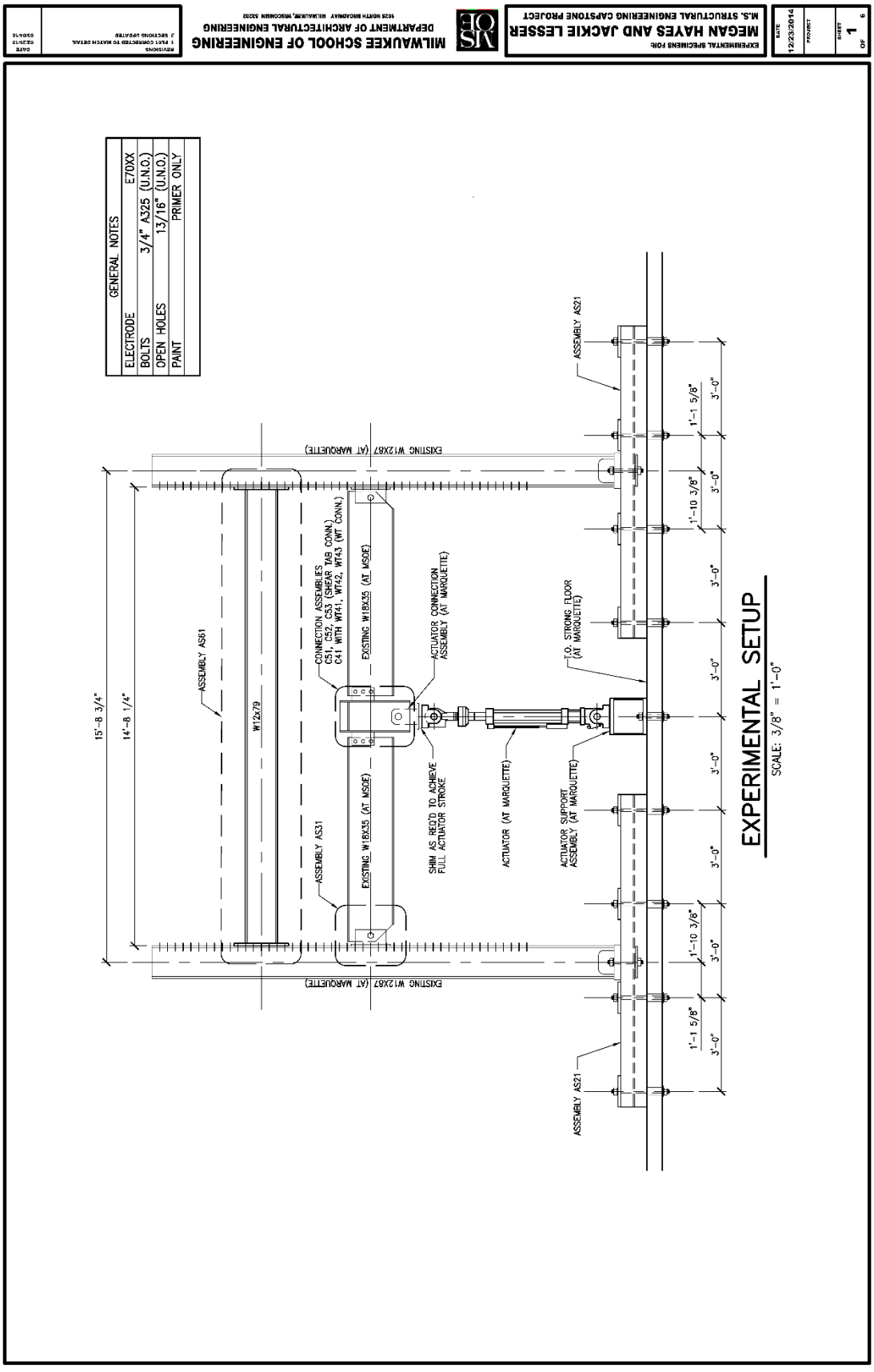

Figure B-1: Experimental Setup.

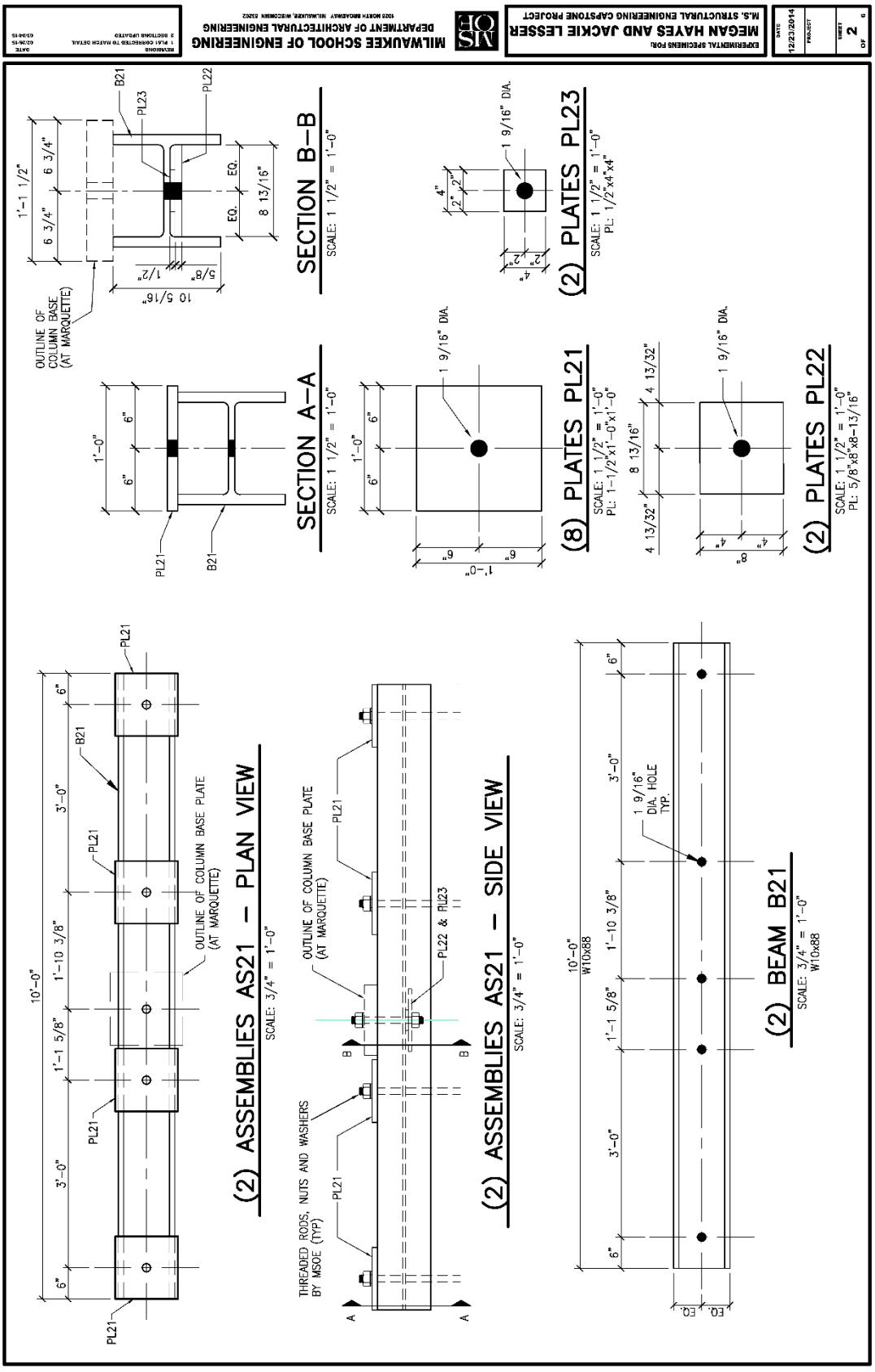

Figure B-2: Test Frame Parts.

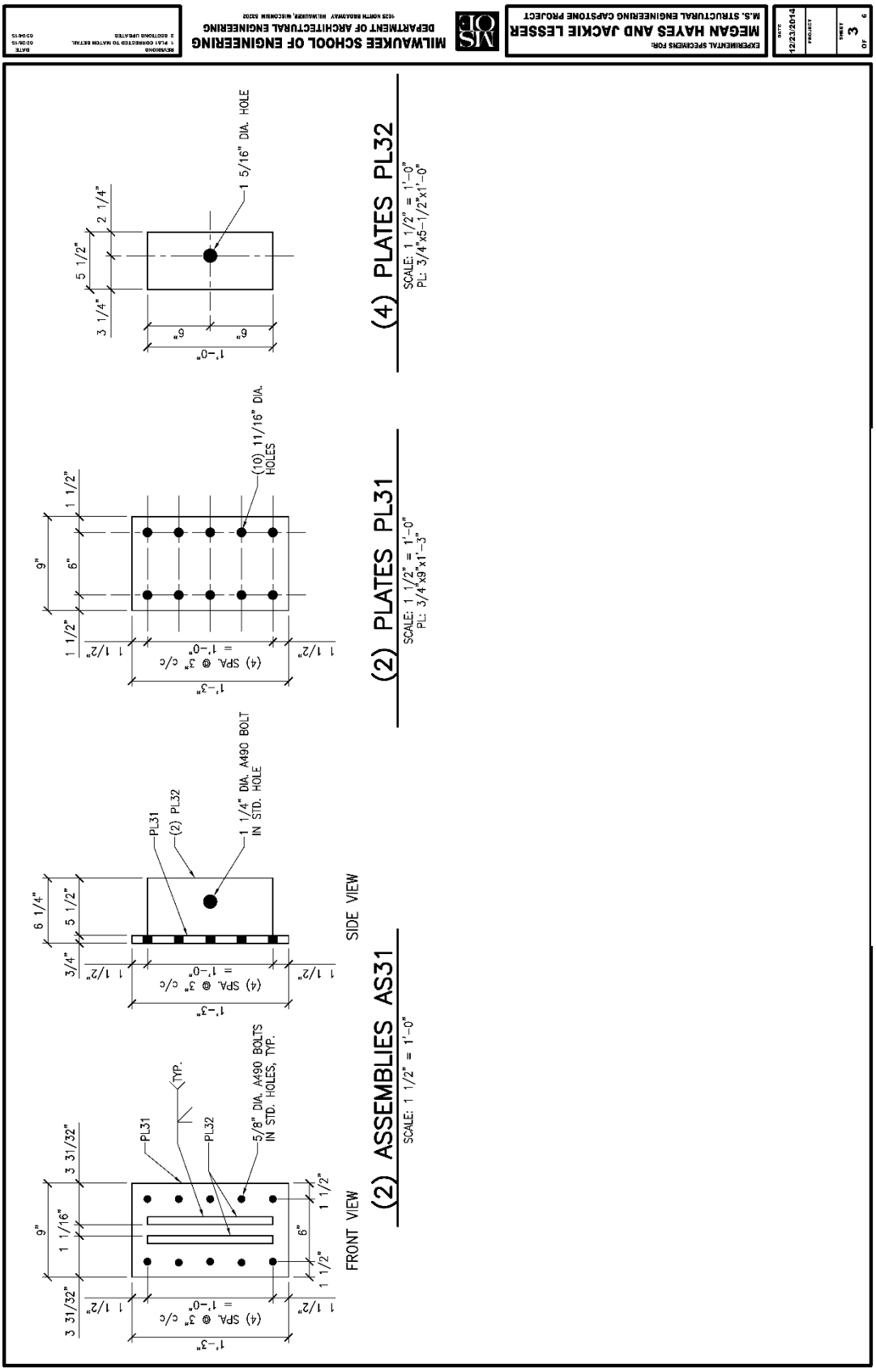

Figure B-3: Test Frame Parts.

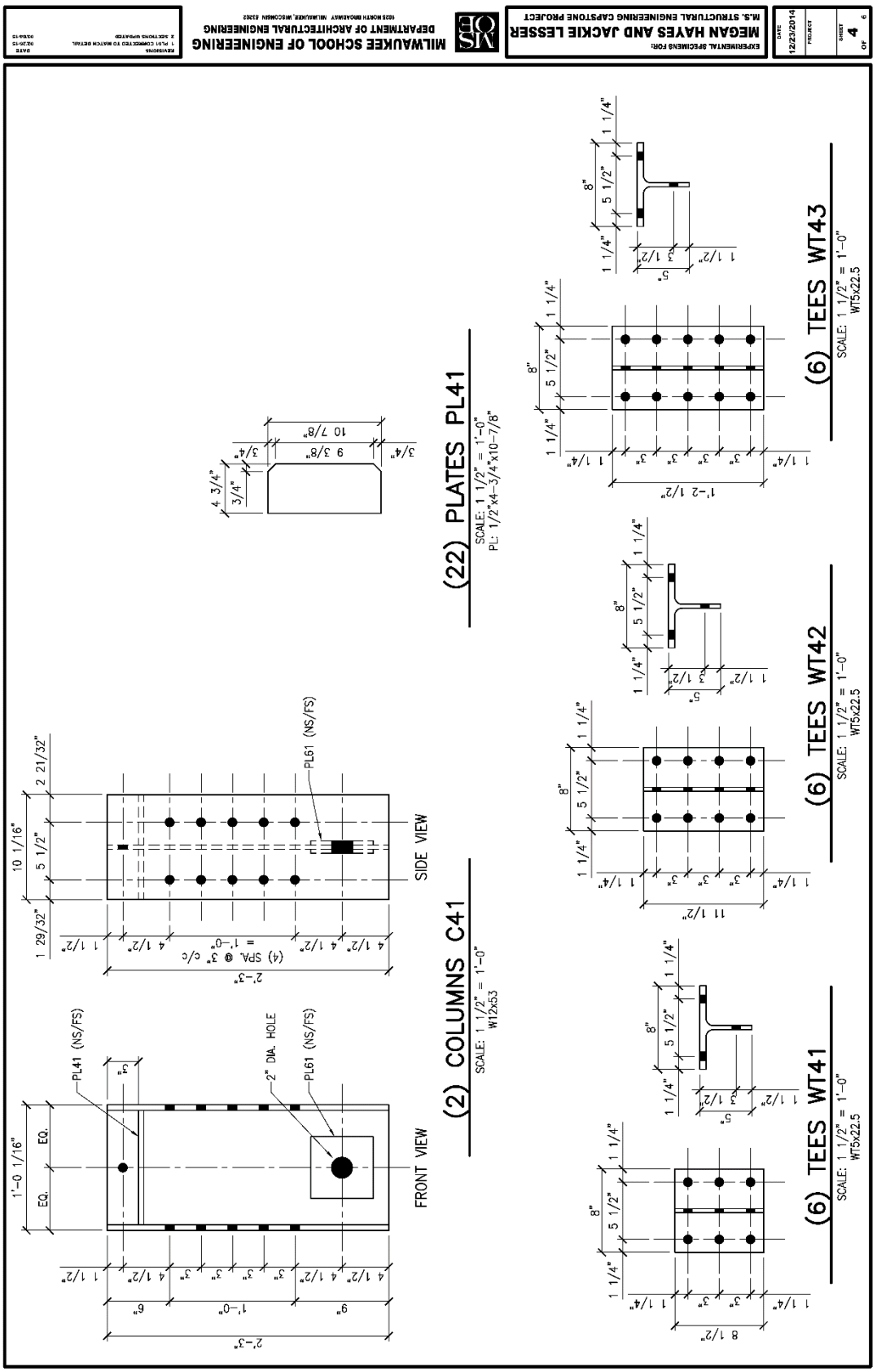

Figure B-4: Columns and WTs.

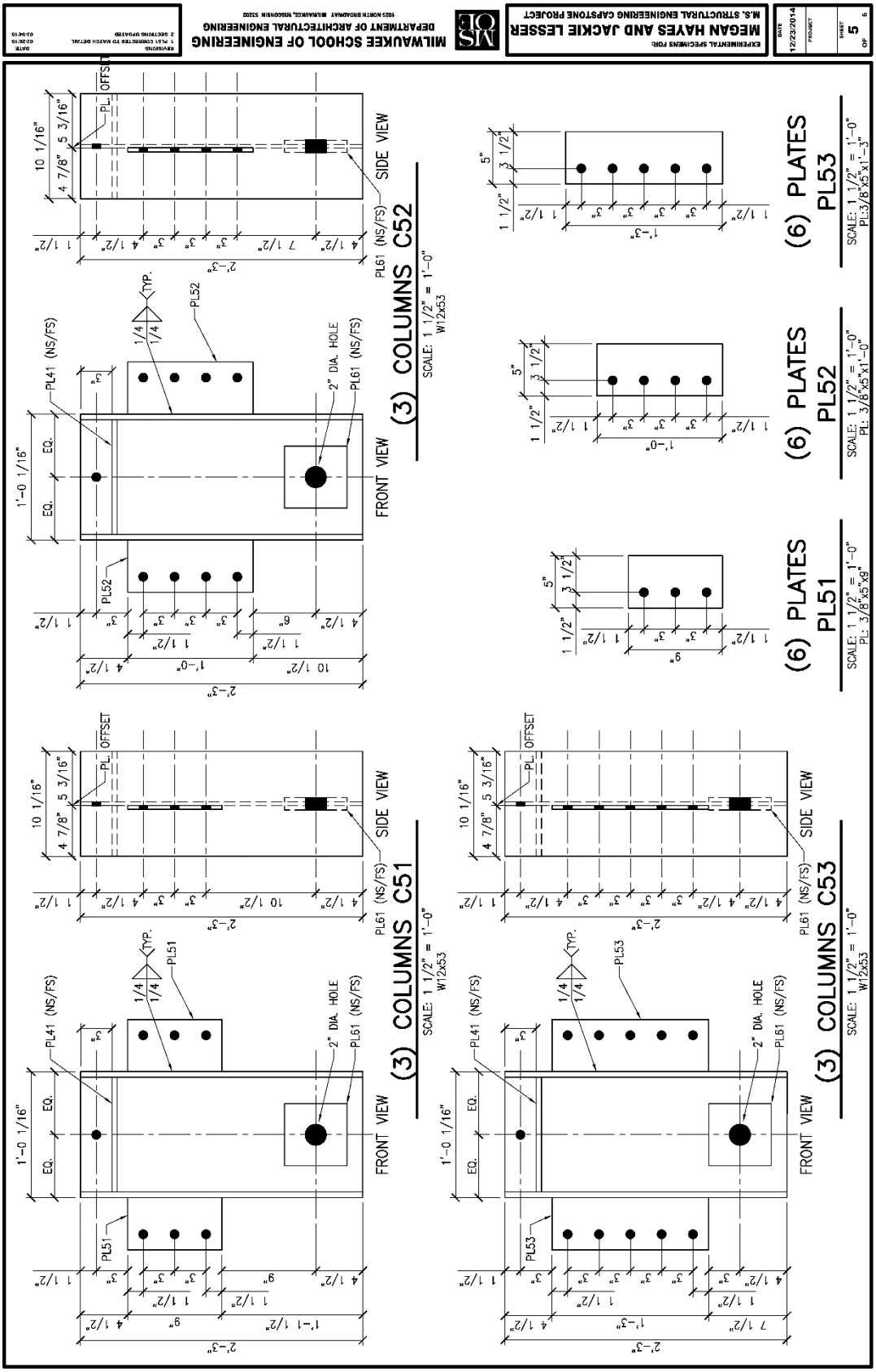

Figure B-5: Columns and Shear Tabs.

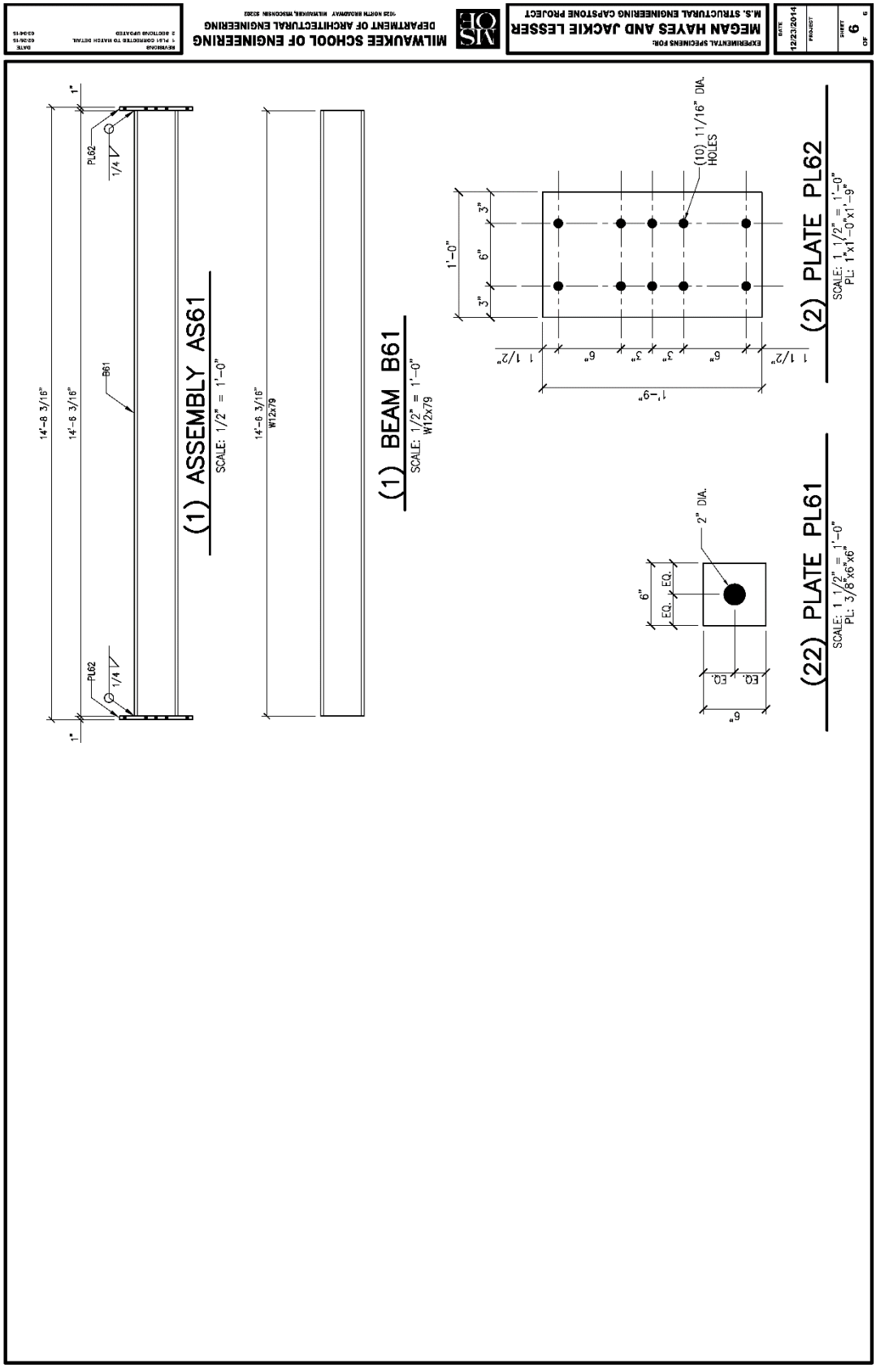

Figure B-6: Test Framing Beam and Parts.

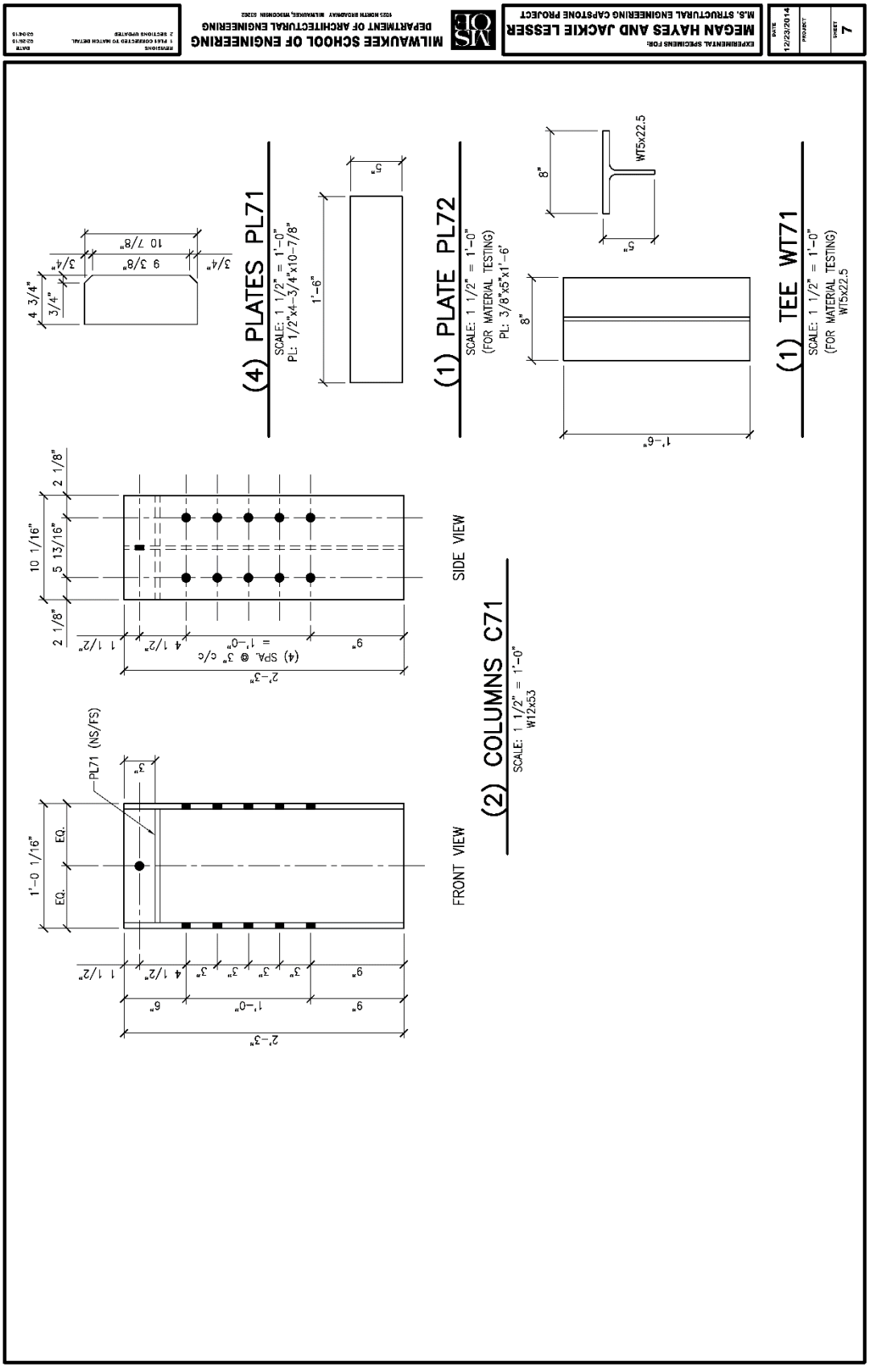

Figure B-7: Plain Material to be used for Material Test.

Appendix C: Material Test

11/20/2015

Sample ID: MSOE flange 1.mss
Specimen Number: 9
Tagged: False

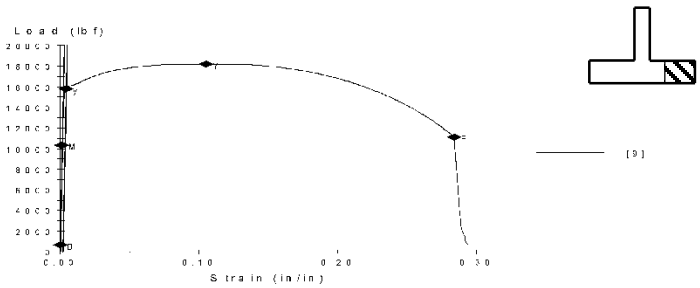

Specimen Results:

Name	Value	Units
Thickness	0.37475	in
Width	0.62440	in
Area	0.23399	in^2
Modulus	31409586.49122	psi
Load At Offset Yield	15806.74642	lbf
Stress At Offset Yield	67551.74639	psi
Load At Yield	18228.18363	lbf
Stress At Yield	77900.00579	psi
Peak Load	18228.18363	lbf
Peak Stress	77900.00579	psi
Break Load	11113.88312	lbf
Break Stress	47496.31543	psi
Strain At Break	0.28366	in/in

Specimen Comment:

11/20/2015

Sample ID: MSOE flange 2.mss
Specimen Number: 10
Tagged: False

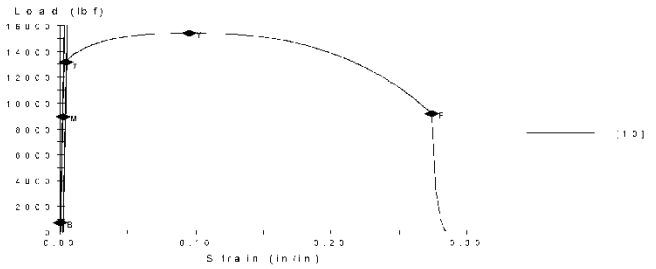

Specimen Results:

Name	Value	Units
Thickness	0.37755	in
Width	0.51885	in
Area	0.19589	in^2
Modulus	28780275.02311	psi
Load At Offset Yield	13183.51188	lbf
Stress At Offset Yield	67299.74990	psi
Load At Yield	15414.88992	lbf
Stress At Yield	78690.58303	psi
Peak Load	15414.88992	lbf
Peak Stress	78690.58303	psi
Break Load	9179.89718	lbf
Break Stress	46861.92799	psi
Strain At Break	0.27395	in/in

Specimen Comment:

11/20/2015

Sample ID: MSOE flange 3.mss
Specimen Number: 11
Tagged: False

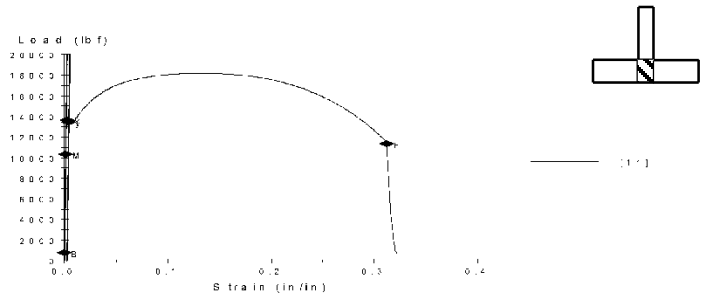

Specimen Results:

Name	Value	Units
Thickness	0.37080	in
Width	0.62345	in
Area	0.23117	in^2
Modulus	28971837.99778	psi
Load At Offset Yield	13426.96991	lbf
Stress At Offset Yield	58081.16138	psi
Load At Yield	13627.73929	lbf
Stress At Yield	58949.63123	psi
Peak Load	18153.29482	lbf
Peak Stress	78525.86647	psi
Break Load	11368.70292	lbf
Break Stress	49177.69782	psi
Strain At Break	0.31241	in/in

Specimen Comment:

11/20/2015

Sample ID: MSOE flange 4.mss
Specimen Number: 12
Tagged: False

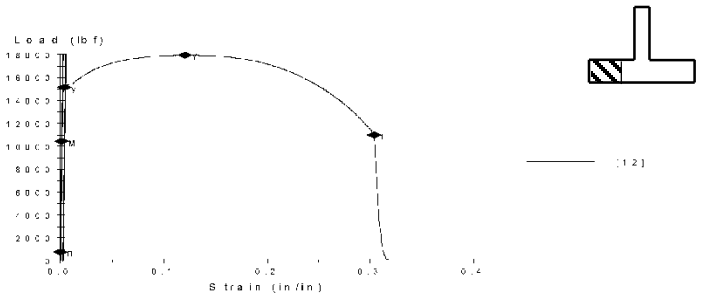

Specimen Results:

Name	Value	Units
Thickness	0.37080	in
Width	0.62345	in
Area	0.23117	in^2
Modulus	28154295.26773	psi
Load At Offset Yield	15133.57503	lbf
Stress At Offset Yield	65463.43812	psi
Load At Yield	17933.18070	lbf
Stress At Yield	77573.71687	psi
Peak Load	17933.18070	lbf
Peak Stress	77573.71687	psi
Break Load	10999.80171	lbf
Break Stress	47581.93865	psi
Strain At Break	0.30375	in/in

Specimen Comment:

11/20/2015

Sample ID: MSOE flange 5.mss
Specimen Number: 13
Tagged: False

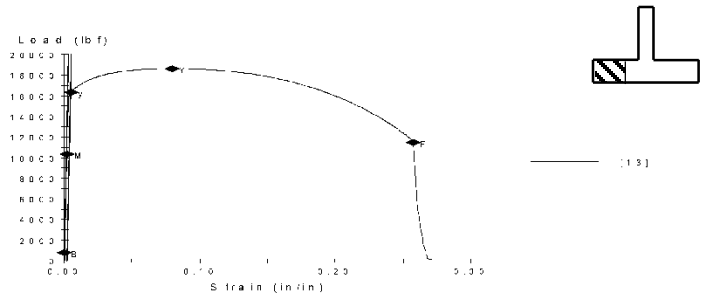

Specimen Results:

Name	Value	Units
Thickness	0.37275	in
Width	0.62325	in
Area	0.23232	in^2
Modulus	28530814.54422	psi
Load At Offset Yield	16336.55582	lbf
Stress At Offset Yield	70320.05353	psi
Load At Yield	18608.24978	lbf
Stress At Yield	80098.46966	psi
Peak Load	18608.24978	lbf
Peak Stress	80098.46966	psi
Break Load	11477.29726	lbf
Break Stress	49403.56872	psi
Strain At Break	0.25749	in/in

Specimen Comment:

11/20/2015

Sample ID: MSOE web 1.mss
Specimen Number: 6
Tagged: False

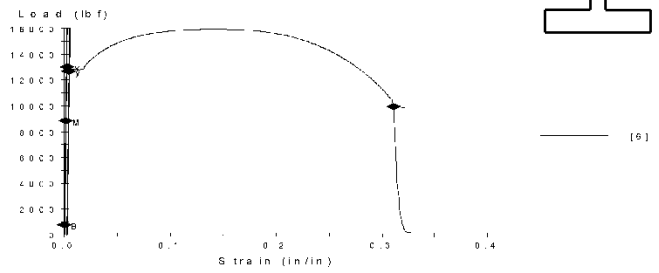

Specimen Results:

Name	Value	Units
Thickness	0.33400	in
Width	0.62350	in
Area	0.20825	in^2
Modulus	27241473.06140	psi
Load At Offset Yield	12700.86411	lbf
Stress At Offset Yield	60988.64373	psi
Load At Yield	13040.80763	lbf
Stress At Yield	62621.02829	psi
Peak Load	15941.96852	lbf
Peak Stress	76552.19600	psi
Break Load	9943.10077	lbf
Break Stress	47746.06083	psi
Strain At Break	0.31068	in/in

Specimen Comment:

11/20/2015

Sample ID: MSOE web 2.mss
Specimen Number: 8
Tagged: False

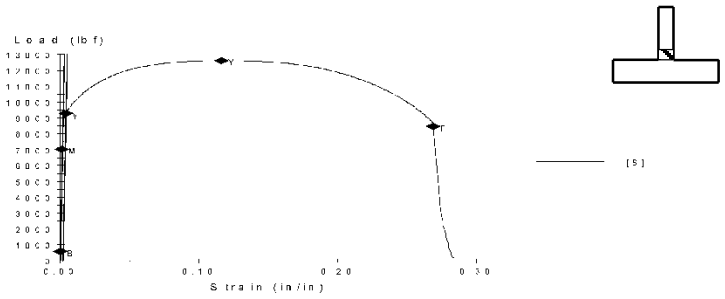

Specimen Results:

Name	Value	Units
Thickness	0.25485	in
Width	0.62325	in
Area	0.15883	in^2
Modulus	31567485.96111	psi
Load At Offset Yield	9304.67648	lbf
Stress At Offset Yield	58580.48773	psi
Load At Yield	12607.55792	lbf
Stress At Yield	79374.80616	psi
Peak Load	12607.55792	lbf
Peak Stress	79374.80616	psi
Break Load	8460.60147	lbf
Break Stress	53266.35071	psi
Strain At Break	0.26916	in/in

Specimen Comment:

Appendix D: Bolt Compensation Report

Analysis

of

Hayes MSST

3/4 Inch Diameter ASTM A325 Bolts

for

Mr. David Newman
Milwaukee, WI

by

Raymond A. Fournelle, Ph.D., P.E.
Metallurgical Consultant
1029 North Jackson Street, #509A
Milwaukee, WI 53202

January 7, 2016

_____
Raymond A. Fournelle, Ph.D., P.E.
Metallurgical Consultant

Summary

The Rockwell C hardness, microstructure and chemical composition of three different ¾ inch ASTM A325 heavy hex bolts were evaluated and compared to ASTM A325 specifications. The bolts were given the following designations: HS Bolt, Chinese JDF Bolt and "n" Bolt. The Rockwell C hardness of all three bolts met the ASTM A325 specification that the hardness be less than HRC 34. All three bolts exhibited quenched and tempered microstructure; however, the microstructure at the center of the shanks of the "n" bolts was different from that in the center of the shanks of the HS bolts and the Chinese JDF bolts. Both the Chinese JDF and HS bolts exhibited uniform tempered martensitic microstructures across the cross section of the shanks, while the "n" bolts exhibited a tempered martensitic microstructure near the outer edge of the cross section and a microstructure consisting of a mixture of tempered martensite, ferrite, pearlite and bainite in the center. As such, the hardness of the "n" bolts was slightly lower in the center. Energy dispersive spectroscopy of the bolt materials shows that the HS bolts and the Chinese JDF bolts are made of alloy steels containing small amounts of chromium, while the "n" bolts are made of carbon steel. This probably explains why the "n" bolts were softer at the center. They did not have enough alloy elements to through harden. Regardless of the differences in the hardness, microstructure and composition, all three bolts meet the requirements of ASTM A325.

Background

Sectioned ¾-10 x 2 ¼ A325 heavy hex bolts from three different manufacturers (HS Bolt, Chinese JDF Bolt and "n" Bolt) were provided by Mr. David Newman for determination of their hardness, microstructure and chemistry. Four cross sections about ¼ inch thick had been cut from the shanks of the bolts with a water cooled band saw. The markings on the heads of the bolts were consistent with them being ASTM A325 Type 1 bolts. According to the specification these can be made of either carbon steel or alloy steel. While the chemical composition specification for carbon steel bolts is straight forward, that for alloy steel bolts allows for a variety of combinations of alloy elements like Mn, Cr, Ni, Mo and Si.

Hardness Testing

The cross section surfaces on one section from each bolt were first ground through 120 grit SiC. Five Rockwell C hardness measurements were then performed on one side of these specimens in the pattern shown in Figure 1 using a Wilson Rockwell Model B523T hardness tester, which was checked against Yamamoto Test Block #437-669 (HRC 31.6) for calibration.

As can be seen in Table 1 the average hardness of each bolt was below HRC 34, which is a requirement of ASTM A325 for ¾ inch x 2 ¼ inch bolts. It can also be seen that the hardness values for the HS and Chinese JDF bolts were uniform over the entire cross section, while the hardness of the "n" bolt was lower in the center. As shown below this is related to the "n" bolt being made of carbon steel and not having enough hardenability to transform to martensite at its center on quenching during heat treatment. Both the HS and Chinese JDF bolts were made of alloy steel and through hardened to 100% martensite at their center on quenching. This difference between the "n" bolt and the HS and Chinese JDF bolts notwithstanding, the "n" bolts still meet ASTM A325 specifications.

Metallography

A second cross section specimen from each bolt was mounted in LECOSET 100 acrylic mounting compound for examination of its microstructure. A third specimen from each bolt was cut in half with an abrasive cut off wheel, and half of it was mounted in LECOSET 100 for examination of the microstructure of the longitudinal section. These metallographic specimens were then ground through 600 grit SiC, polished through 1.0 μm Al_2O_3 and etched for 5 seconds with 3% Nital. They were examined and photographed with an Olympus PME3 metallograph using bright field illumination.

As can be seen in Figures 2 and 3 the HS bolts and the Chinese JDF bolts have uniform tempered martensitic microstructures over their entire cross sections. This is what one would expect in through hardened bolts. As can be seen in Figure 4 the microstructure at

the center of the "n" bolt consisted of a complex mixture of tempered martensite, ferrite, pearlite and bainite, while that ¼ inch from the center consists of tempered martensite. As such, it is not through hardended. This is what one would expect from a carbon steel bolt of this size. Note that, while this bolt is not through hardened, it does meet the hardness, heat treatment and chemistry specified in ASTM A325.

Energy Dispersive X-ray (EDS) Analysis

Energy dispersive analysis of the bolt materials was performed on the center of one of the cross sections of each of the bolts after the cross section had been ground through 240 grit SiC. The EDS was performed using a JEOL JSM 6510LV Scanning Electron Microscope equipped with a NORAN System 7 Spectral Imaging System. The microscope was operated at 20kV and a working distance of 19 mm. A 100 second acquisition time was used to acquire each spectrum, and a standardless filter with a φ-ρ-z correction was used to quantify it.

As can be seen in Figures 5 and 6 and Table 2 both the HS bolts and the Chinese JDF bolts contain a small amount of Cr in combination with a small amount of Mn, which indicates that they are made of alloy steel according to the definition of alloy steel in ASTM A325. This is why these bolts have been through hardened. The Cr and Mn give them sufficient hardenability to through harden. As can be seen in Figure 7 and Table 2 the "n" bolts do not contain any Cr. This means that they are made of carbon steel, which has less hardenability that the alloy steels used for the HS bolts and the Chinese JDF bolts. This is why the "n" bolts did not through harden.

Conclusion

Even though there are differences in hardness, microstructure and chemistry for the three different bolts, they all meet the hardness, heat treatment and chemical requirements of ASTM A325.

Table 1. Rockwell C Hardness Values

Bolt Designation	Measurement Number					Avg.	Std. Dev.
	1	2	3	4	Center		
IIS Bolts	32.2	32.0	32.1	32.9	31.1	32.1	0.6
Chinese JDF Bolts	29.4	29.8	29.5	28.2	27.9	29.0	0.8
"n" Bolts	27.9	27.0	27.3	24.8	25.2	26.4	1.4

Table 2. Bolt Compositions in Comparison to ASTM A325 Specifications (wt.%)

Bolt Designation	Fe	C	Mn	Si	P	S	Cr
ASTM 325 Type 1 Carbon Steel	Bal.	0.30-0.52	0.60 min	0.15-0.30	0.040 max	0.050 max	
ASTM 325 Type 1 Alloy Steel	Bal.	0.30-0.52	0.60 min	0.15-0.35	0.035 max	0.040 max	
IIS Bolts	Bal.	0.37	1.49	0.30			0.27
Chinese JDF Bolts	Bal.	0.38	1.17	0.30			1.10
"n" Bolts	Bal.	0.53	1.50	0.40			

Table 1. Rockwell C Hardness Values

Bolt Designation	Measurement Number					Avg.	Std. Dev.
	1	2	3	4	Center		
IIS Bolts	32.2	32.0	32.1	32.9	31.1	32.1	0.6
Chinese JDF Bolts	29.4	29.8	29.5	28.2	27.9	29.0	0.8
"n" Bolts	27.9	27.0	27.3	24.8	25.2	26.4	1.4

Table 2. Bolt Compositions in Comparison to ASTM A325 Specifications (wt.%)

Bolt Designation	Fe	C	Mn	Si	P	S	Cr
ASTM 325 Type 1 Carbon Steel	Bal.	0.30-0.52	0.60 min	0.15-0.30	0.040 max	0.050 max	
ASTM 325 Type 1 Alloy Steel	Bal.	0.30-0.52	0.60 min	0.15-0.35	0.035 max	0.040 max	
IIS Bolts	Bal.	0.37	1.49	0.30			0.27
Chinese JDF Bolts	Bal.	0.38	1.17	0.30			1.10
"n" Bolts	Bal.	0.53	1.50	0.40			

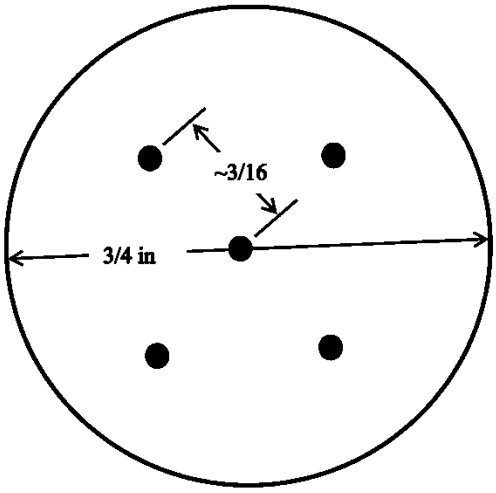

Figure 1. Location of Rockwell C hardness measurements.

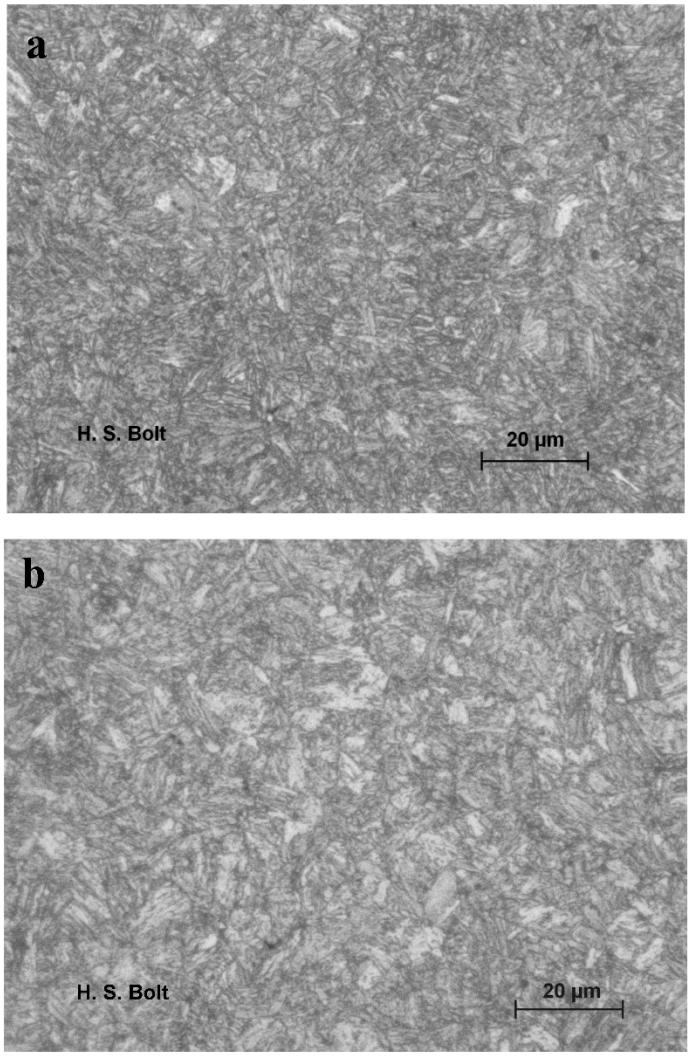

Figure 2. Microstructure of HS bolts. (a) Center. (b) ¼ inch from center. Both microstructures consist of tempered martensite.

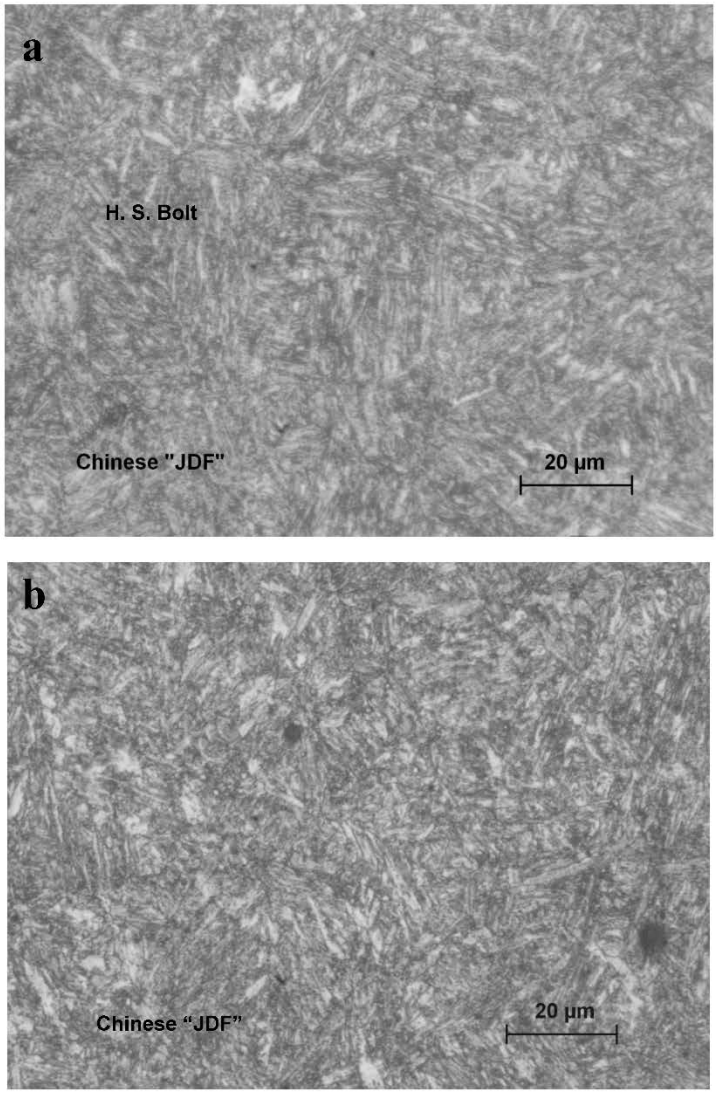

Figure 3. Microstructure of Chinese JDF bolts. (a) Center. (b) ¼ inch from center. Both microstructures consist of tempered martensite.

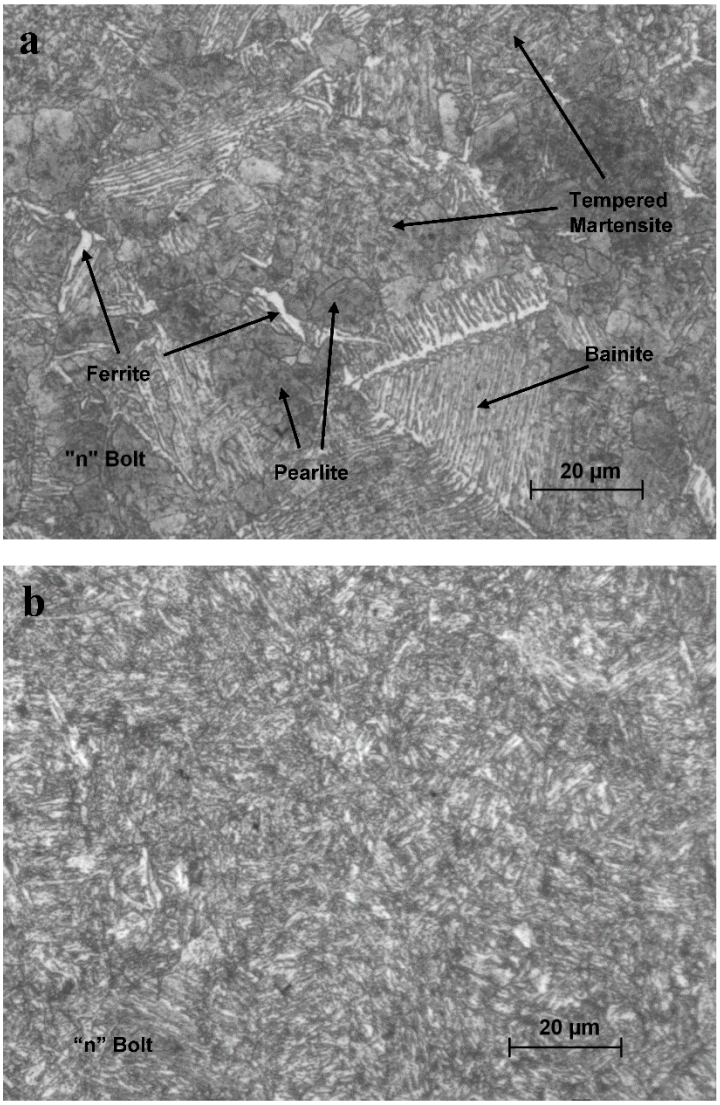

Figure 4. Microstructure of "n" bolts. (a) Center. (b) ¼ inch from center. The microstructure at the center is a complicated mixture of martensite, ferrite, pearlite and bainite. At ¼ inch from the center it is tempered martiensite.

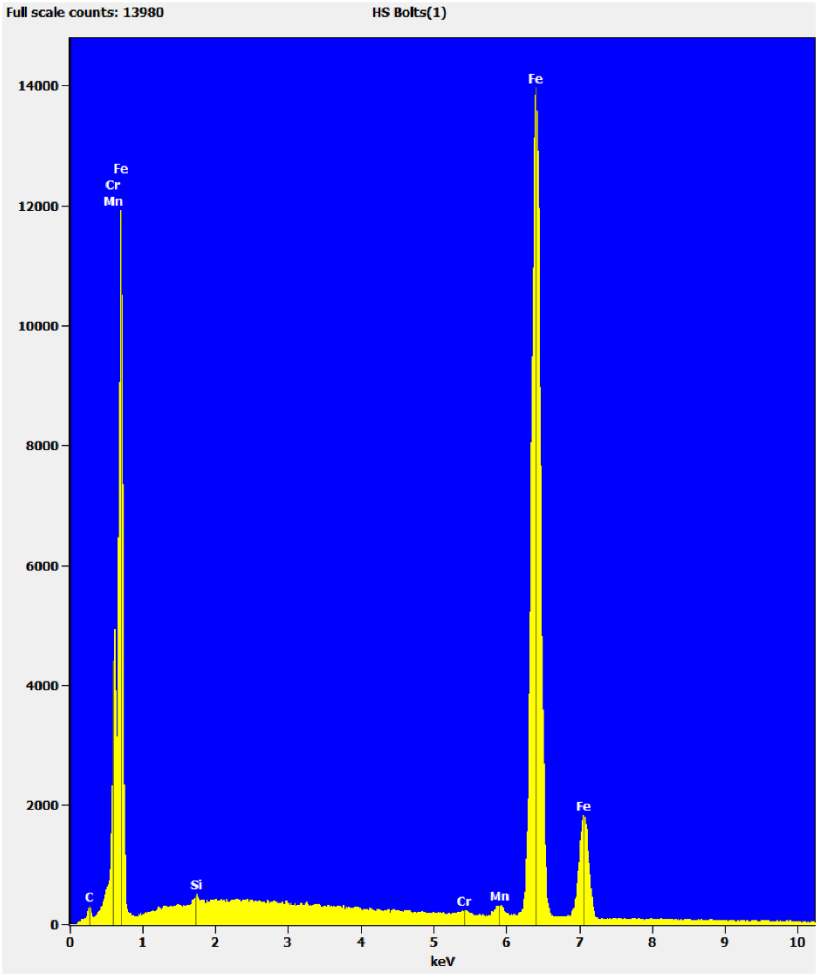

Figure 5. EDS spectrum from HS bolt showing small amounts of Mn and Cr indicating an alloy steel.

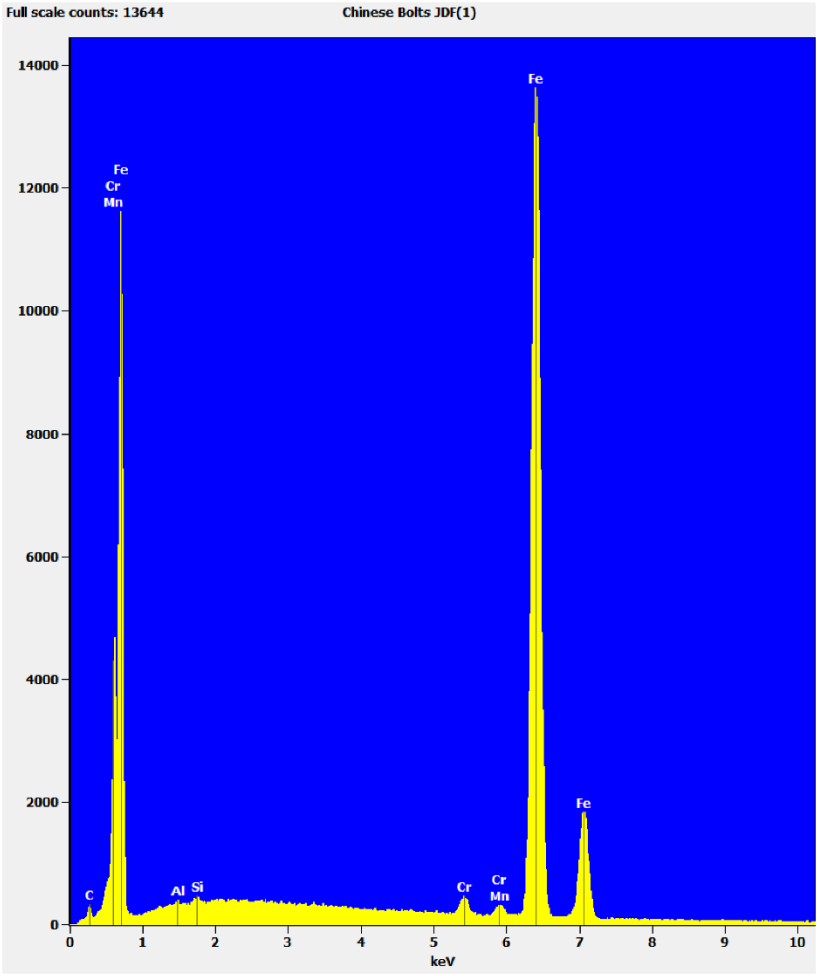

Figure 6. EDS spectrum from Chinese JDF bolt showing small amounts of Mn and Cr indicating an alloy steel.

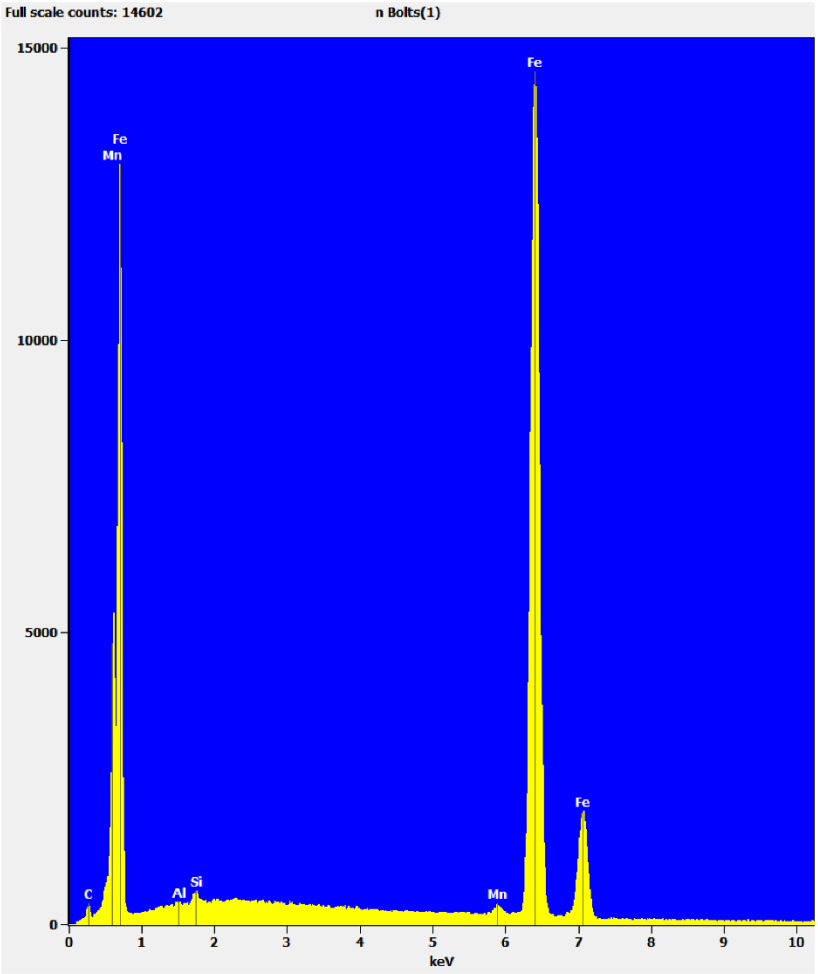

Figure 7. EDS spectrum from "n" bolt showing no Cr indicating a carbon steel.

Appendix E: MATLAB Scripts

D:\MyDocs\Documents\MATLAB\datafilter.m Page 1

```
 1 %% Implemention of a Low pass Butterworth filter using the filtfilt↙
command
 2 %% change the data, sampling frequency, cutoff frequency and order of↙
the filter based on your requirements
 3 % File written by Avinash Parnandi.
 4 % File adjusted to fit parameters of experiment by Megan Hayes
 5 %xx = [1:100];
 6 %data = sin(188*xx)+rand(1,100);  % noisy data; change it to whatever↙
is your data
 7 clear all
 8 clc
 9
10 xx=xlsread('Pre Filter File Name'); %inside the quotes put your file↙
name
11 a=length(xx(1,:));
12
13 A(1:length(xx),1)=xx(:,1);
14 %%
15 for i=2:a;
16     horiz=xx(:,1); %isolate horizontal axis (independent variable)
17     data=xx(:,i); %isolate which column you would like to filter
18
19     f=30;%  sampling frequency --> more or less leave this alone
20     f_cutoff = 0.40; % cutoff frequency
21
22     fnorm =f_cutoff/(f/2); % normalized cut off freq, you can change↙
it to any value depending on your requirements
23
24     [b1,a1] = butter(10,fnorm,'low'); % Low pass Butterworth filter↙
of order 10
25     low_data = filtfilt(b1,a1,data); % filtering
26     low_data = medfilt1(low_data,1000);
27
28     freqz(b1,a1,128,f), title('low pass filter characteristics')
29     figure
30     subplot(2,1,1), plot(horiz,data), title('Actual data')
31     grid on
32     subplot(2,1,2), plot(horiz,low_data), title('Filtered data')
33     grid on
34
35     close all
```

```
    A(:,i)=low_data;
end

cd ('New Location')
xlswrite('New Filter File Name',A)
cd ('Return to Pre Filter File Location')
```

2/25/16 1:06 PM D:\MyDocs\D...\energyfilter.m 1 of 1

```
 1 %% Implemention of a Low pass Butterworth filter using the filtfilt↙
command
 2 %% change the data, sampling frequency, cutoff frequency and order of↙
the filter based on your requirements
 3 clear all
 4 clc
 5
 6 xx=xlsread('Pre Filter File Name'); %inside the quotes put your file↙
name
 7 a=length(xx(1,:));
 8
 9 A(1:length(xx),1)=xx(:,1);
10 %%
11 for i=2:a;
12     horiz=xx(:,1); %isolate horizontal axis (independent variable)
13     data=xx(:,i); %isolate which column you would like to filter
14
15     f=10;%  sampling frequency --> more or less leave this alone
16     f_cutoff = 0.65; % cutoff frequency
17
18     fnorm =f_cutoff/(f/2); % normalized cut off freq, you can change↙
it to any value depending on your requirements
19
20     [b1,a1] = butter(10,fnorm,'low'); % Low pass Butterworth filter↙
of order 10
21     low_data = filtfilt(b1,a1,data); % filtering
22
23     freqz(b1,a1,128,f), title('low pass filter characteristics')
24     figure
25     subplot(2,1,1), plot(horiz,data), title('Actual data')
26     grid on
27     subplot(2,1,2), plot(horiz,low_data), title('Filtered data')
28     grid on
29
30     close all
31     A(:,i)=low_data;
32 end
33
34 cd ('New Location')
35 xlswrite('Filter File Name',A)
36 cd ('Return to Pre Filter File Location')
```

Appendix F: Test Data Output

The experimental data recorded for this research are available upon request. Contact the Milwaukee School of Engineering campus library for further information on how to obtain access to the experimental data.

Structural Engineering

Capstone Report Approval Form

Master of Science in Structural Engineering -- MSST

Milwaukee School of Engineering

This capstone report, entitled “Robustness of WT Steel Connections during Quasi-Dynamic Loading,” submitted by the student Megan E. Hayes, has been approved by the following committee:

Faculty Advisor: _____ Date: _____

Dr. Christopher Raebel

Faculty Member: _____ Date: _____

Dr. Richard DeVries

Faculty Member: _____ Date: _____

Dr. Hans-Peter Huttelmaier

Faculty Member: _____ Date: _____

Dr. Christopher Foley